NOT REMOVE THIS COPY

MSC-R-A-64-1

[redacted]

33

SINGLE COPY ONLY

~~Z 65 · 11218~~

[redacted]

N79-76183

Unclas
00/12 11498

(NASA-TM-X-66755) POSTLAUNCH REPORT FOR APOLLO MISSION A-001 (NASA) 312 p

POSTLAUNCH REPORT FOR APOLLO MISSION A-001 (U)

(BP-12)

CLASSIFICATION CHANGE

To UNCLASSIFIED
By authority of GDS - Eo 11652 Date 12/31/72
Changed by L. Shirley
Classified Document Master Control Station, NASA
Scientific and Technical Information Facility

JUN 1 1964
M A
DOCUMENT
CENTER

GROUP 4
Downgraded at 3-year
intervals; declassified
after 12 years

[redacted]

[redacted]

NATIONAL AERONAUTICS AND SPACE ADMINISTRATION

MANNED SPACECRAFT CENTER

HOUSTON, TEXAS

May 28, 1964

NOT REMOVE THIS COPY

[redacted]

C65-8645

[redacted]

POSTLAUNCH REPORT FOR

APOLLO MISSION A-001 (U)

(BP-12)

[redacted]

Approved for Distribution:

Robert O Piland

for Dr. Joseph F. Shea
Manager, Apollo Spacecraft Program Office

NATIONAL AERONAUTICS AND SPACE ADMINISTRATION

MANNED SPACECRAFT CENTER

HOUSTON, TEXAS

MAY 28, 1964

[redacted]

[redacted]

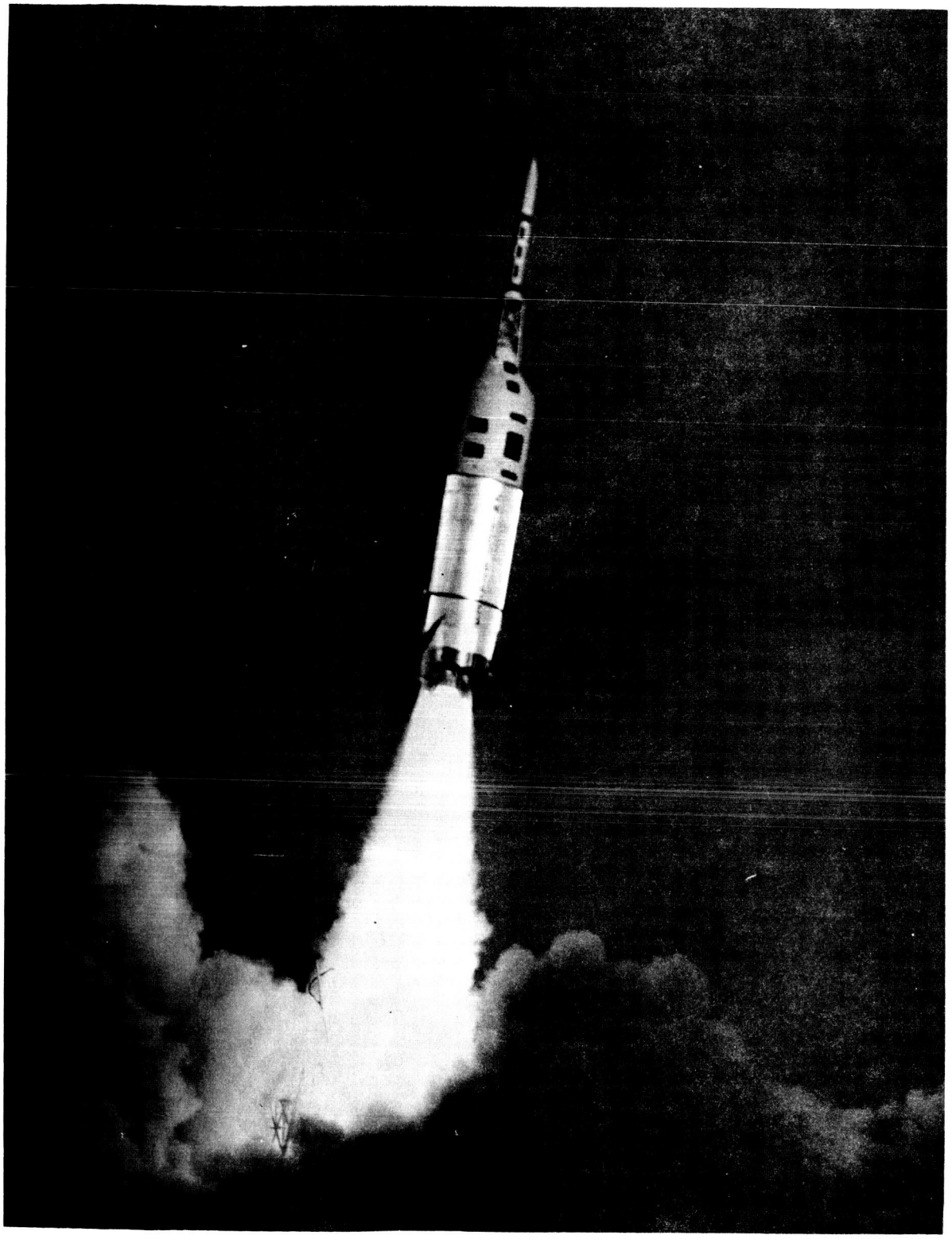

Apollo space vehicle, mission A-001, at lift-off.

[redacted]

[redacted]

TABLE OF CONTENTS

Section		Page
1.0	SUMMARY	1-1
2.0	INTRODUCTION	2-1
3.0	MISSION DESCRIPTION	3-1
4.0	TEST VEHICLE DESCRIPTION	4-1
	4.1 Trajectory Analysis	4-5
	4.1.1 The test point and the real-time-data system	4-5
	4.1.2 Launch vehicle	4-20
	4.1.3 Launch-escape vehicle	4-25
	4.1.4 Spacecraft	4-28
	4.2 Mass Characteristics	4-32
	4.2.1 Propellant weight	4-32
	4.2.2 Spacecraft mass characteristics	4-34
	4.2.3 Launch-vehicle mass characteristics	4-41
	4.2.4 Thrust-vector alinement	4-48
	4.3 Command and Service Module	4-50
	4.3.1 Instrumentation and communications subsystem	4-50
	4.3.2 Electrical and sequential subsystems	4-89
	4.3.3 Launch-escape-propulsion subsystem	4-96
	4.3.4 Spacecraft pyrotechnics	4-110
	4.3.5 Earth-landing subsystem	4-111
	4.3.6 Structures	4-131
	4.3.7 Equipment-cooling subsystem	4-181
	4.3.8 Stability and motion	4-182
	4.4 Launch Vehicle	4-191
	4.4.1 Structures	4-191
	4.4.2 Propulsion and pyrotechnic subsystem	4-193
	4.4.3 Aerodynamic analysis	4-203
	4.4.4 Thrust-termination subsystem	4-207
	4.4.5 Instrumentation subsystem	4-209
	4.4.6 Electrical subsystem	4-213

[redacted]

Section Page

4.5 Inflight Experiments 4-215

4.5.1 Glass samples 4-215
4.5.2 Templaq sensitive paint 4-219

4.6 Postflight Testing 4-222

4.6.1 Launch vehicle postlaunch testing 4-222
4.6.2 Spacecraft postlaunch testing 4-222
4.6.3 Over-all command module electrical subsystem test 4-223
4.6.4 Bench check-out of the ELS sequencer . . 4-223
4.6.5 Bench check-out of the LES sequencer . . 4-223
4.6.6 Investigation of the launch-escape-motor pressure instrumentation 4-224
4.6.7 Investigation of the failure of command module base pressures nos. 5 and 9 . . . 4-224

5.0 MISSION OPERATIONS 5-1

5.1 Prelaunch Operations 5-1

5.1.1 Test vehicle history 5-1
5.1.2 Spacecraft preparation operations 5-3
5.1.3 Launch vehicle preparation operations . . 5-4

5.2 Launch Operations 5-12

5.2.1 Launch procedures 5-12
5.2.2 Launch pad damage assessment 5-13

5.3 Data and Optical Instrumentation Coverage . . . 5-16

5.3.1 Optical instrumentation data 5-16
5.3.2 Meteorological data 5-28
5.3.3 Geodetic data 5-29

5.4 Range Operations 5-31

5.4.1 Communications 5-31
5.4.2 Radio frequency radiation control 5-32
5.4.3 Closed-loop television 5-32
5.4.4 Timing 5-32
5.4.5 Meteorological 5-33
5.4.6 Geodetics 5-33
5.4.7 Telescopes 5-33

Section | Page

5.4.8 Contrave cinetheodolites 5-34
5.4.9 Fixed cameras 5-34
5.4.10 Telemetry 5-34
5.4.11 Radar 5-34
5.4.12 Missile flight surveillance officer . . 5-34
5.4.13 Real-time-data system 5-34

5.5 Recovery Operations 5-36

5.5.1 Recovery teams and equipment 5-36
5.5.2 Command module recovery 5-37
5.5.3 Launch vehicle and service module recovery 5-40
5.5.4 Survey report 5-41

6.0 CONCLUSIONS 6.1

7.0 DISTRIBUTION 7.0

[redacted]

TABLES

Table		Page
2.0-1	TEST OBJECTIVES	2-2
3.0-1	BOILERPLATE 12 EVENT TIMES	3-3
4.1.1-1	THE TEST POINT	4-7
4.2.3-1	MASS PROPERTY DATA	4-42
4.3.1-1	FLIGHT INSTRUMENTATION HARDWARE LIST FOR BOILERPLATE 12	4-56
4.3.1-2	CONTINUOUS TELEMETRY CHANNELS	4-58
4.3.1-3	APOLLO BOILERPLATE MEASUREMENT LIST	4-66
4.3.3-1	MOTOR PERFORMANCE SUMMARY	4-101
4.3.6-1	COMPARISON OF BOILERPLATE 12 TOWER LOADS WITH DESIGN LOADS DURING ABORT	4-131
4.3.6-2	LIMITING FREQUENCY RESPONSE FOR FLUCTUATING PRESSURE	4-137
4.4.1-1	COMPARISON OF BOILERPLATE 12 BOOST PHASE LOADS WITH COMPARABLE DESIGN LOADS	4-192
4.4.5-1	LAUNCH VEHICLE LANDLINE MEASUREMENTS	4-210
4.4.5-2	LAUNCH VEHICLE AIRBORNE MEASUREMENTS	4-212
5.3.1-1	OPTICAL COVERAGE	5-18
5.3.1-2	COVERAGE DETAILS FROM ONBOARD CAMERAS	5-22
5.3.1-3	OPTICAL EVENT DATA	5-23

[redacted]

[redacted]

FIGURES

Figure		Page
3.0-1	Apollo Mission A-001 BP-12 test vehicle configuration .	3-4
3.0-2	Profile of Apollo Mission A-001	3-5
3.0-3	Apollo Mission A-001 launch escape vehicle	3-6
3.0-4	White Sands Missile Range	3-7
4.0-1	Mission A-001 test vehicle	4-3
4.0-2	Test vehicle reference axis system	4-4
4.1.1-1	Altitude plotted against time from launch	4-8
4.1.1-2	Variation of altitude with respect to range	4-9
4.1.1-3	Flight-path angle plotted against time from launch . .	4-10
4.1.1-4	Total velocity plotted against time from launch	4-11
4.1.1-5	Mach number as a function of time from launch	4-12
4.1.1-6	Dynamic pressure plotted against time from launch . . .	4-13
4.1.1-7	Flight-path angle plotted against dynamic pressure . .	4-14
4.1.1-8	Dynamic pressure plotted with respect to Mach number. .	4-15
4.1.1-9	Range resolution error in the real-time-data system	
	(a) Weight flow and Algol thrust with respect to time.	4-16
	(b) Atmospheric pressure, atmospheric temperature and density plotted against time	4-17
	(c) Magnitude of the wind in components and altitude plotted against time	4-18
	(d) Velocity, dynamic pressure, Mach number and flight-path angle plotted against time	4-19

[redacted]

[redacted]

Figure		Page
4.1.2-1	The 4 a.m. m.s.t. meteorological report from Desert Site	
	(a) Temperature and pressure plotted against altitude	4-21
	(b) Wind direction and wind speed plotted against altitude	4-22
4.1.2-2	T-70 minute winds at the launch pad	4-23
4.1.2-3	T-0 winds at the launch pad	4-24
4.1.3-1	Separation distance between the launch-escape vehicle and the predicted Saturn reentry	4-26
4.1.3-2	Altitude with respect to range after abort initiation	4-27
4.1.4-1	Total velocity on the parachutes with respect to time. Computer simulation	4-29
4.1.4-2	Total velocity on the parachutes with respect to time. Cinetheodolite results	4-30
4.1.4-3	The ground track of the command module. Cinethedolite results	4-31
4.2.2-1	Spacecraft predicted weight plotted against time of launch-escape-motor ignition	4-35
4.2.2-2	Spacecraft predicted center-of-gravity (x) location plotted against time of launch-escape-motor ignition	4-36
4.2.2-3	Predicted center-of-gravity (z) location plotted against time of launch-escape-motor ignition . . .	4-37
4.2.2-4	Spacecraft predicted roll moment of inertia plotted against time of launch-escape-motor ignition . . .	4-38
4.2.2-5	Spacecraft predicted pitch moment of inertia plotted against time of launch-escape-motor ignition . . .	4-39

[redacted]

[redacted]

Figure		Page
4.2.2-6	Spacecraft predicted yaw moment of inertia plotted against time of launch-escape-motor ignition . . .	4-40
4.2.3-1	Total test vehicle weight plotted against Little Joe II burning time	4-43
4.2.3-2	Test vehicle center of gravity plotted against Little Joe II burning time	4-44
4.2.3-3	Test vehicle pitch moment of inertia plotted against Little Joe II burning time	4-45
4.2.3-4	Test vehicle roll moment of inertia plotted against Little Joe II burning time	4-46
4.2.3-5	Test vehicle yaw moment of inertia plotted against Little Joe II burning time	4-47
4.2.4-1	Diagram showing thrust-vector angle	4-49
4.3.1-1	Modulation package block diagram	4-75
4.3.1-2	Boilerplate 12 instrumentation block diagram depicting V.C.O. assignment	4-76
4.3.1-3	Communication and instrumentation subsystem block diagram	4-77
4.3.1-4	Communication and instrumentation subsystem component location	4-78
4.3.1-5	Boilerplate 12 camera subsystem block diagram. Each camera has a control subsystem as shown.	4-79
4.3.1-6	Linear accelerometer, gyros, and temperature resistance theromometer	4-80
4.3.1-7	Spacecraft measurement locations	4-81
4.3.1-8	Command module conical surface and fluctuating pressure measurement locations	4-82

[redacted]

[redacted]

Figure		Page
4.3.1-9	Command module aft heat shield pressure measurement locations	4-83
4.3.1-10	Launch-escape subsystem and earth-landing subsystem sequence measurements	4-84
4.3.1-11	Boilerplate 12 physical location of primary instrumentation components	4-85
4.3.1-12	Telemetry transmitter amplifier temperature plotted against time	4-86
4.3.1-13	Command module interior temperature and pressure plotted against time	4-87
4.3.1-14	Transponder A and B trigger pulse repetition rate .	4-88
4.3.2-1	Boilerplate 12 event schedule sequential block diagram	4-91
4.3.2-2	Boilerplate 12 launch-escape subsystem and earth-landing subsystem block diagram	4-92
4.3.2-3	Time histories of pyro bus voltages	4-93
4.3.2-4	Time histories of logic bus voltages	4-94
4.3.2-5	Time histories d-c current and main bus voltages . .	4-95
4.3.3-1	Pitch-control motor thrust correction factor plotted against time	4-102
4.3.3-2	Launch-escape subsystem diagram	4-103
4.3.3-3	Launch-escape motor diagram	4-104
4.3.3-4	Launch-escape motor predicted thrust plotted against time	4-105
4.3.3-5	Pitch-control motor diagram	4-106
4.3.3-6	Pitch-control motor thrust platted against time . .	4-107

[redacted]

[redacted]

Figure		Page
4.3.3-7	Tower-jettison motor diagram	4-108
4.3.3-8	Tower-jettison motor predicted thrust plotted against time	4-109
4.3.5-1	Command module upper deck prior to flight	4-119
4.3.5-2	Top view of command module	4-120
4.3.5-3	Command module attitude changes during main parachute deployment	4-121
4.3.5-4	Reconstruction of routing of failed riser of no. 1 main parachute	4-122
4.3.5-5	Routing of failed riser over no. 2 and no. 3 longerons	4-123
4.3.5-6	Upper portion of failed riser showing abrasion of command module Thermo Fit sleeving and riser . . .	4-124
4.3.5-7	Failed riser showing abrasion of command module skin by parachute connector links	4-125
4.3.5-8	No. 1 main parachute riser damage to no. 2 longeron	4-126
4.3.5-9	Area of no. 1 parachute riser damaged by abrasion over no. 2 longeron	4-127
4.3.5-10	Drogue disconnect assembly showing damaged electrical connector and charge holder. Note nylon tuft at upper right.	4-128
4.3.5-11	Command module showing bent simulated reaction-control-subsystem motor	4-129
4.3.5-12	Chart showing damage to no. 3 parachute	4-130
4.3.6-1	Time history of command module accelerometers during thrust termination	
	(a) X-axis acceleration (high range accelerometer).	4-138
	(b) Z-axis acceleration	4-139
	(c) Y-axis acceleration	4-139

[redacted]

[redacted]

Figure		Page
4.3.6-2	Time histories of command module accelerometers during main parachute deployment	
	(a) X-axis acceleration (high range accelerometer).	4-140
	(b) Z-axis acceleration	4-141
	(c) Y-axis acceleration	4-141
4.3.6-3	Beginning of thrust termination	4-142
4.3.6-4	Thrust termination as fireball engulfs launch vehicle	4-143
4.3.6-5	Launch vehicle disintegrates during thrust termination	4-144
4.3.6-6	Pressure coefficient comparison in the pitch plane +Z quadrant	4-145
4.3.6-7	Pressure coefficient comparison along two rays in the yaw plane	4-146
4.3.6-8	Pressure coefficient comparison in planes between jet plumes	4-147
4.3.6-9	Pressure coefficient comparison at a typical station	4-148
4.3.6-10	Comparison of BP-12 fluctuation pressures with wind-tunnel data	
	(a) M = 0.80 and 0.95	4-149
	(b) M = 0.90 and 0.95	4-150
4.3.6-11	Root mean square pressure time history	
	(a) Fluctuating pressure 1	4-151
	(b) Fluctuating pressure 2	4-152
	(c) Fluctuating pressure 3	4-153
	(d) Fluctuating pressure 4	4-154

[redacted]

[redacted]

Figure | Page

(e) Fluctuating pressure 6 4-155

(f) Fluctuating pressure 8 4-156

(g) Fluctuating pressure 10 4-157

4.3.6-12 Time histories of base pressures

(a) Base pressures 1 and 2 4-158

(b) Base pressures 3 and 4 4-159

(c) Base pressures 6 and 10 4-160

(d) Base pressures 7 and 8 4-161

(e) Base pressures 11 and 12 4-162

4.3.6-13 Time histories of conical surface pressures

(a) Conical surface pressures 1 and 2 4-163

(b) Conical surface pressures 3 and 4 4-164

(c) Conical surface pressures 5 and 6 4-165

(d) Conical surface pressures 7 and 8 4-166

(e) Conical surface pressures 9 and 10 4-167

(f) Conical surface pressures 11 and 12 4-168

(g) Conical surface pressures 14 and 22 4-169

(h) Conical surface pressures 23 and 24 4-170

(i) Conical surface pressures 25 and 26 4-171

(j) Conical surface pressures 21 and 27 4-172

(k) Conical surface pressures 15 and 28 4-173

(l) Conical surface pressures 18 and 29 4-174

Figure Page

(m) Conical surface pressures 30 and 31 4-175

(n) Conical surface pressures 20 and 32 4-176

(o) Conical surface pressures 33 and 34 4-177

(p) Conical surface pressures 35 and 36 4-178

(q) Conical surface pressures 13 and 16 4-179

(r) Conical surface pressures 17 and 19 4-180

4.3.8-1 Predicted and actual launch-escape-vehicle pitch rate time histories 4-184

4.3.8-2 Predicted and actual launch-escape-vehicle yaw rate time histories 4-184

4.3.8-3 Predicted and actual launch-escape-vehicle roll rate time histories 4-185

4.3.8-4 Predicted and actual launch-escape-vehicle roll attitude time histories 4-185

4.3.8-5 Predicted and actual angles of attack and sideslip time histories

(a) Angle of attack 4-186

(b) Angle of sideslip 4-186

4.3.8-6 Time histories of yaw rate and attitude 4-187

4.3.8-7 Time histories of pitch rate and attitude 4-188

4.3.8-8 Time histories of roll rate and attitude 4-189

4.3.8-9 Time histories of Q-ball delta pressures 4-190

[redacted]

Figure		Page
4.4.2-1	Algol rocket motor thrust correction factor	4-195
4.4.2-2	Algol rocket motor chamber pressure plotted against time	4-196
4.4.2-3	Algol rocket motor thrust plotted against time . . .	4-197
4.4.2-4	Recruit rocket motor predicted thrust plotted against time	4-198
4.4.2-5	Launch vehicle total thrust plotted against time . .	4-199
4.4.2-6	Algol ignition subsystem diagram	4-200
4.4.2-7	Recruit ignition subsystem diagram. Typical for all Recruits	4-201
4.4.2-8	Time history of Algol chamber pressure	4-202
4.4.3-1	Launch-vehicle pitch rate time history from lift-off to thrust termination	4-204
4.4.3-2	Launch-vehicle yaw rate time history from lift-off to thrust termination	4-204
4.4.3-3	Launch-vehicle roll attitude time history from lift-off to thrust termination	4-205
4.4.3-4	Launch-vehicle roll rate time history from lift-off to thrust termination	4-205
4.4.3-5	Comparison of estimated drag with flight drag for various Mach numbers	4-206
4.4.4-1	Block diagram of dual thrust termination subsystem .	4-208
4.4.6-1	Variation of ignition battery voltage with time after removal of battery charger	4-214
4.5.1-1	Location of eight 2- by 2-inch glass samples on command module	4-217
4.5.1-2	Location of four 4- by 5-inch glass samples on command module [redacted]	4-218

[redacted]

Figure		Page
4.5.2-1	Location of temperature sensitive paint on command module	4-220
4.5.2-2	Location of heat sensitive paint on launch-escape tower	4-221
5.1.1-1	Launch vehicle 12-50-2 prelaunch milestones	5-6
5.1.1-2	Boilerplate 12 prelaunch milestones	
	(a) Apollo test operations - Downey	5-8
	(b) WSMR facility preparation - Spacecraft assembly and checkout - Integrated operations	5-9
5.1.1-3	Spacecraft and associated facility pre-integrated tests	5-10
5.1.1-4	Launch vehicle and associated facility pre-integrated tests	5-11
5.2.1-1	Pre-count for boilerplate 12	5-14
5.2.1-2	Final countdown for boilerplate 12	5-15
5.3.1-1	Camera and radar locations for boilerplate 12 . . .	5-25
5.3.1-2	Telemetry station locations for boilerplate 12 . .	5-26
5.3.1-3	Data handling time history	5-27
5.4.1-1	Functional block diagram of WSMR timing system . .	5-35
5.5.1-1	Recovery team standby positions and location of predicted and actual landing/impact points . .	5-42
5.5.1-2	Photograph of command module after landing	5-43
5.5.1-3	Closeup photograph of command module after landing	5-44
5.5.1-4	Photograph of command module and parachute after landing	5-45

[redacted]

[redacted]

Figure		Page
5.5.1-5	Photograph showing command module being loaded on Terracruiser	5-46
5.5.1-6	Photograph of command module imprint on ground . .	5-47
5.5.1-7	Photograph showing fiberglass torn from aft heat shield	5-48
5.5.1-8	Photograph of LES after impact	5-49
5.5.1-9	Photograph of LES after removal from ground	5-50
5.5.1-10	Photograph of service module after impact	5-51
5.5.1-11	Photograph of aft section of launch vehicle after impact	5-52

[redacted]

[redacted]

POSTLAUNCH REPORT FOR

APOLLO MISSION A-001

(BP-12)

1.0 SUMMARY

The Apollo boilerplate 12 Mission A-001 was launched on May 13, 1964, at White Sands Missile Range, New Mexico, at 5:59:59.717 a.m. mountain standard time (m.s.t.). Unacceptable wind and dust conditions had forced a 24-hour postponement of the launch from its original schedule of 6:00 a.m. m.s.t., May 12, 1964. Vehicle performance was as predicted. The mission was a success.

All first-order test objectives and two of the three second-order test objectives were satisfied. The second-order test objective which was not satisfied was:

> Demonstrate proper operation of the applicable components of the earth-landing subsystem.

During the deployment of the three main parachutes, a parachute riser chafed against a simulated reaction-control-subsystem motor and drogue disconnect guide assembly (horsecollar). The riser subsequently broke after main parachute line stretch, and the command module descended safely to the ground on the two remaining main parachutes.

[redacted]

2.0 INTRODUCTION

The Apollo Mission A-001 using boilerplate 12 was conducted to determine the aerodynamic characteristics of the launch-escape vehicle and to prove its capability to propel the command module away from the launch vehicle under transonic speed conditions and high dynamic pressure.

To perform this mission, Apollo boilerplate 12 was delivered to White Sands Missile Range (WSMR), New Mexico, on March 2, 1964. Little Joe II launch vehicle, designated 12-50-2, was delivered to WSMR on February 17, 1964. Complete subsystems tests were performed on both the launch vehicle and the test vehicle at WSMR prior to launch operations on May 13, 1964. This was the second flight abort test of an Apollo boilerplate command module test vehicle.

The launch was successfully initiated at 5:59:59.717 a.m. m.s.t. on Wednesday, May 13, 1964. The test was originally scheduled for 6:00 a.m. m.s.t. on May 12, 1964; however, unacceptable wind and dust conditions on that day forced a 24-hour postponement.

There were five first-order and three second-order test objectives formulated for this mission. First-order test objectives are those objectives which define the main purpose for making a flight. These objectives must be achieved for the flight to be a success. Second-order test objectives are those desired to support future Apollo missions or to supply supplementary data for over-all spacecraft evaluation. These test objectives are shown in table 2.0-1. Detailed results pertaining to individual objectives are discussed in subsequent sections of this report.

The definition of terms used in connection with objectives for this report is as follows:

Demonstrate denotes the occurrence of an action or an event during a test. The accomplishment of an objective of this type requires a qualitative answer. The answer will be derived through the relation of this action or event to some other known information or occurrence. This category of objective implies a minimum of airborne instrumentation, and/or that the information be obtained external to the spacecraft.

Determine denotes the measurement of performance of any subsystem or component. This category implies a quantitative investigation of over-all operation which includes, generally, instrumentation for measuring basic inputs and outputs of the subsystem. The information obtained should indicate to what extent the subsystem operated as designed. Instrumentation should allow performance deficiencies to be isolated to either the subsystem or to the subsystem inputs.

[redacted]

TABLE 2.0-1.- TEST OBJECTIVES

Number	First order	Comment
1	Demonstrate the structural integrity of the escape tower.	Satisfied
2	Demonstrate the capability of the escape subsystem to propel the command module to a predetermined distance from the launch vehicle.	Satisfied
3	Determine aerodynamic stability characteristics of the escape configuration for this abort condition.	Satisfied
4	Demonstrate proper operation of the command module to service module separation subsystem.	Satisfied
5	Demonstrate satisfactory recovery timing sequence in the earth-landing subsystem.	Satisfied
Number	**Second order**	**Comment**
1	Demonstrate Little Joe II-spacecraft compatibility.	Satisfied
2	Determine aerodynamic loads due to fluctuating pressures on the command module and service module during a Little Joe II launch.	Satisfied
3	Demonstrate proper operation of the applicable components of the earth-landing subsystem.	Not satisfied

[redacted]

3.0 MISSION DESCRIPTION

Apollo Mission A-001 was executed to determine the aerodynamic and operational characteristics of the launch-escape vehicle during an abort at transonic speed conditions and high dynamic pressure. The test vehicle launch configuration is shown in figure 3.0-1, the mission profile is illustrated in figure 3.0-2, and the launch-escape vehicle in figure 3.0-3.

The test vehicle was launched on May 13, 1964, at 5:59:59.717 a.m. m.s.t.[a] by igniting all Little Joe II launch vehicle motors simultaneously. Launch took place from launch complex 36 at White Sands Missile Range, New Mexico, which is approximately 4,000 feet above mean sea level (m.s.l.). Figure 3.0-4 is a map of the White Sands Missile Range.

The launcher was set at 81°19' elevation and 346°20' azimuth to compensate for predominantly southeast surface winds (south component 5.0 mph, east component 6.0 mph) recorded at T-70 minutes.

The flight proceeded through the series of significant events at the proper times as tabulated in table 3.0-1.

The launch vehicle rated thrust of approximately 300,000 pounds was provided by the six Recruit and one Algol solid-propellant motors. The six Recruit motors were expended after 1.5 seconds; thereafter, thrust was provided by the one Algol motor. At lift-off, a maximum launch-vehicle acceleration of approximately 7g was experienced.

The flight dynamics officer observed the real-time-data system plots of: flight-path angle plotted against dynamic pressure, dynamic pressure plotted against Mach number, and altitude plotted against range and trajectory ground track. When the optimum test-point conditions of dynamic pressure and Mach number were displayed at 28.435 seconds after lift-off, the flight dynamics officer sent the abort signal. This test-point condition corresponded to a dynamic pressure of 633 lb/sq ft, a Mach number of 0.935, and an altitude of 19,444 feet m.s.l.

The abort signal initiated thrust termination of the Little Joe II launch vehicle (by rupturing the Algol motor casing), ignition of the launch-escape and pitch-control motors, and separation of the command module from the service module.

---

[a]All times for data, telemetry, onboard tape recorder, and radar theodolite film are referenced to a maximum 4-inch vehicle rise event as zero time (T-0).

[redacted]

Chamber pressure of the pitch-control motor was first recorded at 28.54 seconds. Telemetry recordings of the pitch-control-motor pressure indicate that performance was slightly below specification. The performance characteristics of the launch-escape motor could not be determined because of the loss of the chamber-pressure measurement. However, evaluation of the flight data indicated that motor performance was acceptable.

At approximately 44 seconds, the tower-jettison motor was ignited and satisfactorily separated the launch-escape tower from the command module.

The drogue parachute mortar fired at 47.2 seconds with full drogue parachute deployment occurring at approximately 48.2 seconds. The command module was subjected to less-than-predicted maximum conditions of pitch, roll, and yaw rates during drogue parachute operation.

At an altitude of approximately 12,500 feet m.s.l., baroswitches initiated the firing of the three pilot parachute mortars. This event occurred at 112.7 seconds. When the three main 88-foot parachutes were deployed, a parachute riser chafed and abraded against a simulated reaction-control-subsystem motor and the drogue disconnect guide assembly (horse-collar). This riser subsequently broke close to the bridle in the chafed area and allowed the main parachute to separate from the command module. The two remaining main parachutes were deployed normally and achieved reefed and then disreefed inflation. Suspension lines of the free parachute inflicted sufficient burn damage to one of the remaining two reefed parachutes to cause the gore failure noted upon disreef.

The command module, supported by the two remaining main parachutes, was lowered at a rate of 30 feet per second, decreasing to 26 feet per second at earth landing rather than the predicted rate of 24 feet per second based on a three-parachute support.

Earth impact for the base of the Little Joe II launch vehicle occurred at 124.5 seconds, 11,592 feet downrange.

Earth landing for the command module occurred at 350.3 seconds, 22,400 feet downrange. Maximum altitude attained was 29,772 feet m.s.l.

Earth impact for the launch-escape subsystem with forward cover occurred at 110.9 seconds, 27,953 feet downrange. Maximum altitude attained was 30,511 feet m.s.l.

Postlaunch recovery operations were underway immediately after launch and all major components were returned to the Vehicle Assembly Building within $10\frac{1}{2}$ hours.

[redacted]

TABLE 3.0-1.- BOILERPLATE 12 EVENT TIMES

[Lift-off: Planned, 6:00 a.m. m.s.t; actual, 5:59:59.717 a.m. m.s.t.]

Event	Commutator channel number	Planned time, t+sec	Actual time, t+sec		Time from abort, sec		
			A	B	Planned	Actual	
						A	B
Abort enable	A-E-45	0	0.08	--	--	--	--
Little Joe thrust termination (system A)	A-E-70	31.39	28.49	--	0	0	--
Little Joe thrust termination (system B)	A-E-79	31.39	--	28.49	0	--	0
Abort initiate relay closure A and B	A-E-55	31.39	28.46	28.46	0	-.03	-.03
Abort initiate relay closure A and B (K-20, 19)	A-E-72	31.39	28.49	28.49	0	0	0
LES pitch-control motor fire relay closure A and B	A-E-48	31.39	28.46	28.56	0	-.03	.07
Command module/service module separation relay closure A and B	A-E-56	31.39	28.46	28.56	0	-.03	.07
Sequencer start signal A	A-E-57	31.39	28.46	--	0	-.03	--
Sequencer start signal B	A-E-58	31.39	--	28.46	0	--	-.03
Backup abort timer A and B	A-E-38	41.10	28.56	41.39	10.36	.07	12.90
Tower jettison-separation A initiate relay closure A and B	A-E-50	46.89	43.94	44.14	15.50	15.45	15.65
Tower jettison-separation B initiate relay closure A and B	A-E-49	46.89	43.74	44.25	15.50	15.25	15.76
Tower jettison-separation relay closure A and B	A-E-61	46.89	44.15	44.26	15.50	15.66	15.77
ELS sequencer A start relay closure A and B	A-E-62	49.89	47.11	47.11	18.50	18.62	18.62
ELS sequencer B start relay closure A and B	A-E-63	49.89	47.11	47.21	18.50	18.62	18.72
Forward heat shield relay closure A and B	A-E-60	49.89	47.11	47.31	18.50	18.62	18.82
Drogue mortar fire	A-E-80	49.89	47.23	--	18.50	18.74	--
Drogue deploy relay closure A and B	A-E-65	49.89	47.11	47.21	18.50	18.62	18.72
Main parachute deploy - Drogue release relay closure A and B	A-E-66	120.57	112.7	112.7	89.18	84.21	84.21
Baroswitch 1 and 2 (25K ft) system A[a]	A-E-46	72.50	--	--	40.89	--	--
Pilot mortar 1 fire	A-E-81	122.86	112.7	--	89.18	84.21	--
Pilot mortar 2 fire	A-E-82	122.86	112.7	--	89.18	84.21	--
Pilot mortar 3 fire	A-E-83	122.86	112.7	--	89.18	84.21	--
Baroswitch 1 and 2 (25K ft) system B[a]	A-E-59	122.86	--	--	89.18	--	--
Main parachute release relay closure A and B[a]	A-E-67	386.47	350.51	--	355.08	322.08	--
Command module landing	--	386.47	350.3	--	355.08	321.8	--

NOTE: All event times from commutator are to be treated as -0, -0.1 second in quoting times.

[a]These events were monitored only.

[redacted]

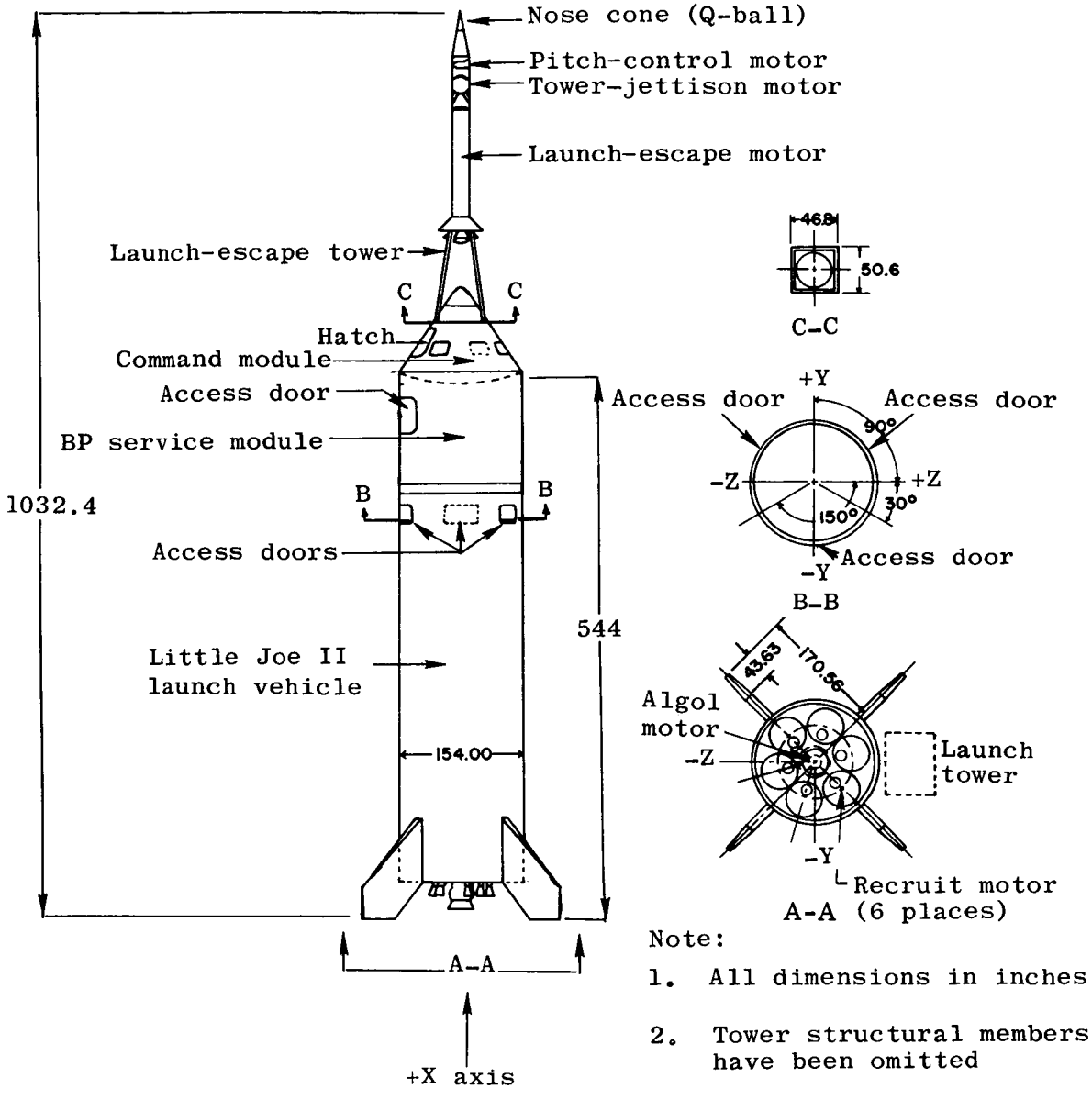

Figure 3.0-1.- Apollo mission A-001 BP-12 test vehicle configuration.

[redacted]

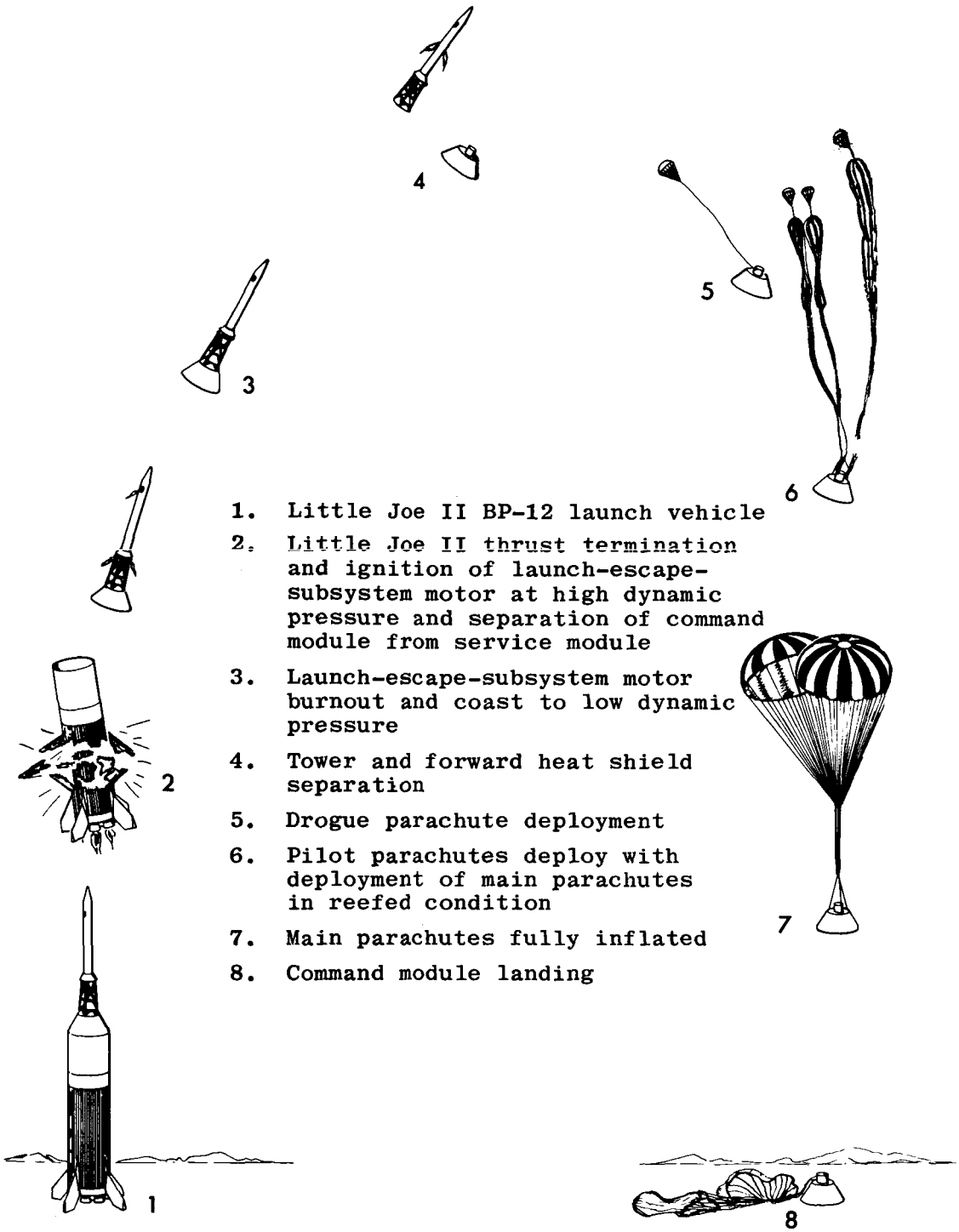

1. Little Joe II BP-12 launch vehicle
2. Little Joe II thrust termination and ignition of launch-escape-subsystem motor at high dynamic pressure and separation of command module from service module
3. Launch-escape-subsystem motor burnout and coast to low dynamic pressure
4. Tower and forward heat shield separation
5. Drogue parachute deployment
6. Pilot parachutes deploy with deployment of main parachutes in reefed condition
7. Main parachutes fully inflated
8. Command module landing

Figure 3.0-2.- Profile of Apollo mission A-001.

[redacted]

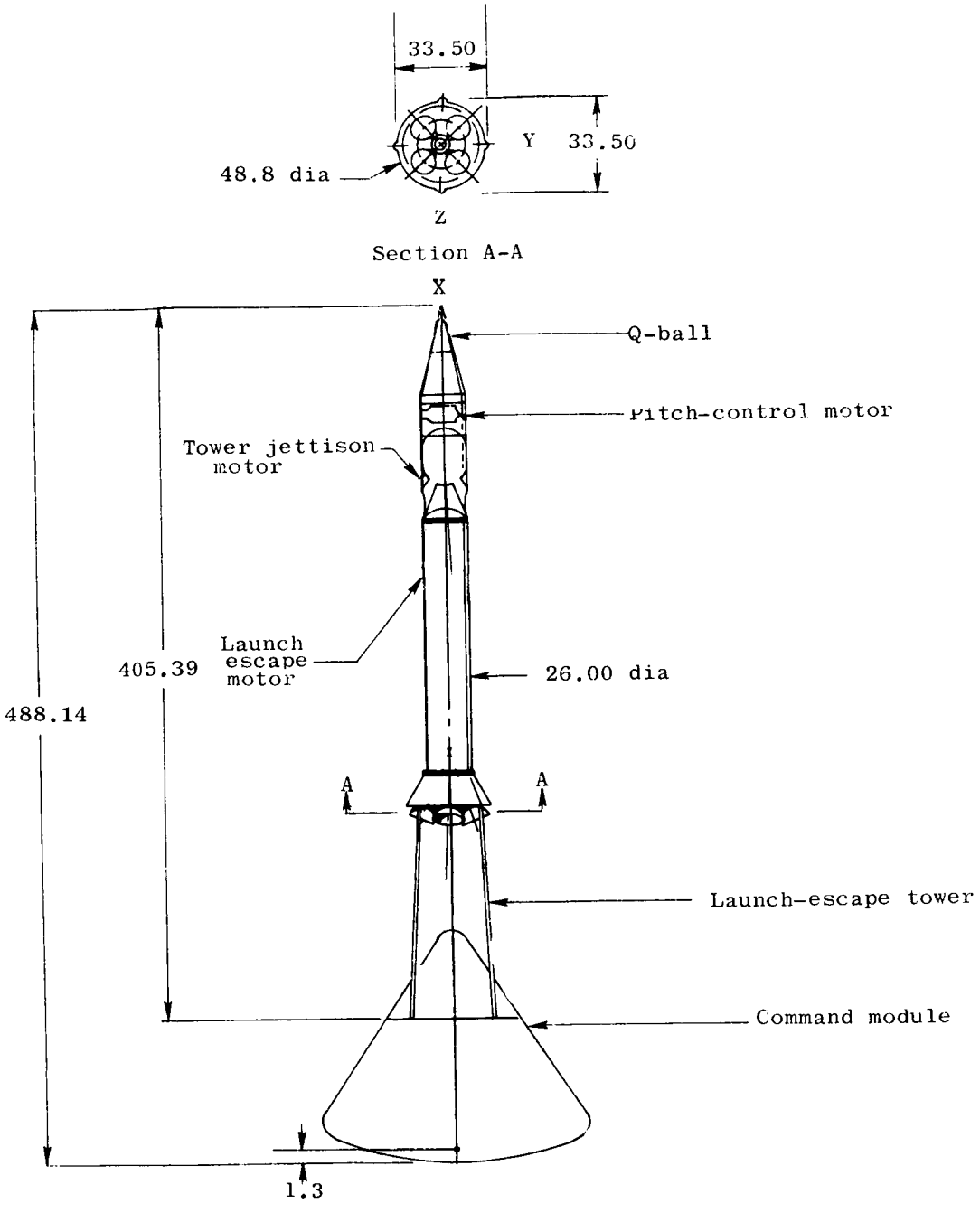

Note 1. All dimensions in inches unless otherwise noted
2. Tower structural members habe been omitted for clarity

Figure 3.0-3.- Apollo mission A-001 launch escape vehicle.

[redacted]

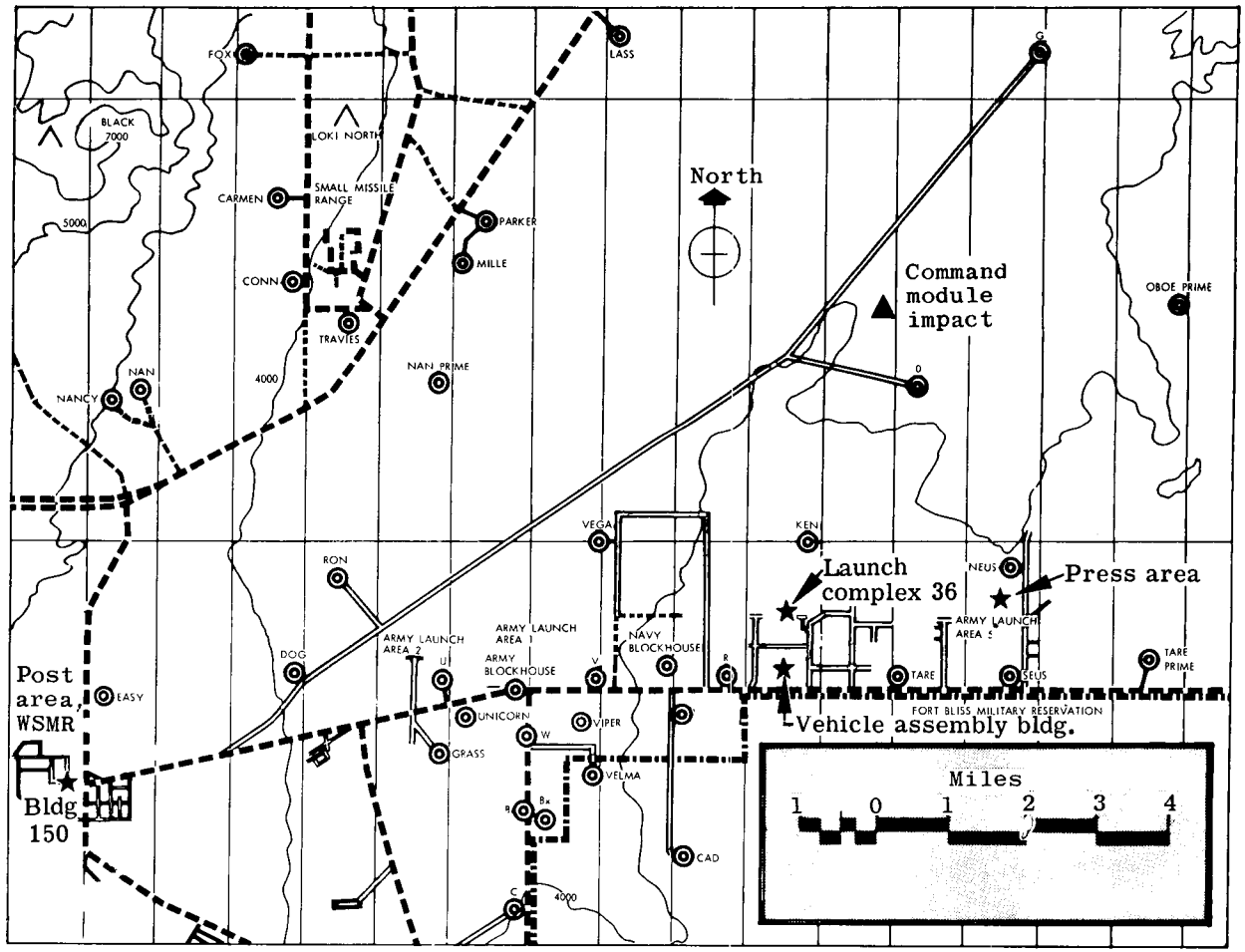

Figure 3.0-4.- White Sands Missile Range.

4.0 TEST VEHICLE DESCRIPTION

The Apollo Mission A-001 test vehicle (BP-12) consisted of two main units: the spacecraft (launch-escape subsystem, boilerplate command module, boilerplate service module), and the launch vehicle.

The Little Joe II launch vehicle no. 12-50-2 was a fin-stabilized airframe in which one Algol ID Mod II and six Recruit solid-propellant rocket motors were installed. The launch vehicle contained or utilized a propulsion and pyrotechnic subsystem, a thrust-termination subsystem, an instrumentation and communication subsystem, and an electrical subsystem.

The launch-vehicle airframe consisted of a cylindrical body and four fixed fins. A diagram of the test vehicle is shown in figure 4.0-1. The test vehicle reference axis system is shown in figure 4.0-2. A sketch of the launch-escape vehicle is shown in figure 3.0-3.

The command module was of aluminum boilerplate construction, conical in shape, 134 inches high and 154 inches maximum diameter. The aft heat shield was constructed of laminated fiber glass as a substitute for the ablative material and substructure. Subsystems contained within the command module were: onboard instrumentation, electrical power, earth-landing subsystem, launch-escape sequencer, and equipment cooling.

The service module was of aluminum boilerplate construction, cylindrical in shape, 158.6 inches long and 154 inches in diameter. Provisions to bolt the service module to launch vehicle were incorporated at the bottom in a 10-inch-long detachable adapter. A protective fiber-glass bulkhead was attached to the inside of the module as a means of protecting the command module during explosive thrust termination of the Little Joe II launch vehicle.

The launch-escape subsystem consisted of a welded tubular launch-escape tower, four explosive bolts, and three solid-propellant motors. The tower, 120 inches long with a base about 46 by 50 inches, formed the intermediate structure between the boilerplate command module and the escape-jettison motors. The tower was attached to the command module by four explosive bolts.

The solid-propellant launch-escape motor was 26 inches in diameter and 183 inches in length. The motor contained four nozzles canted 35° from the motor longitudinal axis, and produced a nominal 155,000-pound thrust.

[redacted]

The solid-propellant pitch-control motor, 9 inches in diameter and 22 inches in length, produced a nominal total impulse of 1,700 pound-seconds. The motor housing formed the structure between the nose cone and the forward end of the jettison motor.

The solid-propellant tower-jettison motor was 26 inches in diameter, and 47 inches in length with a bolt flange at the aft end which allows the jettison motor to be mounted to the head end of the launch-escape motor. The motor contained two thrust nozzles positioned 30° from the resultant thrust center line and produced a nominal 33,000 pounds of thrust for 1 second.

Applicable time histories of measured parameters are included at the end of each subsystem analyses.

[redacted]

[redacted]

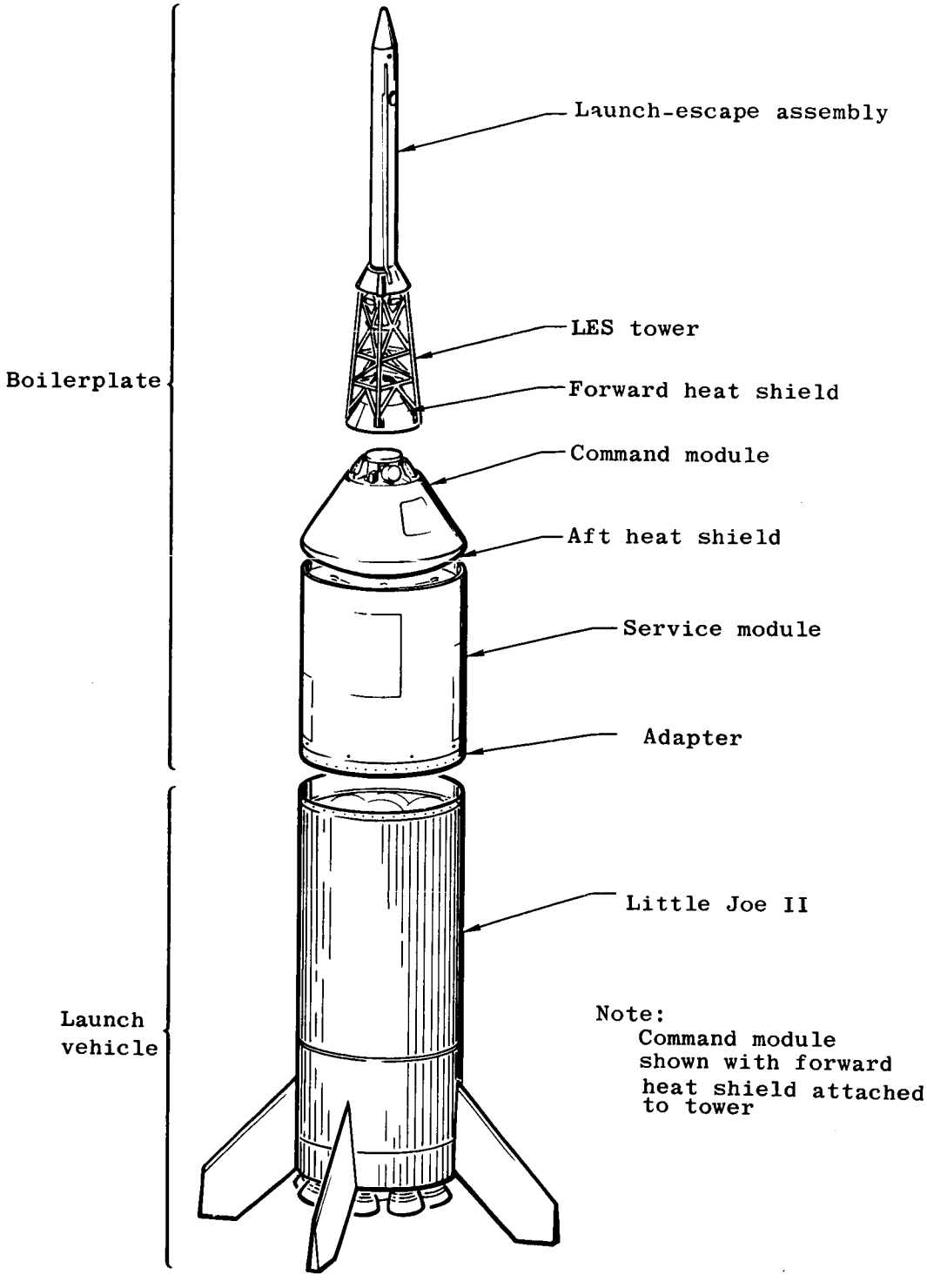

Figure 4.0-1. - Mission A-001 test vehicle.

[redacted]

[redacted]

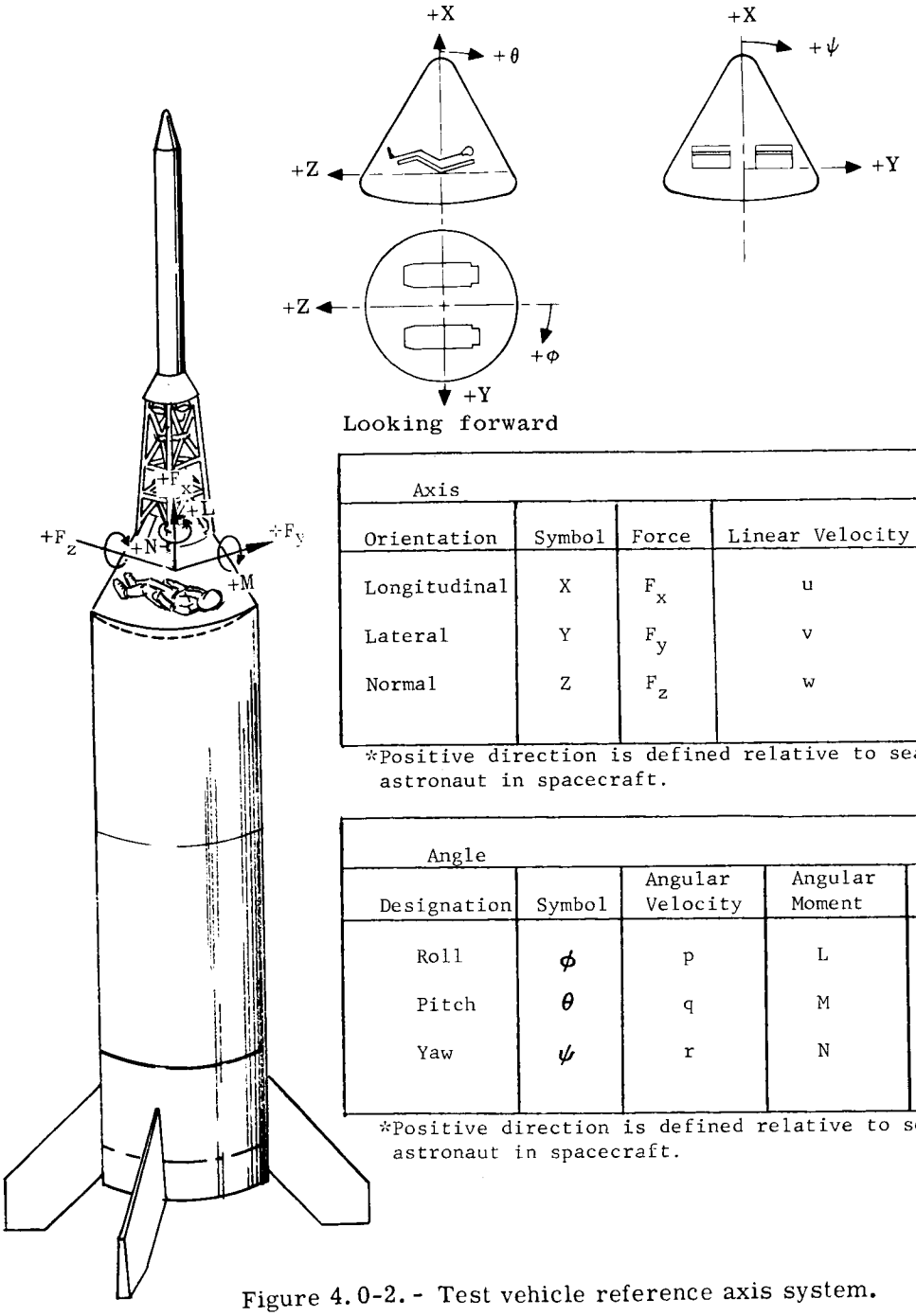

Axis				
Orientation	Symbol	Force	Linear Velocity	Positive Direction*
Longitudinal	X	F_x	u	Forward
Lateral	Y	F_y	v	Right
Normal	Z	F_z	w	Down

*Positive direction is defined relative to seated astronaut in spacecraft.

Angle				
Designation	Symbol	Angular Velocity	Angular Moment	Positive Direction*
Roll	ϕ	p	L	Clockwise
Pitch	θ	q	M	Up
Yaw	ψ	r	N	Right

*Positive direction is defined relative to seated astronaut in spacecraft.

Figure 4.0-2. - Test vehicle reference axis system.

[redacted]

4.1 Trajectory Analysis

4.1.1 The test point and the real-time-daya system.- In an attempt to match conditions at a point on the Saturn trajectory, the test point for the high dynamic pressure at transonic speed conditions (Mission A-001) was selected for a Mach number of 0.94 and dynamic pressure of 585 lb/sq ft.

Manned Spacecraft Center, Houston, provided a digital computer program for use at WSMR to determine the launcher settings on elevation and azimuth which would allow the test vehicle to pass through the test point. This program took into account all known information about the test vehiche as well as the best estimate of the weather and winds at the time of launch. The winds and atmospheric conditions used to make the final launcher setting were for those conditions reported at T-70 minutes before the time of launch.

A primary reason for the flight was to obtain launch-escape-vehicle stability and performance characteristics in the transonic region which corresponds to the foregoint test conditions. To accomplish this objective the real-time-data system of WSMR was utilized to determine in real time several parameters, both in digital display and in plotboards driven by this program. A brief description of the plotboards follows:

a. Plotboard A plotted the flight-path angle of the velocity vector against the dynamic pressure.

b. Plotboard B showed the dynamic pressure with relation to Mach number.

c. Plotboard C displayed both altitude plotted against range and a ground track of the trajectory.

The real-time-data system showed the trajectory of the command module from lift-off to landing by tracking the two beacons on the command module with three radars. Trajectory parameters are shown in figures 4.1.1-1 to 4.1.1-8.

On the basis of the winds which were reported at T-70 minutes during the countdown, a launcher elevation angle of 81°19' and azimuth of 346°21' was computed using the launch-angle program. The launcher was set at 81°19' and 346°20' which was said to be as close as it could be set. A digital computer solution of the trajectory using these launch angles and this wind form the predicted trajectory as shown in figures 4.1.1-1 to 4.1.1-8.

The real-time-data system uses 51-point end-point smoothing. To accumulate these 51 points from which the average is formed takes

[redacted]

2.5 seconds. Thus, whenever radical acceleration changes occur, the real-time-data system develops a temporary error. This error is smoothed out completely in a maximum of 5 seconds but after 2.5 seconds an acceptable agreement is reached between what the real-time-data system presents and what really takes place. Curves of the trajectory as presented by the real-time-data system are shown in figures 4.1.1-1 to 4.1.1-8.

A 2.5-second smoothing interval length was chosen to reduce inherent radar cycling errors caused by range resolution and random radar noise. This range resolution error is a state-of-the-art problem and its effect on the real-time-data system has been thoroughly investigated previous to mission A-001. During this study it was found that this range resolution error will cause one or two deviations from the true value and that this deviation will not reach values which are incompatible with the task to be performed by the real-time-data system.

During the mission at about 12.2 seconds, one step occurred in the data which could be attributed to this error source. During the boost phase, a large increase in velocity was shown in the output of the real-time-data system which did not actually occur in flight. Figures 4.1.1-9(a) to 4.1.1-9(d) show all the parameters that go into the solution of vehicle velocity, such as weight flow, thrust, wind, and weather. All of these parameters changed smoothly. Altitude was also found to increase smoothly. Velocity and the several items calculated from the velocity have a sharp discontinuity. Since Mach number, dynamic pressure, and flight-path angle all change abruptly at this point, there was no indication of an error on the plotboards except that all these quantities appear high. The quantities were so high that the plotboards showed that the vehicle did not pass through the 3σ dispersion about the test point. This error in dynamic pressure has been confirmed by optical tracking and is high by approximately 25 lb/sq ft at the test point. With this error taken into account, the real-time-data system shows the vehicle passing through the ellipse describing the 3σ dispersion around the test point.

Values of several trajectory parameters at the test point are shown in table 4.1.1-1. The test point is Mach number of 0.94 for digital computer solutions, and at the abort time of 28.435 seconds for the actual flight. The values of several parameters shown in figures 4.1.1-1 to 4.1.1-8 and in other simulations are given in the table.

[redacted]

TABLE 4.1.1-1.- THE TEST POINT

Parameter	Trajectory[1]					
	a	b	c	d	e	f
Mach number	0.94	0.94	0.955	0.94	0.94	0.935
Dynamic pressure, lb/sq ft	589.2	585.1	659	612.7	632	634
Altitude, ft m.s.l. . . .	20,512	21,677	19,480	20,641	19,862	19,445
Time, sec	30.587	31.393	28.435	30.853	28.764	28.435
Flight-path angle, deg.	54.3	60.2	56.44	52.0	56.27	54.85
Velocity, ft/sec	973	989	1,015	988	993	998
Range, ft	7,250	6,577	6,870	7,976	6,869	7,020

[1]a = Nominal 84° trajectory, no wind, 1962 ARDC atmosphere.

b = The predicted trajectory, determined at T-70 minutes in the countdown.

c = The trajectory as shown by the real-time-data system.

d = The trajectory corrected for launch time winds.

e = The trajectory corrected for launch time winds and higher Algol thrust.

f = The trajectory as tracked by cinetheodolites.

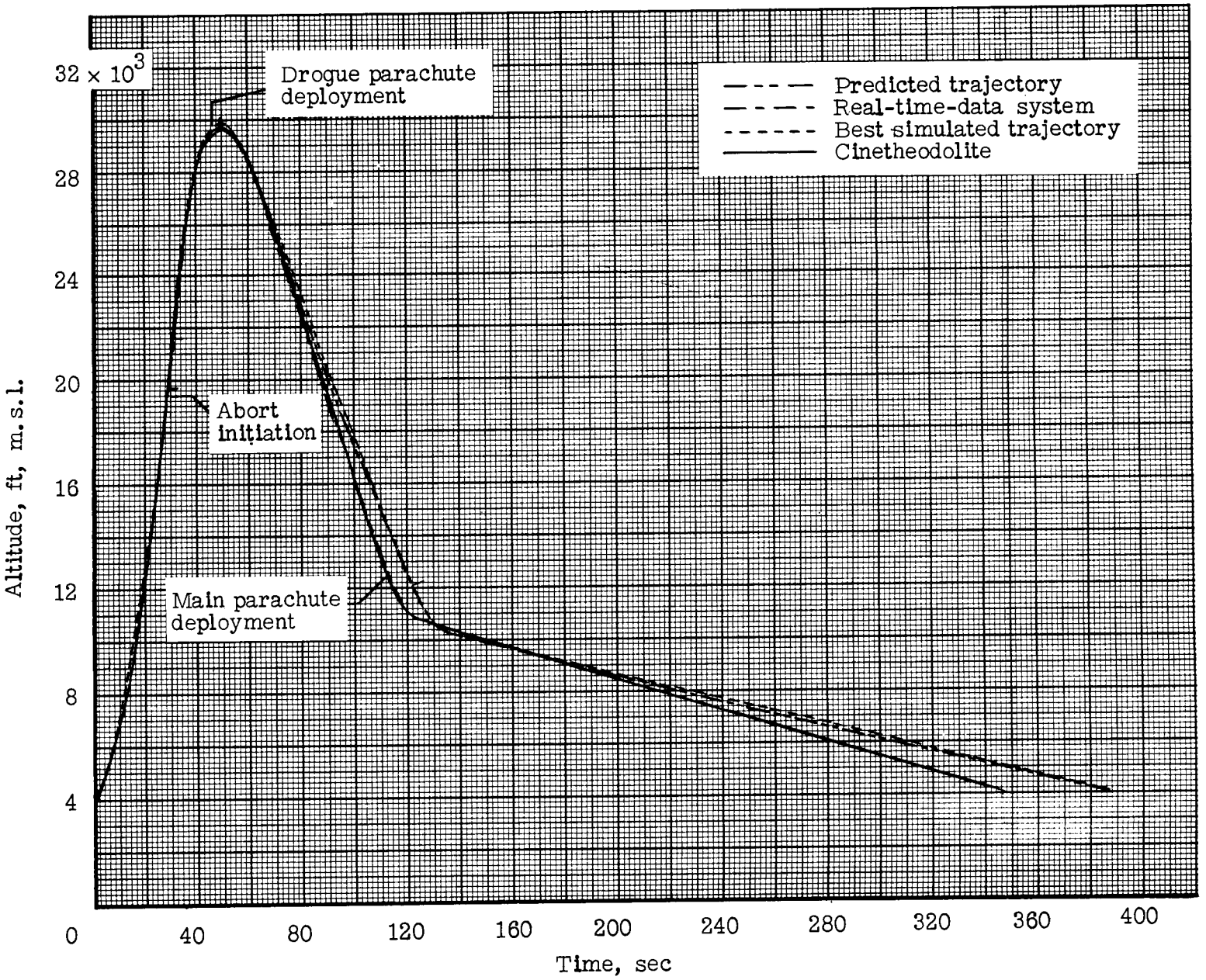

Figure 4.1.1-1. - Altitude plotted against time from launch.

[redacted]

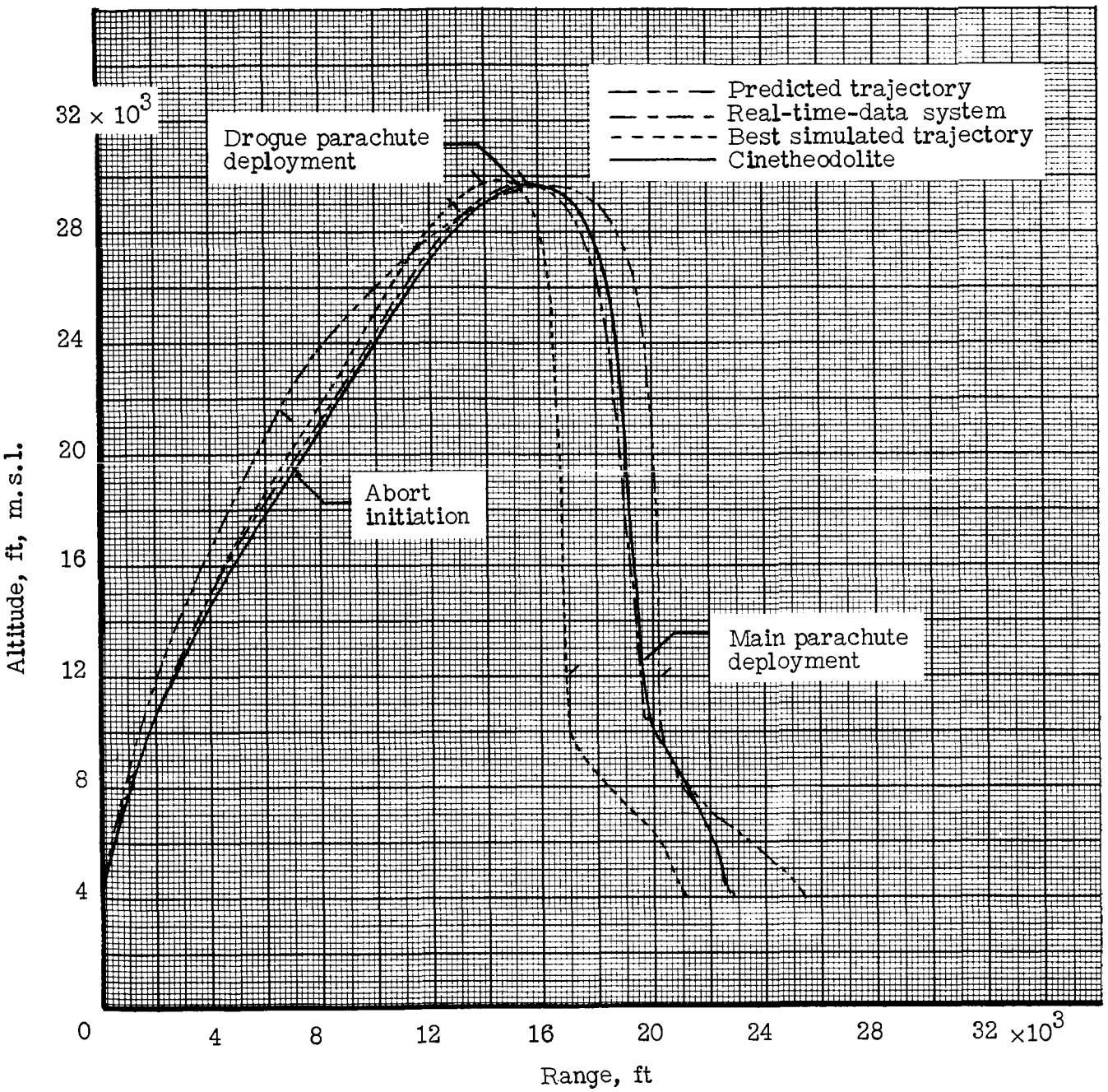

Figure 4.1.1-2. - Variation of altitude with respect to range.

[redacted]

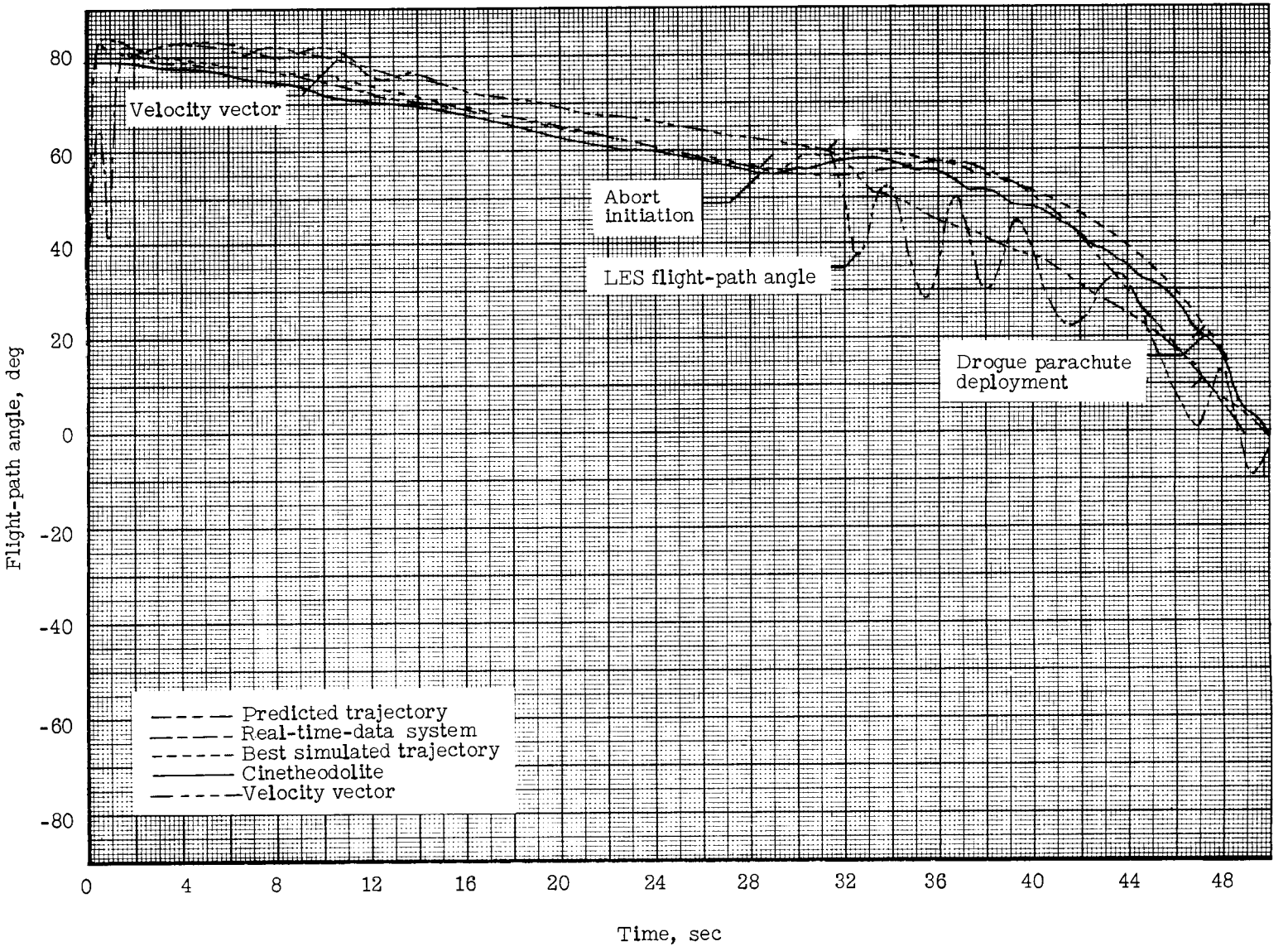

Figure 4.1.1-3. - Flight-path angle plotted against time from launch.

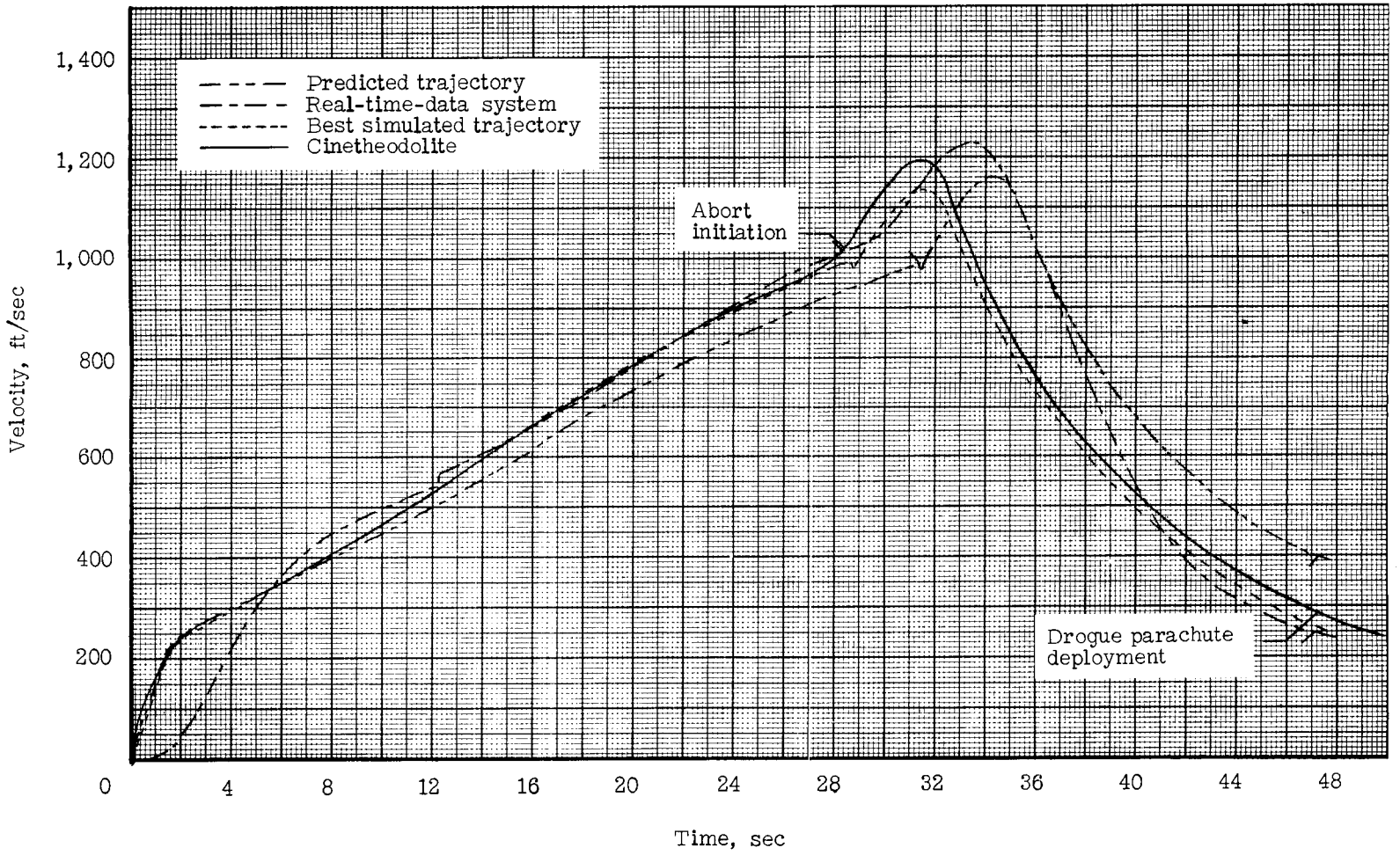

Figure 4.1.1-4. - Total velocity plotted against time from launch.

[redacted]

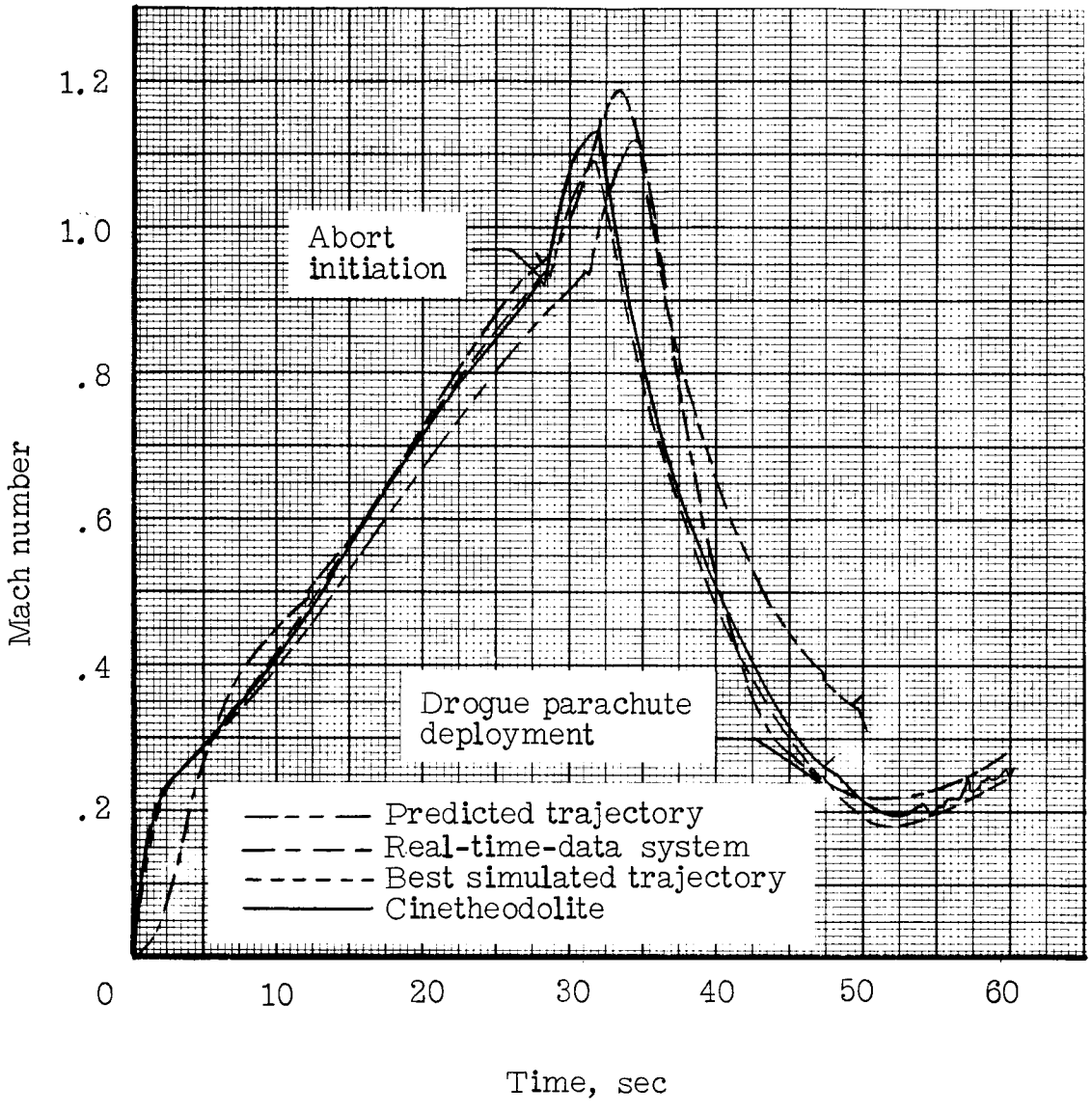

Figure 4.1.1-5. - Mach number as a function of time from launch.

[redacted]

[redacted]

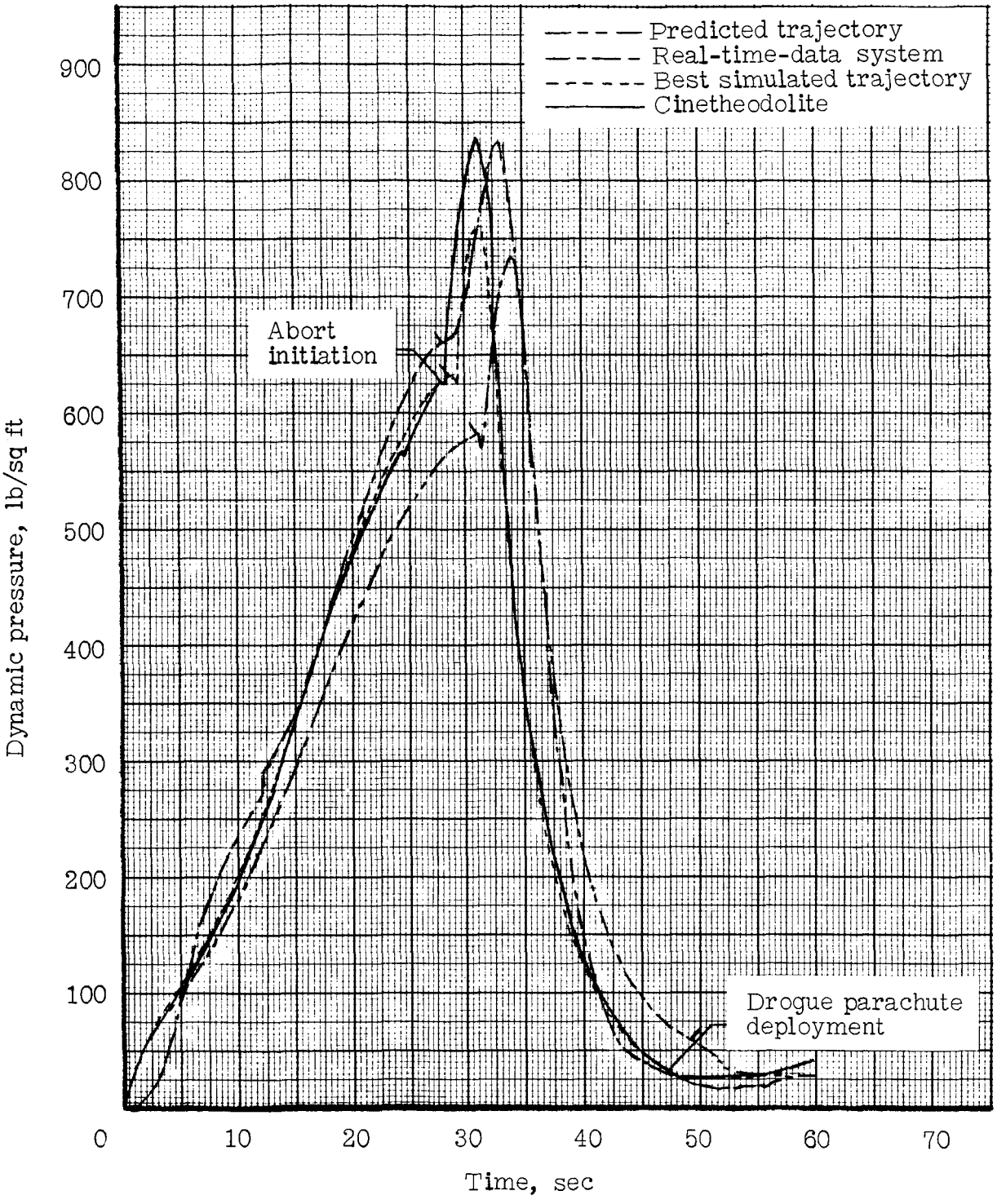

Figure 4.1.1-6. Dynamic pressure plotted against time from launch.

[redacted]

[redacted]

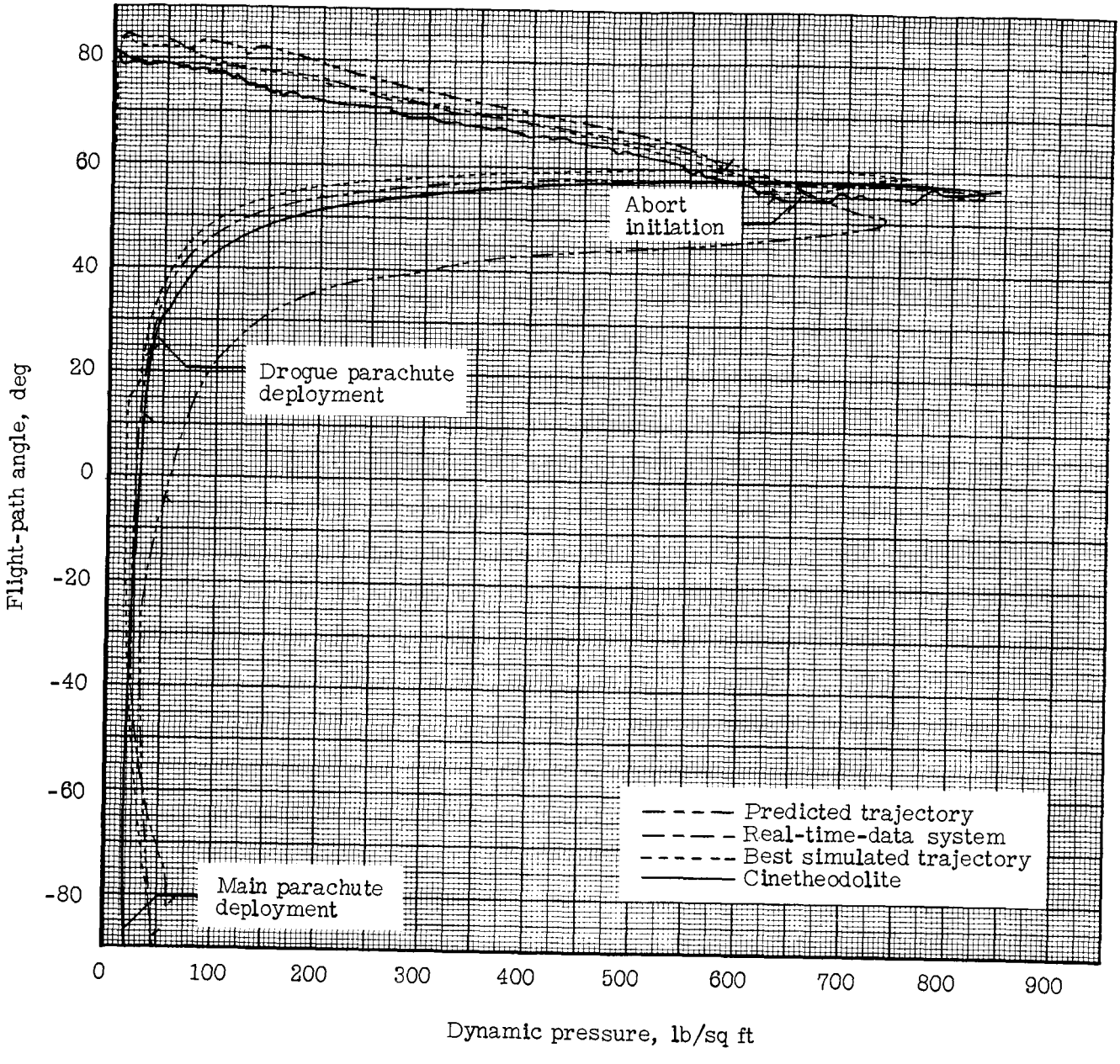

Figure 4.1.1-7 - Flight-path angle plotted against dynamic pressure.

[redacted]

[redacted]

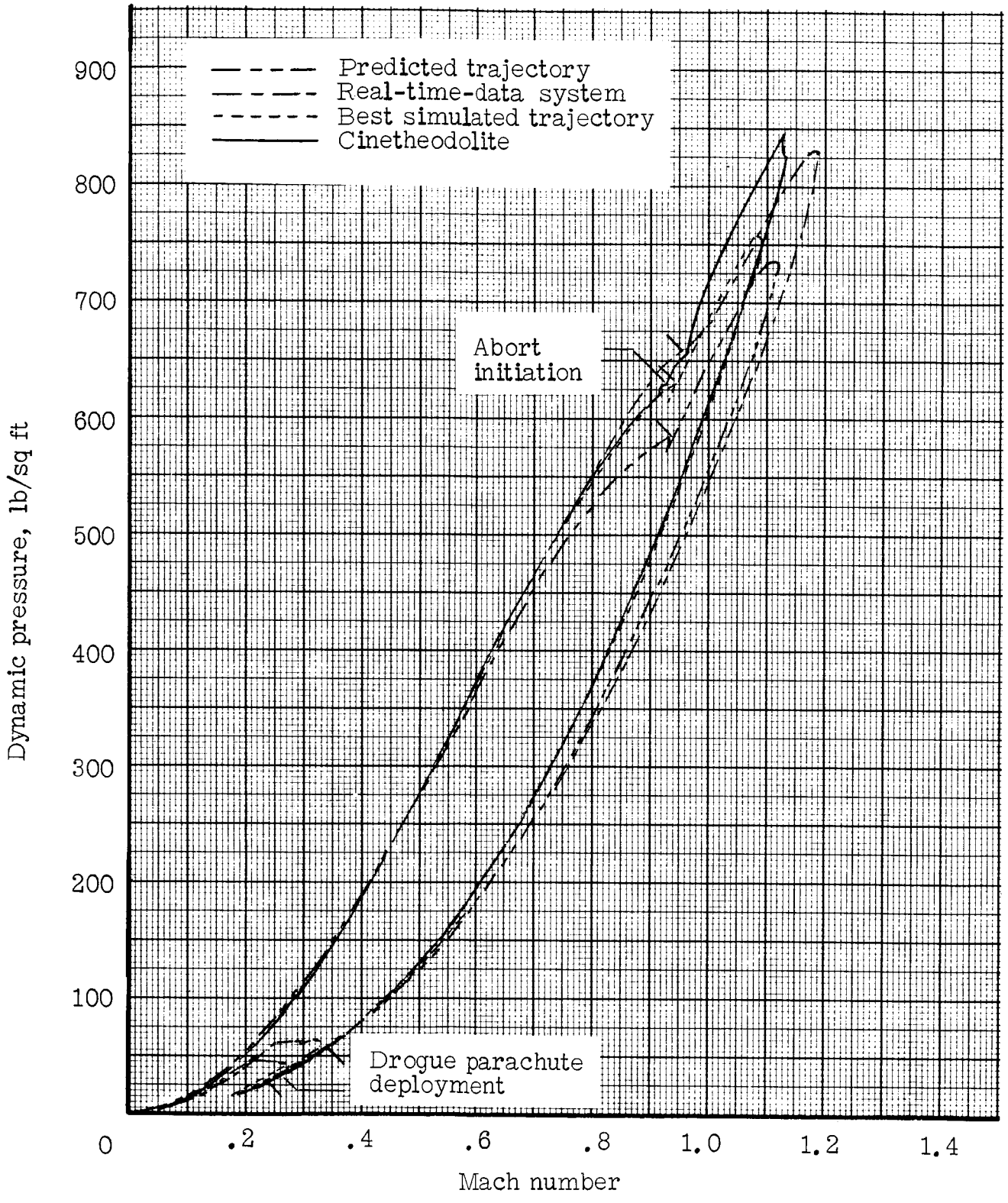

Figure 4.1.1-8. - Dynamic pressure plotted with respect to Mach number.

[redacted]

[redacted]

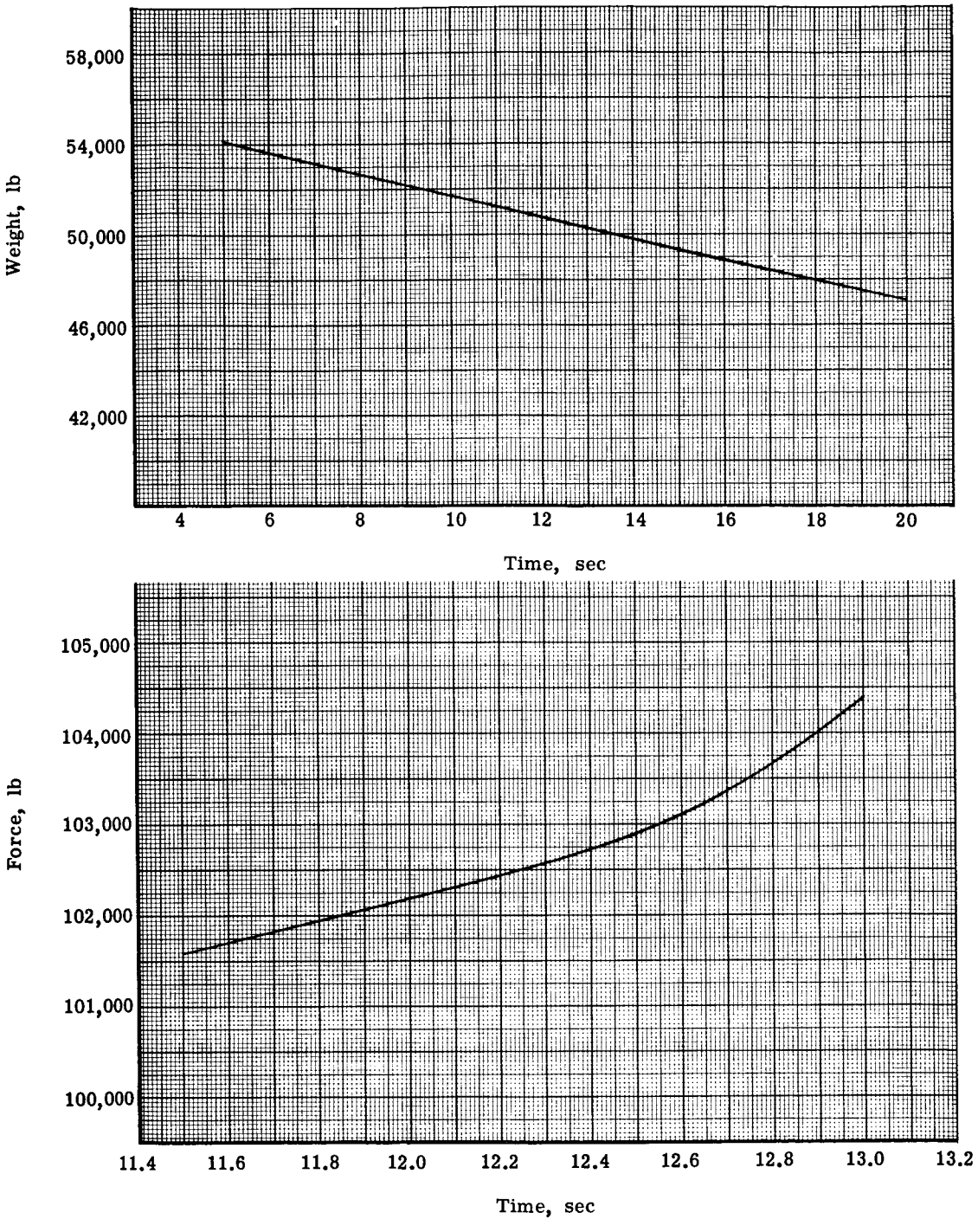

(a) Weight flow and Algol thrust with respect to time.

Figure 4.1.1-9. - Range resolution error in the Real-time-data system.

[redacted]

[redacted]

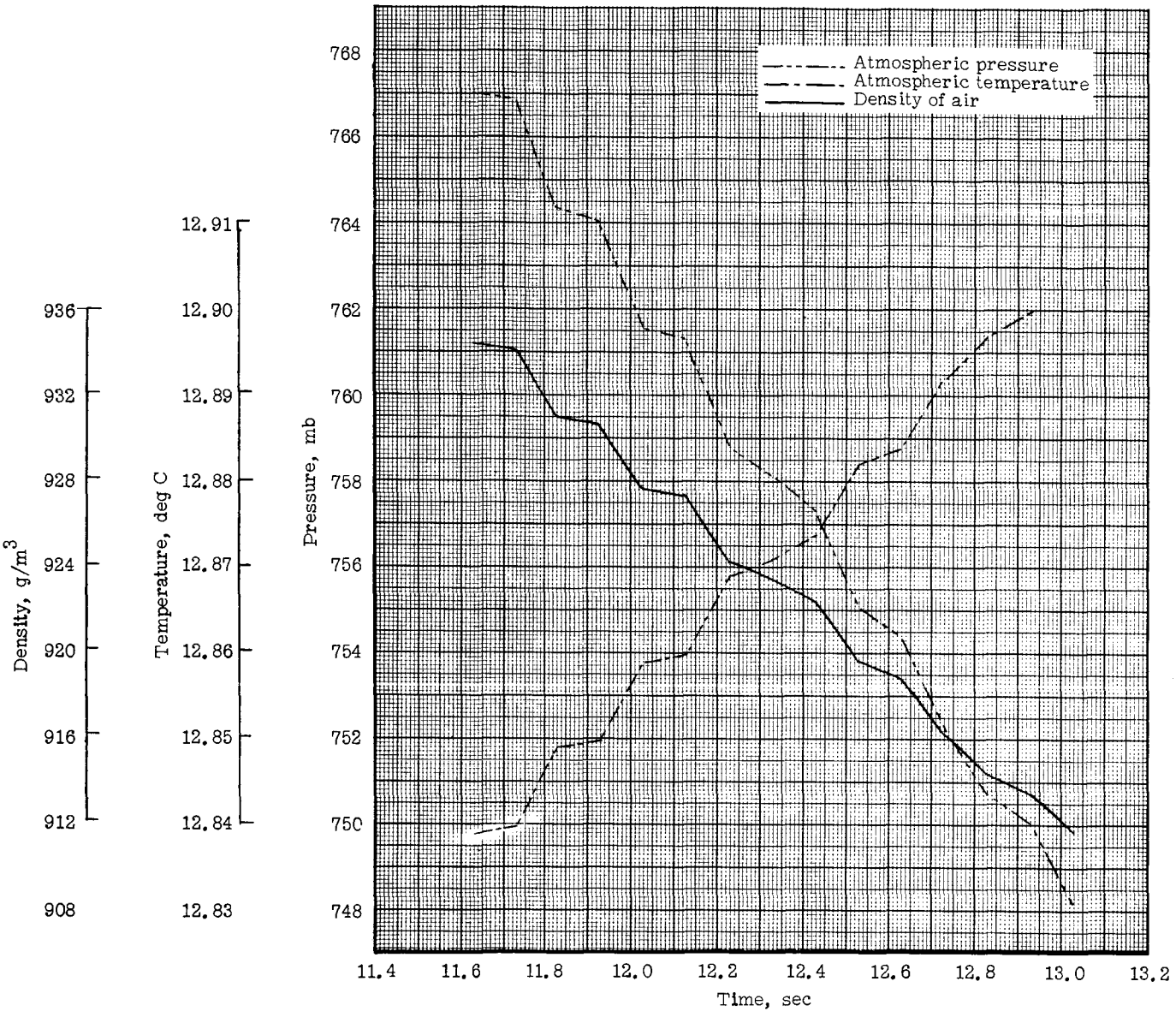

(b) Atmospheric pressure, atmospheric temperature and density plotted against time.

Figure 4.1.1-9 - Continued.

[redacted]

[redacted]

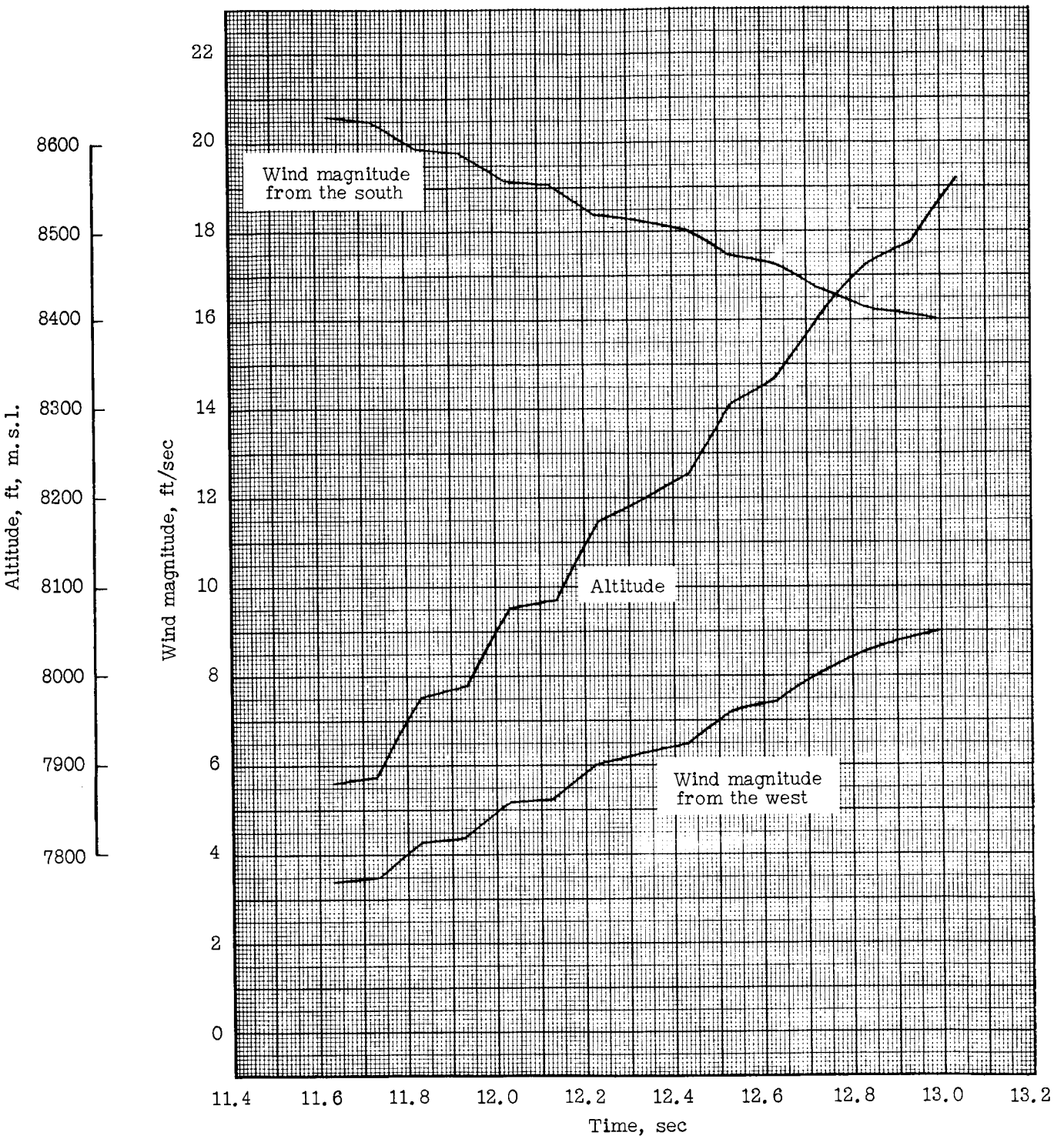

(c) Magnitude of the wind in components and altitude plotted against time.

Figure 4.1.1-9 - Continued.

[redacted]

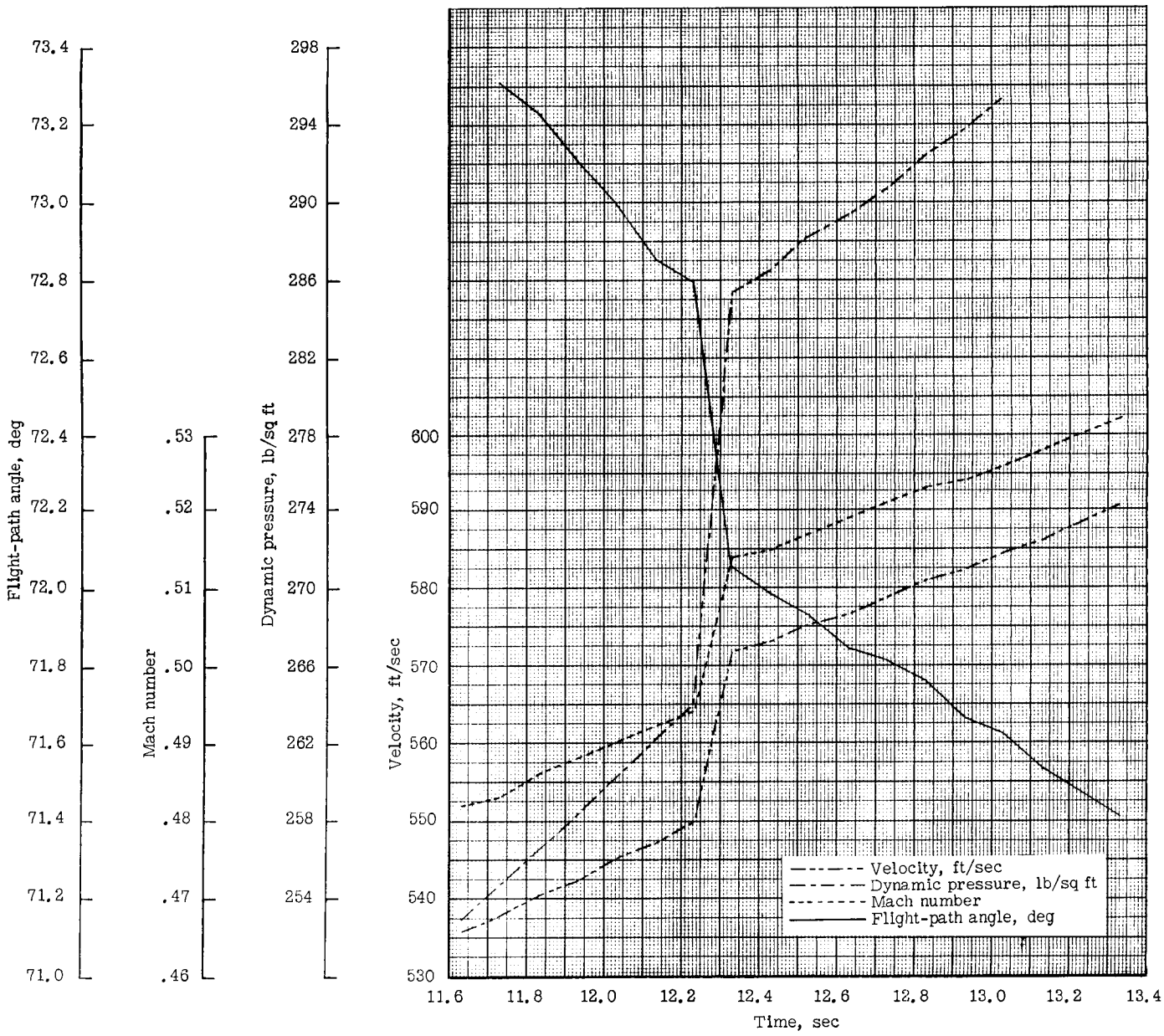

(d) Velocity, dynamic pressure, Mach number and flight-path angle plotted against time.

Figure 4.1.1-9 - Concluded.

[redacted]

4.1.2 Launch vehicle.- The launcher for Little Joe II was set at an elevation angle of 81°19' and an azimuth of 346°20' on the basis of winds reported at T-70 minutes. The winds and weather data for 4 a.m. m.s.t. are plotted in figure 4.1.2-1. The wind shown in this figure indicates a north component on the ground which was not true at the launch pad. These data were measured at Desert Site, some distance from the launch pad. Figure 4.1.2-2 shows the magnitude and direction of the winds reported at T-70 minutes which were used to compute the launcher angle settings. Winds at the launch pad at the time of launch are shown in figure 4.1.2-3. In comparing figures 4.1.2-2 and 4.1.2-3, it is seen that the winds from the south had decreased in magnitude by the time of launch. In effect the launcher had been over-compensated for the actual launch time winds. The results of a digital computer solution, using the launch time winds, are shown in table 4.1.1-1. The predicted trajectory as shown in figures 4.1.1-1 to 4.1.1-8 is based on the reported T-70 minute winds. From these figures, it is evident that when the launcher elevation is lower than it should be for wind compensation, the altitude at a Mach number of 0.94, the test point, is lower and the dynamic pressure higher because of the increased density of the air. The lower flight-path angle also accounts for the increased range at the test point.

Telemetry data indicated about a 5-percent to 7-percent higher Algol motor thrust than had been expected. When this higher thrust was taken into account along with the launch time winds, digital computer solution of the trajectory resulted in a dynamic pressure of 632 lb/sq ft at 28.76 seconds. These results are also shown in figures 4.1.1-1 to 4.1.1-8. Figures 4.1.1-1 to 4.1.1-8 also show results of cinetheodolite or optical tracking. Up to the test point of a Mach number of 0.94 and dynamic pressure of 632 lb/sq ft, the results are virtually identical.

Telemetry data indicated that at the time of abort the launch vehicle had rolled approximately 135° counterclockwise, looking forward from the vehicle base. This roll effect is discussed in section 4.4.3.

A digital computer simulation, using the preliminary weight and balance data derived from the test and the higher Algol thrust, showed even closer agreement with the actual flight than does the simulation shown in figures 4.1.1-1 to 4.1.1-8. At a Mach number of 0.94 the time was 28.432 seconds, the altitude 19,684 ft m.s.l., and the dynamic pressure was 636.5 lb/sq ft.

The plots of the flight-path angle with respect to dynamic pressure shown in figure 4.1.1-7 are of two different forms. The predicted trajectory, which assumes no roll, has a continually decreasing flight-path angle. The curves which show the output of the range tracking facilities and the computer simulation which took the roll into account showed the flight-path angle increasing after abort initiation. The roll caused the launch-escape vehicle to fly at a higher flight-path angle.

[redacted]

[redacted]

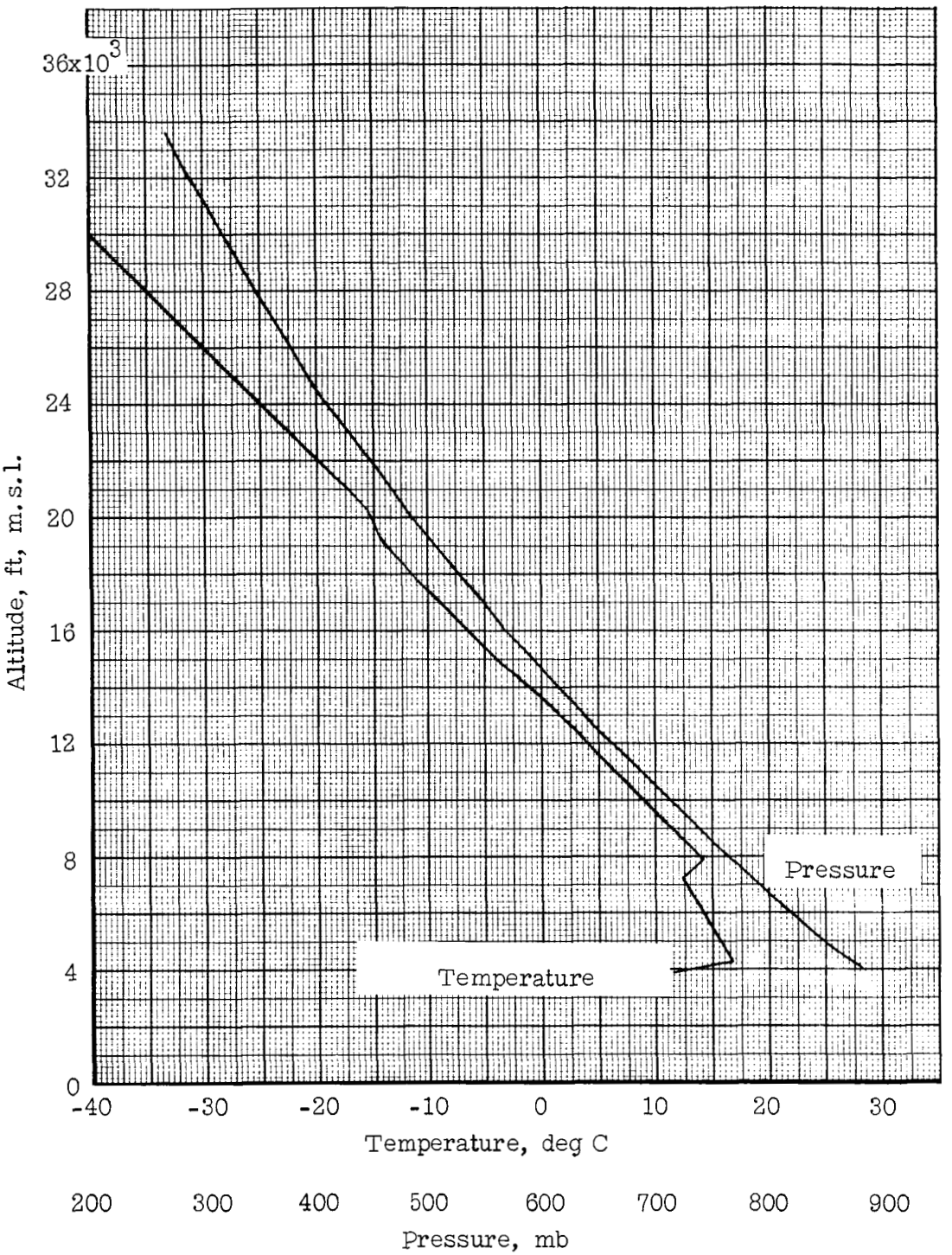

(a) Temperature and pressure plotted against altitude.

Figure 4.1.2-1. - The 4 a.m. m.s.t. meterological report from Desert Site.

[redacted]

[redacted]

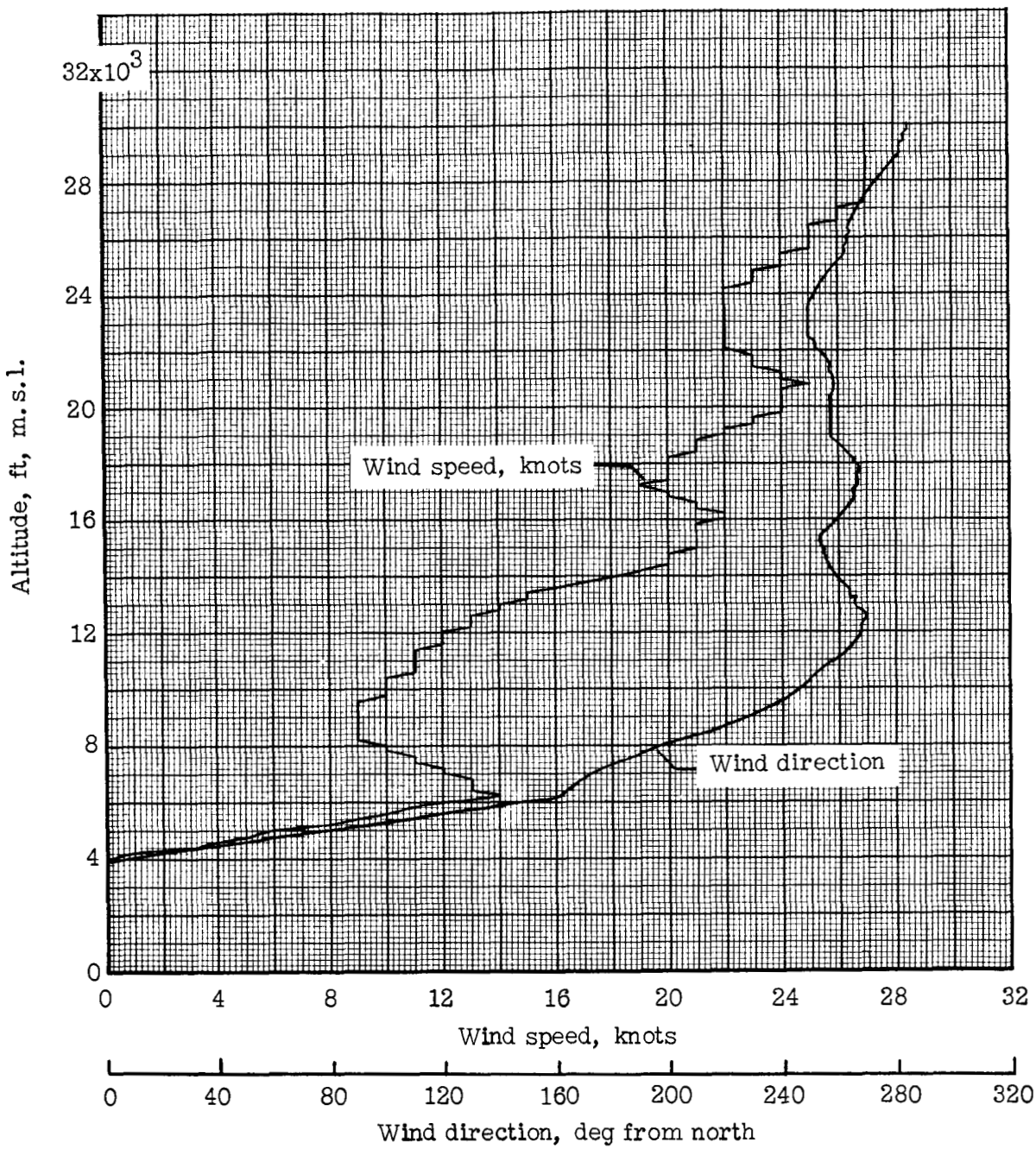

(b) Wind direction and wind speed plotted against altitude.

Figure 4.1.2-1. - Concluded.

[redacted]

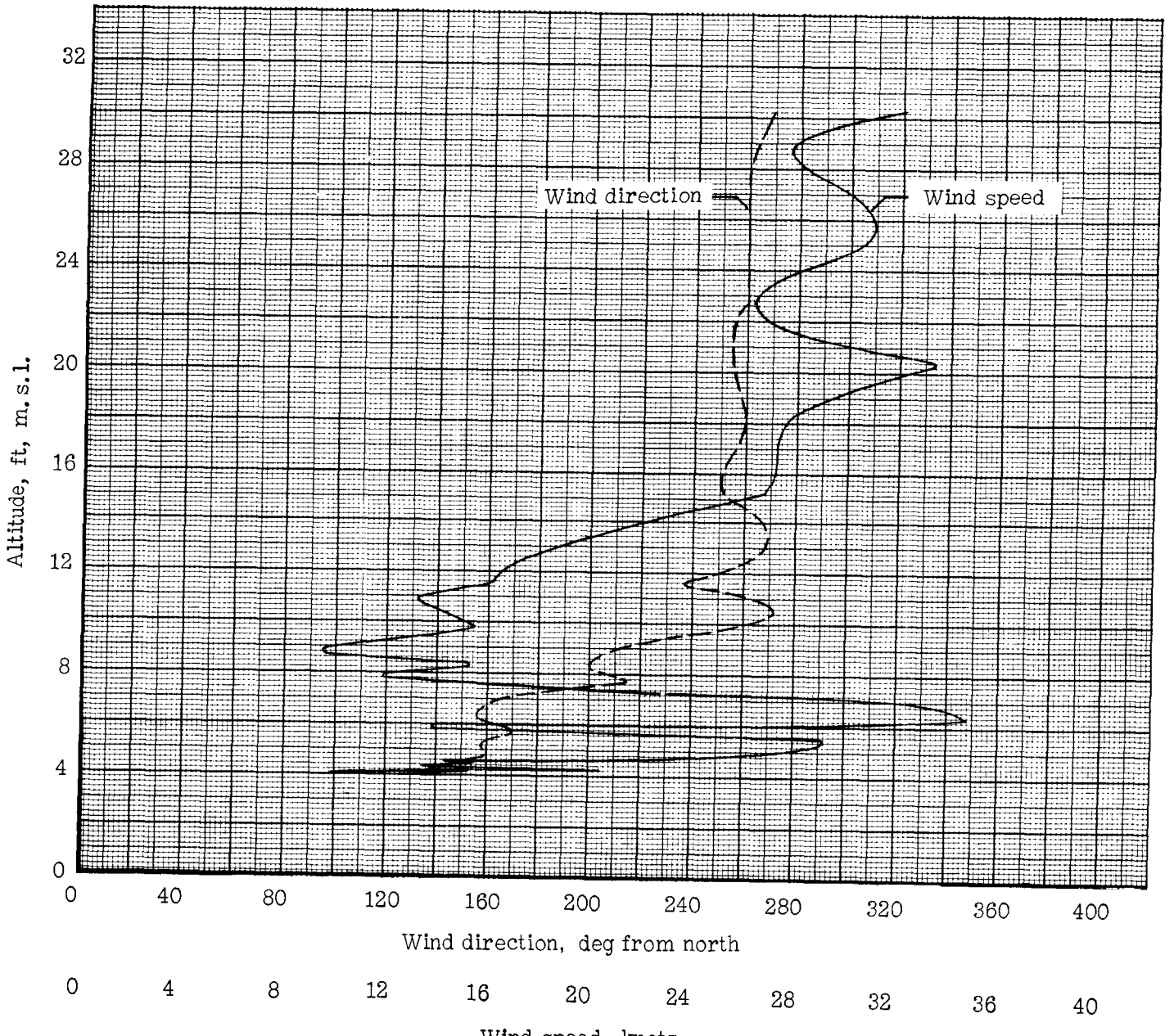

Wind direction and velocity plotted against altitude.

Figure 4.1.2-2. - T-70 minute winds at the launch pad.

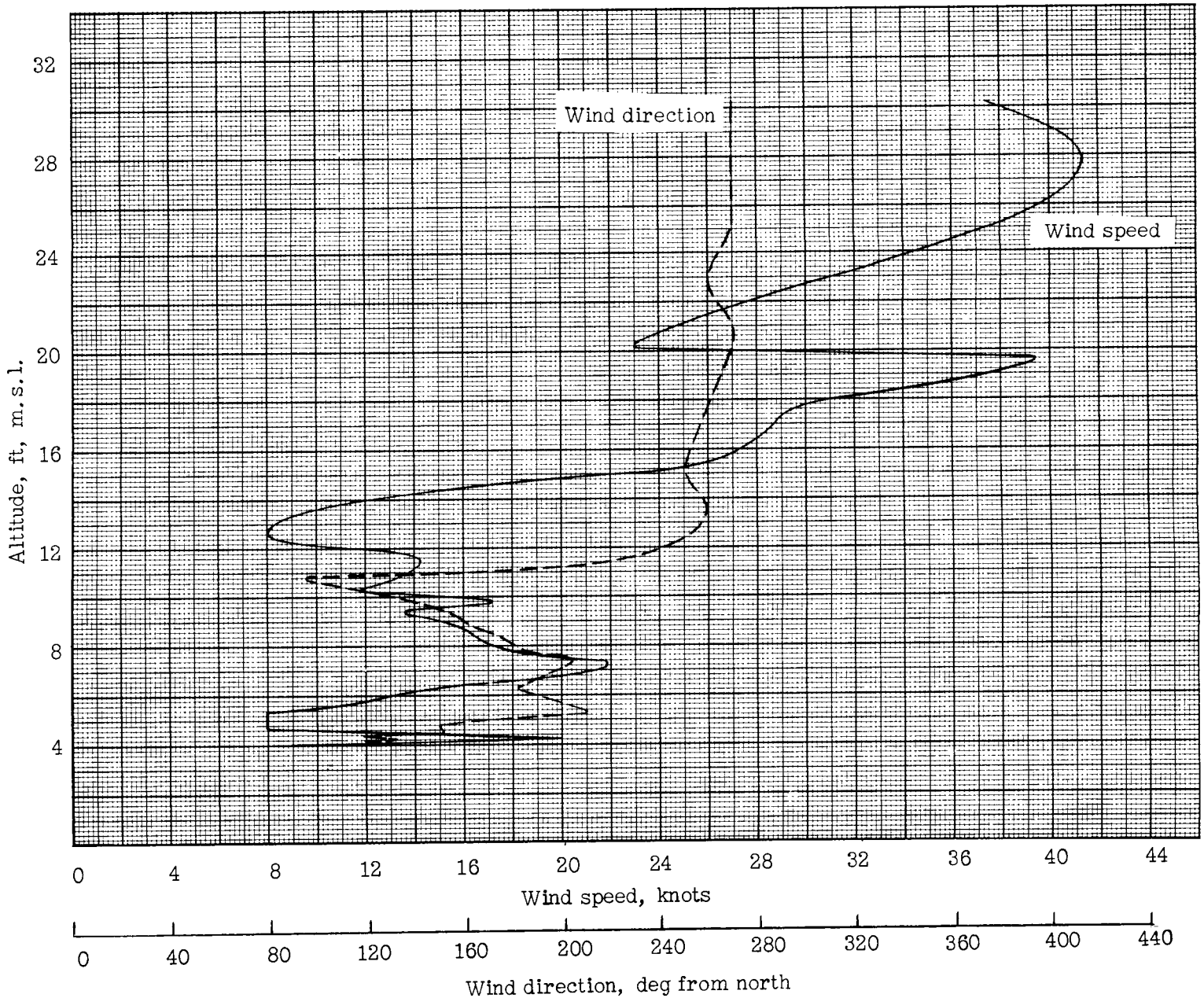

Wind direction and velocity plotted against altitude.

Figure 4.1.2-3 - T-O winds at the launch pad.

4.1.3 Launch-escape vehicle.- Abort was initiated manually when the real-time-data system indicated that the test region had been reached and a Mach number limit had been achieved. A signal was sent to the launch-vehicle thrust-termination subsystem which terminated thrust. Separation of the command module from the service module was accomplished about 0.1 second after the launch-escape vehicle attained full thrust.

Since the Little Joe II launch vehicle had rolled approximately 135° prior to abort, the roll combined with the positive trim angle of the launch-escape vehicle increased the flight-path angle rather than decreased it. This facet of the trajectory is clearly seen in figure 4.1.1-3. This higher flight-path angle resulted in higher maximum altitude than would have been attained if the vehicle had not rolled.

Figure 4.1.3-1 presents a comparison of predicted and demonstrated performance of the launch-escape vehicle with a point mass trajectory for a nonthrusting Saturn IB vehicle. The Saturn simulation assumed the Saturn to be at the point in the sky where the BP-12 abort took place. Range and altitude parameters are compared at specific time intervals subsequent to abort initiation yielding a two-dimensional separation comparison. Figure 4.1.3-2 gives the altitude with respect to range for the actual launch-escape system abort and the simulated Saturn trajectory for a greater time period. The data indicate that separation distances achieved from the theoretical Saturn by the launch-escape vehicle on BP-12 are approximately equal to those predicted. Based on this information, it is evident that the first-order objective, "Demonstrate the capability of the launch-escape subsystem to propel the command module to a predetermined distance from the launch vehicle", was achieved.

The maximum dynamic pressure as computed from the cinetheodolite tracking cameras is almost 90 lb/sq ft higher than that shown by computer simulation and is possibly caused by incomplete knowledge of the aerodynamics of the thrusting launch-escape vehicle, or motor thrust characteristics. The actual Mach number is also higher by 0.05 than predicted.

[redacted]

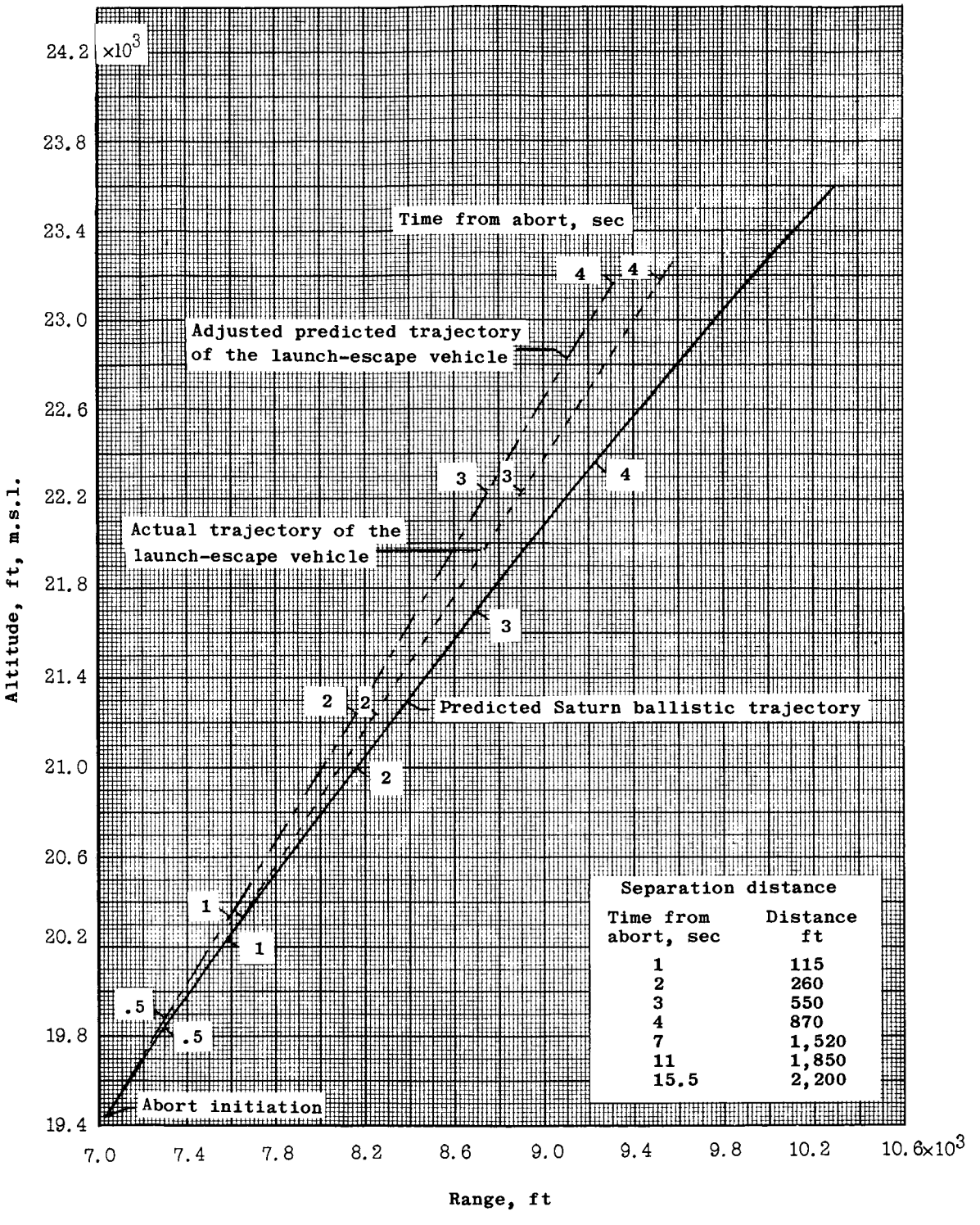

Figure 4.1.3-1.- Separation distance between the launch-escape vehicle and the predicted Saturn reentry.

[redacted]

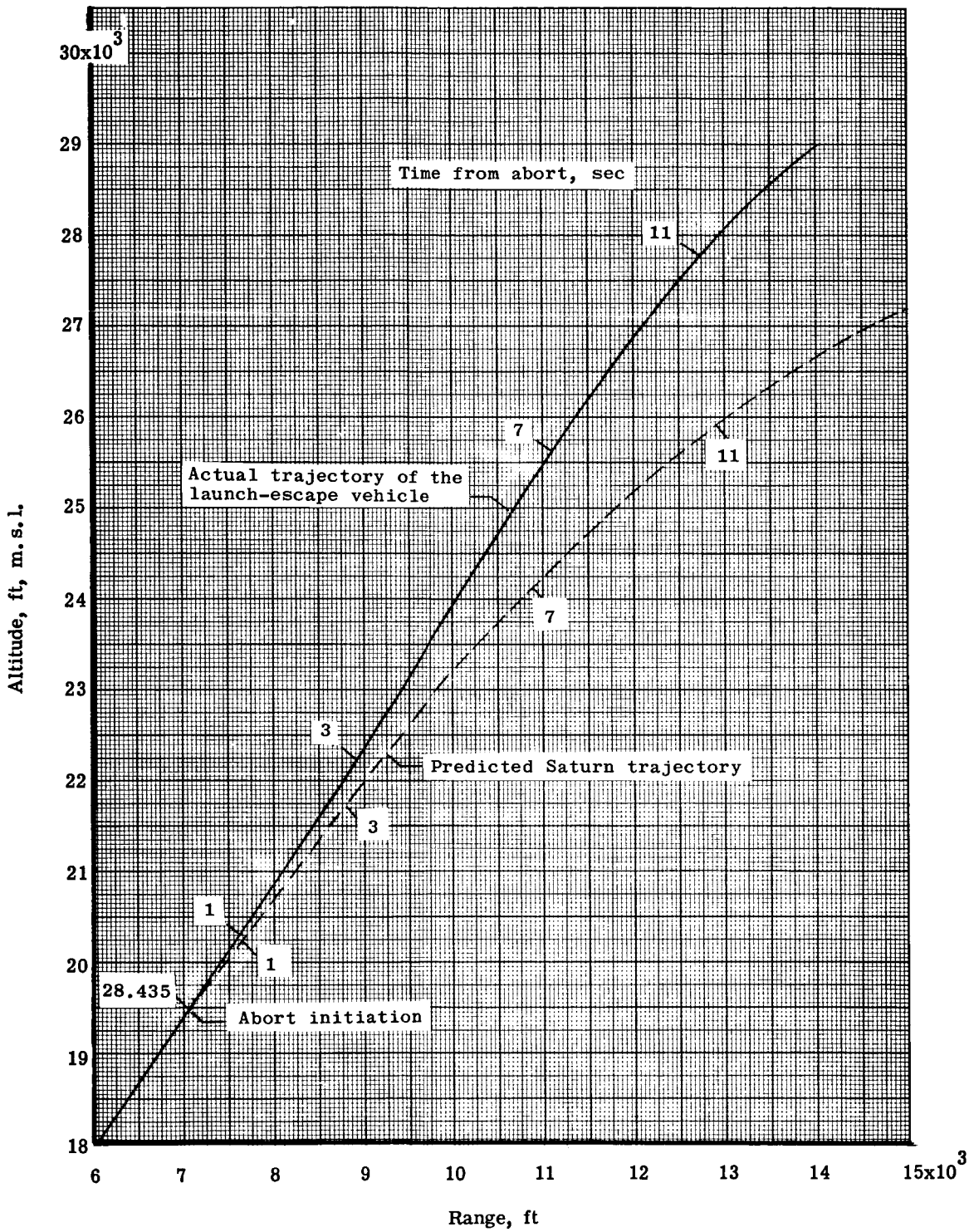

Figure 4.1.3-2. - Altitude with respect to range after abort initiation.

[redacted]

4.1.4 Spacecraft.- Fifteen and one-half seconds after the launch-escape subsystem had separated the command module from the destructed Little Joe II launch vehicle, the launch-escape subsystem tower was jettisoned. About 3 seconds later, the drogue parachute was deployed as expected. From figure 4.1.1-1 it can be seen that the command module apogee of 29,778 feet m.s.l. occurred at 49.8 seconds of flight time, which is about 2.9 seconds after drogue parachute deployment. The rate of descent as seen in this figure is faster than in the simulated trajectory, figure 4.1.1-1. This increase in descent rate and the resulting shorter time to a 12,000-foot altitude, in comparison to the time shown in figure 4.1.1-1, is caused by an incorrect value of drag coefficient on the command module. This value of drag coefficient corresponds to the value for the position of heat shield forward, whereas, in reality, the command module oscillated from 120° to 290°. The drag coefficient for this configuration is approximately 0.7 for the command module alone. A computer simulation to verify this value has not been completed.

At an altitude of 12,525 feet m.s.l., the 12,000-foot baroswitch signalled the release of the drogue parachute and the firing of the pilot parachute mortars. The three main parachutes were pulled off the command module by the pilot parachutes. The main parachutes were designed such that the three parachutes would lower the command module at a rate of 24 feet per second at a pressure altitude of 5,000 feet. However, at 115.5 seconds of flight time, the riser on one of the main parachutes failed, and this parachute was separated from the command module. The total velocity for the descent on the parachutes is shown in figure 4.1.4-1 for computer simulation and figure 4.1.4-2 for cinetheodolite tracking. The simulated trajectory had three main parachutes and, of course, the actual trajectory had only two. Thus, the time to landing of the command module is explained.

The ground track of the command module is shown in figure 4.1.4-3.

[redacted]

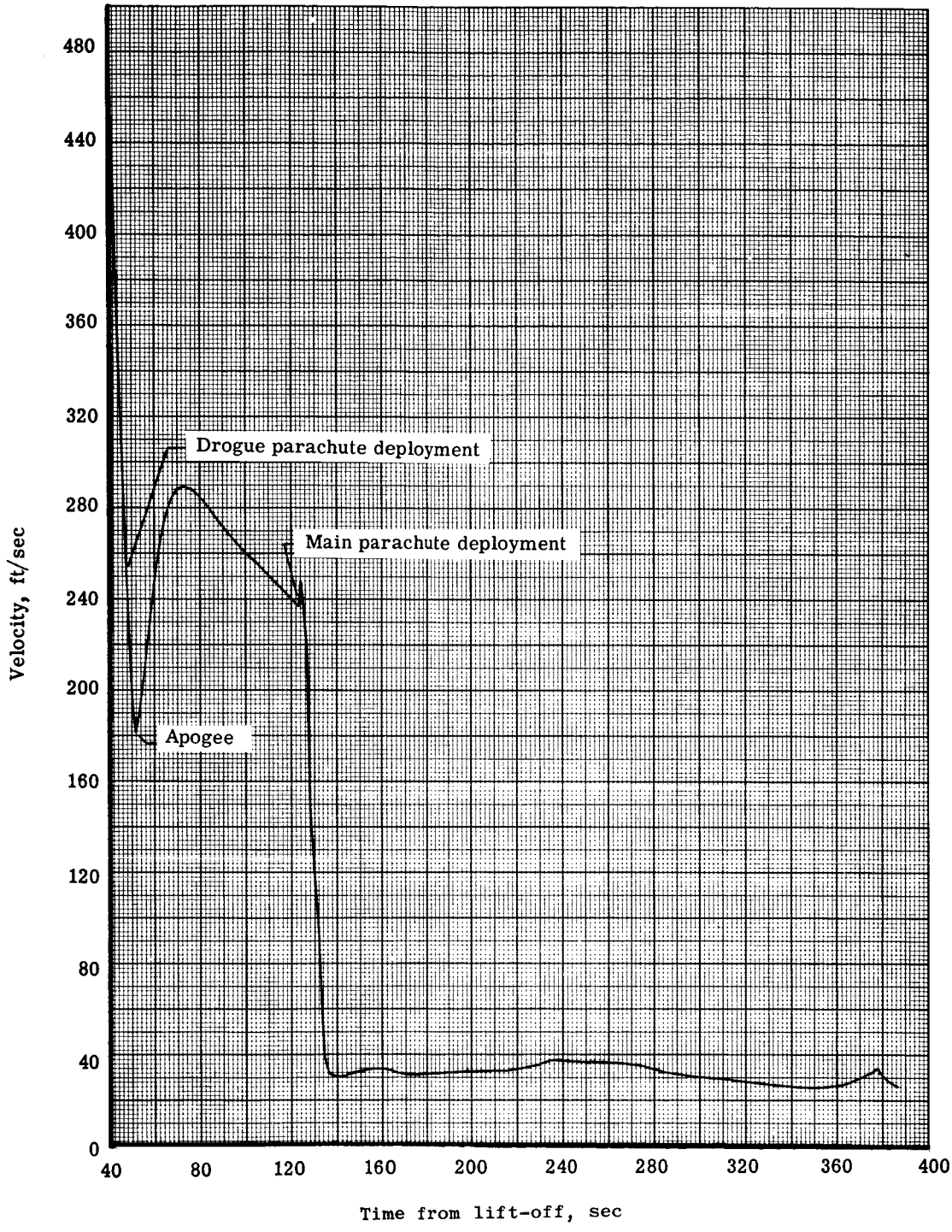

Figure 4.1.4-1. - Total velocity on the parachutes with respect to time. Computer simulation.

[redacted]

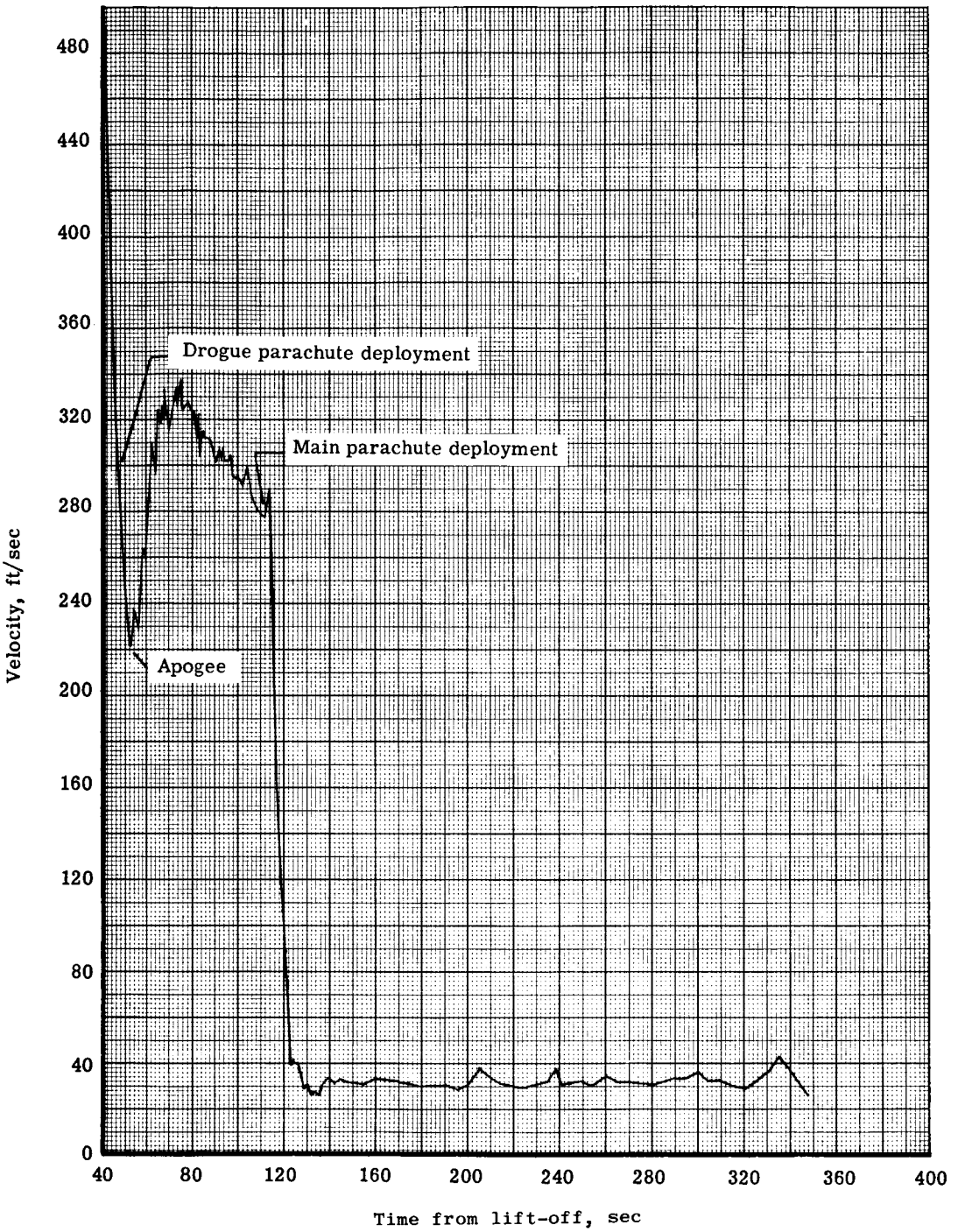

Figure 4.1.4-2. - Total velocity on the parachutes with respect to time. Cinetheodolite results.

[redacted]

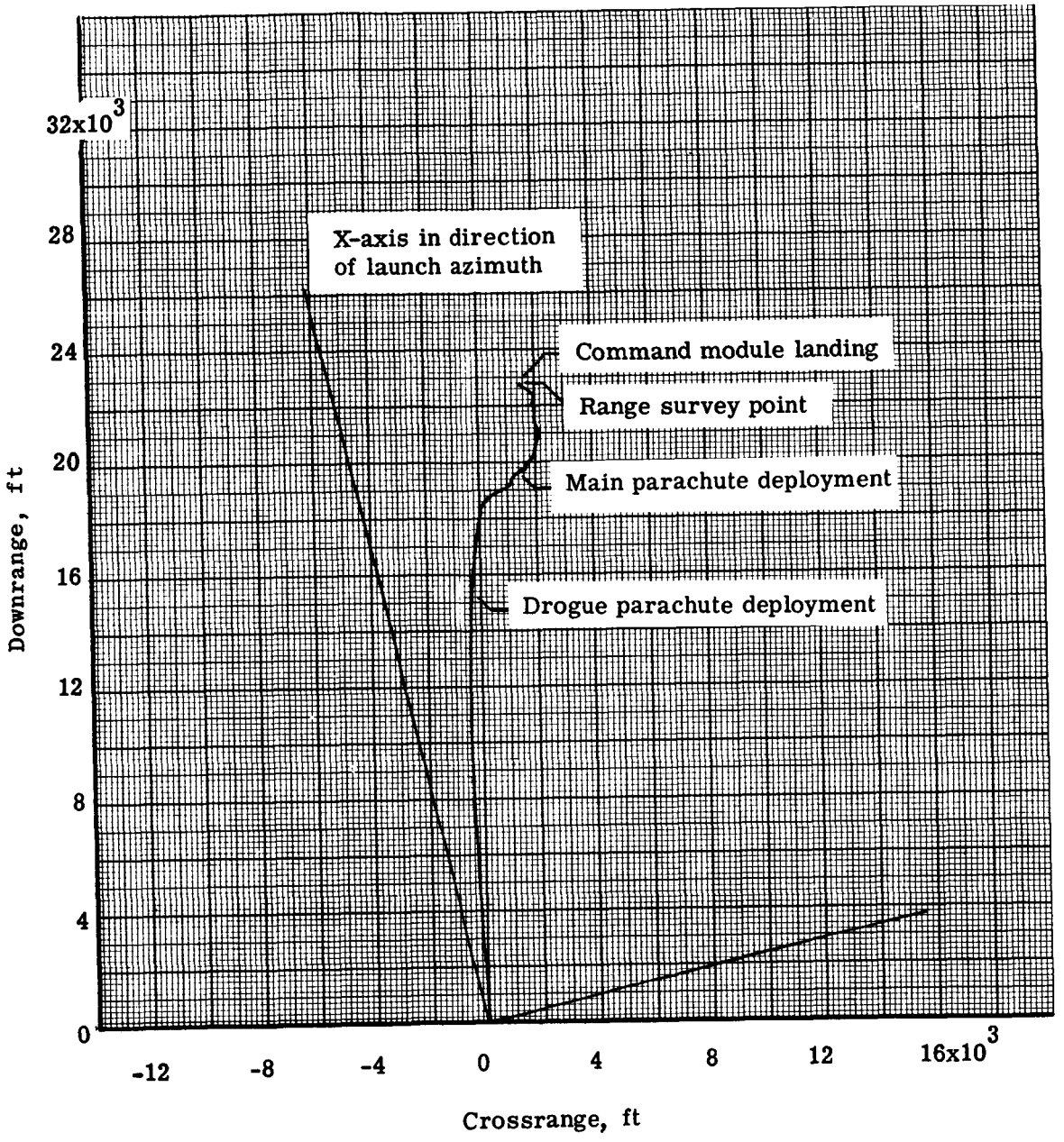

Figure 4.1.4-3. - The ground track of the command module. Cinetheodolite results.

[redacted]

4.2 Mass Characteristics

During flight, mass characteristics change as propellant is burned and inert weight is expended. In order to ascertain the changes of weight and other mass characteristics, the change in weight of propellant as a function of time must be determined. The weight changes for those items expended have been determined previously by actual weighings.

4.2.1 Propellant weight.- Propellant mass is expended for the various motor assemblies during each of the powered phases of the mission. The propellant masses for each particular event can be determined by use of the following expression:

$$W = \frac{A_t g}{c^*} \int_0^t P_c \, dt$$

where:

A_t = throat area, assumed constant

W = weight

g = gravitational constant

c^* = characteristic velocity, assumed constant

P_c = chamber pressure

t = time

Therefore, the propellant weight expended in a given time can be determined by integrating the curve of the rocket-motor chamber pressure P_c plotted against time t.

In order to determine the variation of propellant weight with time, the percentage of area under the curve for chamber pressure P_c plotted against time t at a given time increment is determined. The total weight expended W_t is proportional to the total area under the curve. Likewise, the incremental weight W_i expended is proportional to the incremental area under the curve at any time. This relationship is expressed in the following equation.

[redacted]

$$\frac{W_i}{W_t} = \frac{\frac{A_t g}{c^*} \int_0^t P_c \, dt}{\frac{A_t g}{c^*} \int_0^T P_c \, dT}$$

where:

W_i = incremental weight

W_t = total weight

t = incremental time

T = total time

The total area and incremental area under the curve for chamber pressure P_c plotted against time t is determined by graphical integration. The percentage area at each time is proportional to the percentage weight expended. The propellant weight remaining at each time is the difference between the initial loading determined from the motor initial loaded weight and that determined to have been expended.

The actual change in weight for the Little Joe II launch vehicle has been determined by this relationship. However, this change cannot be evaluated for the launch-escape subsystem since the loss of telemetry signal of the chamber pressure prevented the determination of these values.

[redacted]

4.2.2 Spacecraft mass characteristics.- The mass properties of the spacecraft are based on actual weights and measurements. Weight history logs were maintained and actual weight data updated as changes were accomplished. Spacecraft inertia values have been calculated from these values since no facility exists for the measurement of these properties.

The variation of spacecraft mass properties with propellant burning time was calculated and is presented in figures 4.2.2-1 to 4.2.2-6. Loss of the chamber pressure measurement of the launch-escape motor prevented the comparison of actual experienced mass properties with those calculated for the spacecraft. Inertial values for the launch-escape vehicle have been corrected for launch-escape subsystem offset produced by LES thrust-vector alinement.

Included as part of the mass property curves are mass characteristics determined for a deviation of ±6 percent from predicted motor performance. (Statistically calculated limits from the development motor program indicate that 95 percent of the motors to be tested will perform within the predicted performance value ±6 percent.) Mass property characteristics for these upper and lower values of performance are included to evaluate the spacecraft performance and dynamics since actual performance deviation from that predicted for the motor cannot be determined because of loss of launch-escape motor pressure data during this test.

The variation of the spacecraft Y-coordinate with propellant burning time has not been presented graphically because the computer program used to calculate these data rounds off values to the nearest 0.1 inch. The value of the Y-coordinate varies from Y = 0.2 inch at the initial or zero point to Y = 0.3 inch for the final point at 8 seconds.

[redacted]

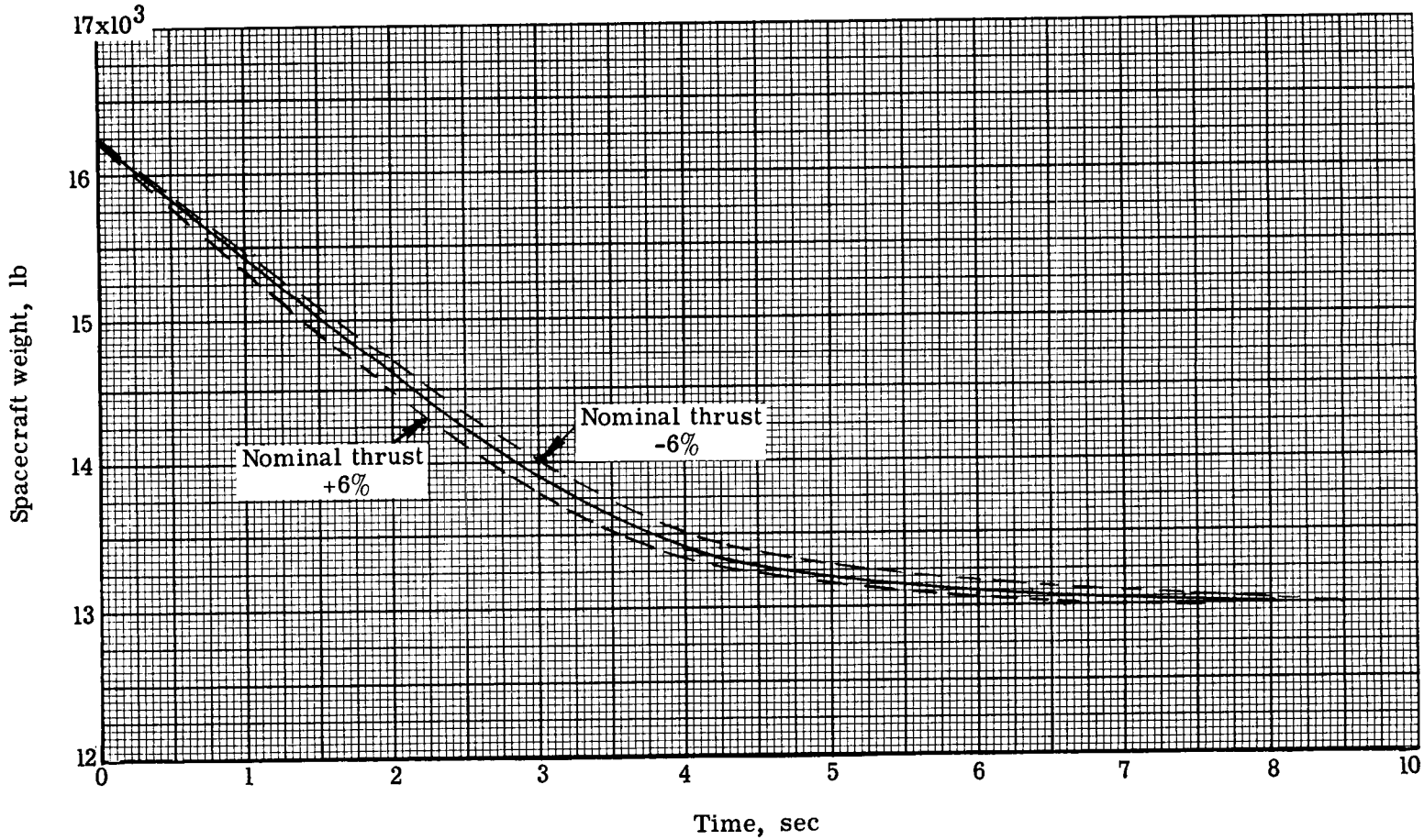

Figure 4.2.2-1.- Spacecraft predicted weight plotted against time of launch-escape-motor ignition.

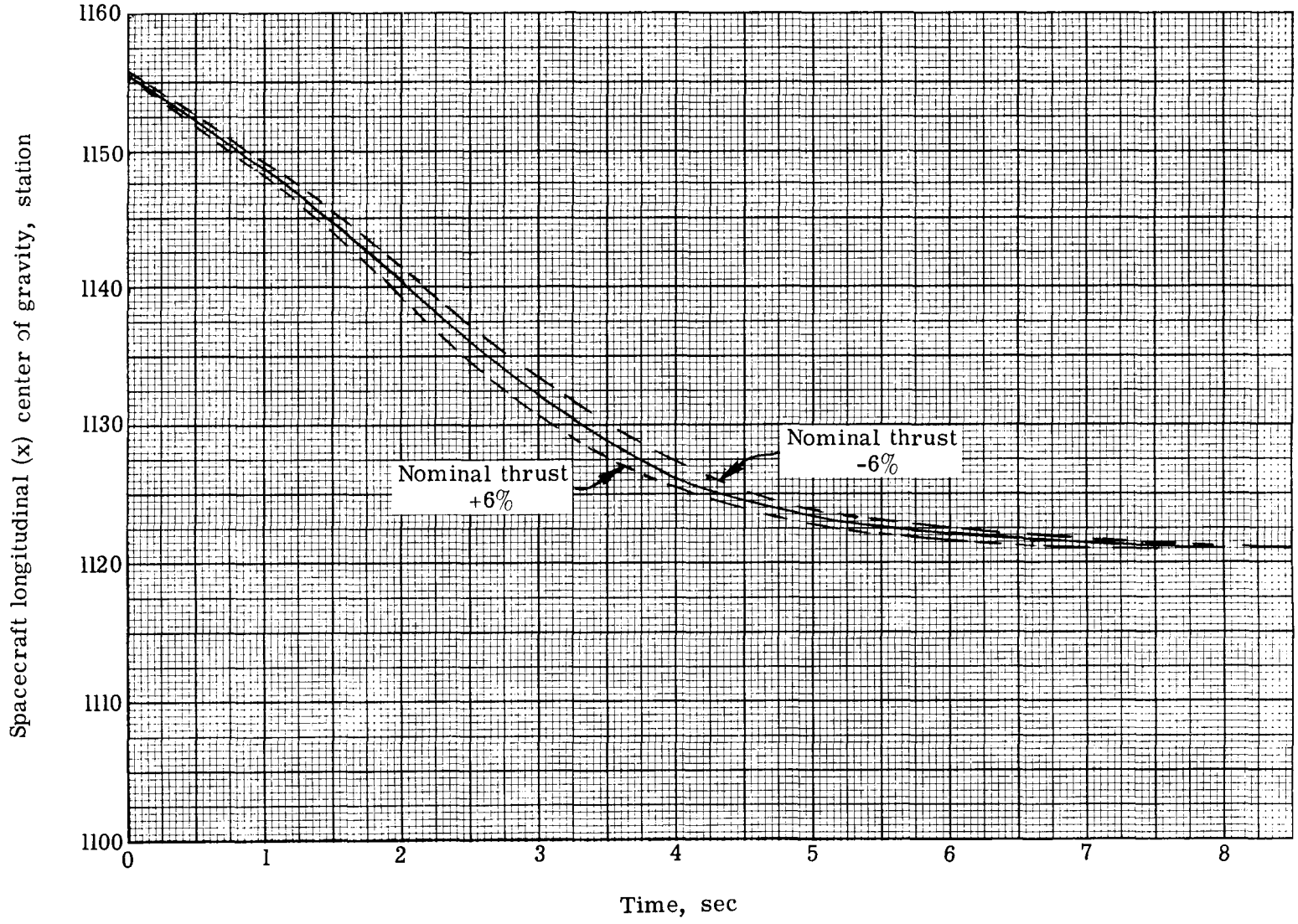

Figure 4.2.2-2.- Spacecraft predicted center-of-gravity (x) location plotted against time of launch-escape-motor ignition.

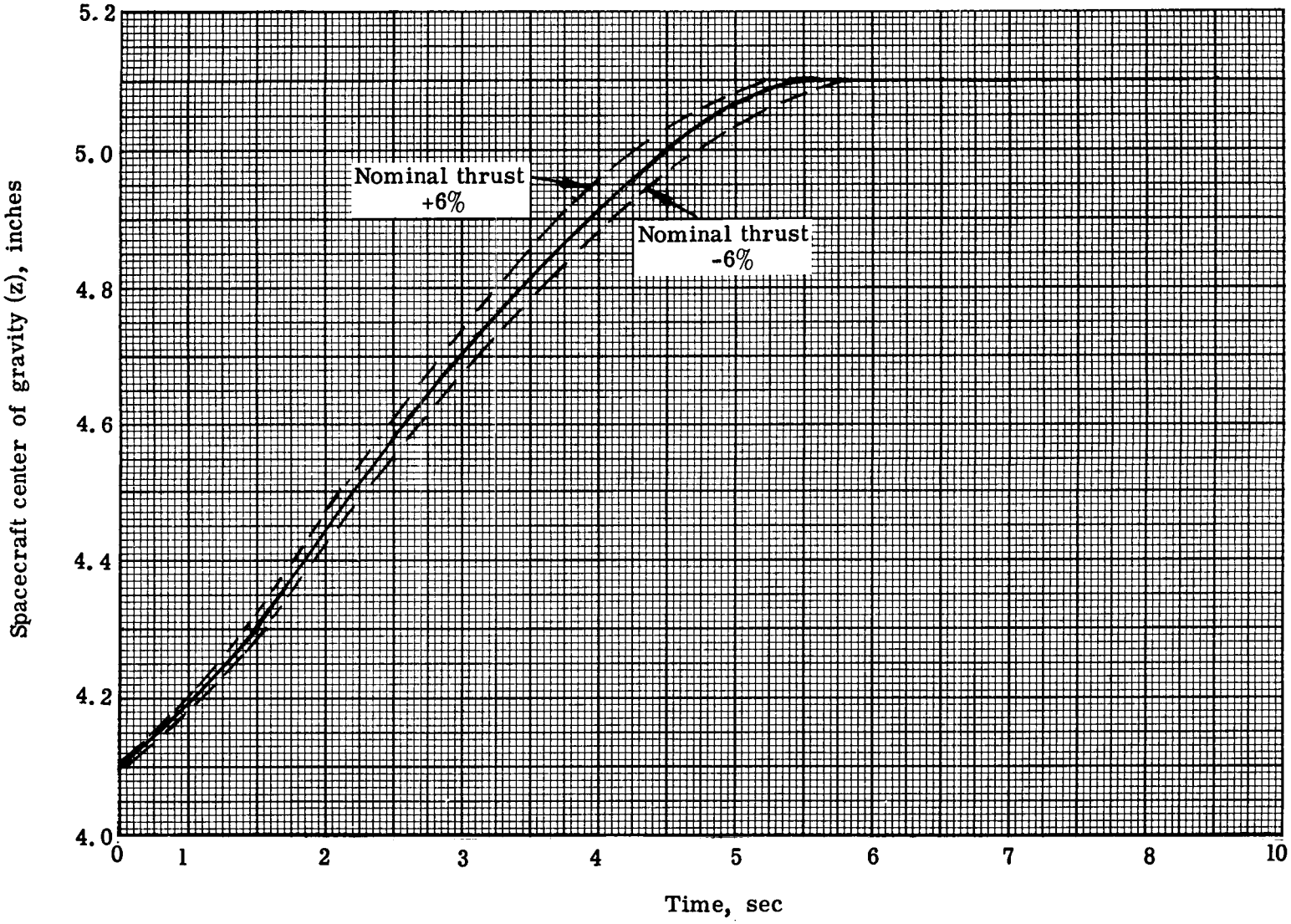

Figure 4.2.2-3.- Predicted center-of-gravity (z) location plotted against time of launch-escape-motor ignition.

[redacted]

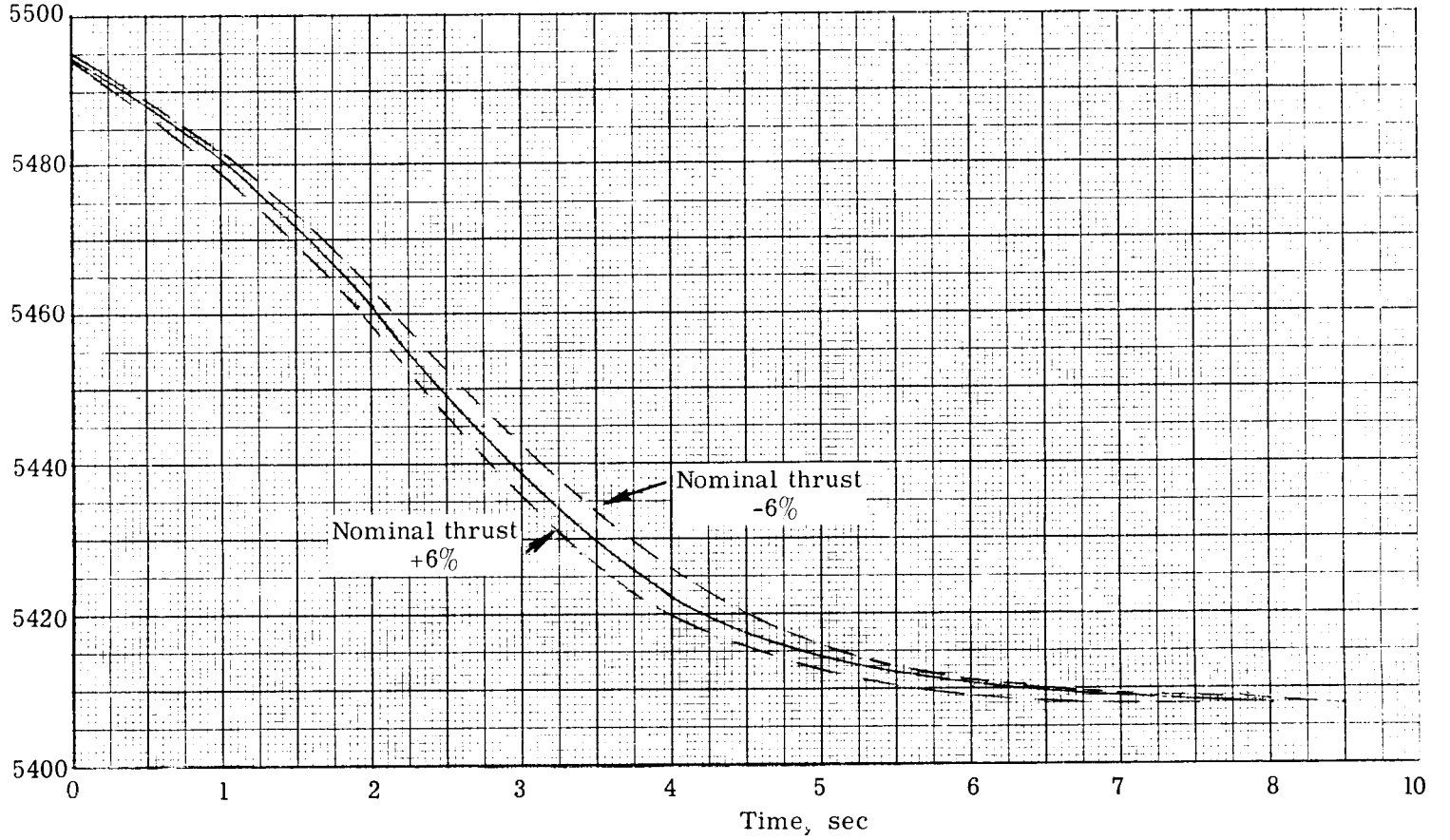

[redacted]

Figure 4.2.2-4.- Spacecraft predicted roll moment of inertia plotted against time of launch-escape-motor ignition.

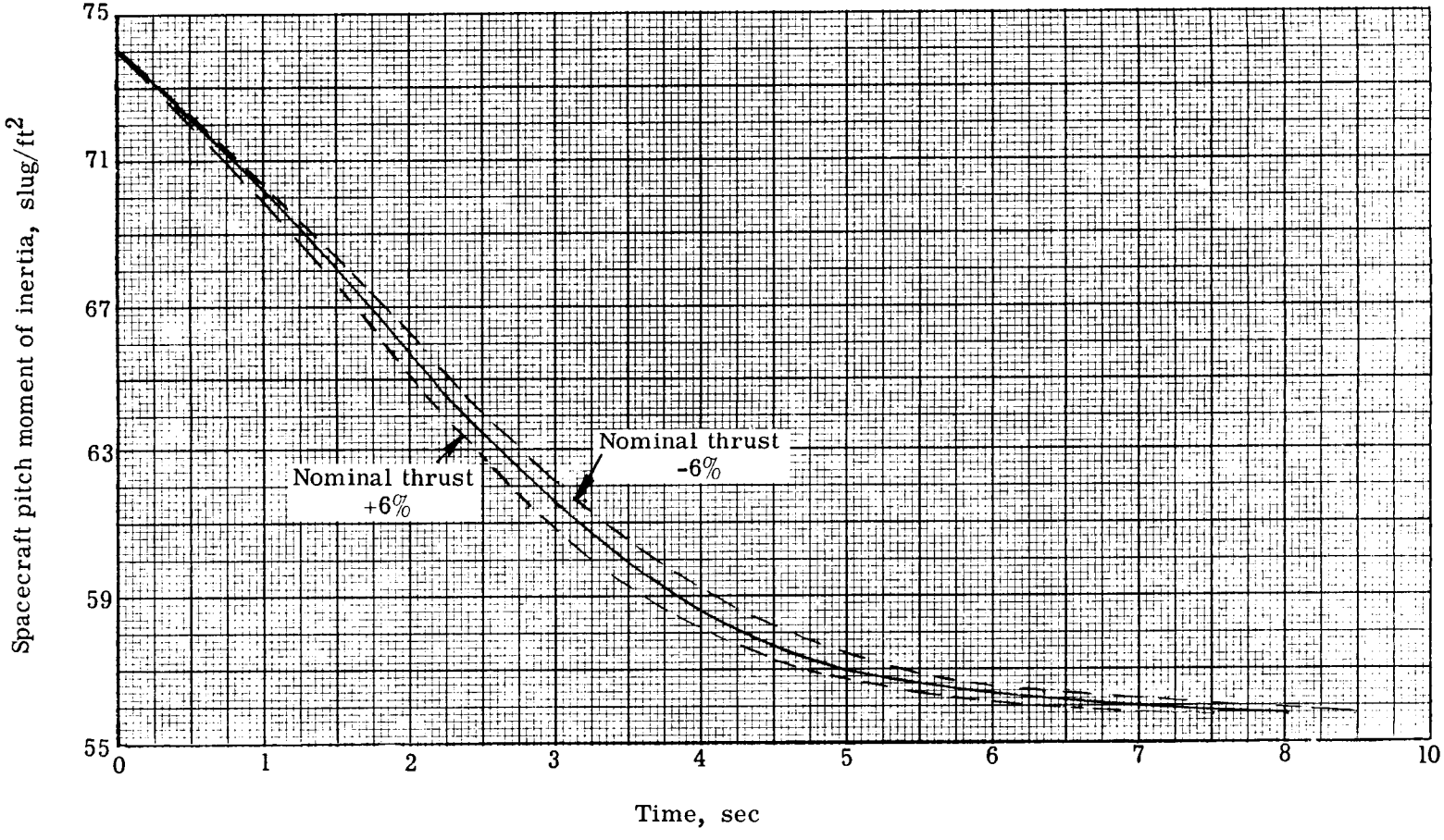

Figure 4.2.2-5.- Spacecraft predicted pitch moment of inertia plotted against time of launch-escape-motor ignition.

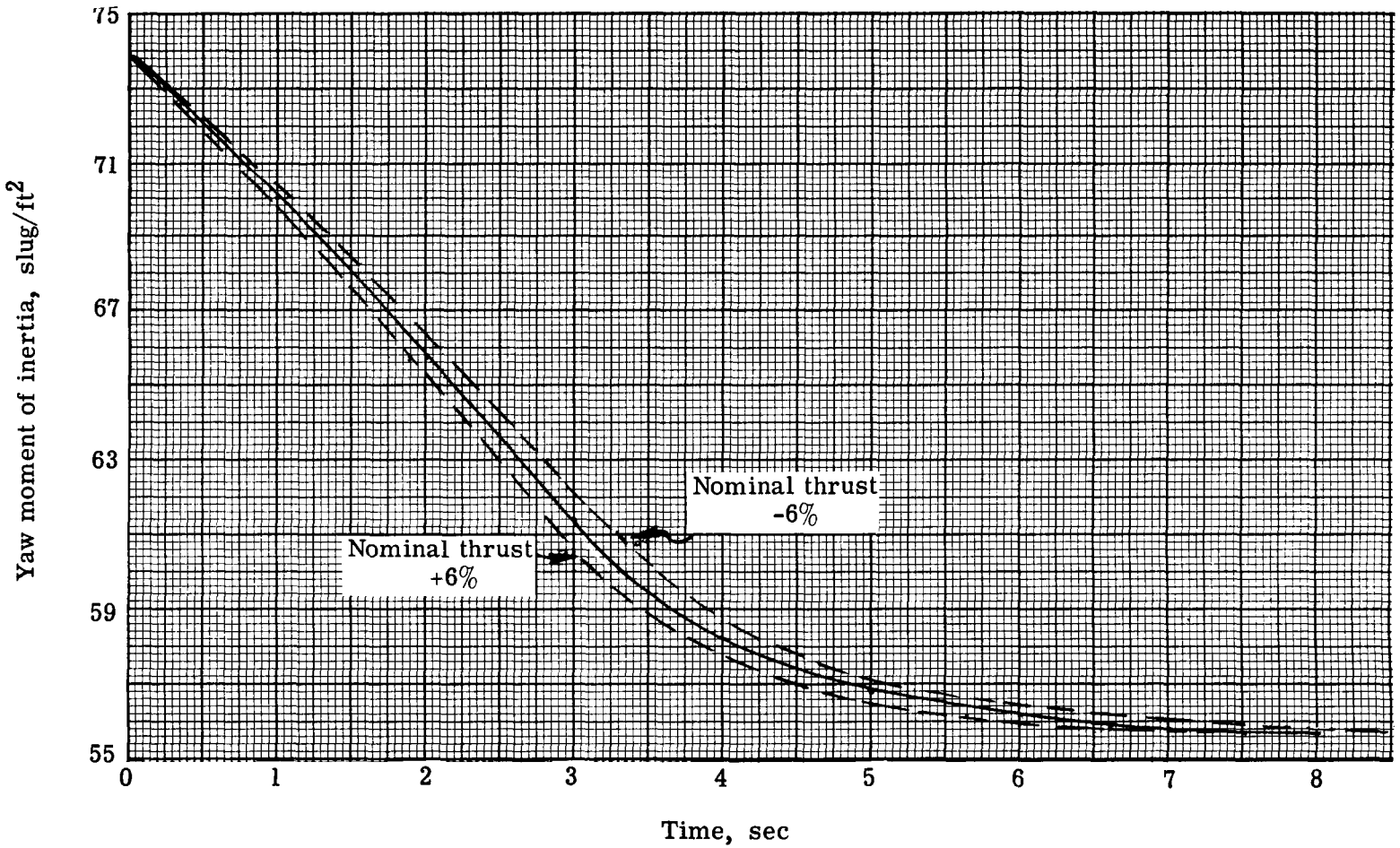

Figure 4.2.2-6.- Spacecraft predicted yaw moment of inertia plotted against time of launch-escape-motor ignition.

4.2.3 Launch-vehicle mass characteristics.- The mass properties of the Little Joe II launch vehicle are based on actual weights. Inertia values were calculated from these actual weights. These calculated values were then utilized in calculating the test-vehicle mass properties plotted against burning time as shown in figures 4.2.3-1 to 4.2.3-5. Comparison of actual values with those predicted is also shown in these figures. The variation of the actual mass properties from those predicted was caused by the thrust of the Little Joe II launch vehicle being higher than predicted.

Table 4.2.3-1 presents the mass properties of the total vehicle for significant points during the mission. The values are based on actual weights for the initial conditions and the remaining points were calculated on nominal propellant burning rates furnished by the motor manufacturer.

The center of gravity for the test vehicle varies only 0.1 inch in the Y- and Z-coordinate system. This accuracy resulted from the fact that the machine program rounded off the values to the nearest 0.1 inch. Therefore, no attempt has been made to present these values graphically.

The variations in the Y- and Z-coordinates are:

Axis	Distance from center line, in.
Y	-0.1 to -0.2
Z	0.0 to 0.1

Variations in the X-coordinate are presented in figure 4.2.3-2 as the variation of center of gravity with time.

TABLE 4.2.3-1.- MASS PROPERTY DATA

Event	Weight, lb	Center of gravity[a,b]			Moment of inertia,[a] slug-ft		
		X	Y	Z	I_{xx}	I_{yy}	I_{zz}
Test vehicle at launch	57,946[c]	827.9	-0.1	0.0	28,971	828,113	826,797
Launch payload	25,355[c]	1,075.8	-.2	-.1	16,370	147,174	145,860
Launch-escape vehicle	16,218[c]	1,155.7	.2	4.1	5,494	74,052	73,907
Launch-escape vehicle at burnout	13,024[d]	1,121.2	.3	5.1	5,408	55,815	55,684
Command module prior to drogue deployment	8,806[d]	1,040.0	.3	7.3	5,132	4,308	4,209
Command module at touchdown	8,351[d]	1,037.2	.3	7.4	5,082	4,010	3,893

[a]Little Joe II reference stations have been changed to calculate center of gravity and inertia values for total vehicle.

[b]Centers of gravity are in the NASA reference system except that the longitudinal axis has an origin 998.7 inches below the tangency of the command module structure mold line.

[c]Weight of test vehicle at launch, the payload, and the launch-escape vehicle are actual values.

[d]Weights are derived from predicted values.

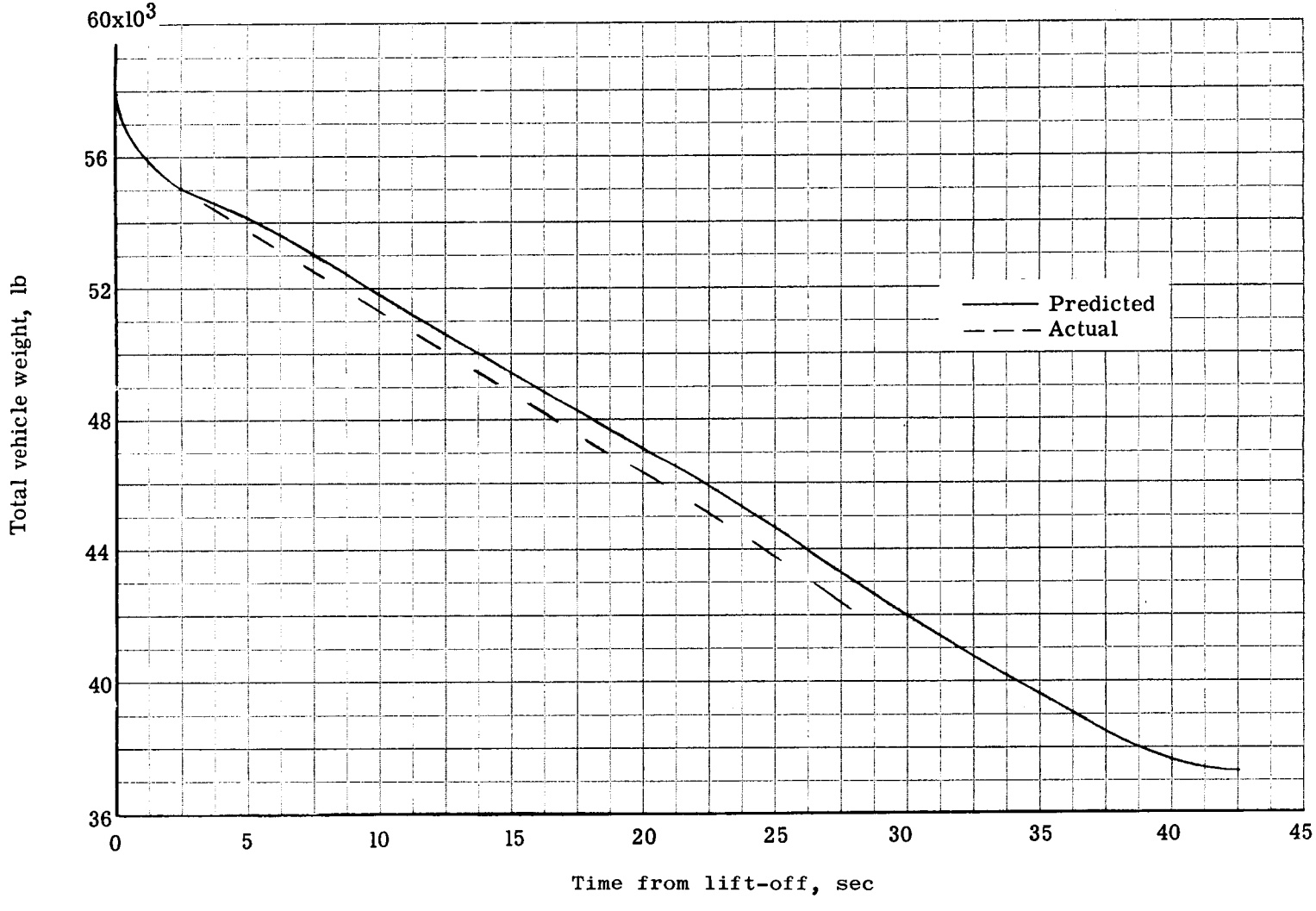

Figure 4.2.3-1.- Total test vehicle weight plotted against Little Joe II burning time.

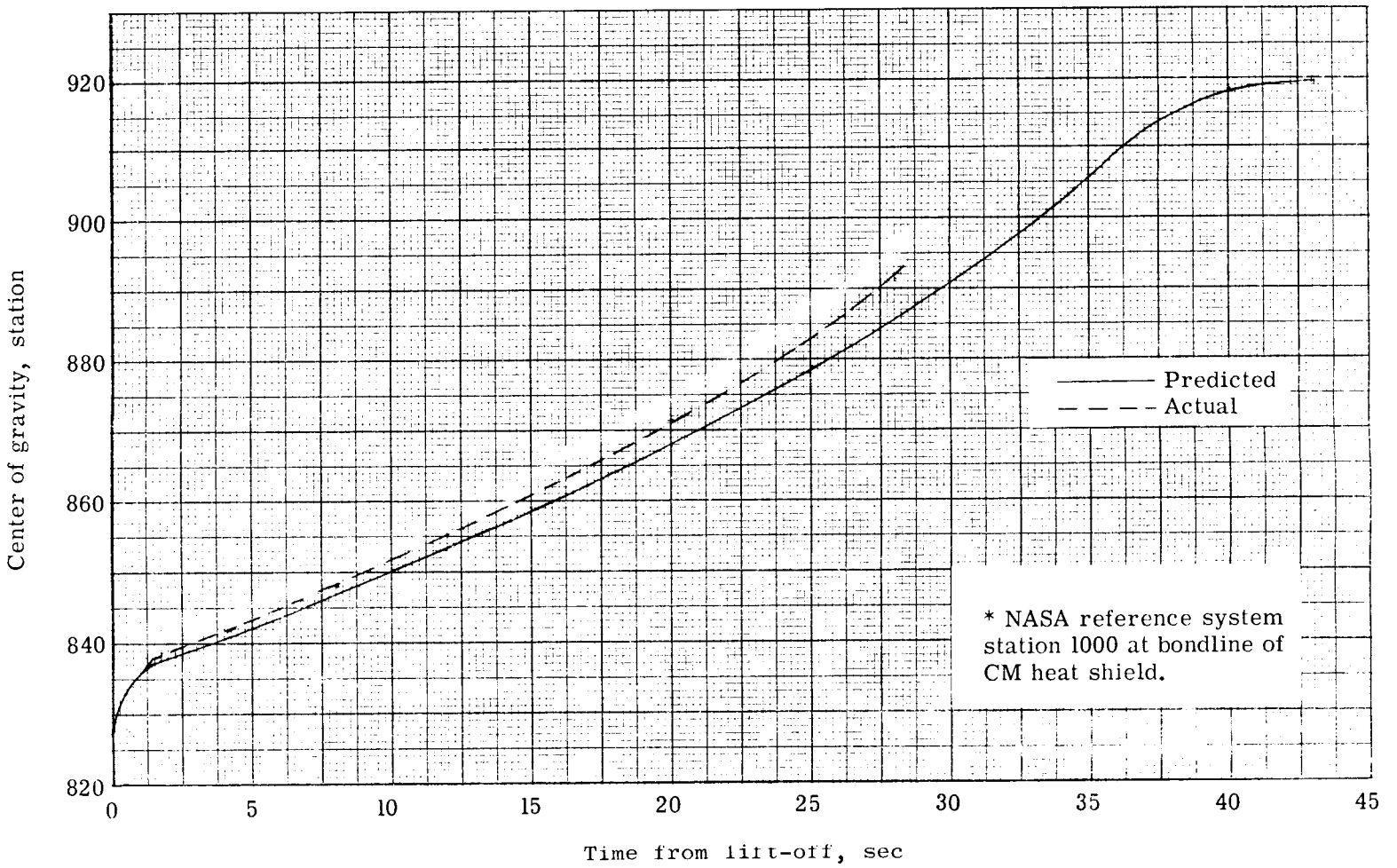

Figure 4.2.3-2.- Test vehicle center of gravity plotted against Little Joe II burning time.

[redacted]

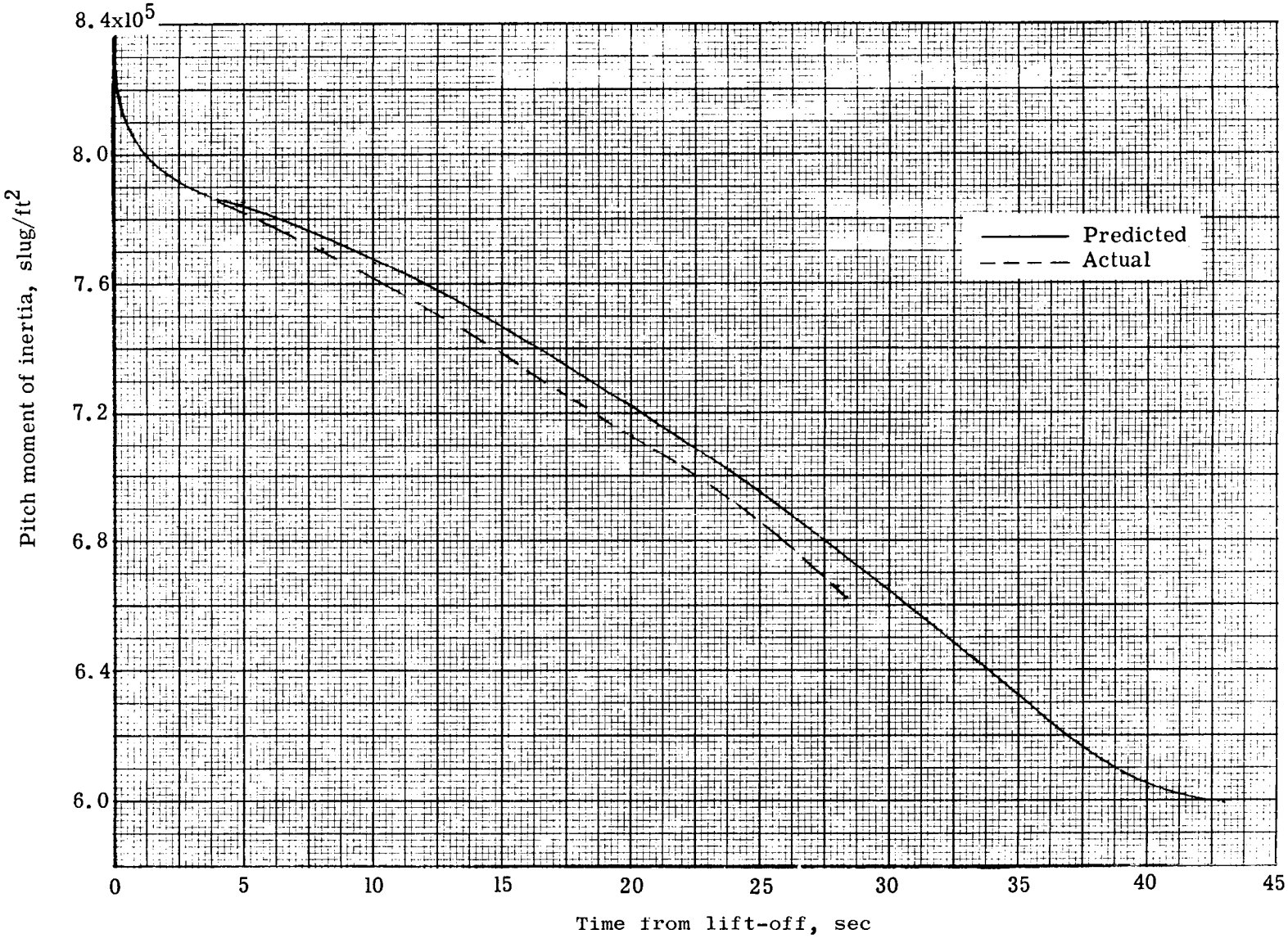

[redacted]

Figure 4.2.3-3.- Test vehicle pitch moment of inertia plotted against Little Joe II burning time.

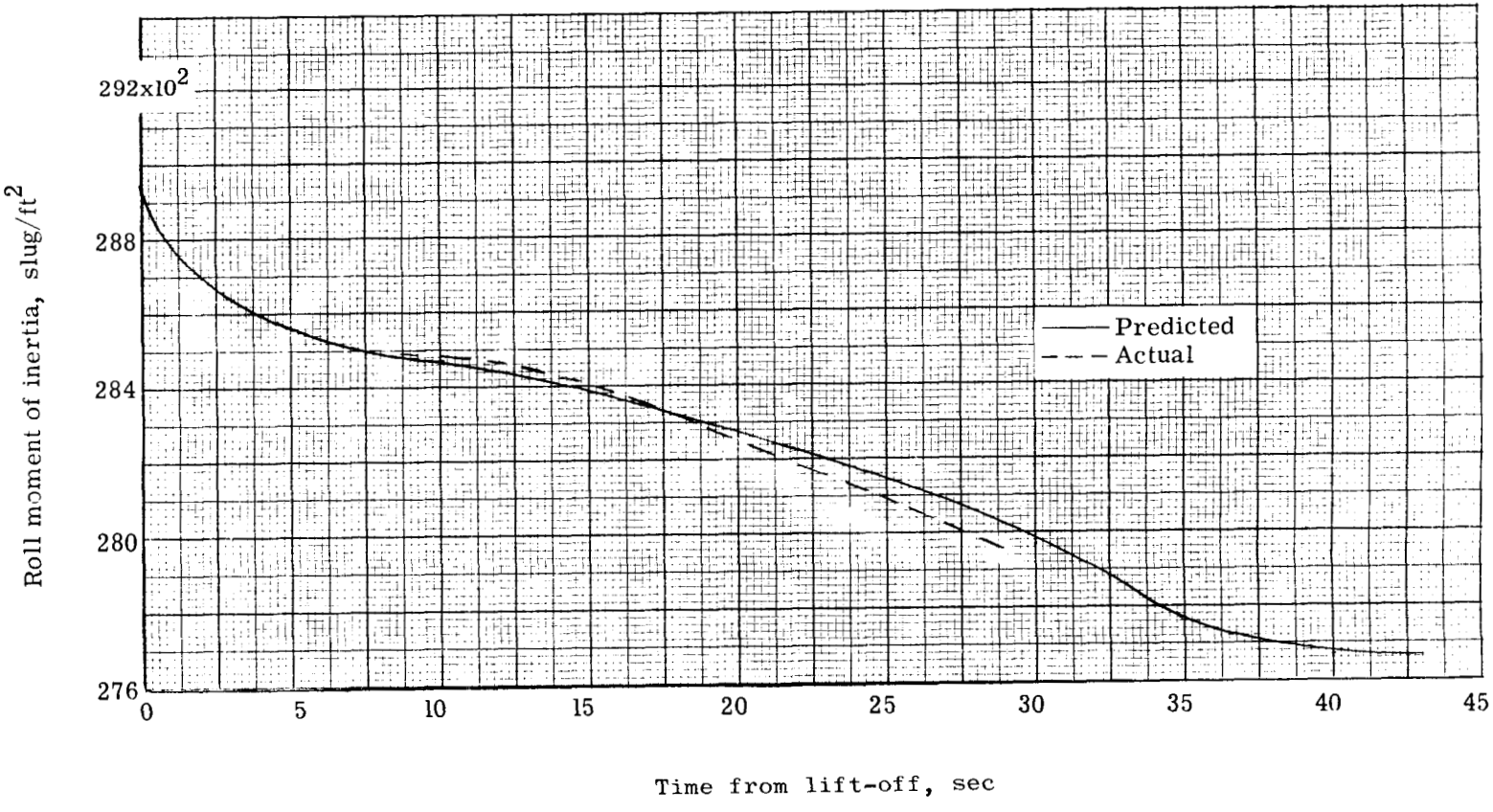

Figure 4.2.3-4.- Test vehicle roll moment of inertia plotted against Little Joe II burning time.

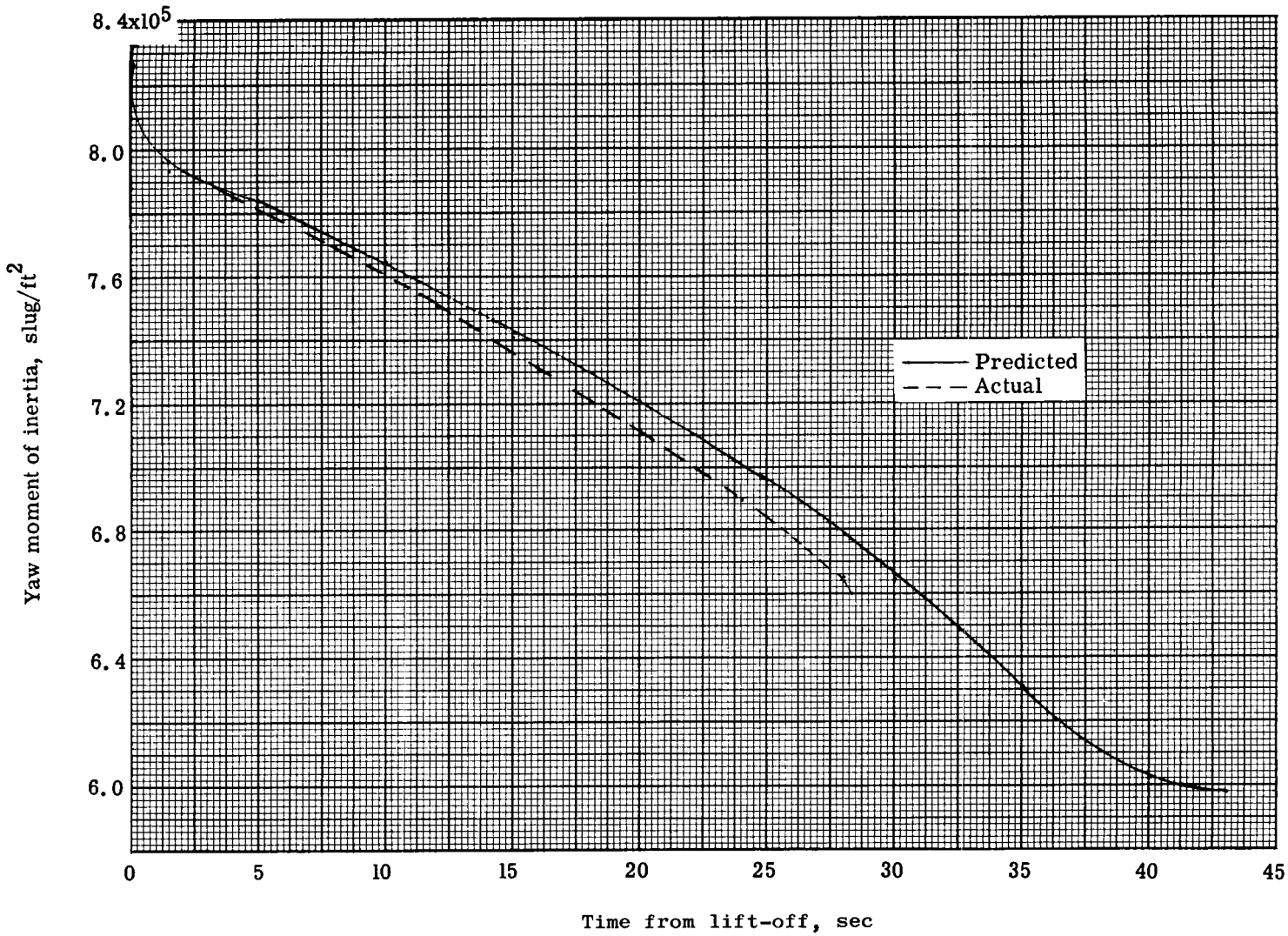

Figure 4.2.3-5.- Test vehicle yaw moment of inertia plotted against Little Joe II burning time.

[redacted]

4.2.4 Thrust-vector alinement.- Thrust-vector alinement of the launch-escape motor was performed on March 26 and 27 at the Vehicle Assembly Building, White Sands Missile Range. This alinement was performed by optical projection of an image on a grid placed between the tower legs. (See fig. 4.2.4-1.) After setting the thrust-vector angle optically, the grid was removed and the image projected and scribed on metal-faced tape placed on the command module. This method permitted resetting of the proper thrust angle after demating the launch-escape subsystem for transportation to the launch site. After reassembly at the launch site, the projection was reinstalled and the image was found to coincide with the scribed point on the command module.

Thrust-vector angle from the motor log book was 2°48'56" in the X-Z plane, and 90°2'16" in the X-Y plane (both with reference to the motor center line). Thrust-vector alinement resulted in the center line of the launch-escape motor being canted, relative to the command module X-axis, approximately 13 minutes in the -Y direction and no measureable amount in the Z direction.

[redacted]

[redacted]

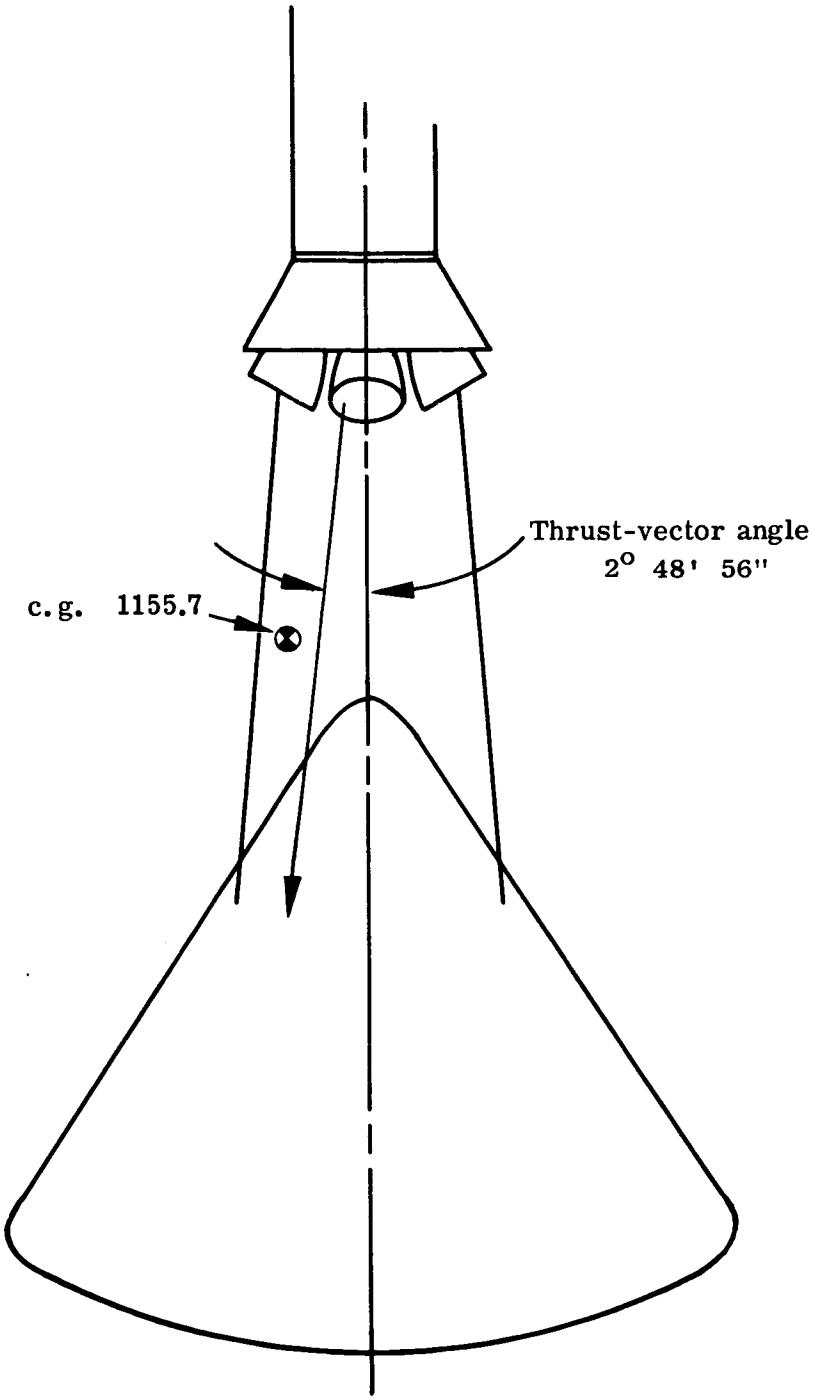

Figure 4.2.4-1.- Diagram showing thrust-vector angle.

[redacted]

[redacted]

4.3 Command and Service Module

4.3.1 Instrumentation and communications subsystem.- The telemetry subsystem used on Apollo boilerplate 12 was not a prototype flight system. It was a standard PAM/FM/FM system consisting of a 90 × 10 commutator, 16 voltage-controlled oscillators, one mixer, one tape input amplifier, one line-matching amplifier, one 5-point calibrator, one transmitter input amplifier, and one RF power amplifier. The block diagram of the telemetry modulation package is shown in figure 4.3.1-1. Table 4.3.1-1 is the instrumentation and communications subsystem flight hardware list for boilerplate 12. A 90 × $1\frac{1}{4}$ commutator was used in conjunction with the TMS-1090 temperature subsystem. This commutator was external to the telemetry modulation package.

The RF power amplifier boosts the output of the telemetry transmitter to 10 watts. All of the 16 voltage-controlled oscillators used were standard IRIG channels, and the total RF carrier deviation used was 125 kc.

The telemetry antennas consisted of four H-shaped, slot antennas flush-mounted with the exterior skin of the command module. The antennas are spaced 90° apart around the circumference of the command module and located at station X_c = 57.45 inches. Figures 4.3.1-2 and 4.3.1-3 show a block diagram of the subsystem, and figure 4.3.1-4 shows the antenna installation.

A 1-inch, 14-track Leach onboard tape recorder was used on boilerplate 12. Ten wideband frequency modulation channels were used for high frequency fluctuating pressure and base pressure measurements. The differentiated PDM output of the 90 × 10 commutator was recorded on a direct input track. The onboard tape recorder was the only data-gathering source for the pressures that were recorded on the 10 FM tracks.

Two C-band beacons with four antennas spaced at 90° were used for radar tracking. The beacon system transmits at a nominal frequency of 5500 megacycles in conjunction with two C-band transponders. The installation of the beacon antenna is shown in figure 4.3.1-4.

Three 16-mm motion-picture camera subsystems were installed. Each was a self-contained unit, consisting of a high-speed camera, a timing pulse generator, a control unit, an inertia switch, and a 28-volt, 5-ampere-hour battery. Power was applied to all cameras at lift-off by the closure of an inertia switch. The frame rate of the tower camera and service module camera was 200 frames per second and the frame rate of the command module camera was 100 frames per second. Figures 4.3.1-4 and 4.3.1-5 show the relative installation and subsystem configuration.

[redacted]

The instrumentation subsystem was powered by one 28-volt silver-zinc-oxide battery rated at 120 ampere-hours. Power from the battery was taken to the power-control box which provides power to the A bus, B bus, and instrumentation bus.

The instrumentation subsystem voltage reference was provided by a 5-volt, 0.5-ampere regulated power supply located within the signal conditioner box. Time reference was provided by a Gulton Coded timer which was recorded onboard and transmitted. The instrumentation subsystem transducers included those to measure voltages, current, pressure, temperature rates, accelerations, attitudes, and events. The acceleration transducers and the amplifier for fluctuating pressures, current, and temperatures had the capability of being remotely calibrated for range and zero values, referred to as R and Z calibrates. A block diagram of the instrumentation subsystem is shown in figure 4.3.1-3. Refer to figures 4.3.1-6 to 4.3.1-9 for relative instrumentation installation positions, and to figure 4.3.1-10 for launch-escape and earth-landing-subsystem-sequencer measurement points. A photograph of the installation of primary instrumentation components is shown in figure 4.3.1-11.

The two C-band beacons were interrogated by three radars during flight. The three radars tracked the command module throughout flight and satisfactory return signals were received from both transponders. The transponder trigger levels remained constant at 4.6 v d-c during flight.

In general, the instrumentation subsystem operated satisfactorily. Of the 140 total measurements made, only 3 failed to provide data, and 3 others provided only partial data. For analysis by channel, refer to table 4.3.1-2. The measurement list by subsystems is shown in table 4.3.1-3.

A telemetry subsystem disturbance occurred at T+28.470 seconds and lasted 0.002 second. This brief disturbance was noted by all telemetry receiving stations. This disturbance was also noted on the onboard tape recorded data but for a period of approximately 0.3 second. The cause of this disturbance cannot be positively established but may be attributable to the large shock loading imposed on the launch-escape vehicle at thrust termination. The uncompensated tape had a speed and flutter variation of approximately 2 to 3 percent. However, very clean data with minimal noise content were obtained using the 50-kc reference to compensate the data. The data from the onboard tape recorder indicate an increasing noise level during the powered phase of flight which is believed to have been caused by engine-induced vibration on the tape recorder.

No data were obtained for the launch-escape motor chamber pressure, LD0013P. Postflight tests indicated that the malfunction was caused by either the transducer itself or the launch-escape-vehicle wiring. See

[redacted]

section 4.6 for further discussions of the postflight testing.

Conical surface pressure no. 16, CA0043P, provided valid data until approximately 44 to 47 seconds from lift-off, after which time the reading remained constant for the remainder of the flight. The orifice for this measurement was located near the forward heat shield and command module separation plane. Postflight inspection did not reveal any orifice problem. The pressure transducer was removed and sent to the calibration laboratory where it was found to be functioning properly.

Two base pressures, numbers 5 and 9, did not provide data. These measurements were to be switched in after tower separation. Two fluctuating pressures measured on the same channels of the onboard tape recorder were active prior to thrust termination; however, the two base pressures which shared these channels did not afford any data at switchover. Base pressure transducers numbers 5 and 9 were sent to the laboratory for analysis and were found to be operative. Upon further postflight investigation it was found that there was an open circuit in the +28 v d-c line common to both transducer power supplies within the signal conditioning box.

As part of the postflight investigation, the aft heat shield was lowered to examine the damage in the aft compartment of the command module. Two additional base pressure transducers (nos. 2 and 4) were found to have their pressure lines kinked and broken at the pressure orifices.

The performance of the relay box was satisfactory. Switching at T+28.435 seconds to time-share high response telemetry and tape recorder channels was provided.

Several instruments received stimuli which exceeded their range. The limits of accelerometer CA0002A, X-axis spacecraft acceleration low, were exceeded several times during flight, as expected, since its range had been selected to measure accelerations of small magnitude accurately. The limit of -10g to 20g for accelerometer CA0001A, X-axis spacecraft acceleration high, was exceeded briefly at touchdown, as was the limit of ±10g for accelerometer CA0007A, Z-axis spacecraft acceleration.

The rate gyros performed satisfactorily throughout flight even though their limit of ±60 deg/sec was exceeded in both the pitch and yaw axis. The limits of the roll rate accelerometer were not exceeded. Spacecraft orientation is shown in figure 4.3.1-6.

The attitude gyros used in boilerplate 12 are ±175°, 2-axes gyros. Several design characteristics of the attitude gyros must be understood before attempting to understand the analysis of the gyro data as observed during the flight mission of boilerplate 12.

[redacted]

The gyro inner gimbal action which is not telemetered moves into alinement of the sensing axis at approximately ±80°. When this happens, the gyro rotor will shift away from its initial inertial reference point. This change would invalidate any additional data which are referenced to a calibration using the initial inertial reference point.

The mechanical positioning of the gyros within the command module must also be considered. The positioning of the yaw and pitch gyros were such that the inner gimbals of these gyros were affected by a roll attitude. (Refer to fig. 4.3.1-6 for spacecraft orientation.) Therefore, if roll attitude exceeded approximately ±80°, the inner gimbal of the pitch and yaw gyros would be forced into alinement with the sensing axis. The positioning of the roll and yaw gyros were such that a pitch attitude would not affect their inner gimbal action.

Additional design characteristics that must be considered are the mechanical and electrical characteristics of the potentiometer associated with the outer gimbal which converts the gyroscopic motion into an electrical analogy. The potentiometer winding encompasses approximately 354° of angular rotation. Taps for electrical excitation are provided at approximately 2.5° from each end of the potentiometer. No mechanical stops are employed in the design of the potentiometer. The potentiometer wiper is normally at a center position when the gyro is in a caged condition. The wiper will pass the tap point when the maximum range of the unit is exceeded and will continue to follow the motion of the gyro rotor. As the motion continues, the wiper will cross over a dead-band area between the ends of the potentiometer. The output signal will exhibit an abrupt reversal in polarity when the wiper arm completes the crossover of the dead-band area. The data after such a reversal can be replotted to reflect the total motion of the vehicle by using the following equation:

$$360 + (\alpha) = A$$

where

A = true attitude value after discontinuity

α = observed attitude value after the discontinuity

However, certain inaccuracies may exist because of switching dead bands.

Both the yaw and pitch attitude gyros provided valid data from T+0 until T+22.3 seconds, at which time roll the attitudes exceeded 80°. The roll attitude gyro provided valid data throughout the flight except for a very brief period at thrust termination, or command module—service module separation.

The three 16-mm flight motion-picture cameras provided some flight data. The service module camera and 95 percent of its support bracketry

[redacted]

were missing from the service module on landing. The bottom of this plate carries the impression pattern of the fiber-glass bulkhead; the top of this plate has impressions of the camera film footage indicator. One side of the camera body also left an indention in the steel plate. This indicates the camera was torn loose from its internal mount and hit the bottom plate with considerable force at the Little Joe II destruct. The aft heat shield of the command module shows evidence of the individual plates of the camera case striking at three widely separated points.

The camera was not found despite a 7-hour search. The camera system control units remained on the service module until ground impact, at which time the camera control unit and tri-pulse generator were torn loose.

The camera control units showed very little damage, whereas the generator, being of lighter construction, was severely damaged. The inertia switch and the battery remained mounted and suffered little surface damage although the battery showed some internal damage. The pressure transducers and associated wiring, and the amplifiers and camera components showed little evidence of damage as a result of the force of the Algol engine top and fiber-glass bulkhead being blown through the center of the service module to the command module aft heat shield.

The command module camera and approximately 400 feet of film were recovered. The recovered film covered the flight time from T+0 through the launch-escape-motor ignition and touchdown. The command module camera was set to run at 100 frames per second and did so until after launch-escape subsystem ignition at which time the camera apparently stopped since tower separation was not photographed. At drogue deployment, photographic coverage resumed at an unscheduled frame rate of approximately 10 frames per second to touchdown. The cause for the stoppage and slow speed is not known but apparently caused the motor to heat excessively and cause damage to the film. The excess heat caused emulsion to transfer in spots to the back of the film.

The film timing marks were largely obliterated. However, the film format throughout the film contained a true image as evidenced by the sharp and clean fiducial markers. Considerable care was required to salvage the damaged film.

The launch-escape-tower camera had been turned on inadvertently during prelaunch check. When the camera was installed and plugged in, the camera started. It was found that the reset relay had not been reset prior to delivery to the vehicle. As a result, when the camera was turned on at launch, the film was not driven by the sprocket, and thus no coverage was obtained from the tower camera. The camera was recovered and, although damaged, the film would have been useable.

[redacted]

Data plots for basic instrumentation subsystem parameters, command module interior temperature, and telemetry package temperature are shown in figures 4.3.1-12 to 4.3.1-14.

The performance of the instrumentation subsystem was satisfactory and telemetry transmission continued until the recovery crew turned off the instrumentation power.

[redacted]

TABLE 4.3.1-1.- FLIGHT INSTRUMENTATION HARDWARE LIST FOR BOILERPLATE 12

Component	Manufacturer	Manufacturer model	Range	Quantity flight
Telemetry modulation package	Bendix	TATP-316	Channel 2-16/E	1
Telemetry RF package	Bendix	TATP-316	244.8 mc 10 w	1
C-band transponder	Motorola	AM/DPN-66		2
Beacon line filter	NASA	SB 510-216		2
Tape recorder	Leach	MTR-1200	14 tracks	1
Timer	Gulton	CGT-100	60 minutes	1
Signal conditioning box	NASA Brown	CH-150	150 channels	1
Junction box	NASA	JB-1		1
Main battery	Eagle-Picher	MAP 4095-3	120 amp-hour	1
Battery	Eagle-Picher	MAR 4090-9	5 amp-hour	7
Power control box	NASA	PC-3		1
Rate gyro package	US Time	400455	±60°/second	1
Attitude gyro	Giannini	3416 DV-06	±175°	3
Linear accelerometer	Donner	4310	±10g (30 cps)	4
Linear accelerometer	Donner	4310	±2g (30 cps)	1
Linear accelerometer	Donner	4310	-10g to 20g	1
Relay box	NASA	RB-1		1
Pressure transducer	Wiancko	P2-3236-1	0 to 15 psia	9
Pressure transducer	Wiancko	P2-3136-2	0 to 2500 psia	2
Pressure transducer	Wiancko	P2-3236-3	15 to 2 psia	4
Pressure transducer	Wiancko	P2-3236-2	2 to 22 psia	36

[redacted]

TABLE 4.3.1-1.- FLIGHT INSTRUMENTATION HARDWARE LIST FOR BOILERPLATE 12 - Concluded

Component	Manufacturer	Manufacturer model	Range	Quantity flight
Pressure transducer	Statham	PA-288TG	0 to 15 psia	12
Amplifier rack	NASA	1-A	2 channels	9
Amplifier	Engineered Magnetics	EM 2000D-1	100 gain, 5 cps	1
Amplifier	Engineered Magnetics	EM 2000D-1	100 gain, 300 cps	4
Amplifier	Engineered Magnetics	EM 2000D-1	100 gain, 400 cps	4
Amplifier	Engineered Magnetics	EM 2000D-1	100 gain, 600 cps	4
Temperature system	Engineered Magnetics	EMT 111B	0 to 150° C	2
Amplifier	Engineered Magnetics	EM 2000A-3	1,000 gain	2
Resistance thermometer	Trans-Sonics	2168A	0 to 150° C	2
Temperature system	Engineered Magnetics	EMT 111B	0 to 150° C	1
Amplifier	Engineered Magnetics	EM 2000A-3	1,000 gain	1
Resistance thermometer	Trans-Sonics	T4082C-8	0 to 150° C	1
Temperature signal conditioning box	Microdot	401-0110-1		1
Temperature simulator box	NASA	TS-1		1
Commutator	Fifth Dimension	LDA 12-N-432	$90 \times 1\frac{1}{4}$	1
Camera	Milliken	DBM-5A	100 fps	1
Camera	Milliken	DBM-5A	200 fps	2
Lens	Kinoptik	5.7mm		3

TABLE 4.3.1-2.- CONTINUOUS TELEMETRY CHANNELS

Measurement number	Channel	Comment
CK0003R	A-2	Satisfactory
CK0002R	A-3	Good data from T-0 to T+53.5 seconds at which time instrument limits were exceeded.
CK0001R	A-4	Good data from T-0 until T+48.2 seconds at which time instrument limits exceeded.
CA0007A	A-5	Good data from T-0, command module landing instrument limits exceeded.
CA0005A	A-6	Satisfactory
CT0001W	A-7	Satisfactory
CA0001A	A-8	Good data from T-0 until command module landing at which time instrument limit exceeded.
LA0011A	A-9	Good data from T-0 to tower separation.
LA0012A	A-10	Good data from T-0 to tower separation.
CA0002A	A-11	Good data except when instrument bottomed on several times during flight.
LD0013P	A-12	No data. See section 4.3.1.3
$90 \times 1\frac{1}{4}$	A-13	Good data throughout flight observed from commutated wave train.
LD0012P	A-14	Good data from T-0 to tower separation.
SA0184P[a]	A-15	Good data from T-0 to CM-SM separation.
CA0107P[b]	A-15	Good data from SM-CM separation throughout flight.
BS0109P[a]	A-16	Good data from T-0 until CM-SM separation.
CA0111P[b]	A-16	Good data begins from CM-SM separation.
90×10	A-E	Satisfactory

TABLE 4.3.1-2.- Continued

Channel A-E, 90 × 10 commutator segments

Measurement number	Channel	Comment	Measurement number	Channel	Comment
CT0025V	A-E-1	Satisfactory	CA0044P	A-E-23	Satisfactory
CT0026V	A-E-2	Satisfactory	CA0045P	A-E-24	Satisfactory
CA0100P	A-E-3	Satisfactory	CA0046P	A-E-25	Satisfactory
CA0101P	A-E-4	Satisfactory	CA0047P	A-E-26	Satisfactory
CA0102P	A-E-5	Satisfactory	CA0048P	A-E-27	Satisfactory
CA0103P	A-E-6	Satisfactory	CA0049P	A-E-28	Satisfactory
CA0028P	A-E-7	Satisfactory	CA0050P	A-E-29	Satisfactory
CA0029P	A-E-8	Satisfactory	CA0051P	A-E-30	Satisfactory
CA0030P	A-E-9	Satisfactory	CA0052P	A-E-31	Satisfactory
CA0031P	A-E-10	Satisfactory	CA0053P	A-E-32	Satisfactory
CA0032P	A-E-11	Satisfactory	CA0054P	A-E-33	Satisfactory
CA0033P	A-E-12	Satisfactory	CA0055P	A-E-34	Satisfactory
CA0034P	A-E-13	Satisfactory	LK0023H[c]	A-E-35	Satisfactory
CA0035P	A-E-14	Satisfactory	LK0024H[c]	A-E-36	Satisfactory
CA0036P	A-E-15	Satisfactory	LK0025P[c]	A-E-37	Satisfactory
CA0037P	A-E-16	Satisfactory	CD0151X CD0150X[c]	A-E-38	Satisfactory
CA0038P	A-E-17	Satisfactory	CA0056P	A-E-39	Satisfactory
CA0039P	A-E-18	Satisfactory	CA0057P	A-E-40	Satisfactory
CA0040P	A-E-19	Satisfactory	CA0058P	A-E-41	Satisfactory
CA0041P	A-E-20	Satisfactory	CA0059P	A-E-42	Satisfactory
CA0042P	A-E-21	Satisfactory	CT0002V	A-E-43	Satisfactory
CA0043P[d]	A-E-22	Satisfactory	CT0003V	A-E-44	Satisfactory

[redacted]

TABLE 4.3.1-2.- Continued

Channel A-E, 90 × 10 commutator segments

Measurement number	Channel	Comment	Measurement number	Channel	Comment
CD0154X CD0155X	A-E-45	Satisfactory	CD0025X CD0026X	A-E-62	Satisfactory
CE0022X CE0023X	A-E-46	Satisfactory	CD0027X CD0028X	A-E-63	Satisfactory
CA0611P	A-E-47	Satisfactory	CC0002V	A-E-64	Satisfactory
LD0190X LD0191X	A-E-48	Satisfactory	CE0001X CE0002X	A-E-65	Satisfactory
CD0031X CD0032X	A-E-49	Satisfactory	CE0003X CE0004X	A-E-66	Satisfactory
CD0029X CD0030X	A-E-50	Satisfactory	CE0005X CE0006X	A-E-67	Satisfactory
CC0001V	A-E-51	Satisfactory	CD0005V	A-E-68	Satisfactory
CC0003V	A-E-52	Satisfactory	CD0006V	A-E-69	Satisfactory
CC0004V	A-E-53	Satisfactory	BS0110X[a]	A-E-70	Satisfactory
CC0005C	A-E-54	Satisfactory	Spare	A-E-71	
CD0021X CD0022X	A-E-55	Satisfactory	CD0152X CD0153X	A-E-72	Satisfactory
CE0023X CE0024X	A-E-56	Satisfactory	CK0017H	A-E-73	Satisfactory
CD0008V	A-E-57	Satisfactory	CK0018H	A-E-75	Satisfactory
CD0009V	A-E-58	Satisfactory	CA0610T	A-E-76	Satisfactory
CE0028X CE0029X	A-E-59	Satisfactory	CT0202T	A-E-77	Satisfactory
CE0007X CE0008X	A-E-60	Satisfactory	CT0201T	A-E-78	Satisfactory
LD0033X LD0034X	A-E-61	Satisfactory	BS0111X[a]	A-E-79	Satisfactory
			CE0014X	A-E-80	Satisfactory
			CE0011X	A-E-81	Satisfactory

[redacted]

TABLE 4.3.1-2.- Continued

Channel A-E, 90 X 10 commutator segments

Measurement number	Channel	Comment	Measurement number	Channel	Comment
CE0012X	A-E-82	Satisfactory	CA0063P	A-E-87	Satisfactory
CE0013X	A-E-83	Satisfactory	CT0007X	A-E-88	Satisfactory
CA0060P	A-E-84	Satisfactory	CT0027V	A-E-89	Satisfactory
CA0061P	A-E-85	Satisfactory	CT0028V	A-E-90	Satisfactory
CA0062P	A-E-86	Satisfactory			

General Note: It was noted that a momentary telemetry dropout occurred at 28.470 seconds and lasted until 28.472 seconds. This dropout was on all continuous and commutated channels.

Note a: These measurements were time-shared and switched out at command module—service module separation or measurement terminated with CM—SM separation.

Note b: These measurements were time-shared and were switched in at CM—SM separation for the remainder of the flight.

Note c: These measurements were active from lift-off until tower separation.

Note d: See flight performance section 4.3.1.3.

[redacted]

TABLE 4.3.1-2.- Concluded

Onboard tape recorder channel assignment

Measurement number	Channel	Comment
SA0186P[a]	TRK1	Satisfactory
CA0110P[b]	TRK1	Satisfactory
SA0188P	TRK2	Satisfactory
CT0020V	TRK3	Satisfactory
Spare	TRK4	
SA0187P[a]	TRK5	Satisfactory
CA0106P[b]	TRK5	Satisfactory
CT0021V	TRK6	Satisfactory
50 kc compensation	TRK7	
CA0179P	TRK8	Satisfactory
CA0180P	TRK9	Satisfactory
CA0181P	TRK10	Satisfactory
SA0189P[a]	TRK11	Satisfactory
CA0108P[b]	TRK11	No data. See section 4.3.1.3.
SA0182P[a]	TRK12	Satisfactory
CA0105P[b]	TRK12	Satisfactory
SA0190P[a]	TRK13	Satisfactory
CA0109P[b]	TRK13	Satisfactory
SA0183P[a]	TRK14	Satisfactory
CA0104P	TRK14	No data. See section 4.3.1.3.

Note: Tape recorder turned off at ≈ T+416.5 seconds.

[redacted]

LIST CODING AND NOMENCLATURE FOR TABLE 4.3.1-3

The measurement requirement list consists of all flight measurement parameters, and these parameters are grouped by functional spacecraft systems to aid in system evaluation.[1] The format and nomenclature are briefly described as follows:

The measurement identification number consists of seven characters: two letters followed by four numbers and one letter.

The first letter (module code) designates the measurement location by module.

A	Adapter
B	Booster
C	Command module
L	Launch-escape tower
S	Service module

The second letter (functional system code) denotes the subsystem within which the measurement originates.

A	Structures
C	Electrical power
D	Launch escape
E	Earth landing
F	Environmental control
G	Guidance and navigation
H	Stabilization and control
J	Life systems
K	Flight technology
L	Inflight test
P	Propulsion
R	Reaction control
S	Crew safety
T	Communications and instrumentation

Characters three through six are numbers assigned sequentially or grouped for clarity within each subsystem. The seventh character, a letter, denotes the measurement classification.

---

[1]Total system accuracy for each measurement is assumed to be 5 percent (or better) of full scale, unless otherwise noted.

[redacted]

A	Acceleration	M	Mass
B	Phase	P	Pressure
C	Current	Q	Quantity
D	Vibration	R	Rate
E	Power	S	Strain
F	Frequency	T	Temperature
G	Force	V	Voltage
H	Position	W	Time
J	Biomedical	X	Discrete event
K	Radiation	Y	Acoustical
L	Velocity	Z	Ph-acidity

The measurement description is a brief, definitive title given to each measurement. Standard abbreviations are used, where applicable, to keep the measurement description length within 32 characters, including spaces.

Channel or Track

1. Link (LK). LK designates the telemetry package of the r-f carrier as package A, package B, or package C.

2. Subcarrier Number (SC No.). SC No. designates the telemetry channel in terms of Channels 1 through 18.

3. Commutator Segment (COM SEG). COM SEG designates the telemetry commutator segment assigned to the measurement for that vehicle.

4. Track (TRK). TRK designates the tape recorder track assigned to the measurement for that vehicle.

Data Range

Data range denotes the minimum and maximum values for a parameter in engineering units.

Priority

The priority column indicates the criticality of each measurement.

1. P (primary) denotes the measurements that must be available at launch for mission success and/or for attainment of the flight objectives.

2. S (secondary) denotes the measurements that are highly desirable but will not abort or delay the mission.

[redacted]

3. M (multiple) designates a group of related measurements of which no more than a specified percentage may be inoperative.

Response

Response rate denotes the rate, in engineering units, required to provide satisfactory data resolution to time or wave form. Response for continuous data monitoring (telemetry or recorder) will be specified in cycles per second (cps), and response for sampled-data monitoring (PCM or PACE), in samples per second (s/s).

Location

The location column denotes the physical location within the spacecraft where the measurement is taken. When the location is given in polar coordinates, it is referenced from the +Y axis (+Y = 0°). The angle increases as the measurement location changes progressively from the +Y axis to the +Z axis.

TABLE 4.3.1-3.- APOLLO BOILERPLATE MEASUREMENT LIST

Boilerplate 12

(a) Structures subsystem

Measurement identification	Measurement description	Channel			Data Range			Priority	Response		Location
		IK	SC no.	Com. seg.	Low	High	Unit		Rate	Unit	
C A0001 A	X-axis, spacecraft accel., high	A	8		-10	+20	g	P	0-30	cps	XC78, YC0, ZC21
C A0002 A	X-axis, spacecraft accel., low	A	11		- 2	+ 2	g	P	0-30	cps	XC78, YC0, ZC21
C A0005 A	Y-axis, spacecraft accel	A	6		-10	+10	g	P	0-20	cps	XC78, YC0, ZC21
C A0007 A	Z-axis, spacecraft accel.	A	5		-10	+10	g	P	0-20	cps	XC78, YC0, ZC21
L A0011 A	Y-axis, tower accel.	A	9		-10	+10	g	P	0-30	cps	XL380, YL0, ZL6
L A0012 A	Z-axis, tower accel.	A	10		-10	+10	g	P	0-30	cps	XL380, YL6, ZL0
C A0028 P	Conical surface pressure 1	A	E	7	+ 2	+22	psia	M	10	s/s	XC30, 359°
C A0029 P	Conical surface pressure 2	A	E	8	+ 2	+22	psia	M	10	s/s	XC30, 21.5°
C A0030 P	Conical surface pressure 3	A	E	9	+ 2	+22	psia	M	10	s/s	XC30, 40.75°
C A0031 P	Conical surface pressure 4	A	E	10	+ 2	+22	psia	M	10	s/s	XC30, 84°
C A0032 P	Conical surface pressure 5	A	E	11	+ 2	+22	psia	M	10	s/s	XC30, 179.5°
C A0033 P	Conical surface pressure 6	A	E	12	+ 2	+22	psia	M	10	s/s	XC30, 203.75°
C A0034 P	Conical surface pressure 7	A	E	13	+ 2	+22	psia	M	10	s/s	XC30, 221.25°
C A0035 P	Conical surface pressure 8	A	E	14	+ 2	+22	psia	M	10	s/s	XC30, 246.5°
C A0036 P	Conical surface pressure 9	A	E	15	+ 2	+22	psia	M	10	s/s	XC30, 276°
C A0037 P	Conical surface pressure 10	A	E	16	+ 2	+22	psia	M	10	s/s	XC30, 293.25°
C A0038 P	Conical surface pressure 11	A	E	17	+ 2	+22	psia	M	10	s/s	XC30, 318.75°
C A0039 P	Conical surface pressure 12	A	E	18	+ 2	+22	psia	M	10	s/s	XC30, 335.5°
C A0040 P	Conical surface pressure 13	A	E	19	+ 2	+22	psia	M	10	s/s	XC100, 357°
C A0041 P	Conical surface pressure 14	A	E	20	+ 2	+22	psia	M	10	s/s	XC50.5, 21.5°
C A0042 P	Conical surface pressure 15	A	E	21	+ 2	+22	psia	M	10	s/s	XC71, 41.916°
C A0043 P	Conical surface pressure 16	A	E	22	+ 2	+22	psia	M	10	s/s	XC100, 40.75°

TABLE 4.3.1-3.- APOLLO BOILERPLATE MEASUREMENT LIST - Continued

Boilerplate 12

(a) Structures subsystem - Continued

Measurement identification	Measurement description	Channel			Data Range			Priority	Response		Location
		IK	SC no.	Com. seg.	Low	High	Unit		Rate	Unit	
C A0044 P	Conical surface pressure 17	A	E	23	+ 2	+22	psia	M	10	s/s	XC100, 221.25°
C A0045 P	Conical surface pressure 18	A	E	24	+ 2	+22	psia	M	10	s/s	XC71, 221.25°
C A0046 P	Conical surface pressure 19	A	E	25	+ 2	+22	psia	M	10	s/s	XC100, 318.75°
C A0047 P	Conical surface pressure 20	A	E	26	+ 2	+22	psia	M	10	s/s	XC71, 318.75°
C A0048 P	Conical surface pressure 21	A	E	27	+ 2	+22	psia	M	10	s/s	XC50.5, 335.5°
C A0049 P	Conical surface pressure 22	A	E	28	+ 2	+22	psia	M	10	s/s	XC50.5, 359°
C A0050 P	Conical surface pressure 23	A	E	29	+ 2	+22	psia	M	10	s/s	XC50.5, 40.75°
C A0051 P	Conical surface pressure 24	A	E	30	+ 2	+22	psia	M	10	s/s	XC50.5, 84.0°
C A0052 P	Conical surface pressure 25	A	E	31	+ 2	+22	psia	M	10	s/s	XC50.5, 221.25°
C A0053 P	Conical surface pressure 26	A	E	32	+ 2	+22	psia	M	10	s/s	XC50.5, 276°
C A0054 P	Conical surface pressure 27	A	E	33	+ 2	+22	psia	M	10	s/s	XC50.5, 318.75°
C A0055 P	Conical surface pressure 28	A	E	34	+ 2	+22	psia	M	10	s/s	XC71, 21.5°
C A0056 P	Conical surface pressure 29	A	E	39	+ 2	+22	psia	M	10	s/s	XC71, 203.75°
C A0057 P	Conical surface pressure 30	A	E	40	+ 2	+22	psia	M	10	s/s	XC71, 246.5°
C A0058 P	Conical surface pressure 31	A	E	41	+ 2	+22	psia	M	10	s/s	XC71, 293.25°
C A0059 P	Conical surface pressure 32	A	E	42	+ 2	+22	psia	M	10	s/s	XC71, 335.5°
C A0060 P	Conical surface pressure 33	A	E	84	+ 2	+22	psia	M	10	s/s	XC79, 359°
C A0061 P	Conical surface pressure 34	A	E	85	+ 2	+22	psia	M	10	s/s	XC79, 84°
C A0062 P	Conical surface pressure 35	A	E	86	+ 2	+22	psia	M	10	s/s	XC80.3, 179.5°
C A0063 P	Conical surface pressure 36	A	E	87	+ 2	+22	psia	M	10	s/s	XC79, 276°
C A0100 P	Base pressure 1	A	E	3	+ 2	+15	psia	M	10	s/s	Bottom, 50R, 90°
C A0101 P	Base pressure 2	A	E	4	+ 2	+15	psia	M	10	s/s	Bottom, 50R, 0°

TABLE 4.3.1-3.- APOLLO BOILERPLATE MEASUREMENT LIST - Continued

Boilerplate 12

(a) Structures subsystem - Continued

Measurement identification	Measurement description	Channel			Data Range			Priority	Response		Location
		IK	SC no.	Com. seg.	Low	High	Unit		Rate	Unit	
C A0102 P	Base pressure 3	A	E	5	+ 2	+15	psia	M	10	s/s	Bottom, 50R, 270°
C A0103 P	Base pressure 4	A	E	6	+ 2	+15	psia	M	10	s/s	Bottom, 50R, 180°
C A0104 P	Base pressure 5	TRK		14	+ 0	+15	psia	M	5	cps	Bottom, 65, 0°
C A0105 P	Base pressure 6	TRK		12	+ 0	+15	psia	M	5	cps	Bottom, 65, 90°
C A0106 P	Base pressure 7	TRK		5	+ 0	+15	psia	M	5	cps	Bottom, 65, 180°
C A0107 P	Base pressure 8	A	15		+ 0	+15	psia	M	5	cps	Bottom, 65, 270°
C A0108 P	Base pressure 9	TRK		11	+ 0	+15	psia	M	5	cps	Bottom, 77, 0°
C A0109 P	Base pressure 10	TRK		13	+ 0	+15	psia	M	5	cps	Bottom, 77, 90°
C A0110 P	Base pressure 11	TRK		1	+ 0	+15	psia	M	5	cps	Bottom, 77, 180°
C A0111 P	Base pressure 12	A	16		+ 0	+15	psia	M	5	cps	Bottom, 77, 270°
C A0179 P	Fluctuating pressure 1	TRK		8	+ 0	+15	psia	M	0-300	cps	XC119, 7°
C A0180 P	Fluctuating pressure 2	TRK		9	+ 0	+15	psia	M	0-300	cps	XC70, 357°
C A0181 P	Fluctuating pressure 3	TRK		10	+ 0	+15	psia	M	0-300	cps	XC40, 357°
C A0182 P	Fluctuating pressure 4	TRK		12	+ 0	+15	psia	M	0-300	cps	XA1012, 357°
C A0183 P	Fluctuating pressure 5	TRK		14	+ 0	+15	psia	M	0-300	cps	XA1012, 177°
C A0184 P	Fluctuating pressure 6	A	15		+ 0	+15	psia	M	0-300	cps	XA974, 357°
C A0186 P	Fluctuating pressure 8	TRK		1	+ 0	+15	psia	M	0-300	cps	XA974, 177°
C A0187 P	Fluctuating pressure 9	TRK		5	+ 0	+15	psia	M	0-600	cps	XA974, 267°
C A0188 P	Fluctuating pressure 10	TRK		2	+ 0	+15	psia	M	0-600	cps	XA930, 357°
C A0189 P	Fluctuating pressure 11	TRK		11	+ 0	+15	psia	M	0-600	cps	XA881, 357°
C A0190 P	Fluctuating pressure 12	TRK		13	+ 0	+15	psia	M	0-600	cps	XA881, 177°

TABLE 4.3.1-3.- APOLLO BOILERPLATE MEASUREMENT LIST - Continued

Boilerplate 12

(a) Structures subsystem - Concluded

Measurement identification	Measurement description	Channel			Data Range			Priority	Response		Location
		IK	SC no.	Com. seg.	Low	High	Unit		Rate	Unit	
C A0610 T	CM interior temperature	A	E	76	+ 0	+150	°C	S	10	s/s	CM interior
C A0611 P	CM interior pressure	A	E	47	+ 0	+15	psia	S	10	s/s	CM interior
(b) Electrical subsystem											
C C0001 V	d-c voltage main bus A	A	E	51	+22	+32	vd-c	P	10	s/s	Power control box
C C0002 V	d-c voltage main bus B	A	E	64	+22	+32	vd-c	P	10	s/s	Power control box
C C0003 V	d-c voltage logic bus A	A	E	52	+ 0	+36	vd-c	P	10	s/s	LES sequencer
C C0004 V	d-c voltage logic bus B	A	E	53	+ 0	+36	vd-c	P	10	s/s	LES sequencer
C C0005 C	Total d-c current	A	E	54	+ 0	+35	amps	P	10	s/s	Power control box
(c) Launch-escape subsystem											
C D0005 V	d-c voltage LES pyro bus A	A	E	68	+ 0	+36	vd-c	P	10	s/s	LES sequencer
C D0006 V	d-c voltage LES pyro bus B	A	E	69	+ 0	+36	vd-c	P	10	s/s	LES sequencer
C D0008 V	Sequencer start signal A	A	E	57	+ 0	+36	vd-c	P	10	s/s	LES sequencer
C D0009 V	Sequencer start signal B	A	E	58	+ 0	+36	vd-c	P	10	s/s	LES sequencer
L D0012 P	Pitch control motor chamber pressure	A	14		+ 0	+2,500	psid	P	0-45	cps	XL345, YLO, ZL-13
L D0013 P	Escape motor chamber pressure	A	12		+ 0	+2,500	psid	P	0-45	cps	XL290, YLO, ZLO
C D0021 X	Abort initiate relay close A	A	E	55			step	P	10	s/s	LES sequencer
C D0022 X	Abort initiate relay close B	A	E	55			step	P	10	s/s	LES sequencer
C D0023 X	CM-SM separation relay close A	A	E	56			step	P	10	s/s	LES sequencer
C D0024 X	CM-SM separation relay close B	A	E	56			step	P	10	s/s	LES sequencer
C D0025 X	ELS sequencer A start relay close A	A	E	62			step	P	10	s/s	LES sequencer
C D0026 X	ELS sequencer A start relay close B	A	E	62			step	P	10	s/s	LES sequencer
C D0027 X	ELS sequencer B start relay close A	A	E	63			step	P	10	s/s	LES sequencer

TABLE 4.3.1-3.- APOLLO BOILERPLATE MEASUREMENT LIST - Continued

Boilerplate 12

(c) Launch-escape subsystem - Concluded

Measurement identification	Measurement description	Channel			Data Range			Priority	Response		Location
		IK	SC no.	Com seg.	Low	High	Unit		Rate	Unit	
C D0028 X	ELS sequencer B start relay close B	A	E	63			step	P	10	s/s	LES sequencer
C D0029 X	TWR jettison and separation A initiate relay close A	A	E	50			step	P	10	s/s	LES sequencer
C D0030 X	TWR jettison and separation A initiate relay close B	A	E	50			step	P	10	s/s	LES sequencer
C D0031 X	TWR jettison and separation B initiate relay close A	A	E	49			step	P	10	s/s	LES sequencer
C D0032 X	TWR jettison and separation B initiate relay close B	A	E	49			step	P	10	s/s	LES sequencer
L D0033 X	TWR jettison and separation relay close A	A	E	61			step	P	10	s/s	TWR LES sequencer
L D0034 X	TWR jettison and separation relay close B	A	E	61			step	P	10	s/s	TWR LES sequencer
L D0190 X	LES pitch-control motor fire relay close A	A	E	48			step	P	10	s/s	TWR LES sequencer
L D0191 X	LES pitch-control motor fire relay close B	A	E	48			step	P	10	s/s	TWR LES sequencer
C D0150 X	Backup abort timer start A	A	E	38			step	P	10	s/s	TWR LES sequencer
C D0151 X	Backup abort timer start B	A	E	38			step	P	10	s/s	TWR LES sequencer
C D0152 X	Abort initiate relay close A (K-20)	A	E	72			step	P	10	s/s	TWR LES sequencer
C D0153 X	Abort initiate relay close B (K-19)	A	E	72			step	P	10	s/s	TWR LES sequencer
C D0154 X	Abort enable GSE system A	A	E	45			step	P	10	s/s	TWR LES sequencer
C D0155 X	Abort enable GSE system B	A	E	45			step	P	10	s/s	TWR LES sequencer

TABLE 4.3.1-3.- APOLLO BOILERPLATE MEASUREMENT LIST - Continued

Boilerplate 12

(d) Earth-landing subsystem

Measurement identification	Measurement description	Channel			Data Range			Priority	Response		Location
		IK	SC no.	Com. seg.	Low	High	Unit		Rate	Unit	
C E0001 X	Drogue deploy relay close A	A	E	65			step	P	10	s/s	ELS sequencer
C E0002 X	Drogue deploy relay close B	A	E	65			step	P	10	s/s	ELS sequencer
C E0003 X	Main parachute deploy-drogue release relay A	A	E	66			step	P	10	s/s	ELS sequencer
C E0004 X	Main parachute deploy-drogue release relay B	A	E	66			step	P	10	s/s	ELS sequencer
C E0005 X	Main parachute release relay close A	A	E	67			step	P	10	s/s	ELS sequencer
C E0006 X	Main parachute release relay close B	A	E	67			step	P	10	s/s	ELS sequencer
C E0007 X	Forward heat shield release relay close A	A	E	60			step	P	10	s/s	ELS sequencer
C E0008 X	Forward heat shield release relay close B	A	E	60			step	P	10	s/s	ELS sequencer
C E0011 X	Physical monitor pilot parachute 1	A	E	81			event	P	10	s/s	Pilot Mortar
C E0012 X	Physical monitor pilot parachute 2	A	E	82			event	P	10	s/s	Pilot Mortar
C E0013 X	Physical monitor pilot parachute 3	A	E	83			event	P	10	s/s	Pilot Mortar
C E0014 X	Physical monitor drogue parachute	A	E	80			event	P	10	s/s	Drogue mortar
C E0022 X	Baro switch 1, 25,000 ft A	A	E	46			step	P	10	s/s	ELS sequencer
C E0023 X	Baro switch 2, 25,000 ft A	A	E	46			step	P	10	s/s	ELS sequencer
C E0028 X	Baro switch 1, 25,000 ft B	A	E	59			step	P	10	s/s	ELS sequencer
C E0029 X	Baro switch 2, 25,000 ft B	A	E	59			step	P	10	s/s	ELS sequencer

TABLE 4.3.1-3.- APOLLO BOILERPLATE MEASUREMENT LIST - Continued

Boilerplate 12

(e) Flight technology

Measurement identification	Measurement description	Channel			Data Range			Priority	Response		Location
		LK	SC no.	Com. seg.	Low	High	Unit		Rate	Unit	
C K0001 R	Pitch rate gyro output	A	4		-60	+60	°S	P	0-10	cps	XC78, YCO, ZC21
C K0002 R	Yaw rate gyro output	A	3		-60	+60	°S	P	0-10	cps	XC78, YCO, ZC21
C K0003 R	Roll rate gyro output	A	2		-60	+60	°S	P	0-10	cps	XC78, YCO, ZC21
C K0016 H	Pitch attitude gyro output	A	E	74	-175	+175	°	P	10	s/s	XC78, YCO, ZC21
C K0017 H	Roll attitude gyro output	A	E	73	-175	+175	°	P	10	s/s	XC78, YCO, ZC21
C K0018 H	Yaw attitude gyro output	A	E	75	-175	+175	°	P	10	s/s	XC78, YCO, ZC21
L K0023 H	Angle of attack	A	E	35	-40	+40	°	P	10	s/s	XL399, YLO, ZLO
L K0024 H	Angle of sideslip	A	E	36	-40	+40	°	P	10	s/s	XL399, YLO, ZLO
L K0025 P	Dynamic pressure	A	E	37	+ 0	+1,250	psf	P	10	s/s	XL399, YLO, ZLO
L K0120 N	Forward heat shield view camera						photo		100	fps	XL85, YLO, ZLO
C K0121 N	LES tower view camera						photo		200	fps	XC124, YCO, ZCO
S K0122 N	CM aft heat shield view camera						photo		200	fps	SA870, YAO, ZAO
(f) Crew safety											
B S0109 P	ALGOL chamber press	A	16		+ 0	+500	psia		0-70	cps	Little Joe II booster
B S0110 X	Little Joe II thrust term. fire system A	A	E	70			event		10	s/s	Little Joe II booster
B S0111 X	Little Joe II thrust term. fire system B	A	E	79			event		10	s/s	Little Joe II booster

TABLE 4.3.1-3.- APOLLO BOILERPLATE MEASUREMENT LIST - Continued

Boilerplate 12

(g) Communications and instrumentation

Measurement identification	Measurement description	Channel			Data Range			Priority	Response		Location
		IK	SC no.	Com. seg.	Low	High	Unit		Rate	Unit	
C T0001 W	On-board timer	A	7					P	0-35	cps	CM interior
C T0002 V	Transponder A trigger	A	E	43	+ 0	+ 5	vd-c	S	10	s/s	Transponder A
C T0003 V	Transponder B trigger	A	E	44	+ 0	+ 5	vd-c	S	10	s/s	Transponder B
C T0007 X	R and Z calibration monitor	A	E	88			step	P	10	s/s	SIG cond box
C T0201 T	TM RF transmitter A, temperature	A	E	78	+ 0	+150	°C	S	10	s/s	TM RF transmitter A
C T0202 T	TM RF amp A, temperature	A	E	77	+ 0	+150	°C	S	10	s/s	TM RF amp A
C T0025 V	0V system reference	A	E	1		0	vd-c	P	10	s/s	Signal conditioner box
C T0026 V	5V system reference	A	E	2		5	vd-c	P	10	s/s	Signal conditioner box

TABLE 4.3.1-3.- APOLLO BOILERPLATE MEASUREMENT LIST - Concluded

Boilerplate 12

(h) GSE measurements

Measurement identification	Measurement description	Channel			Data Range			Priority	Response		Location
		LK	SC no.	Com. seg.	Low	High	Unit		Rate	Unit	
C F0401 T	R/D ECS cold plate inlet temperature	GSE			+ 0	+100	°F				Cold plate inlet
C F0402 T	R/D ECS cold plate outlet temperature	GSE			+ 0	+100	°F				Cold plate outlet
C F0403 P	R/D ECS tank inlet pressure	GSE			+ 0	+ 50	psid				Cool tank inlet
L D2070 T	Temperature LES motor star point	GSE		Monitor	+ 0	+160	°F				XL260, 270°
L D2071 T	Temperature LES motor star valley	GSE		Monitor	+ 0	+160	°F				XL260, 270°
L D2072 T	Temperature LES motor	GSE		Monitor	+ 0	+160	°F				XL260, 270°
L D2073 T	Temperature LES motor	GSE		Monitor	+ 0	+160	°F				XL210, 30°
L D2074 T	Temperature LES motor	GSE		Monitor	+ 0	+160	°F				XL160, 150°

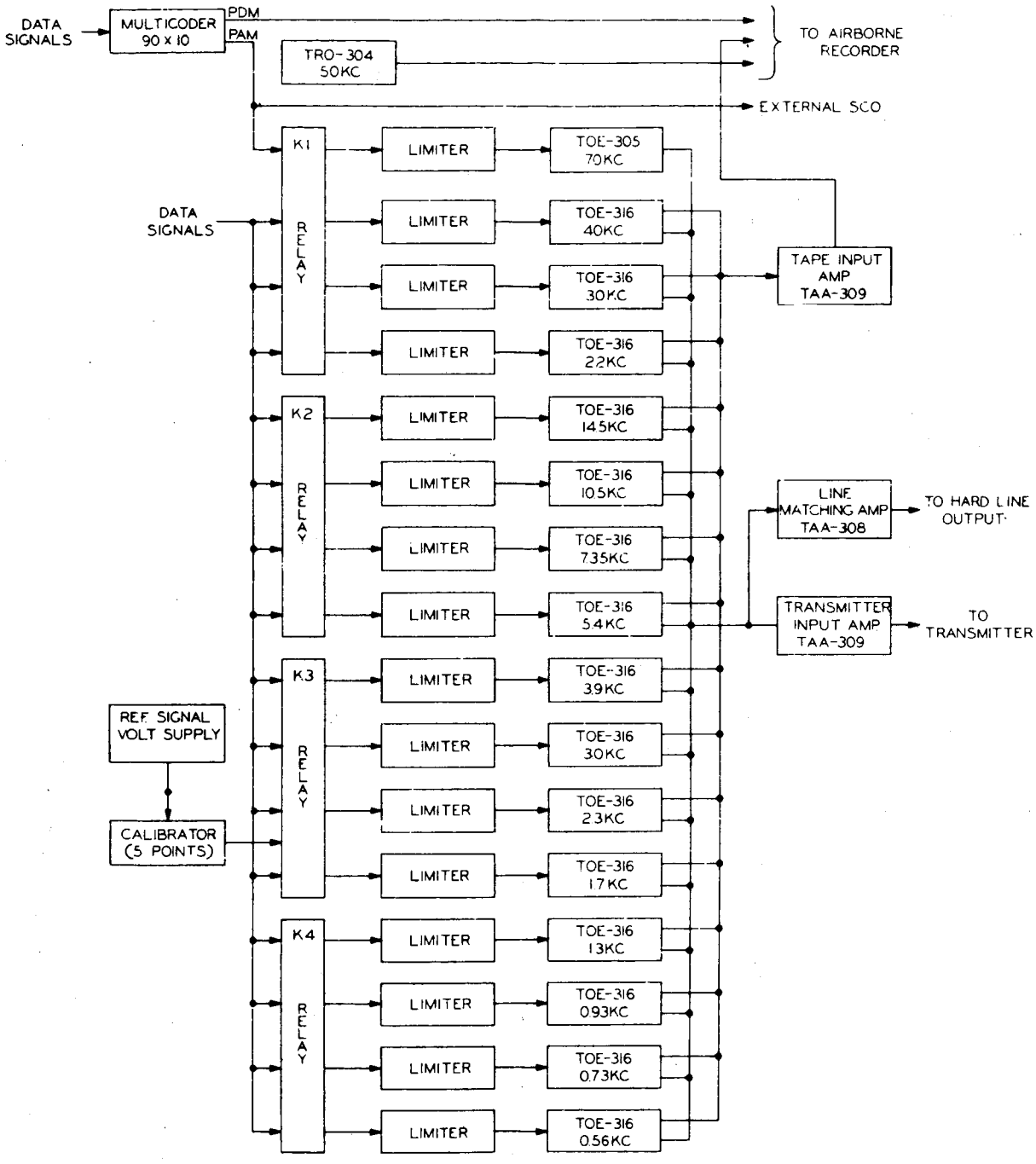

Figure 4.3.1-1. - Modulation package block diagram.

[redacted]

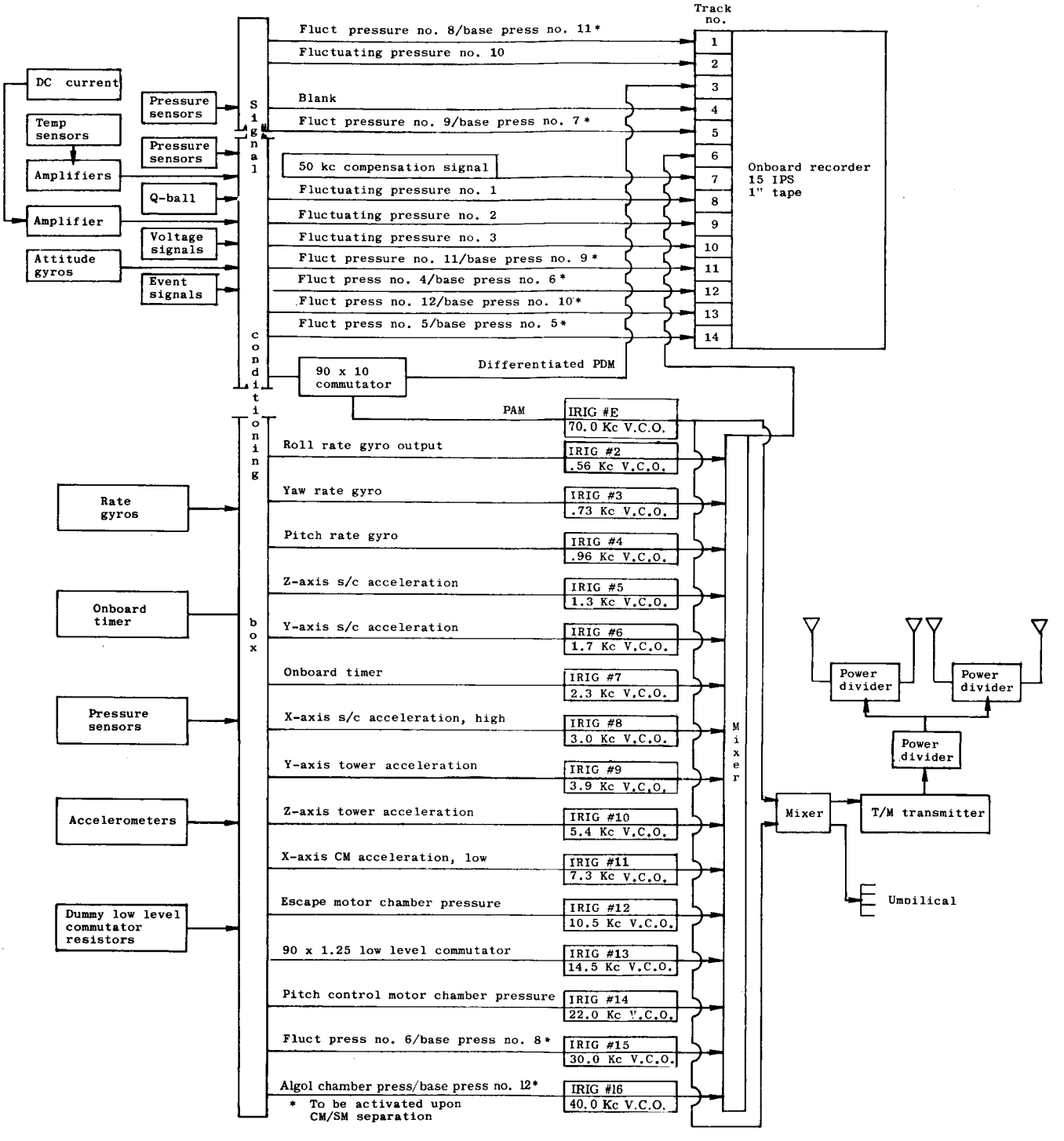

Figure 4.3.1-2. - Boilerplate 12 instrumentation block diagram depicting V. C. O. assignment.

[redacted]

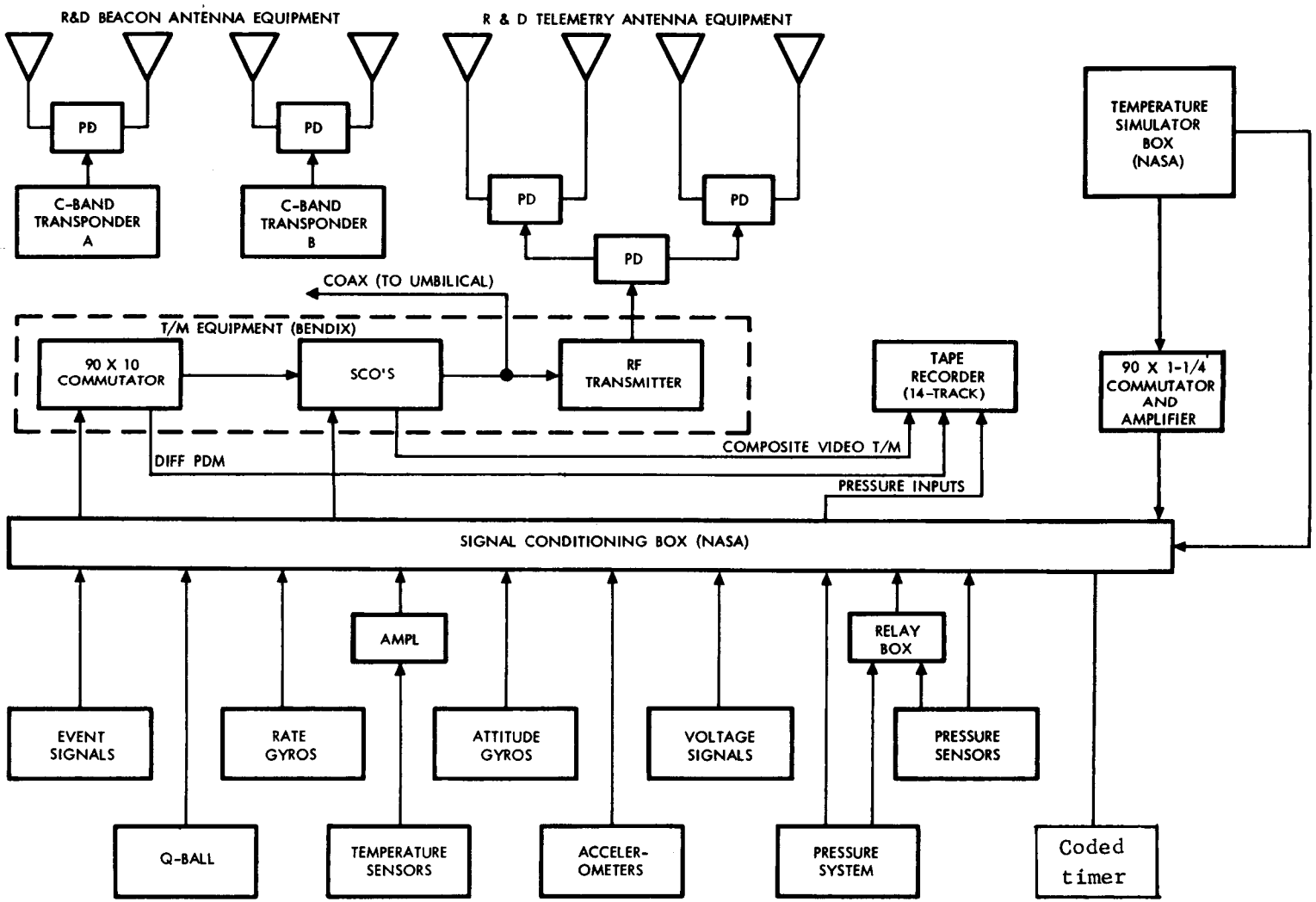

Figure 4.3.1-3.- Communication and instrumentation subsystem block diagram.

[redacted]

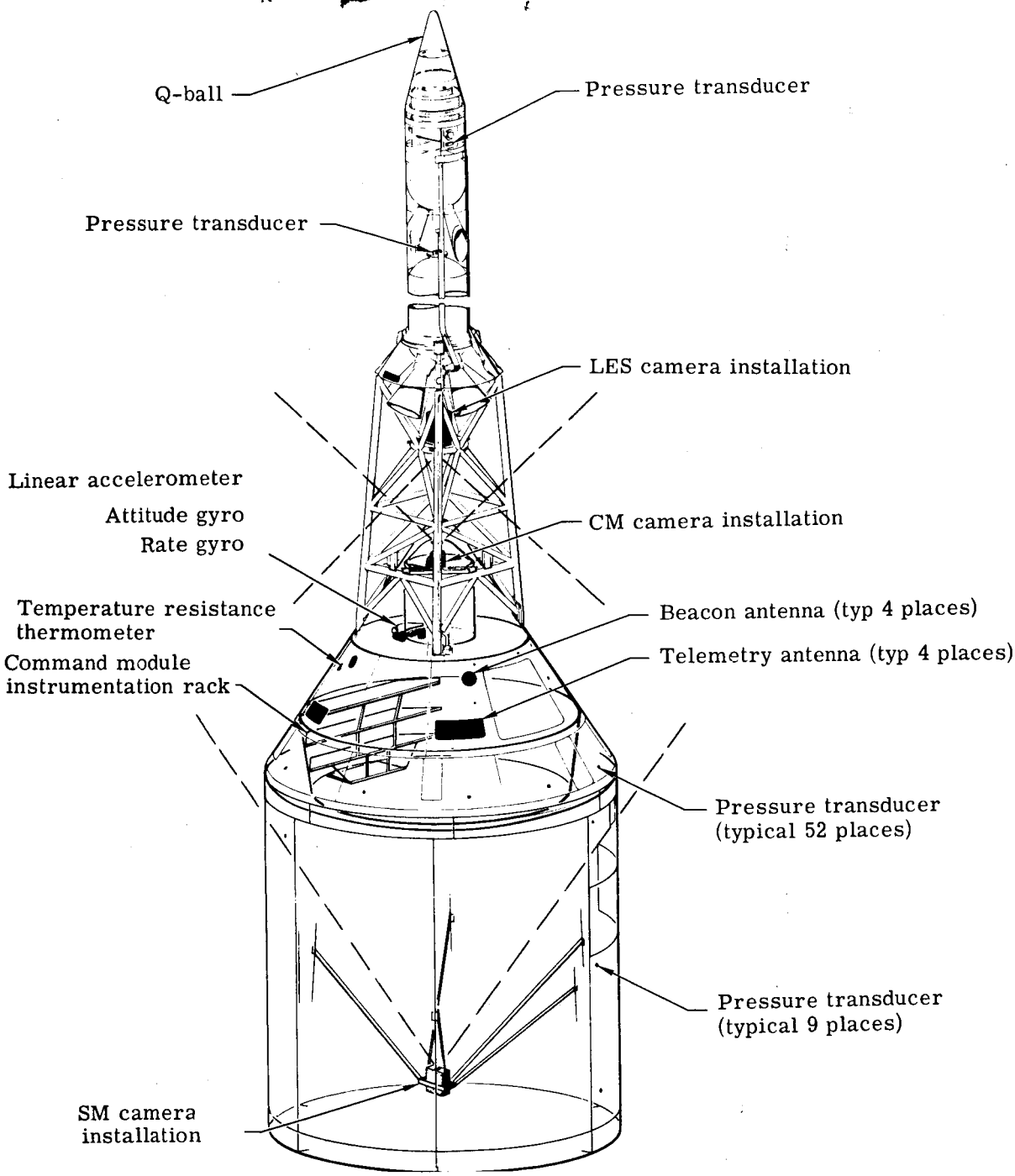

Figure 4.3.1-4.- Communication and instrumentation subsystem component location.

[redacted]

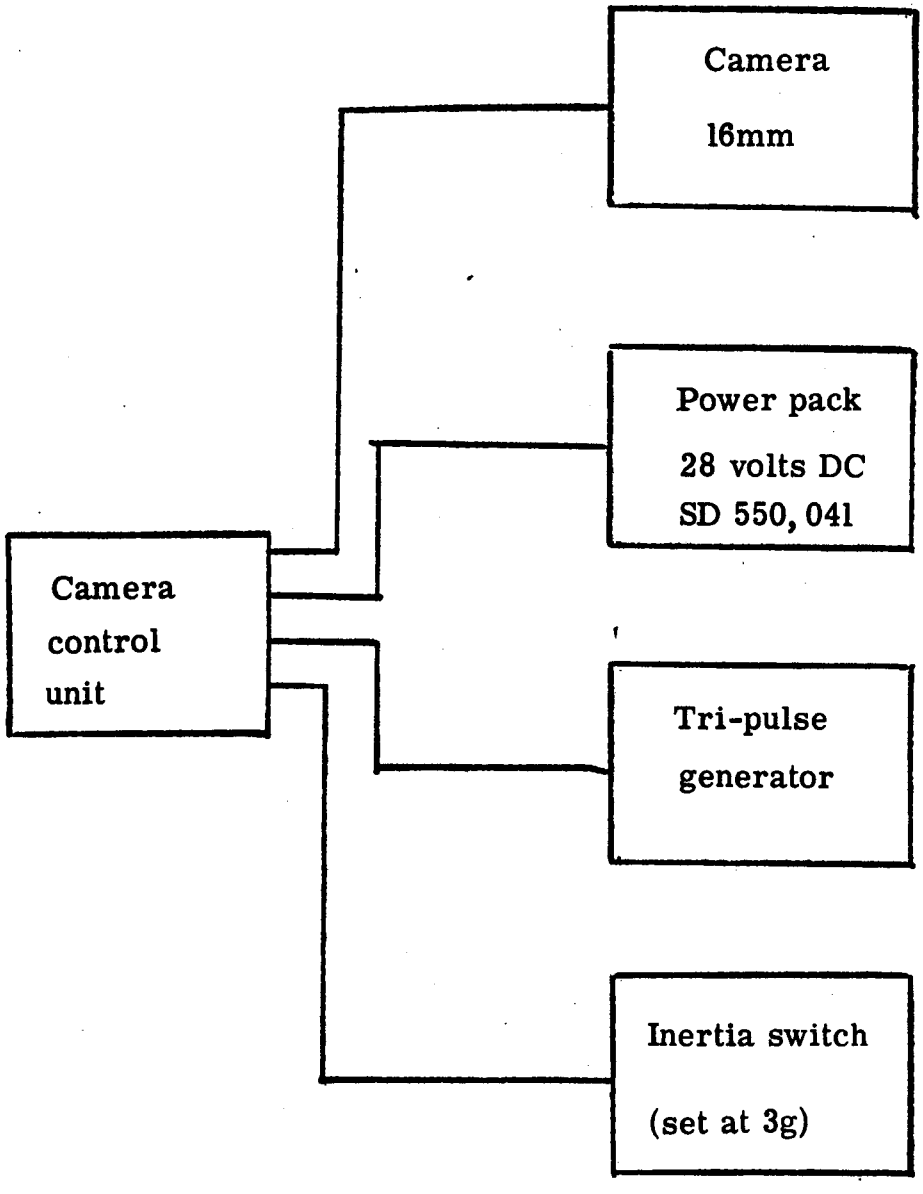

Figure 4.3.1-5.- Boilerplate 12 camera subsystem block diagram. Each camera has a control subsystem as shown.

[redacted]

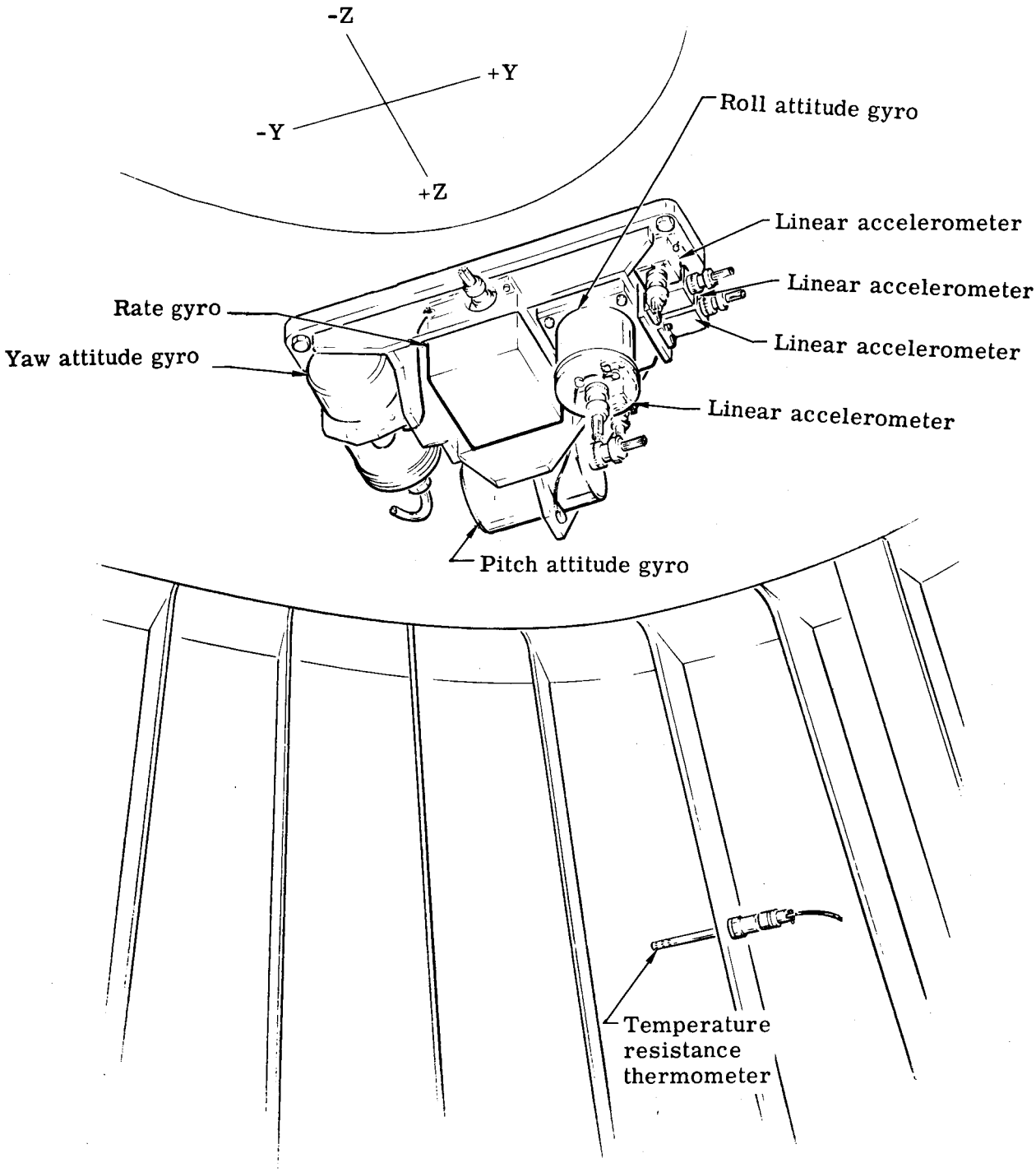

Figure 4.3.1-6. - Linear accelerometer, gyros, and temperature resistance thermometer.

[redacted]

[redacted]

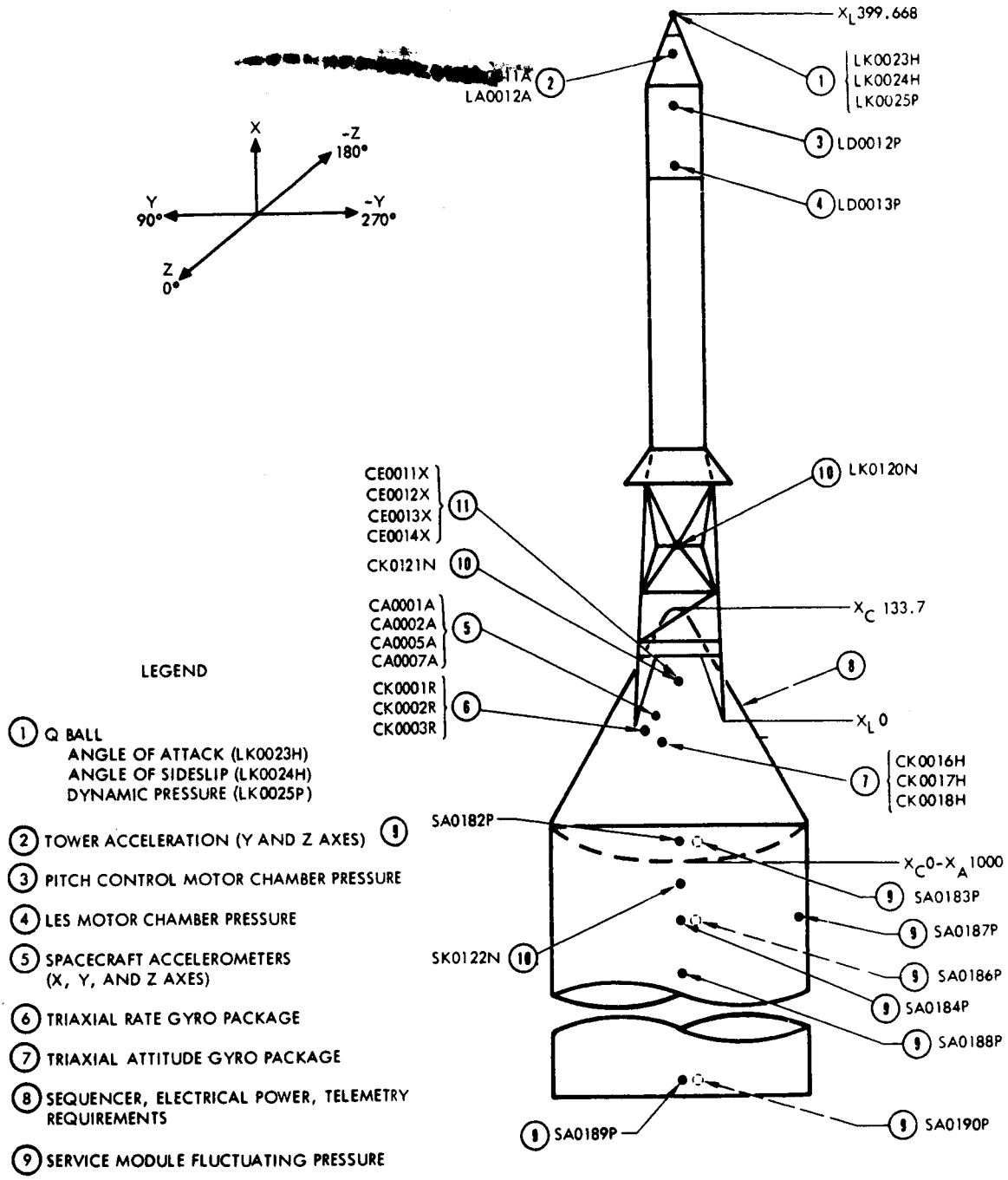

LEGEND

1. Q BALL
   - ANGLE OF ATTACK (LK0023H)
   - ANGLE OF SIDESLIP (LK0024H)
   - DYNAMIC PRESSURE (LK0025P)
2. TOWER ACCELERATION (Y AND Z AXES)
3. PITCH CONTROL MOTOR CHAMBER PRESSURE
4. LES MOTOR CHAMBER PRESSURE
5. SPACECRAFT ACCELEROMETERS (X, Y, AND Z AXES)
6. TRIAXIAL RATE GYRO PACKAGE
7. TRIAXIAL ATTITUDE GYRO PACKAGE
8. SEQUENCER, ELECTRICAL POWER, TELEMETRY REQUIREMENTS
9. SERVICE MODULE FLUCTUATING PRESSURE
10. PHOTOGRAPHIC CAMERA
11. PARACHUTE PHYSICAL MONITOR

● EXPOSED

◌ HIDDEN

Figure 4.3.1-7. - Spacecraft measurement locations.

[redacted]

[redacted]

[redacted]

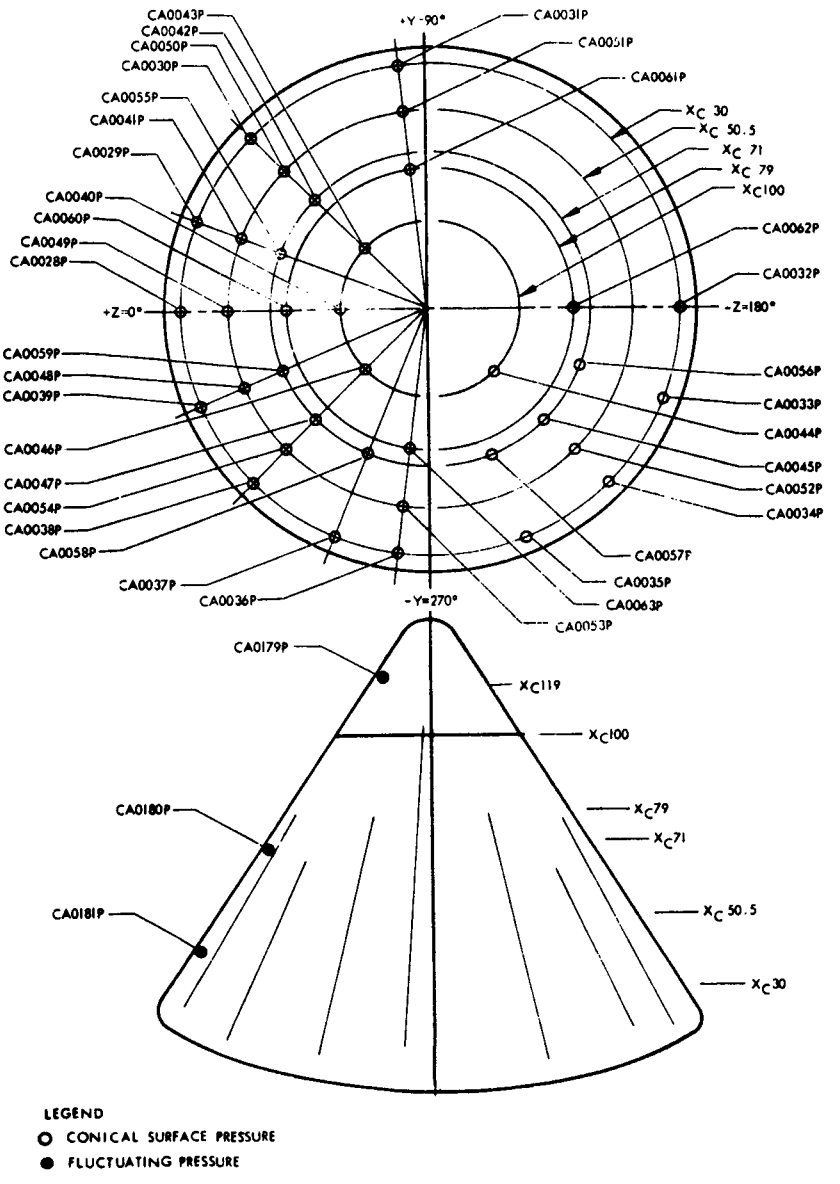

Figure 4.3.1-8. - Command module conical surface and fluctuating pressure measurement locations.

[redacted]

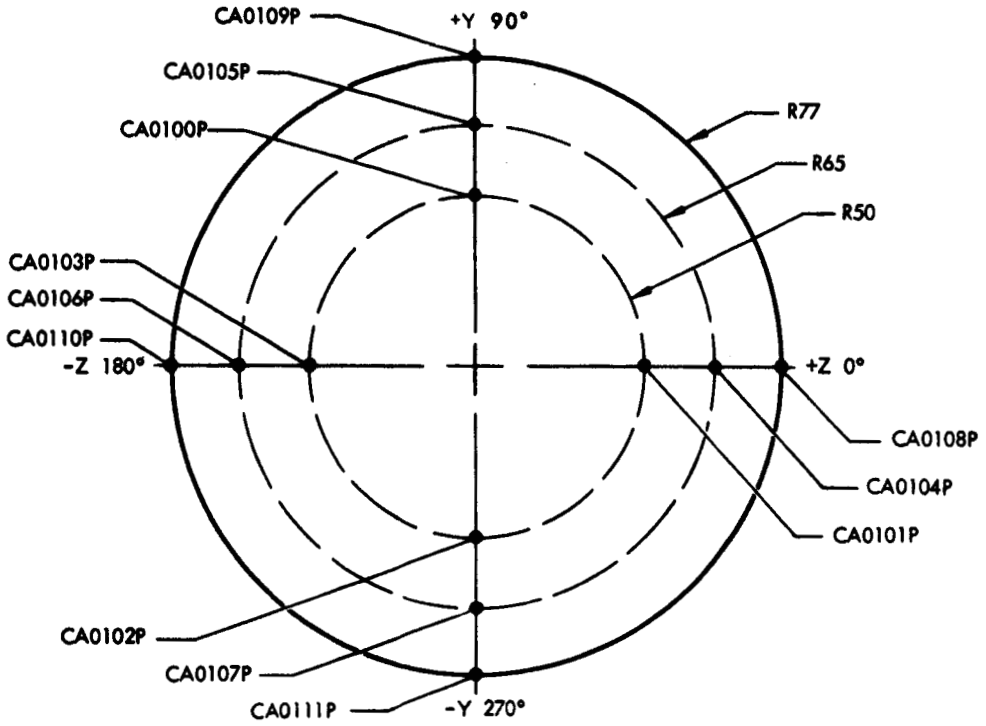

Looking forward

Figure 4.3.1-9. - Command module aft heat shield pressure measurement locations.

[redacted]

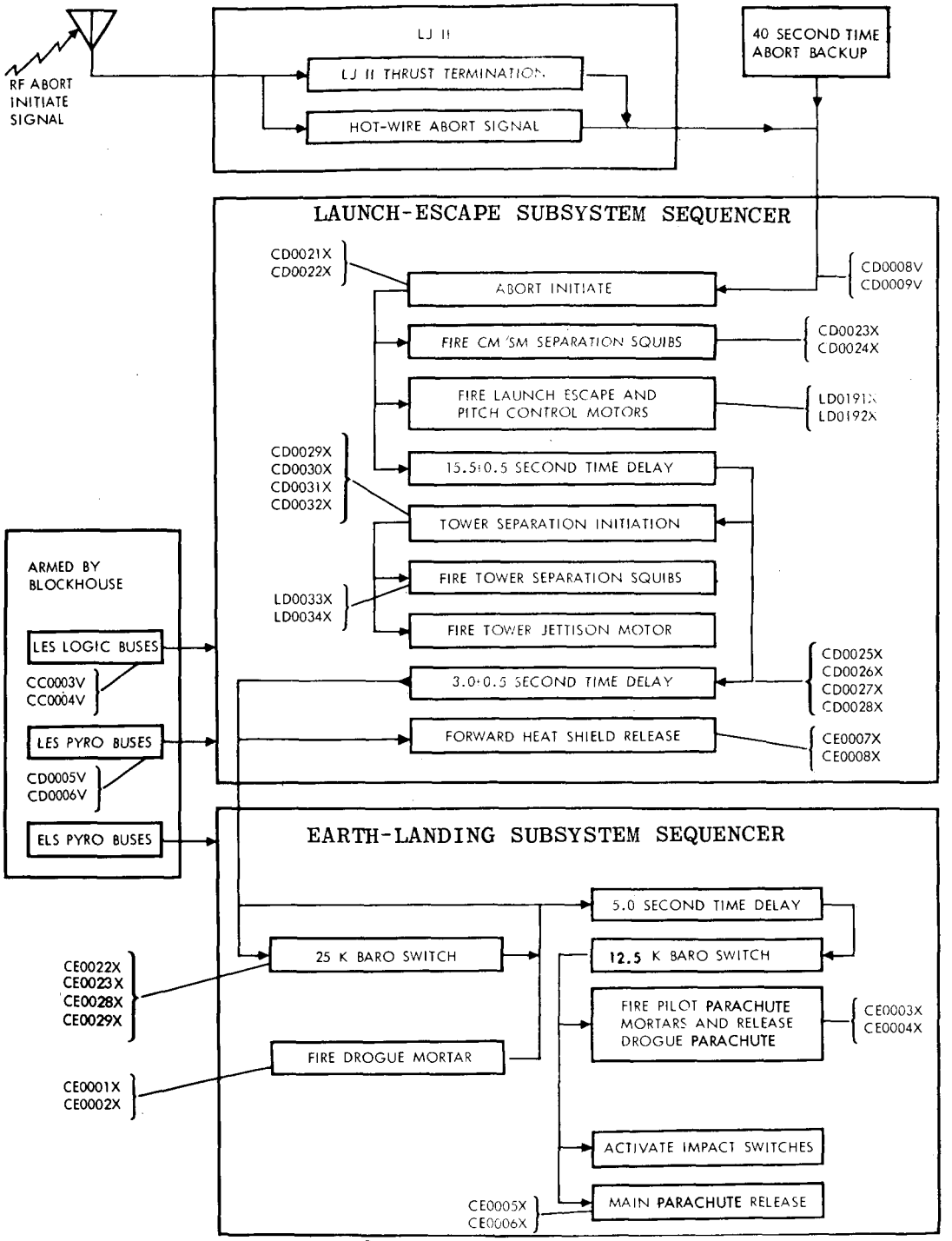

One side of redundant system

Figure 4.3.1-10.- Launch-escape subsystem and earth-landing subsystem sequence measurements.

[redacted]

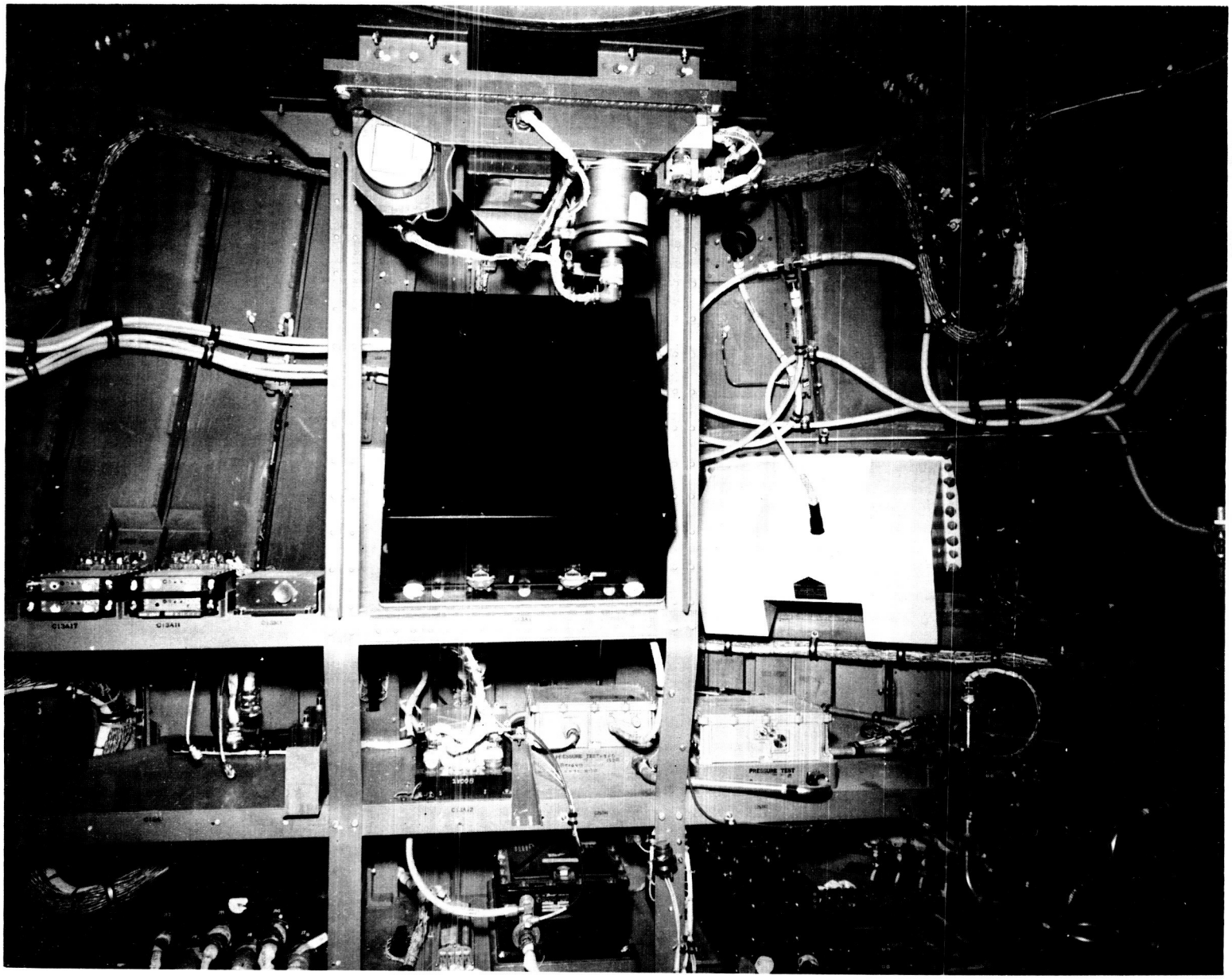

Figure 4.3.1-11. - Boilerplate 12 physical location of primary instrumentation components.

00:00:28.5 CM-SEPARATION
00:00:28.4 LES AND P/C MTR IGNITION
00:00:43.7 LES TOWER JETTISON
00:00:47.1 DROGUE DEPLOYMENT

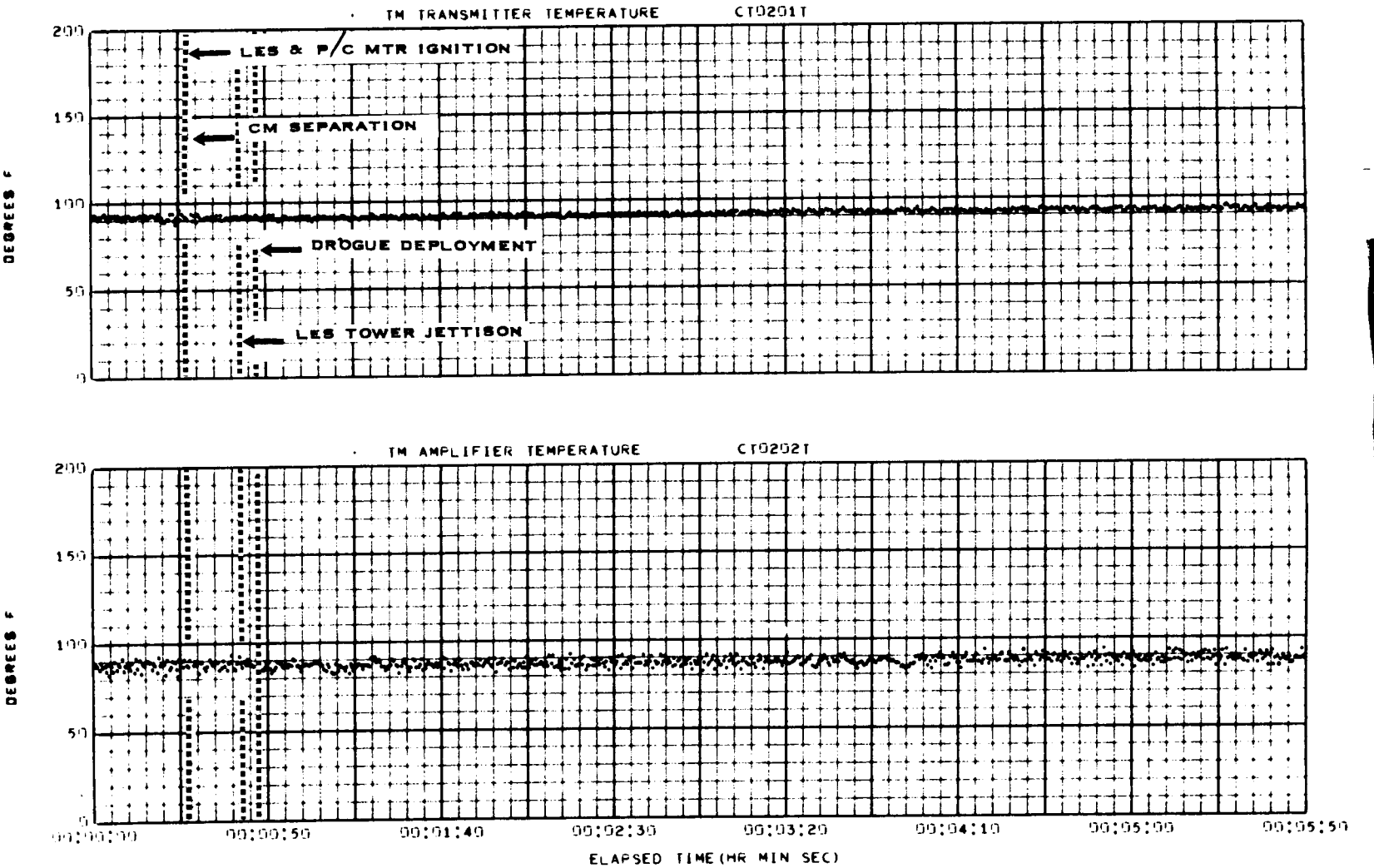

Figure 4.3.1-12. - Telemetry transmitter amplifier temperature plotted against time.

00:00:28.5 CM-SEPARATION
00:00:28.4 LES AND P/C MTR IGNITION
00:00:43.7 LES TOWER JETTISON
00:00:47.1 DROGUE DEPLOYMENT

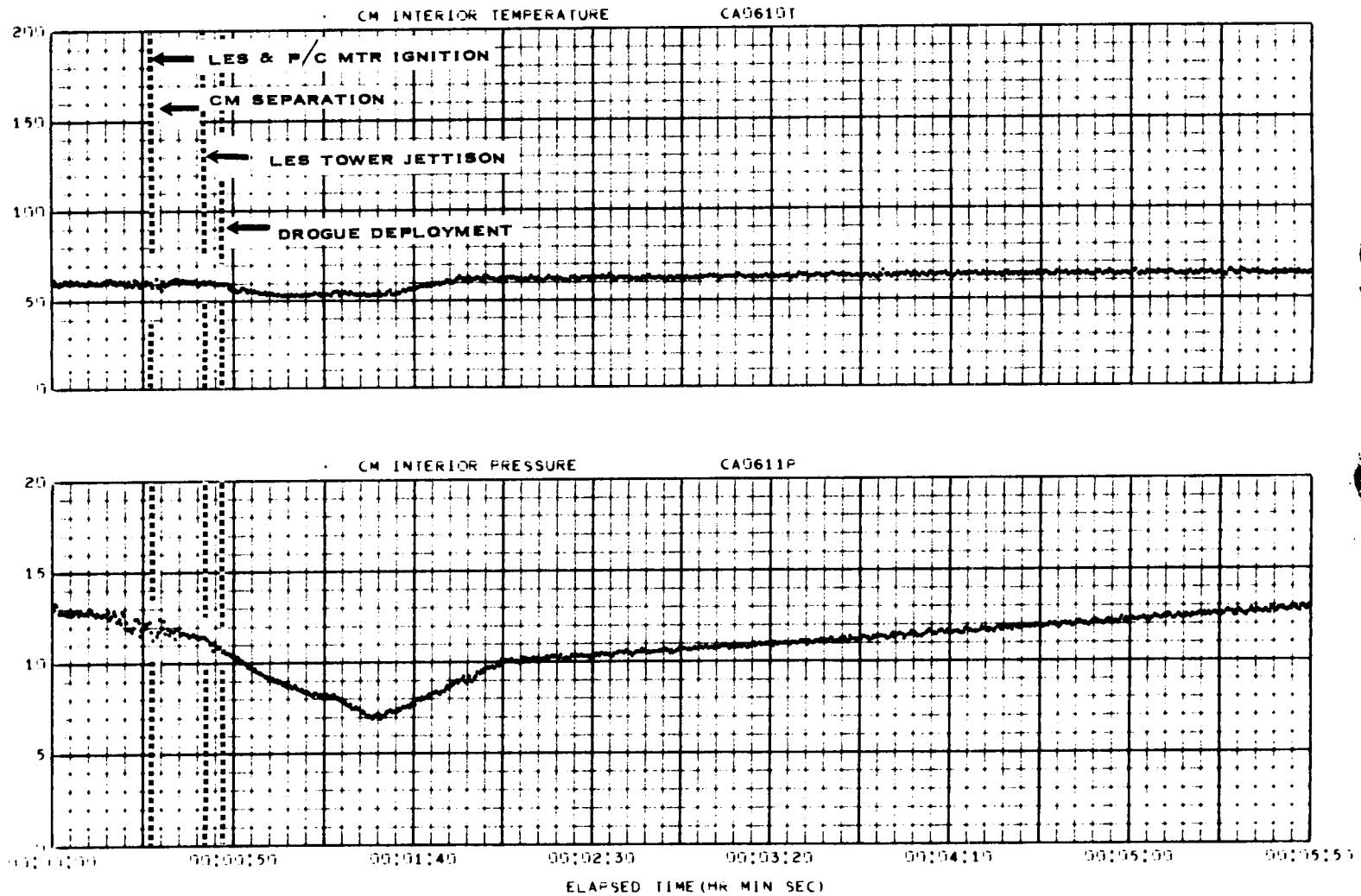

Figure 4.3.1-13. - Command module interior temperature and pressure plotted against time.

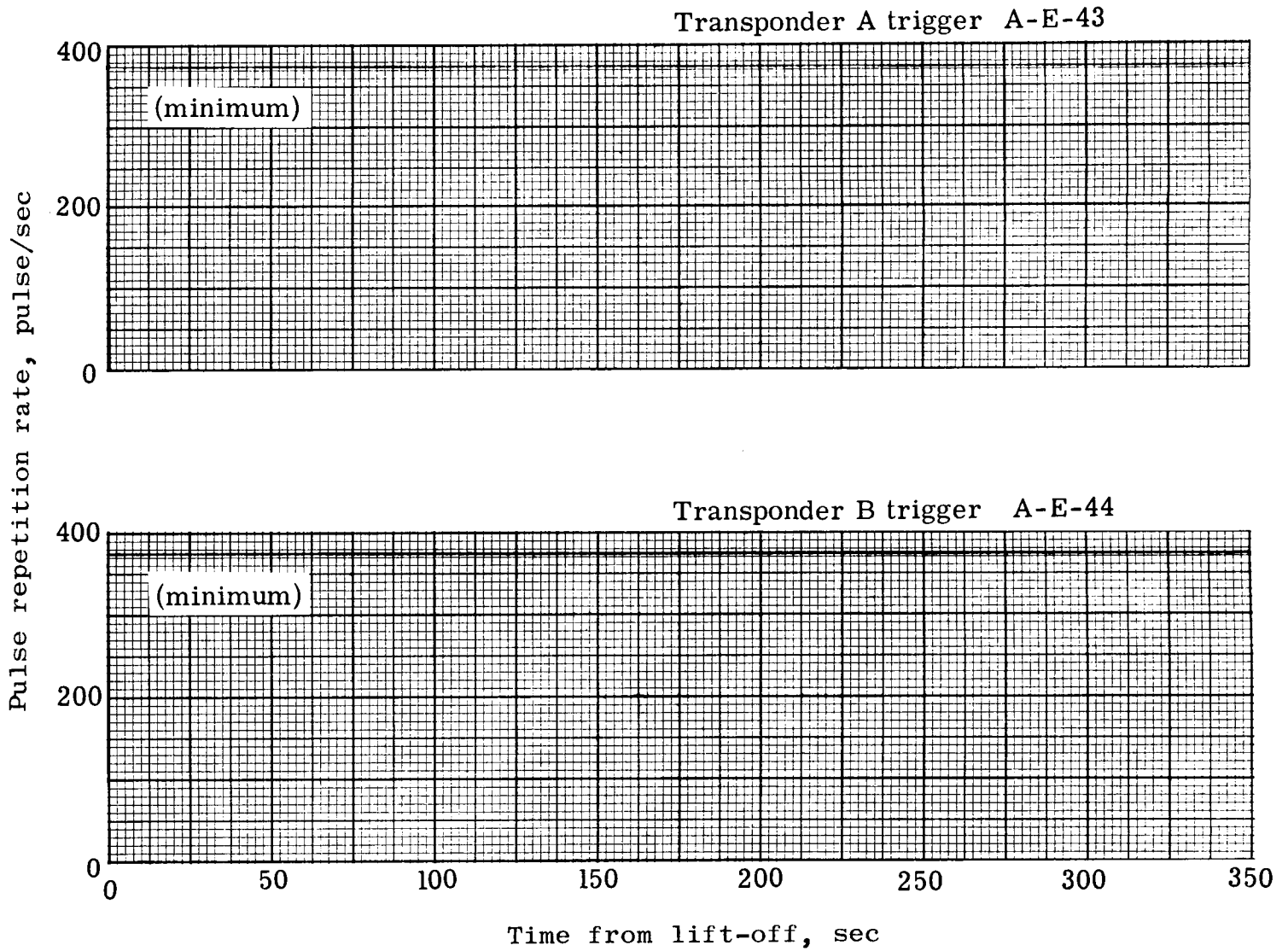

Figure 4.3.1-14.- Transponder A and B trigger pulse repetition rate.

4.3.2 Electrical and sequential subsystems.- The electrical and sequential subsystems on Apollo boilerplate 12 were designed to provide electrical sequencing of electrical power to all power subsystems installed on BP-12.

4.3.2.1 Sequential subsystem: The launch-escape-subsystem (LES) sequencer provides three distinct sequences: command and service module separation and launch-escape and pitch-control motor ignition, jettison-motor ignition and tower separation, and initiation of the earth-landing-subsystem (ELS) sequencer. Figures 4.3.2-1 and 4.3.2-2 show the LES and ELS sequencers in block diagram form.

The LES sequencer operated properly during the flight and all time delays operated within acceptable time limits. The 15.5-second tower jettison/separation from abort time delays operated at 15.66 and 15.76 seconds for channels A and B, respectively. Only side B of channels A and B on the tower jettison-separation 15.5-second timer was monitored. The 3.0-second (from tower jettison) earth-landing subsystem start time delays operated at 2.96 and 2.96 seconds for channel A and 2.96 and 3.06 seconds for channel B.

The ELS sequencer (started by the LES sequencer 3.0 seconds after launch-escape-tower separation) provided the drogue deployment event and the drogue release and pilot parachute mortar firing (5 sec after drogue deployment or upon baroswitch command at an altitude of about 12,500 feet m.s.l).

The ELS sequencer operated properly during the flight and all time delays operated within acceptable time limits during postflight bench tests. The spacecraft did not exceed the 30,000-foot altitude m.s.l. required to operate the 25,000-foot baroswitches during ascent; consequently, no change in telemetry indications was received. These baroswitches have a large deadband, are normally closed at launch, and normally require altitudes in excess of 30,000 feet before they will open. They will close again at 25,000 feet during descent.

The 12,500-foot baroswitches closed at approximately 112.7 seconds after lift-off during descent of the command module. During postflight bench tests, these baroswitches exhibited proper operation by activating at their specified tolerances.

The sequential subsystem contained redundant 41.1-second timers which were to function as a backup event to start the LES sequencer in the event that the radio command abort signal failed to initiate the Little Joe II thrust termination and the LES sequencer. These backup timers allowed sufficient time for the Algol engine to burn out before commencing the abort sequence.

Telemetry data indicated that the 41.1-second timer (backup abort timer), system A, timed out prematurely, approximately at 28.56 seconds +0 -0.1 second after lift-off. Abort occurred at 28.44 seconds after lift-off. System B timed out at 41.39 seconds +0 -0.1 second. The malfunction of the backup timer, system A, occurred 0.12 second +0 -0.1 second subsequent to thrust termination and launch-escape-subsystem sequencer start signal. It is thought at this time that the high g loads experienced by the command module at thrust termination caused the premature time-out of system A. Qualification g loading tests were run on this type of timer. The test required that the timer be subjected to and withstand 20g loading for 5 minutes in all three axes. This qualification test was a centrifuge-type test and not equivalent to a shock acceleration. Further investigation of this inflight malfunction is underway.

4.3.2.2 Electrical subsystem: The electrical subsystem consisted of one 12-ampere-hour (MAP 4095-3) and seven 5-ampere-hour (MAR 4090-9) silver-zinc batteries. Four batteries (MAR 4090-9) supplied power to the redundant logic and pyro busses for the earth-landing-subsystem and launch-escape-subsystem sequencers. Three batteries (MAR 4090-9) supplied power to the command module camera, service module camera, and tower camera. All batteries provided the proper voltage and current to the pyrotechnic devices. Figure 4.3.2-3 shows that the voltage of pyro bus A and B dropped from 33 volts to approximately 30 volts at time of abort. This voltage drop is normal for this type of silver-zinc battery (MAR 4090-9) under pyrotechnic load conditions.

The terminal voltage of the MAR 4090-9 batteries during the postflight load check was approximately the same as for preflight.

At lift-off, the bus B current was approximately 19 amperes, then dropped to approximately 17 amperes at 44 seconds as a result of the Q-ball heater being jettisoned with the launch-escape subsystem.

After flight, the main battery was found to be damaged on a bottom corner. Postflight inspection showed two cells were severely damaged. This damage, however, did not incapacitate the battery during flight.

Each cell (20 total) of the mission A-001 main battery contained 125cc of electrolyte (potassium hydroxide) for flight.

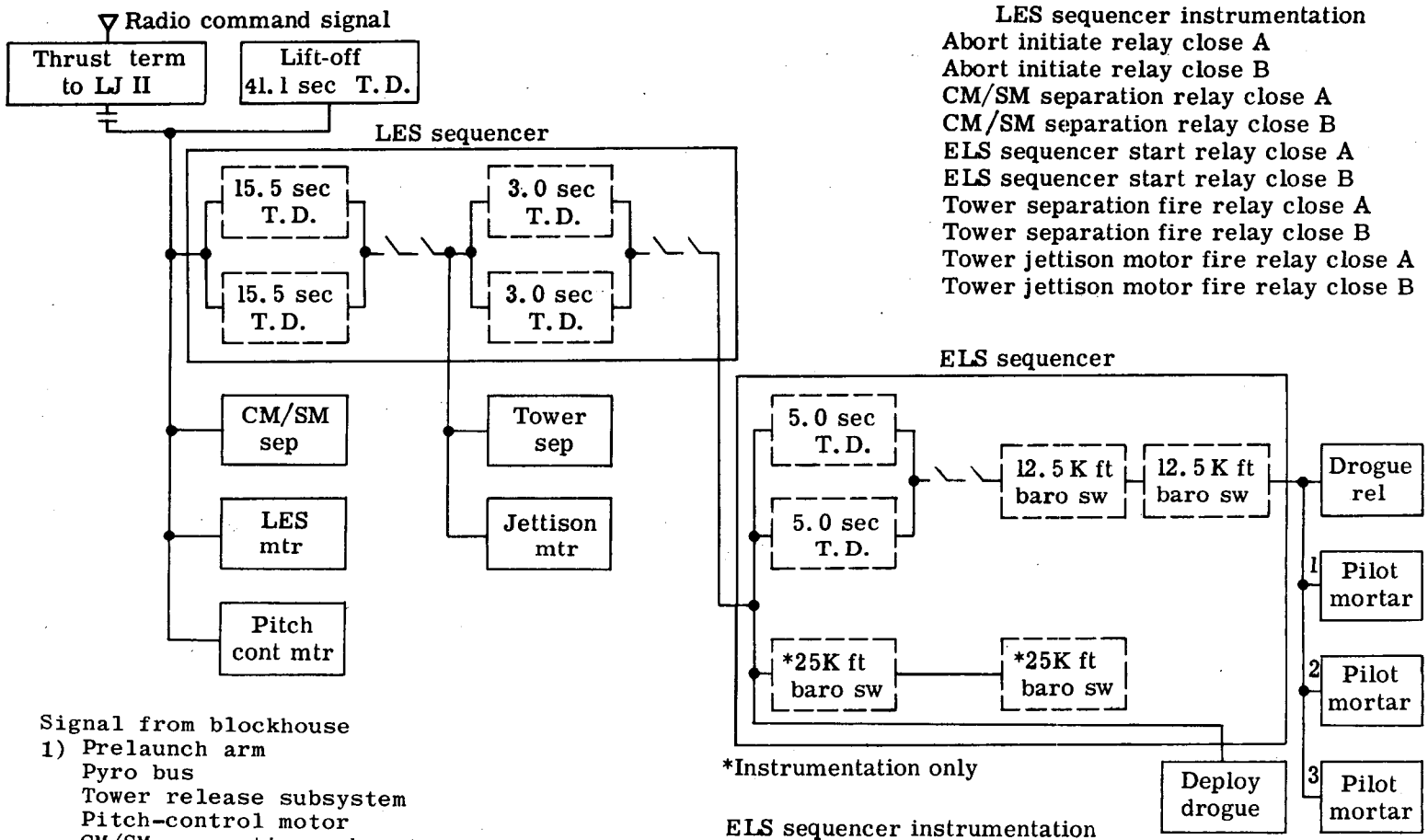

LES sequencer instrumentation
Abort initiate relay close A
Abort initiate relay close B
CM/SM separation relay close A
CM/SM separation relay close B
ELS sequencer start relay close A
ELS sequencer start relay close B
Tower separation fire relay close A
Tower separation fire relay close B
Tower jettison motor fire relay close A
Tower jettison motor fire relay close B

Signal from blockhouse
1) Prelaunch arm
   Pyro bus
   Tower release subsystem
   Pitch-control motor
   CM/SM separation subsystem
   Launch-escape motor
   Earth-landing subsystem
   Arm jettison motor
2) Launch command to LJ II
3) Lift-off, T-0

*Instrumentation only

ELS sequencer instrumentation
Drogue deploy relay close A
Drogue deploy relay close B
Main chute deploy drogue release relay close A
Main chute deploy drogue release relay close B
Barometric switch 1 25,000 feet A
Barometric switch 2 25,000 feet B

Figure 4.3.2-1. - Boilerplate 12 event schedule sequential block diagram.

[redacted]

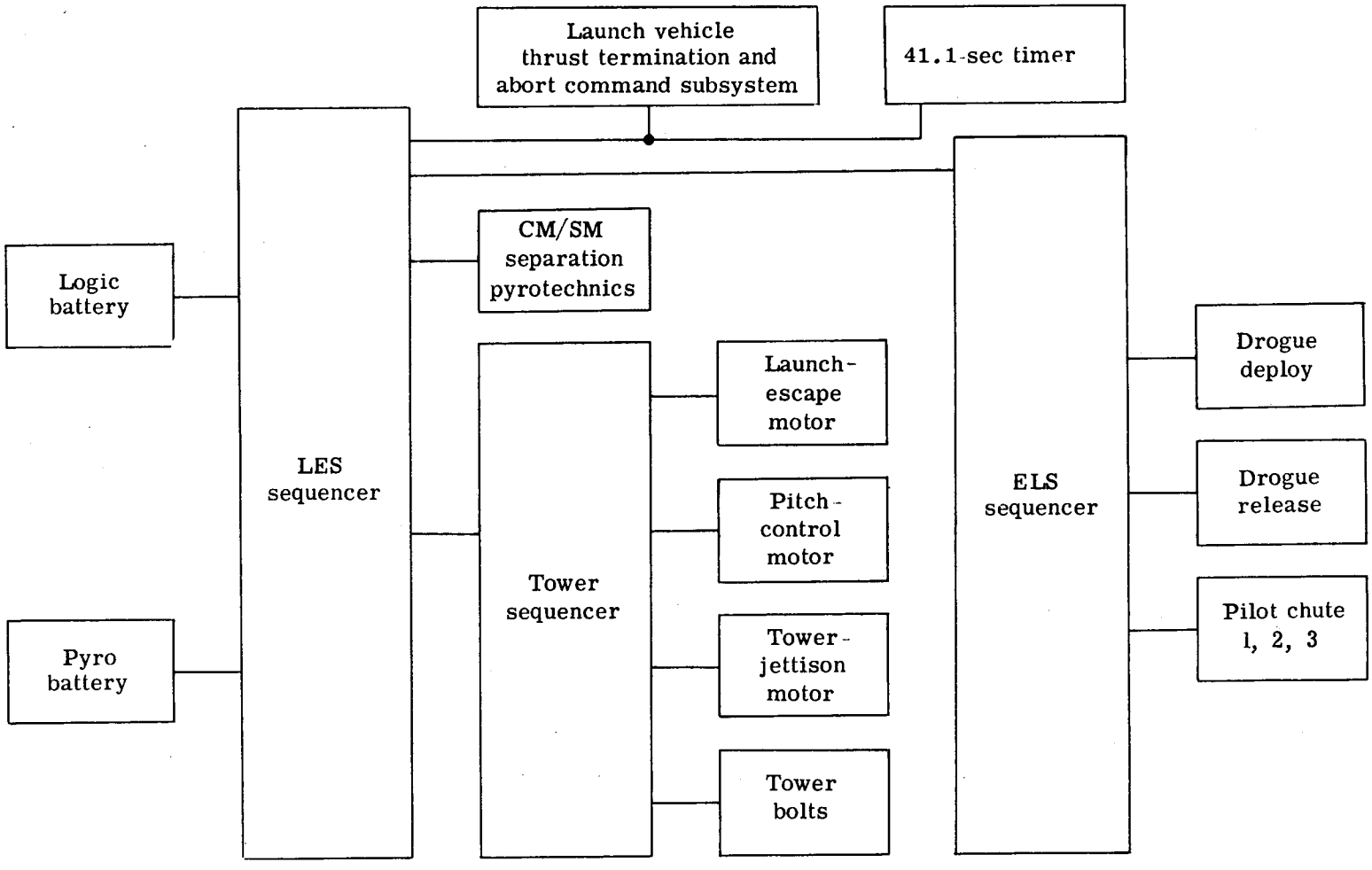

*Note: One side of redundant subsystem

[redacted]

Figure 4.3.2-2. - Boilerplate 12 launch-escape subsystem and earth-landing subsystem block diagram.

00:00:28.5 CM-SEPARATION
00:00:28.4 LES AND P/C MTR IGNITION
00:00:47.1 DROGUE DEPLOYMENT
00:01:52.7 MAIN CHUTE DEPLOYMENT

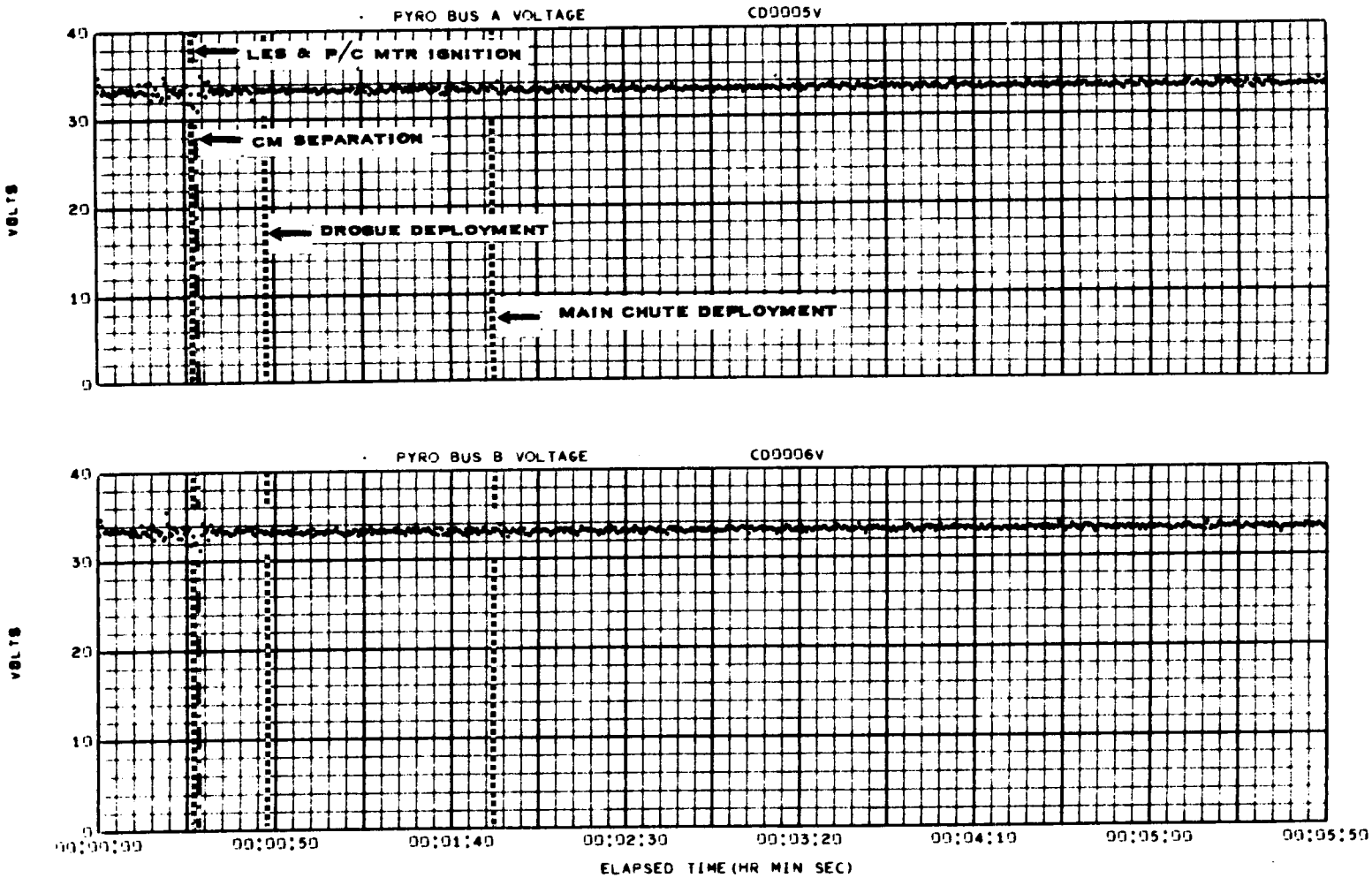

Figure 4.3.2-3. - Time histories of pyro bus voltages.

00:00:28.5 CM-SEPARATION
00:00:28.4 LES AND P/C MTR IGNITION
00:00:47.1 DROGUE DEPLOYMENT
00:01:52.7 MAIN CHUTE DEPLOYMENT

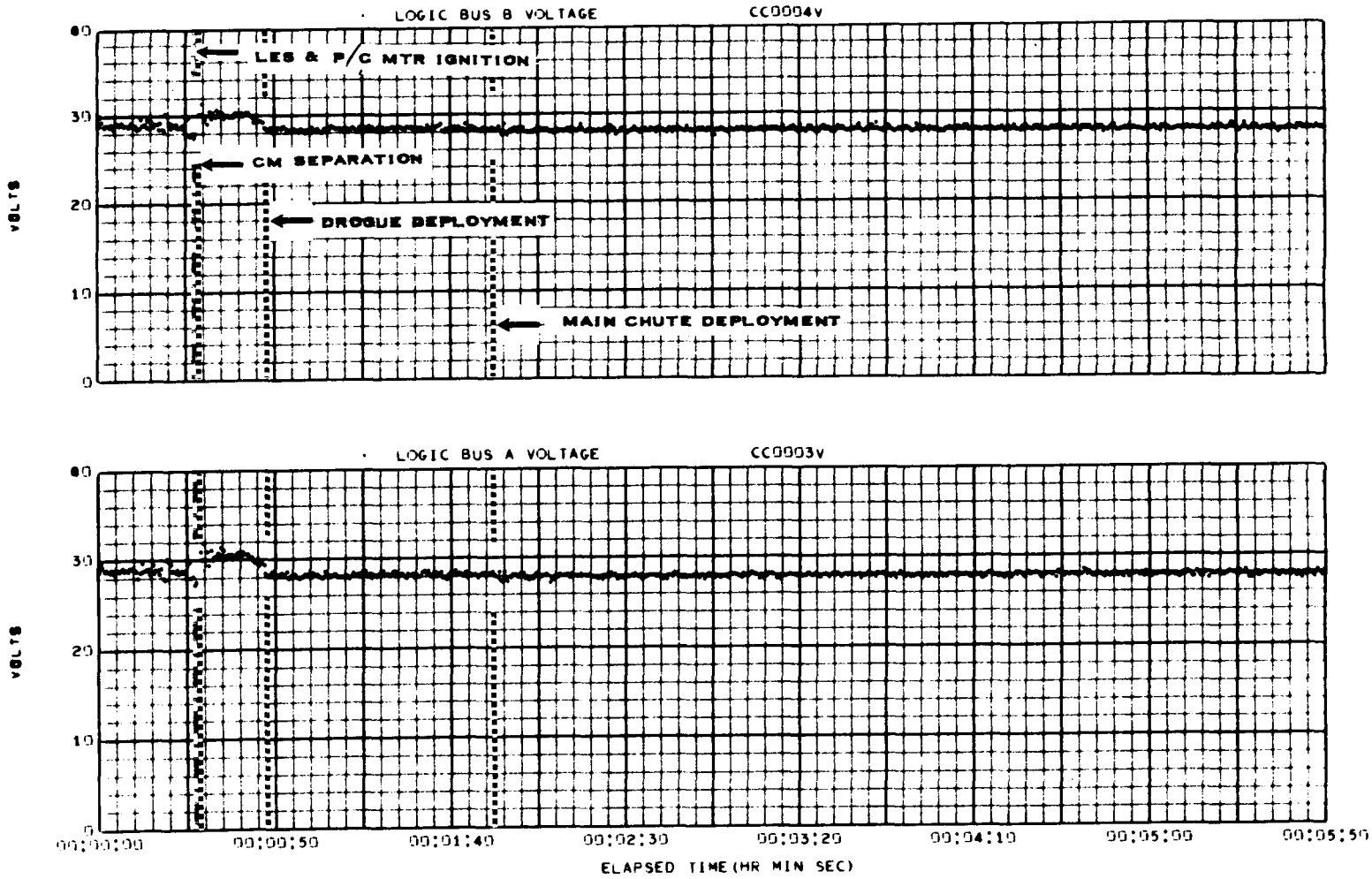

Figure 4.3.2-4. - Time histories of logic bus voltages.

00:00:28.5 CM-SEPARATION
00:00:28.4 LES AND P/C MTR IGNITION
00:00:47.1 DROGUE DEPLOYMENT
00:01:52.7 MAIN CHUTE DEPLOYMENT

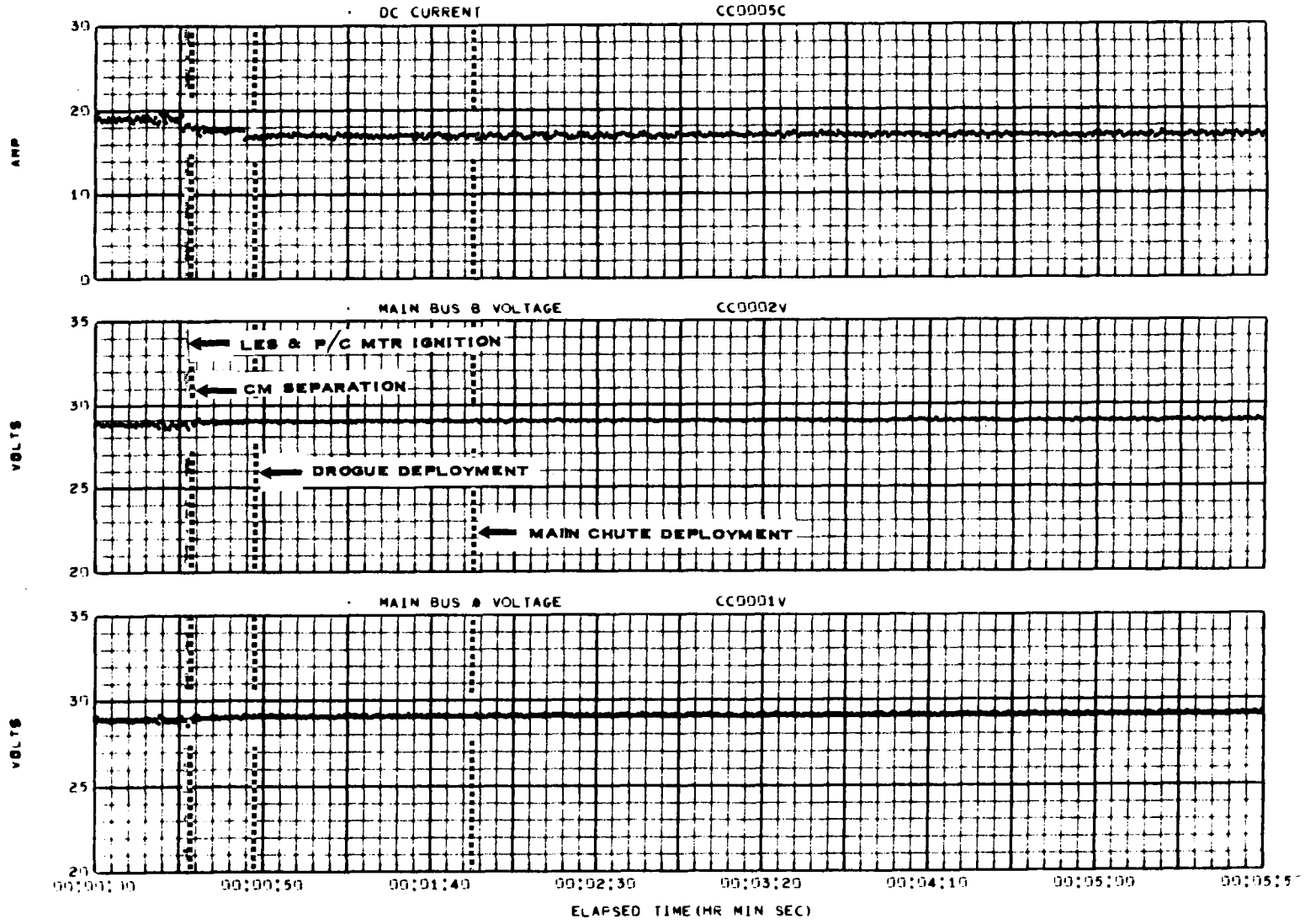

Figure 4.3.2-5.- Time histories d-c current and main bus voltages.

[redacted]

4.3.3 Launch-escape-propulsion subsystem.- The launch-escape-propulsion subsystem (LES) adequately performed its intended purposes of removing the command module from the launch vehicle, applying a pitching moment to the LES to remove it from the flight path of the launch vehicle, and removing the launch-escape tower from the command module and from the flight path of the command module.

Motor performance instrumentation (chamber pressure measurement) was programed for the launch-escape and pitch-control motors. During the test, the pressure data for the launch-escape motor were lost because of an instrumentation malfunction. Pressure data obtained from the pitch-control motor indicated below specification operation for that motor. No instrumentation was programed for the tower-jettison motor.

The thrust level of the pitch-control motor was calculated from the recorded chamber pressure by the equation

$$F = P_c A_t C_{f(VAC)} C_D - P_a A_e$$

where:

F = actual delivered thrust at altitude, lb

P_c = corrected delivered chamber pressure, psia

A_t = nozzle throat area = 1.19 sq in.

$C_{f(VAC)}$ = vacuum thrust coefficient = 1.28

C_D = thrust correction factor at time of thrust

P_a = ambient pressure at time of thrust, psia

A_e = nozzle exit area = 1.404 sq in.

The thrust correction values used for the pitch-control motor are shown in figure 4.3.3-1. Ambient pressure data were obtained from meteorological and cinetheodolite data, figures 4.1.2-1 and 4.1.2-2, respectively.

[redacted]

The grain condition temperatures of the launch-escape motor, pitch-control motor, and tower-jettison motor were approximately 70° F. Since the predicted data for the motors assumed a grain temperature of 70° F, no adjustment to the data was necessary for temperature differences.

4.3.3.1 Launch-escape motor: The launch-escape motor was designed to provide propulsive force to remove the command module safely from the launch vehicle for a mission abort during the time period from final countdown until approximately 35 seconds into Saturn V second-stage burning.

Location of the motor, with respect to the complete test vehicle, is shown in figure 3.0-1, and with respect to the LES in figure 4.3.3-2. A motor configuration diagram is shown in figure 4.3.3-3.

The motor uses a case-bonded, solid propellant of polysulfide fuel binder and ammonium perchlorate oxidizer in an 8-point, internal-burning, star configuration. Four nozzles spaced 90° apart are canted 35° outward from the longitudinal axis. The purpose of the nozzle cant angle is to reduce the flame impingement on the command module. A nominal thrust-vector offset of 2°45' (from the motor center line) is provided by an oversize and an undersize nozzle in the pitch plane. The thrust-vector offset is provided so that the thrust vector passes more nearly through the center of gravity of the launch-escape vehicle. The four nozzles have graphite throat inserts and fiberglass-phenolic exit cones. Polyurethane blowout closures are glued in each nozzle throat to provide a sealed environment inside the motor during handling and storage.

The launch-escape motor is ignited by a pyrogen-type igniter, which incorporates redundant initiators. The igniter is mounted in the forward end of the motor, concentric with the longitudinal axis. The igniter propellant is the same formulation as the propellant used in the motor. Redundant pyrotechnic initiators of the hot bridgewire type are used to ignite boron-potassium nitrate pellets which ignite the igniter propellant. The nominal thrust level for the launch-escape motor during the first 2 seconds of burning is 155,000 pounds at an altitude of 36,000 feet when the motor grain is conditioned to an average temperature of 70° F. Because of the instrumentation malfunction of the launch-escape-motor pressure data, no valid determination of motor thrust can be made. A postflight test, conducted on the instrumentation circuitry for the pressure measurement to the point where the electrical wiring was separated from the command module, revealed that the instrumentation malfunction occurred in the tower electrical circuitry or in the pressure transducer itself. The electrical wiring from the command module to the launch-escape motor pressure transducer was destroyed as a result of the mission and could not be checked.

[redacted]

In an effort to define the performance of the motor more clearly, the maximum expected deviation of predicted motor performance of ±6 percent was determined and appropriate flight trajectories were calculated at the maximum and minimum performance conditions. (Statistically calculated limits from the development motor program indicate that 95 percent of the motors to be tested will perform within the predicted performance value ±6 percent.) The trajectory calculations reveal that the launch-escape motor did perform within the predicted limits. Analysis of accelerometer data also indicates that web burning time occurred approximately as predicted.

The predicted performance data for the launch-escape motor are presented in table 4.3.3-1. The maximum and minimum thrust values used in the trajectory analysis are presented in figure 4.3.3-4. Review of the flight motion pictures reveals that the first indication of flame from the motor occurred at 28.56 seconds after vehicle lift-off.

4.3.3.2 Pitch-control motor: The pitch-control motor is designed to provide a positive pitching moment to change the initial attitude of the command module in order to remove the command module from the flight path of the launch vehicle. The location of the motor with respect to the complete test vehicle is shown in figure 3.0-1, and with respect to the LES in figure 4.3.3-2. A motor configuration diagram is shown in figure 4.3.3-5.

The pitch-control motor utilizes a case-bonded, polysulfide-ammonium perchlorate, solid propellant cast into a 14-point, internal-burning, star configuration. It has one nozzle containing a graphite throat insert housed in a steel structural shell. A polyurethane blowout closure is glued into the nozzle to provide a sealed environment inside the motor during handling and storage.

The motor is ignited by a pellet-type igniter which is mounted in the head end of the motor, concentric with the longitudinal axis. Redundant hot bridgewire pyrotechnic initiators are used to ignite the boron potassium nitrate pellets which ignite the motor propellant. Total nominal impulse for the motor is 1,700 ±51 pound-seconds (specification value).

The pitch-control motor ignited satisfactorily, and performed its intended function of applying a positive pitching moment to the LES. The motor ignition signal was received by the flight vehicle at 28.44 seconds after vehicle lift-off. First indication of pressure occurred 28.54 seconds after lift-off and 0.10 second after the signal was received. Flight motion pictures reveal that first flame from the motor occurred at 28.51 seconds after lift-off.

[redacted]

The actual pitching moment applied by the pitch-control motor was below the value predicted because of a low performance of the motor. Actual total impulse of the motor was 1,607 pound-seconds, which is below the minimum value of 1,649 pound-seconds. At present, no explanation for the low performance has been found. Complete performance data are presented in table 4.3.3-1 and figure 4.3.3-6.

4.3.3.3 Tower-jettison motor: The tower-jettison motor was designed to provide the propulsive force for removing the launch-escape subsystem from the flight vehicle for a normal mission after approximately 35 seconds of Saturn V second-stage burning, and from the command module during an abort mission, when the abort occurs prior to approximately 35 seconds of Saturn second-stage burning.

The location of the motor with respect to the complete test vehicle is shown in figure 3.0-1 and with respect to the LES in figure 4.3.3-2. A motor configuration diagram is shown in figure 4.3.3-7.

The motor uses a case-bonded, polysulfide-ammonium perchlorate, solid propellant cast into an internal-burning, 10-point, star configuration.

Two scarfed nozzles spaced 180° apart are canted 30° outward from the motor longitudinal axis. The nozzles are scarfed for aerodynamic consideration of the launch-escape subsystem. A thrust-vector offset of 2°30' from the motor longitudinal axis is provided by a 10-percent larger throat area in one nozzle. The purpose of the thrust-vector offset is to remove the launch-escape subsystem from the flight path of the command module. The two nozzles have graphite throat inserts and steel exit cones. Polyurethane blowout closures are glued in each nozzle throat to provide a sealed environment inside the motor during handling and storage. The motor has an integral interstage structure which houses the nozzles.

The tower-jettison motor is ignited by a pyrogen-type igniter which is mounted in the aft end of the motor between the nozzles concentric with the motor centerline. The igniter propellant is of the same formulation as the propellant used in the motor. Redundant hot bridgewire pyrotechnic initiators ignite the boron potassium nitrate pellets, which ignite the igniter propellant.

The nominal thrust level of the tower-jettison motor is 33,000 pounds at 70° F and sea-level atmospheric pressure. The nominal web burning time is 1 second and total operating time is 1.3 seconds.

The tower-jettison motor operated satisfactorily and successfully removed the launch-escape tower from the command module. No instrumentation capability was provided and therefore specific motor performance

[redacted]

data are unavailable. Trajectory data indicated that the motor performed approximately as predicted. Tabulated motor predicted performance data are presented in table 4.3.3-1 and graphical presentation of the predicted motor thrust is presented in figure 4.3.3-8.

Upon impact, the launch-escape motor forward section, pitch-control motor, and tower-jettison motor were compressed into the central chamber area of the launch-escape motor. The aft closure and nozzle bases of the launch-escape motor were still intact upon recovery. The nozzle exit cones and tower structure were completely broken away from the launch-escape motor (see fig. 5.5.1-8), all damage occurring upon impact. The graphite throat insert of the launch-escape motor contained cracks and the forward portion of two inserts were broken off, but the general condition of the inserts was very good, with very little throat erosion being exhibited. The forward chamber area of the launch-escape motor was ripped in numerous strips along the longitudinal axis (see fig. 5.5.1-9).

The launch-escape motor aft closure and nozzle bases exhibited slight blistering and discoloration of the painted surface as a result of heat soak and/or recirculation of the exhaust gases.

4.3.3.4 Postflight analysis: A visual inspection of the command module revealed considerable areas of soot and smoke deposits in line with the launch-escape-motor nozzles. The most severe case of deposit was in the +Z plane, where a small area of the paint on the aft heat shield was burned away. Heat and soot effects upon the command module of BP-12 appeared slightly more severe than those experienced on the BP-6 (pad abort test) conducted on November 7, 1963.

The operational performance of the launch-escape-propulsion subsystem was satisfactorily demonstrated with the test flight of the Apollo boilerplate 12 test vehicle. The launch-escape motor removed the command module from the launch vehicle and the pitch-control and launch-escape motors successfully removed the command module from the flight path of the launch vehicle; however, actual pitch-control motor performance was below the minimum specification value. The tower-jettison motor successfully removed the launch-escape tower from the command module.

One malfunction concerning the launch-escape-propulsion subsystem occurred during the test: the failure of the pressure data instrumentation for the launch-escape motor. The failure has been isolated to have occurred within the tower electrical circuitry or the pressure transducer on the motor which was substantially damaged at impact precluding further analysis.

[redacted]

TABLE 4.3.3-1.- MOTOR PERFORMANCE SUMMARY

Parameter	Launch-escape motor[a]	Pitch-control motor		Tower-jettison motor[d]
	Predicted	Predicted	Actual	Predicted
Web burn time average thrust, lb	145,000	2,315	2,000	31,500
Maximum thrust, lb	157,300	2,535	2,490	33,700
Total impulse, lb-sec	586,000	1,726	1,607	36,650
Web burn time average pressure, psia . .	1,340	1,480	1,350	1,368
Maximum chamber pressure, psia	1,473	1,611	1,637	1,450
Action time, sec	6.00	1.10	1.01	1.28
Web burn time, sec	3.11	0.68	0.67	1.08
Total time, sec	8.55	1.52	1.50	1.35
Thrust rise time, sec	0.099	0.10	NA[b]	0.105
Ignition delay time, sec	0.043	0.018	0.07[c]	0.03 to 0.04
Propellant weight, lb	3,153	9.42	9.42	205.6

[a]Launch-escape motor chamber pressure data not obtained.

[b]Noise in data prevents accurate determination of this value.

[c]Accuracy of this parameter is questionable because of noise in data.

[d]Tower-jettison motor not instrumented.

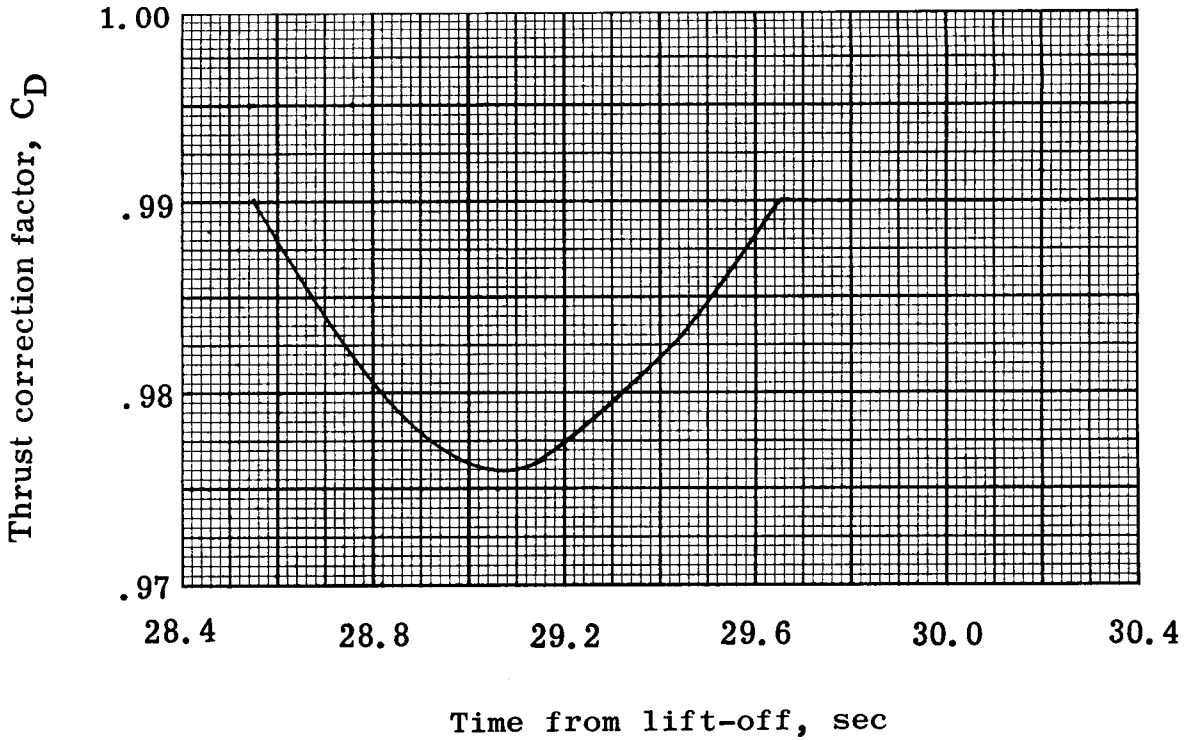

Figure 4.3.3-1.- Pitch-control motor thrust correction factor plotted against time.

[redacted]

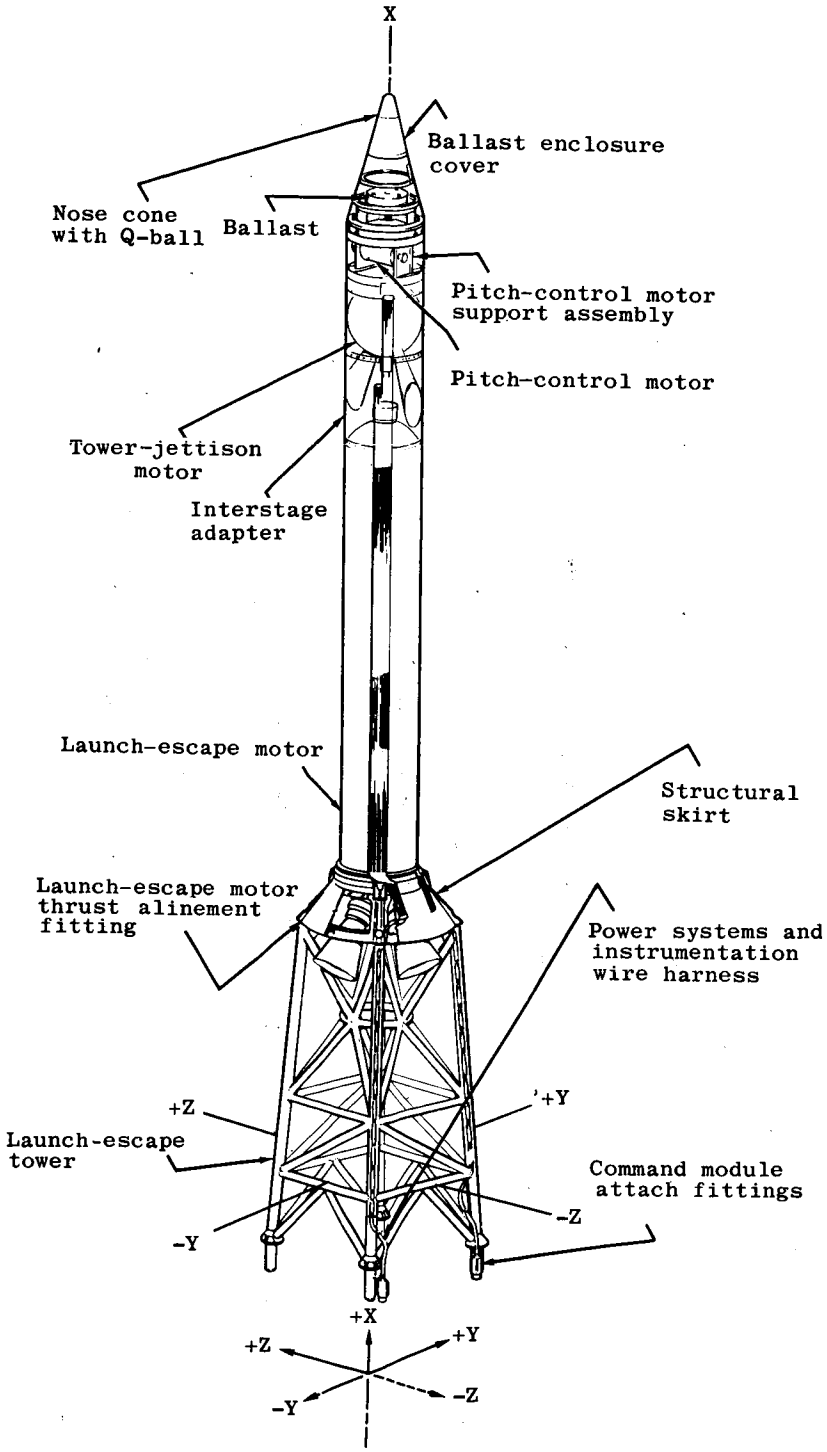

Figure 4.3.3-2. - Launch-escape subsystem diagram.

[redacted]

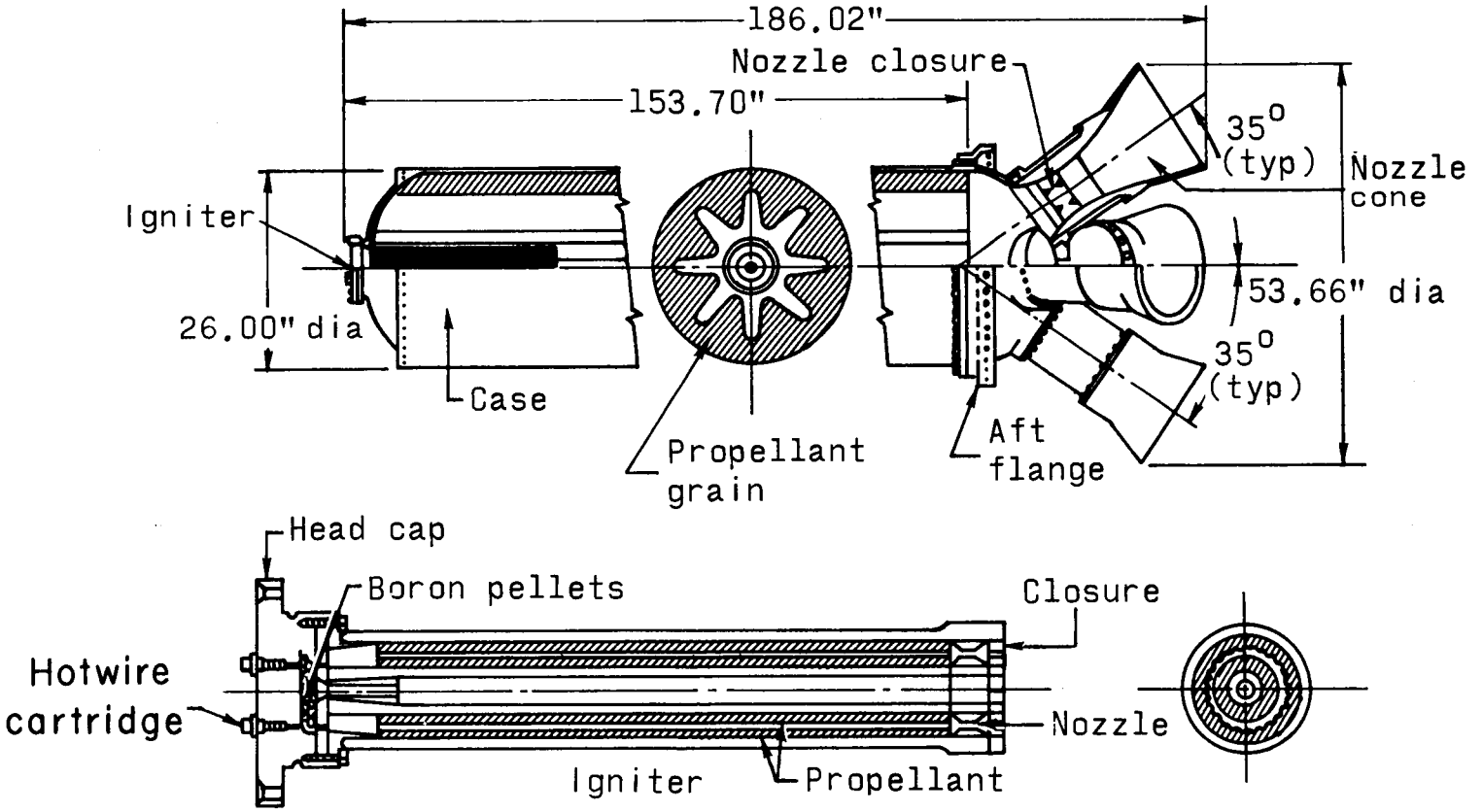

Figure 4.3.3-3. - Launch-escape motor diagram.

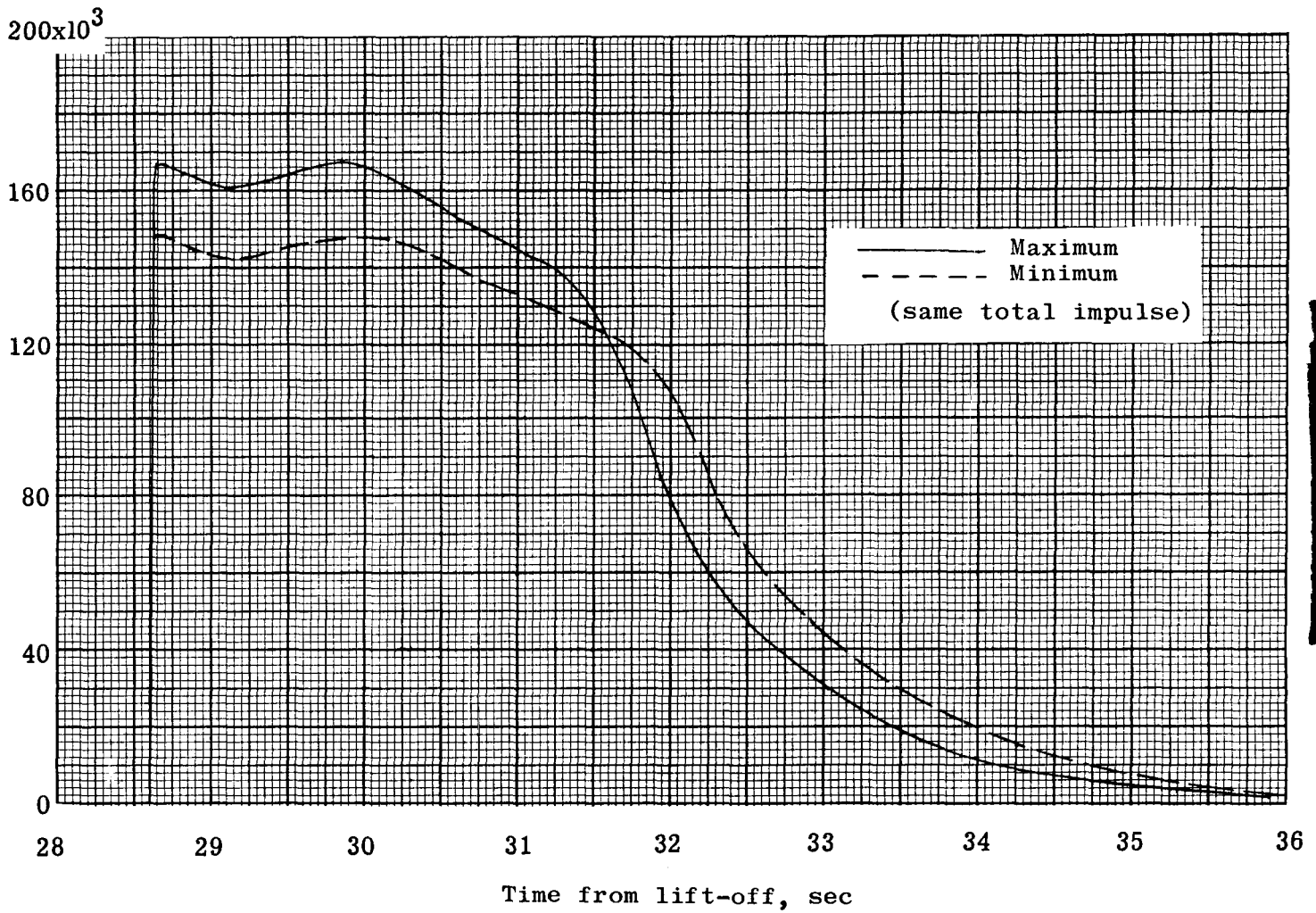

Figure 4.3.3-4. - Launch-escape motor predicted thrust plotted against time.

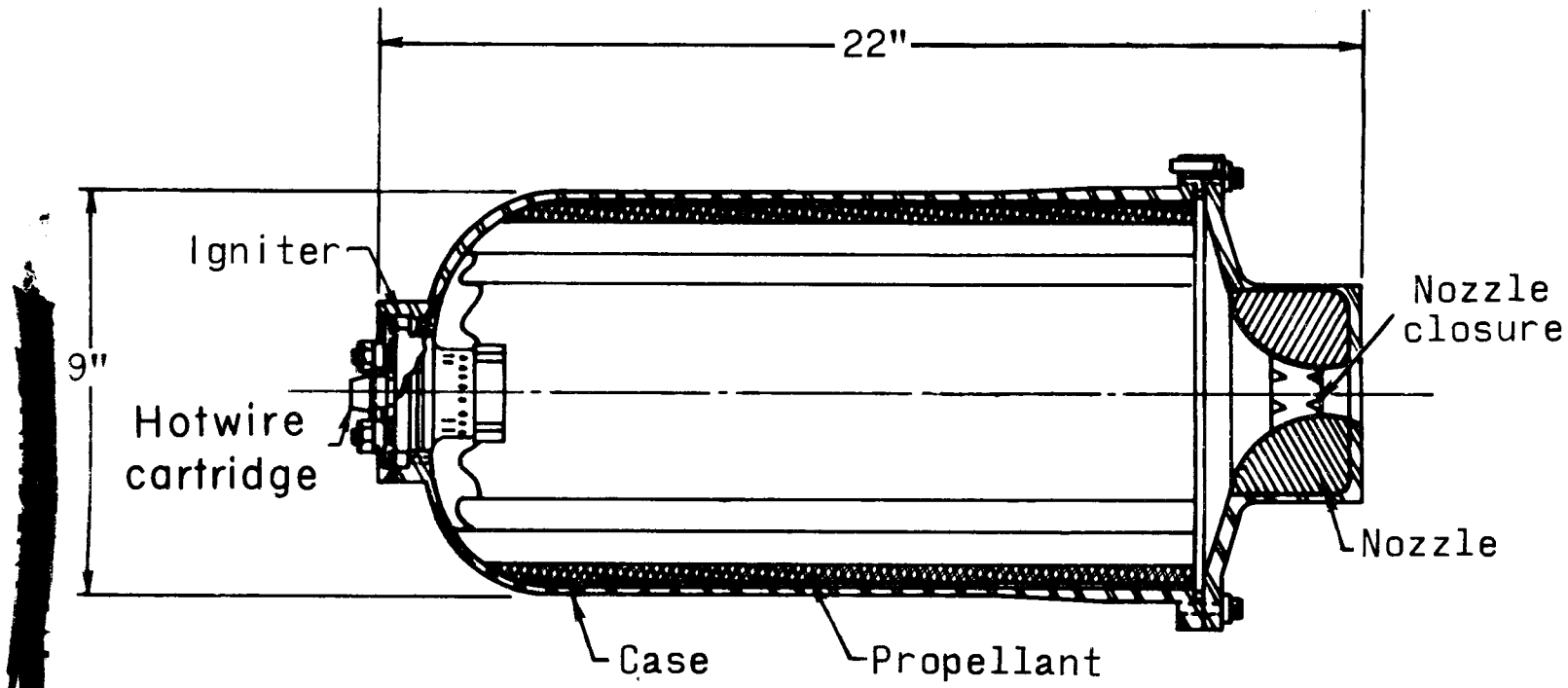

Figure 4.3.3-5. - Pitch-control motor diagram.

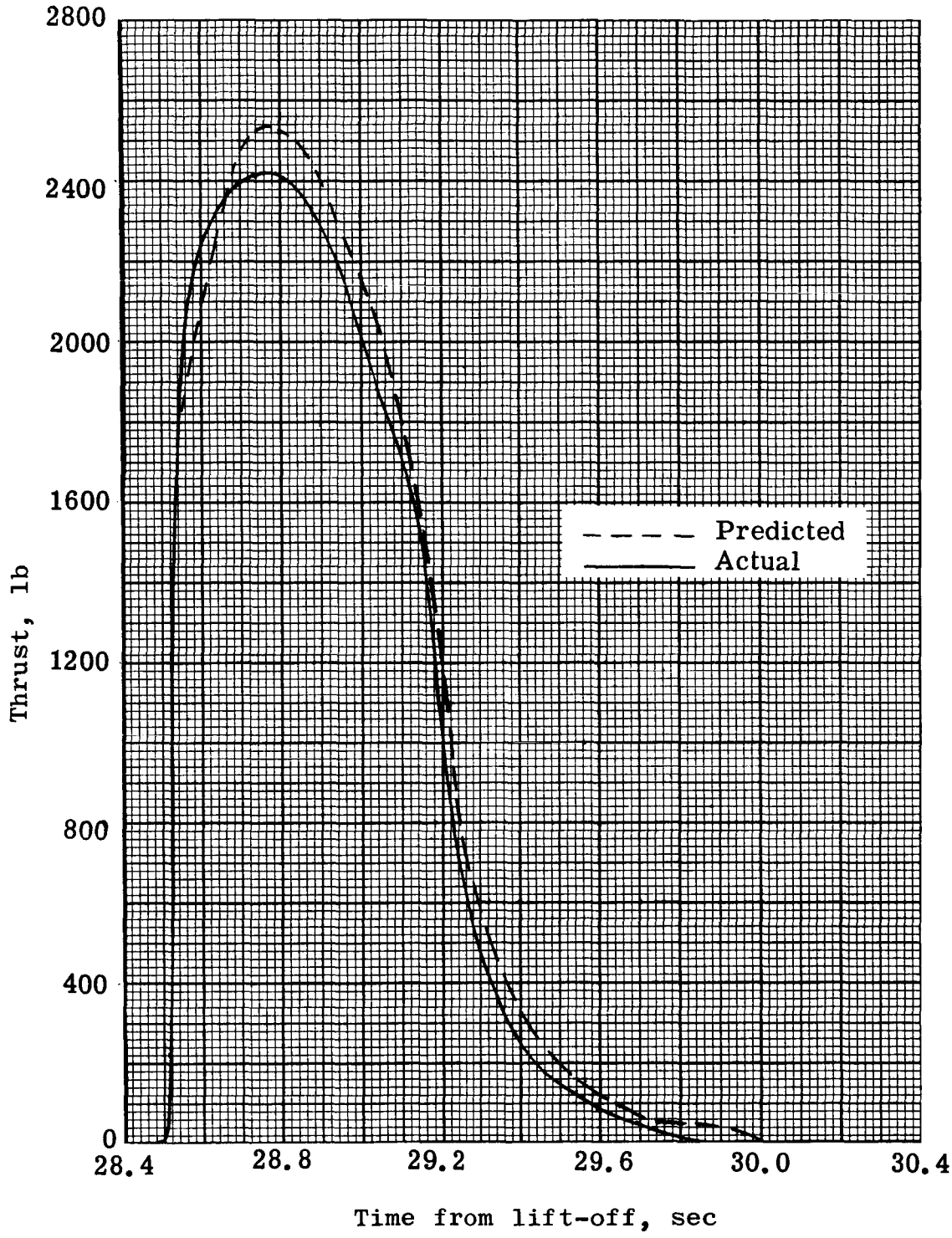

Figure 4.3.3-6.- Pitch-control motor thrust plotted against time.

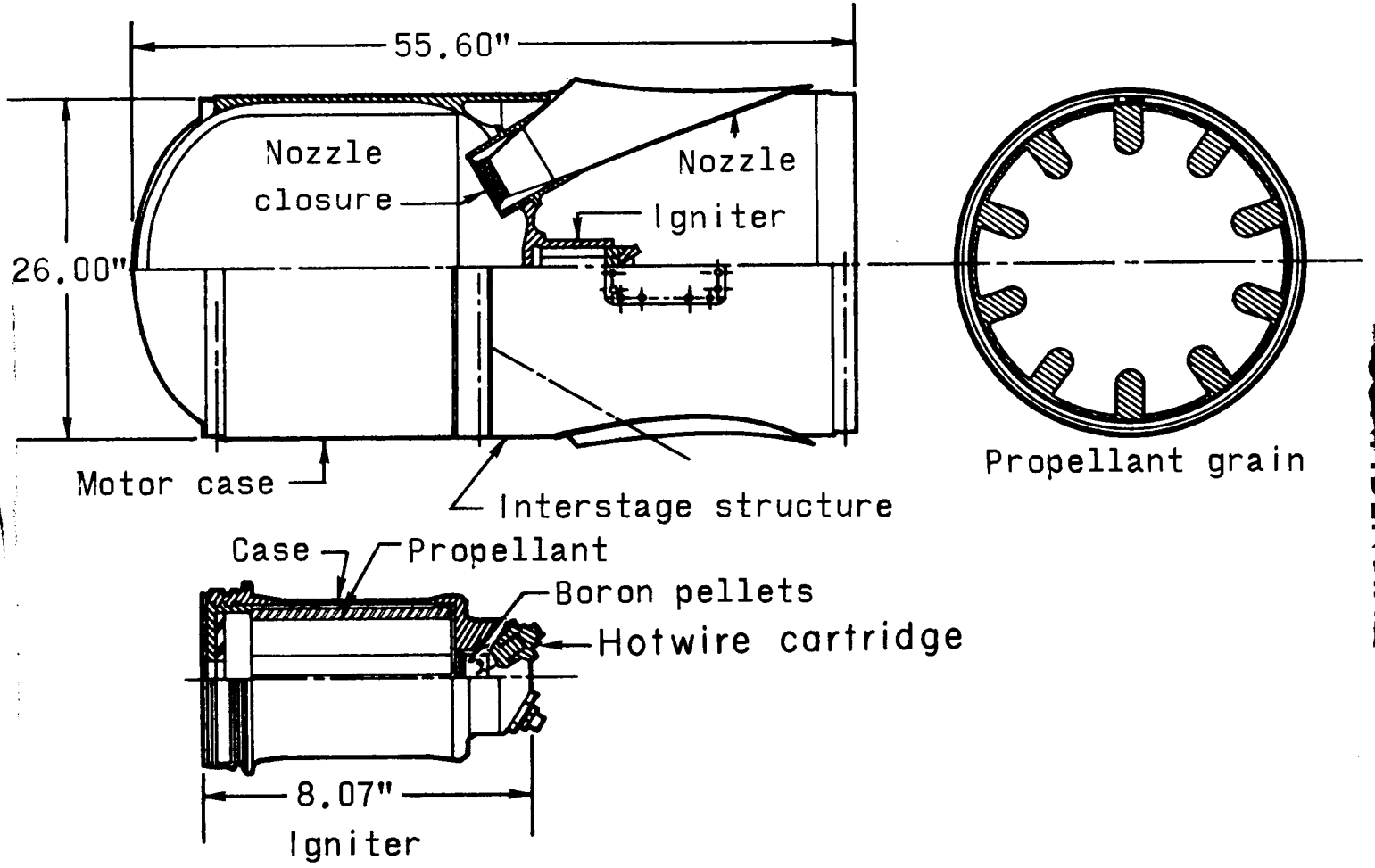

Figure 4.3.3-7. - Tower-jettison motor diagram.

[redacted]

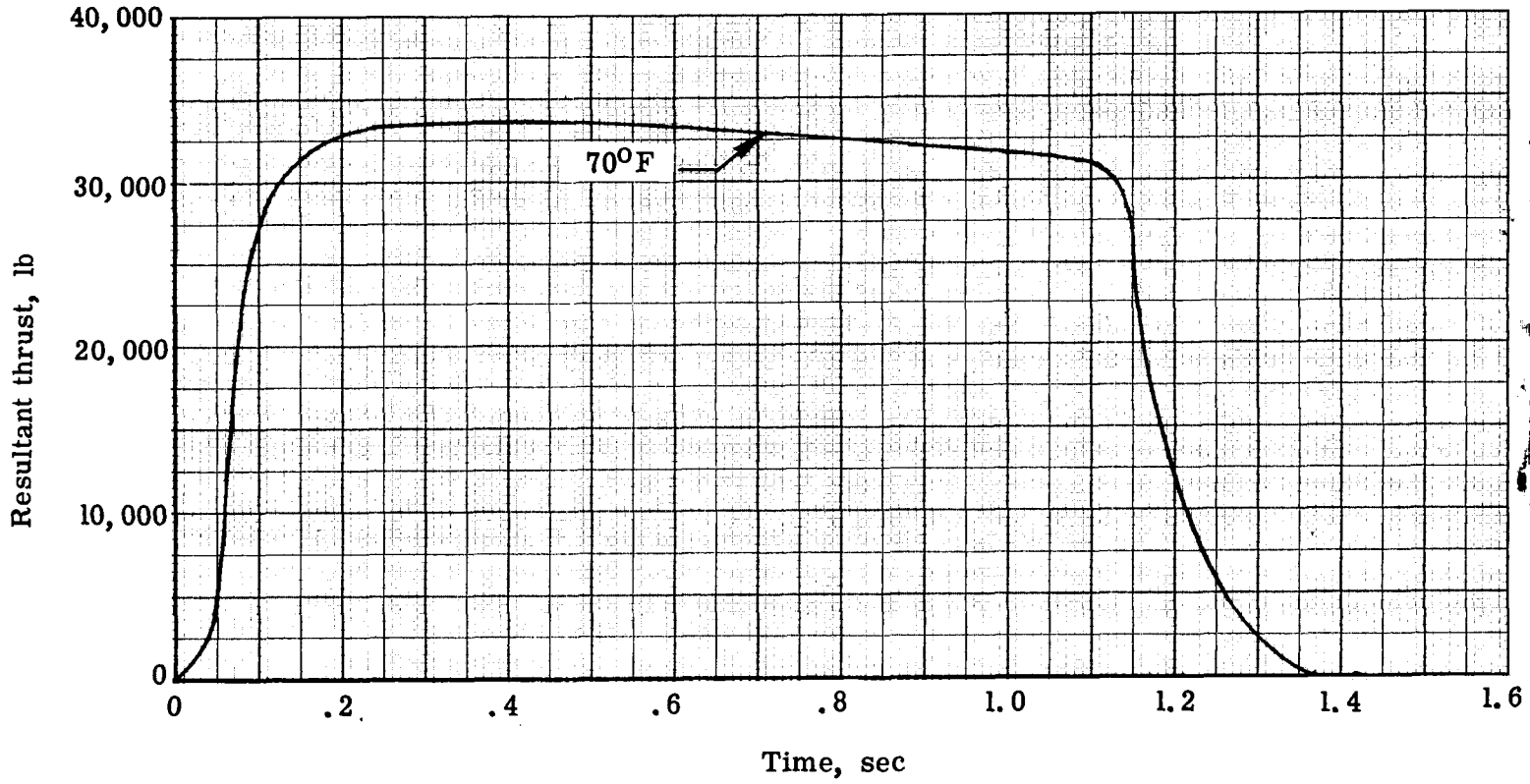

[redacted]

Figure 4.3.3-8. - Tower-jettison motor predicted thrust plotted against time.

[redacted]

4.3.4 Spacecraft pyrotechnics.- Postflight visual, mechanical, and galvanometer checks on the many pyrotechnic devices incorporated in the spacecraft have shown that this subsystem performed as expected.

Functions performed by the pyrotechnic subsystem are listed in sequential groups.

Group I (10 initiators)		
Function	Number of initiators	Remarks
Launch-escape motor ignition.	2	Not recovered
Pitch-control motor ignition.	2	Not recovered
Command module-service module separation. Three tension ties cut by shaped charges.	6	Two initiators recovered
Group II (10 initiators)		
Tower-jettison motor ignition.	2	Not recovered
Tower separation. Four explosive bolts.	8	Eight initiators recovered
Group III (2 initiators)		
Drogue parachute deployment. Two mortar cartridges.	2	Two initiators recovered
Group IV (8 initiators)		
Drogue parachute disconnect. One tension tie cut by shaped charge.	2	Two initiators recovered
Pilot parachute deployment (3). Six mortar cartridges.	6	Six initiators recovered

Instrumentation was not provided to show that each of the redundant pyrotechnics was electrically expended. However, visual examination of all recovered pyrotechnics gave evidence that all explosives in these devices had been expended.

Inactive bridgewires in each initiator had their ends shorted together.

[redacted]

4.3.5 Earth-landing subsystem.- The earth-landing subsystem (ELS) installed on boilerplate 12 performed as expected with the exception of a main parachute riser failure and subsequent failure of a main parachute. The cause of the riser failure was determined to be abrading and cutting of the riser over sharp edges in the area of the drogue disconnect guide assembly (horsecollar) mounted on the command module top deck. Failure of the simulated reaction-control pitch motor supporting structure by the main riser allowed it to slip beneath the horsecollar. One of the two remaining main parachute canopies was damaged by the suspension lines of the parachute with the failed riser. This canopy remained inflated. The command module was successfully recovered on the two remaining main parachutes.

4.3.5.1 Sequencing system description: The ELS on boilerplate 12 was based on timing compatible with the tower-flap concept for abort and recovery. As designed, a signal from the launch-escape-subsystem sequence controller, 3.0 seconds after tower jettison, energized the earth-landing-subsystem sequencer and fired the drogue parachute mortar. After a nominal 5.0-second delay, the 12,000-foot baroswitches were energized. At 12,000 feet m.s.l., electrical signals simultaneously fired the drogue disconnect and the pilot parachute mortars. A nominal 6 seconds after main parachute line stretch, pyrotechnic reefing line cutters disreefed the main parachutes.

4.3.5.2 Drogue parachute: Boilerplate 12 had one 13.7-foot nominal diameter, FIST ribbon, 25° conical drogue parachute with a geometric porosity of 24 percent. The canopy was permanently reefed by the use of pocket bands to an apparent 12.4-foot diameter. The drogue parachute riser was 56.6 feet long and was attached to a shaped-charge-type disconnect. The lower 14.4 feet of the drogue riser was protected with Thermo Fit Sleeving, a plastic which is resistant to abrasion. The drogue parachute was deployed by a mortar which incorporated redundant initiators.

4.3.5.3 Pilot parachutes: Three 10-foot nominal diameter, ringslot pilot parachutes were deployed simultaneously. The pilot parachute risers were 43.5 feet long and were protected with Thermo Fit Sleeving on the lower 4.9 feet. The pilot parachutes were deployed by mortars which incorporated redundant initiators.

4.3.5.4 Main parachutes: Three 88.1-foot nominal diameter ringsail parachutes were independently deployed by the pilot parachutes. The three main parachutes were sized such that proper operation of two parachutes would give a rate of descent of less than 33 ft/sec at a pressure altitude of 5,000 feet. The main parachutes were reefed to 13 percent of the nominal diameter for a period of 6 seconds. Three pyrotechnic cutters, mechanically initiated at main parachute line stretch, were used to sever each reefing line. Two reefing lines were installed in each main parachute and operation of any one cutter per line would have resulted in

normal disreefing.

The three main parachute risers were attached to a common clevis, and 9.7 feet of each riser were covered with Thermo Fit Sleeving. Based on the failure analysis of boilerplate 3 and subsequent rigging requirements, the main parachute disconnect and upper harness legs had been removed. Four lower harness legs were attached to the clevis and to the main parachute attachment fittings located near the top of the egress tunnel, just above each longeron. The lower harness legs were approximately 60 inches long and were protected with Thermo Fit Sleeving. The harness was designed to land the command module at an angle of 5°.

It should be emphasized that the earth-landing subsystem, as tested on boilerplate 12, was not a production subsystem. The significant differences between the production spacecraft and boilerplate 12 are:

a. Dual simultaneously deployed drogue parachutes will be installed, one on either side of the reaction-control-subsystem motor.

b. Reaction-control-subsystem motor mount and drogue disconnect will be redesigned to replace the drogue disonnect guide assembly, or horsecollar, and its associated structural supports.

c. The main parachute harness will have a two-point attach. The harness attach points will be located on the parachute deck and will eliminate the four attach points near the top of the parachute compartment.

d. The ELS sequence controller of the production spacecraft is installed in one of the parachute deck longerons and the impact switch is located in the lower equipment bay.

The installation of the parachutes on the upper deck of the BP-12 command module is shown in figure 4.3.5-1.

4.3.5.5 Events: The following times for events 1 to 9 were recorded and are compared with those expected. Actual times for other significant events are included. Also noted are the dynamic pressures during earth-landing-subsystem operation.

Event	Elapsed time, sec			Dynamic pressure, lb/sq ft
	Expected	A	B	
1. LES tower jettison-separation relay closure	46.9	44.1	44.2	
2. ELS sequence A start relays A and B	49.9	47.1	47.1	
3. ELS sequence B start relays A and B	49.9	47.1	47.2	
4. Forward heat shield release relays A and B	49.9	47.1	47.3	
5. 25,000-foot baroswitch 1 and 2 closure	72.5	----	----	
6. Drogue deploy relay A and B	49.9	47.1	47.2	
7. Drogue mortar fire	49.9	47.2	----	39.8
8. Drogue release - pilot mortar fire relay A and B	122.9	112.7	112.7	57.4
9. Pilot mortar no. 1 fire (-Y)	122.9	112.7	----	57.4
Pilot mortar no. 2 fire (+Z)	122.9	112.7	----	57.4
Pilot mortar no. 3 fire (+Y)	122.9	112.7	----	57.4

Event	Actual time, sec	Dynamic pressure, lb/sq ft
10. Main parachute no. 1 off deck (-Y)	113.7	68.4
Main parachute no. 2 off deck (+Z)	113.8	67.9
Main parachute no. 3 off deck (+Y)	113.6	67.9
11. Main parachute no. 1 line stretch (-Y)	114.6	68.8
Main parachute no. 2 line stretch (+Z)	114.8	64.4
Main parachute no. 3 line stretch (+Y)	114.6	68.8
12. Main parachute no. 1 riser failure (-Y)	115.5	51.2
13. Main parachute no. 1 disreef (-Y)	----	
Main parachute no. 2 disreef (+Z)	120.7	8.6
Main parachute no. 3 disreef (+Y)	120.6	8.2
14. Main parachute no. 3 failure	121.3	4.5
15. Main parachute no. 1 full open (-Y)	----	
Main parachute no. 2 full open (+Z)	127.9	1.0
Main parachute no. 3 full open (+Y)	121.2	2.4
16. Impact	350.3	

[redacted]

Event no. 5, closure of the 25,000-foot baroswitches, did not occur because altitude at apogee was insufficient to open these baroswitches. These baroswitches were not active except for instrumentation of contact closures.

4.3.5.6 Drogue parachute performance: The drogue parachute was deployed by mortar at T+47.2 seconds. Angle of attack at drogue mortar fire was approximately 30°. The drogue deployed and became effective in 1.0 second. Oscillations of the command module while on the drogue parachute were as predicted and previously observed on the boilerplate 12 simulated tests at El Centro, California. The drogue mortar functioned normally with no apparent indication of excessive recoil loads. The drogue parachute was undamaged and there was no scuffing or abrasion of the drogue riser or Thermo Fit Sleeving. The drogue parachute was disconnected and the pilot parachutes were deployed by mortars at T+112.7 seconds.

4.3.5.7 Pilot parachute performance: The three pilot parachutes were simultaneously deployed by mortars. Command module angle of attack was approximately 160° at pilot mortar fire. All pilot parachutes deployed and inflated normally. Postflight inspection revealed no major damage to the pilot parachutes or risers, including the Thermo Fit Sleeving. Each of the pilot parachute mortars functioned normally with no apparent indication of excessive recoil loads.

4.3.5.8 Main parachute performance: All main parachute deployment bags left the upper deck between T+113.6 seconds and T+113.8 seconds. Average angle of attack was approximately 70°. During deployment, the command module continued to rotate apex forward, and at line stretch the angle of attack was approximately 20°. At T+115.5 seconds, the main riser of the no. 1 main parachute failed, as described in detail in paragraph 4.3.5.9. Severe aerodynamic interference between the remaining two parachutes was noted. Disreef of the main parachutes occurred at approximately the same time; however, because of aerodynamic interference, a 6-second difference was noted in the full open times. At T+121.3 seconds, the no. 3 main parachute split from vent to skirt as described in detail in paragraph 4.3.5.11. The skirt band of the failed parachute remained intact and the canopy remained inflated. Major inflight damage to the main parachutes, risers, and harness is described in paragraph 4.3.5.11. Descent after canopy failure was uneventful and the command module remained upright after landing.

Terminal descent rate on the main parachutes was reached at a pressure altitude of 10,550 feet, or approximately 10,800 feet mean sea level. The preliminary trajectory data indicate that the descent rate at a pressure altitude of 5,000 feet was 29.9 feet per second, which is within the operative requirements of the earth-landing subsystem with two main parachutes. Rate of descent at landing was 25.7 ft/sec. The total

[redacted]

velocity at a pressure altitude of 5,000 feet was 30.2 ft/sec and at landing was 26.5 ft/sec. Total velocity components at landing were 5.1 ft/sec north, 3.6 ft/sec east, and 25.7 ft/sec down.

4.3.5.9 Main parachute riser failure: Figure 4.3.5-2 is a top view of the command module showing the location of the drogue and pilot mortars, "horsecollar", and simulated RCS motor. Also shown are forward compartment Y/Z axis and longeron identification markings. Figure 4.3.5-3(a) to (d) present sketches of the command module illustrating the attitude changes during main parachute deployment. As shown in figure 4.3.5-3(a), command module attitude at pilot mortar fire was very favorable; however, pitch and roll rates of the spacecraft resulted in the pilot parachute from the -Y bay being deployed around the no. 3 longeron while the pilot parachutes from the +Y and +Z bays deployed around the other side of the airlock. The command module continued to rotate, apex forward and roll left, as the parachutes left the deck and deployed. At main parachute line stretch (fig. 4.3.5-3(c), the command module was oriented apex forward and had rolled approximately 80° left from its original position. As the inflating main parachutes exerted an increasing drag load on the upper deck area of the command module, it began to rotate rapidly heat shield forward. The command module overshot the 180° angle-of-attack position, and figure 4.3.5-3(d) illustrates command module attitude at main parachute riser failure. Command module oscillations during reefed inflation were heavily damped and at disreef the command module was not oscillating.

The parachute subsystem was installed as specified in OTP-A-3027A-BP12.

The risers were held in position by cotton cord and released when parachute loads became large enough to break the cord. As noted in the preceding paragraph, the pilot and main parachute no. 1 from the -Y bay deployed around longeron no. 3. The continuous left roll and apex forward pitch of the command module insured that the -Y riser could not free itself from its position on the no. 2 longeron. At line stretch the -Y riser was bearing across the no. 2 and no. 3 longerons and down the side of the command module. Figures 4.3.5-4 to 4.3.5-7 show the routing of the -Y riser and abrasions on the skin of the command module from parachute connector link covers and riser protective covering. Also noted was white paint from the command module imbedded in the riser covering. At line stretch, or shortly thereafter, the no. 2 longeron was damaged as shown in figure 4.3.5-8 by the -Y riser. The structural deformation of the no. 2 longeron broke away aerodynamic putty installed to smooth sharp edges and cut through the Thermo Fit Sleeving and partly through one layer of the -Y riser as shown in figure 4.3.5-9. Fragments of the riser Thermo Fit Sleeving were found imbedded in the damaged area of the no. 2 longeron. The no. 3 longeron was not damaged.

[redacted]

As the command module began to rotate heat shield forward, the -Y riser moved up the side of the command module until it was bearing on the simulated RCS motor. The loads on the simulated RCS motor were in excess of the design loads and the upper edge of the simulated RCS motor was permanently depressed approximately 3 inches, allowing the -Y main parachute riser to slip beneath the drogue disconnect guide assembly.

At this time, the clevis was deployed from its position in the +Z pilot mortar bay by the +Z and +Y main parachute loads. This resulted in the -Y main parachute riser being pulled across the underside of the horsecollar. Figure 4.3.5-10 is a close-up view of the area beneath the horsecollar. The edges of the horsecollar structural gusset can be seen as can the drogue disconnect. The electrical connector on the end of the drogue disconnect was pulled upward with sufficient force to split the top of the outer shell of the connector. Insulating material on a wire bundle at the connector was also chafed through. The upper charge holder of the disconnect was severely deformed by the shaped charge fired to disconnect the drogue parachute. A $3\frac{3}{4}$-inch piece of this charge holder was found in the position shown in figure 4.3.5-10. This fragment was extremely sharp on its inner edge. Postflight inspection of the disconnect revealed nylon fibers imbedded in the end of the disconnect near the electrical connector. Also noted were rub marks and a tuft of nylon fibers imbedded in the drogue disconnect guide assembly itself. This tuft of fibers can also be seen in figure 4.3.5-10. The -Y main parachute riser failed at T+115.5 seconds, 0.3 second after it slipped beneath the horsecollar. It could not be definitely determined what sharp edge failed the riser; however, it is surmised that the cause of riser failure was abrasion over the horsecollar and cutting by the horsecollar. Figure 4.3.5-11 is a photograph of the bent simulated RCS motor.

4.3.5.10 Fabric analysis: The riser of the no. 1 main parachute failed across a 10-inch area beginning 66 inches from the clevis attach point. An additional damaged area was noted 3 feet from the clevis attach point where the riser abraded against the no. 2 longeron. The main parachute riser was constructed of 6 layers of 10,000-pound nylon webbing. The riser was 13.5 feet long with the lower 9.7 feet covered with Thermo Fit Sleeving.

In the area of the riser failure, the Thermo Fit Sleeving was ripped open for 8 inches below the break. There were other minor cuts in the sleeving in this area and abrasion marks. Beginning with the layer of webbing nearest the horsecollar at failure, the following damage was noted.

[redacted]

No. 1 - Zinc chromate and a black substance imbedded in the inside riser surface; heavy surface abrasion as evidenced by fusing of no. 1 and no. 2 layers for 3 inches; a $1\frac{1}{2}$-inch cut; and a $\frac{1}{4}$-inch tensile failure.

No. 2 - Surface burns with imbedded zinc chromate; fusing with layer no. 1 indicated; tensile failure of material weakened by abrasion.

No. 3 - Zinc chromate and burns on surface and edge of webbing; some unraveling at edges above break; a $1\frac{1}{2}$-inch cut; and $1\frac{1}{4}$-inch tensile failure.

No. 4 - Zinc chromate and burns on edge of material; surface burns; some unraveling at edges above break; a $1\frac{1}{2}$-inch cut; and a $\frac{1}{4}$-inch tensile failure.

No. 5 - Edges burnt with zinc chromate imbedded in material on one edge; a $\frac{3}{4}$-inch cut; and a 1-inch tensile failure.

No. 6 - No burns on material; tensile failure.

In the area of secondary damage, the Thermo Fit Sleeving was split approximately 80 percent around the circumference of the riser. Five layers of webbing were intact and unburnt. The outside layer was cut cleanly across a $\frac{7}{8}$-inch width of riser as shown in figure 4.3.5-9.

Severe abrasion was noted starting about 18 inches below the riser webbing confluence point and extended for 14 inches. The white paint imbedded in the Thermo Fit Sleeving was traced to the command module skin.

The connector link covers were also found to have white paint imbedded in the material. Fifty-nine suspension lines were burnt to some degree by abrading on the command module skin.

4.3.5.11 Main parachute gore failure: The no. 3 main parachute was severely damaged shortly after disreef when it split from vent to skirt band at gore 14. A detailed examination of test film revealed that the failed canopy could not have been damaged by the broken riser from the no. 1 main parachute, since the riser passed a safe-distance from the inflating parachutes. The suspension lines on the no. 1 main parachute, however, appeared to contact the canopy of the no. 3 main parachute. At T+121.3 seconds, which was 0.7 second after disreef, a tear appeared in

[redacted]

the canopy of the no. 3 main parachute. The tear started in the area of the 6th ring at gore 14 and traveled the length of the gore almost instantly. The skirt band remained intact.

Major damage to all parachutes was charted by North American Aviation. A damage chart of the no. 3 main parachute is shown as figure 4.3.5-12. Detailed damage charts will be constructed when the parachutes are returned to Northrop-Ventura. Of particular interest are the burns in the no. 3 main parachute. These burns were all in the area of failure and, when coupled with the high loads on this parachute at disreef resulting from aerodynamic blanketing of the other main parachute and failure of a main riser, are the most probable cause of canopy failure. Examination of the suspension lines of the no. 1 main parachute disclosed a slight amount of burning; however, it is most probable that the line burns noted occurred as the suspension lines were extracted from the deployment bag. Damage to the no. 2 main parachute was minor. All deployment bags were damaged at the pilot parachute attachment point. This is normal damage and occurs when the deployment bag turns inside out after deployment.

4.3.5.12 Conclusions: The earth-landing subsystem did not fully satisfy one of the second-order test objectives. This objective was:

> Demonstrate proper operation of applicable components of the earth-landing subsystem.

The only applicable component of the earth-landing subsystem which did not demonstrate proper operation was the reefing, disreefing, and inflation of one of the three main parachutes. This parachute broke loose from the spacecraft when the parachute riser parted shortly after line stretch because of abrading and cutting on the sharp edges of the drogue disconnect guide assembly structural gusset.

[redacted]

[redacted]

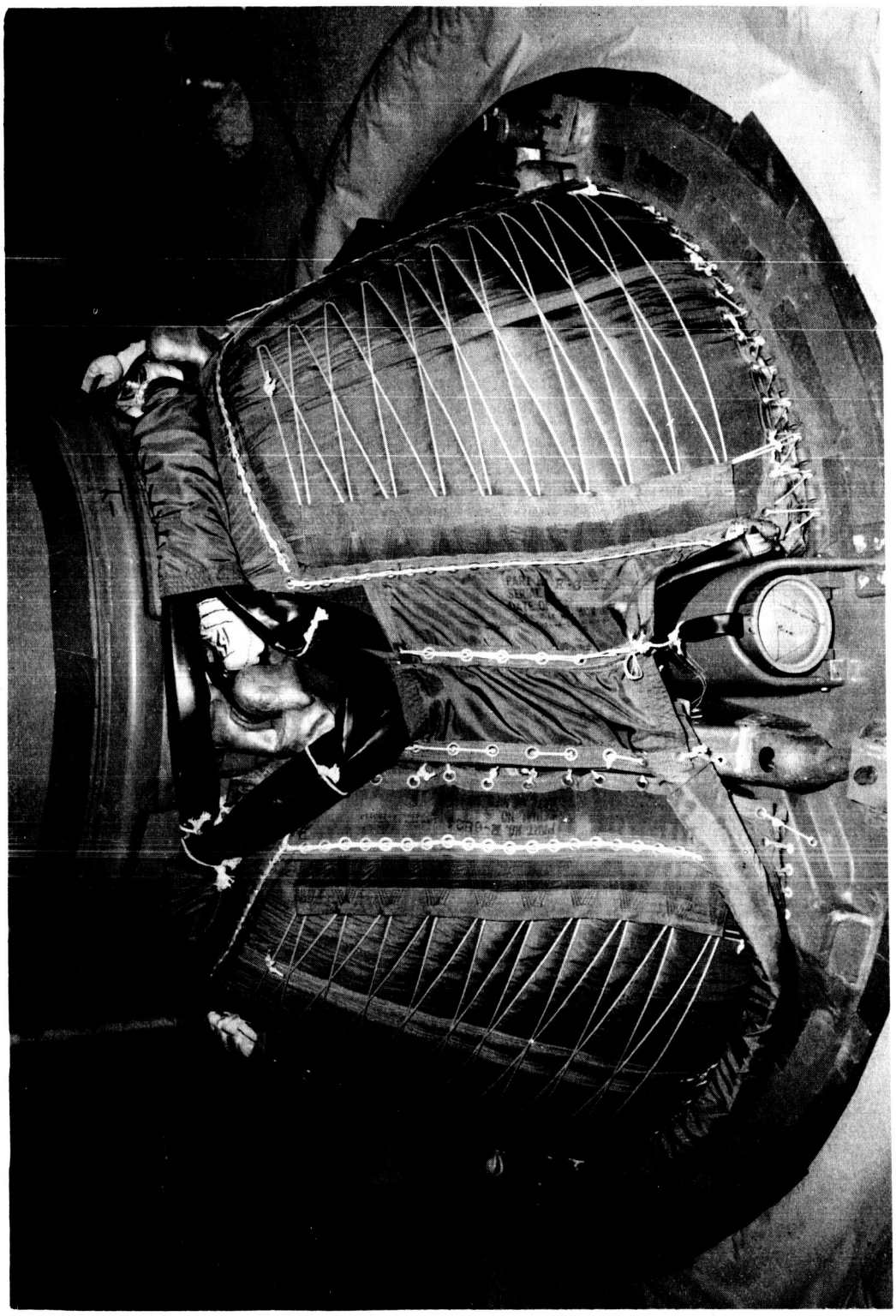

Figure 4.3.5-1. - Command module upper deck prior to flight.

[redacted]

[redacted]

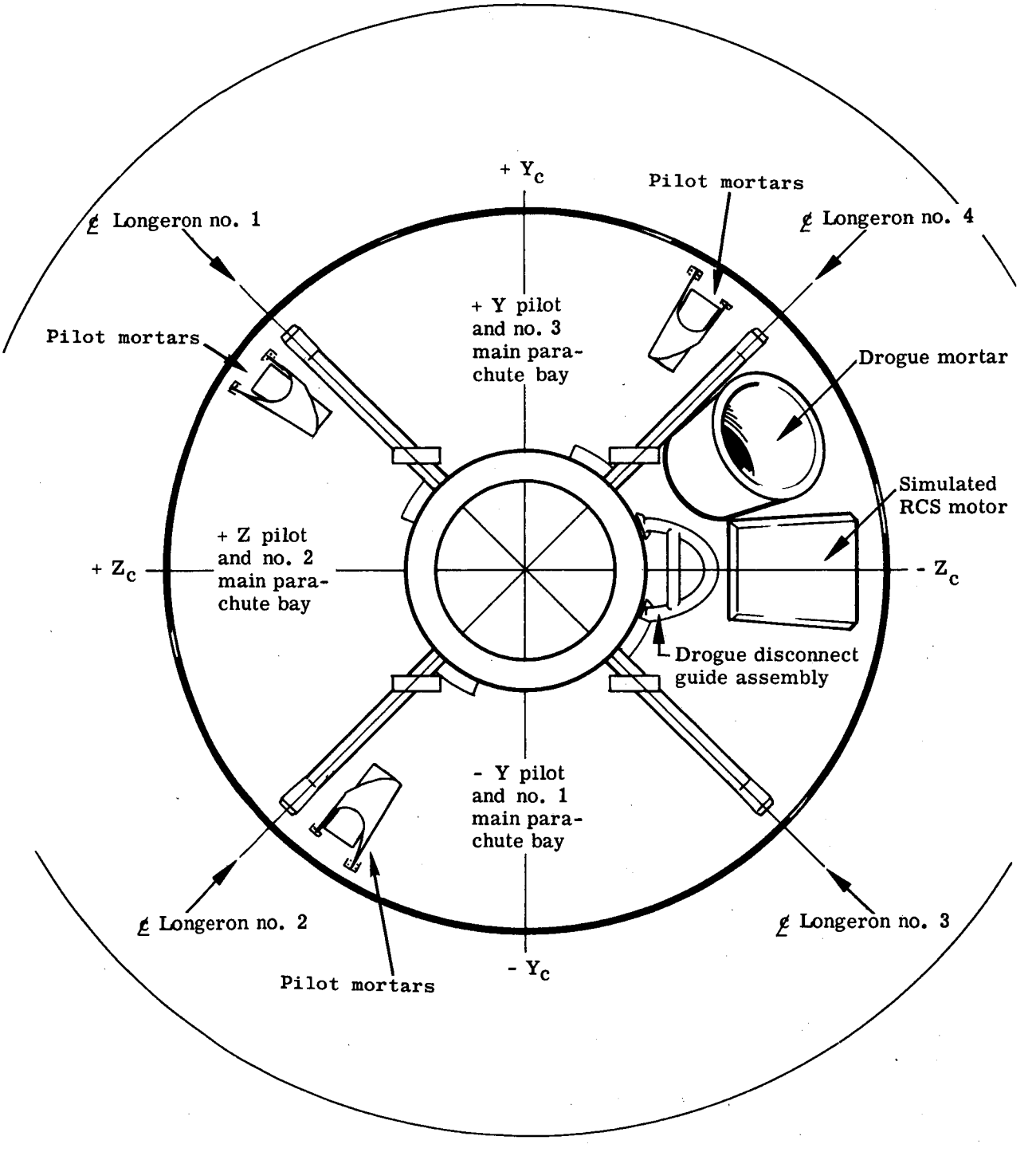

Figure 4.3.5-2.- Top view of command module.

[redacted]

[redacted]

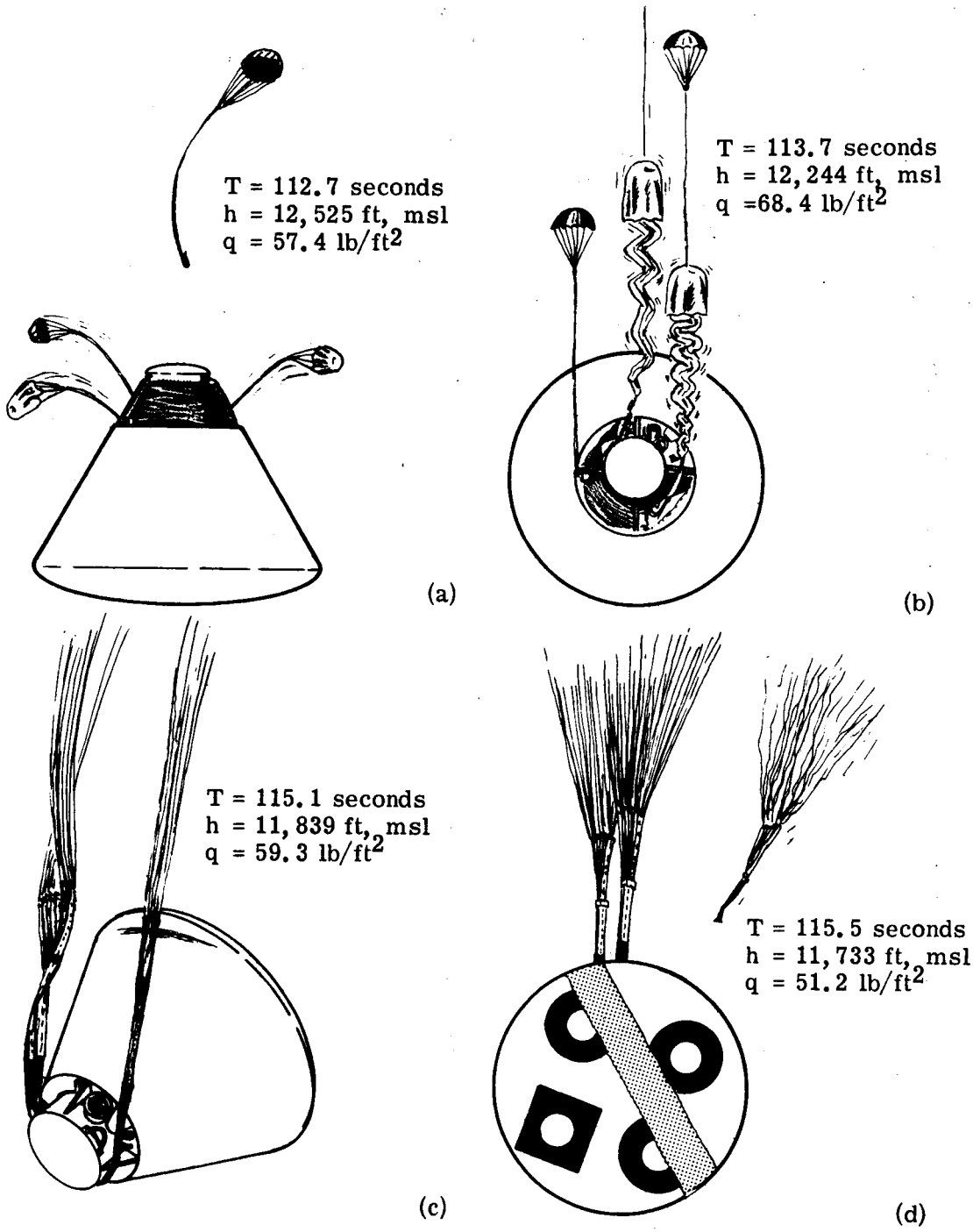

Figure 4.3.5-3. - Command module attitude changes during main parachute deployment.

[redacted]

Figure 4.3.5-4. - Reconstruction of routing of failed riser of no. 1 main parachute.

Figure 4.3.5-5.- Routing of failed riser over no. 2 and no. 3 longerons.

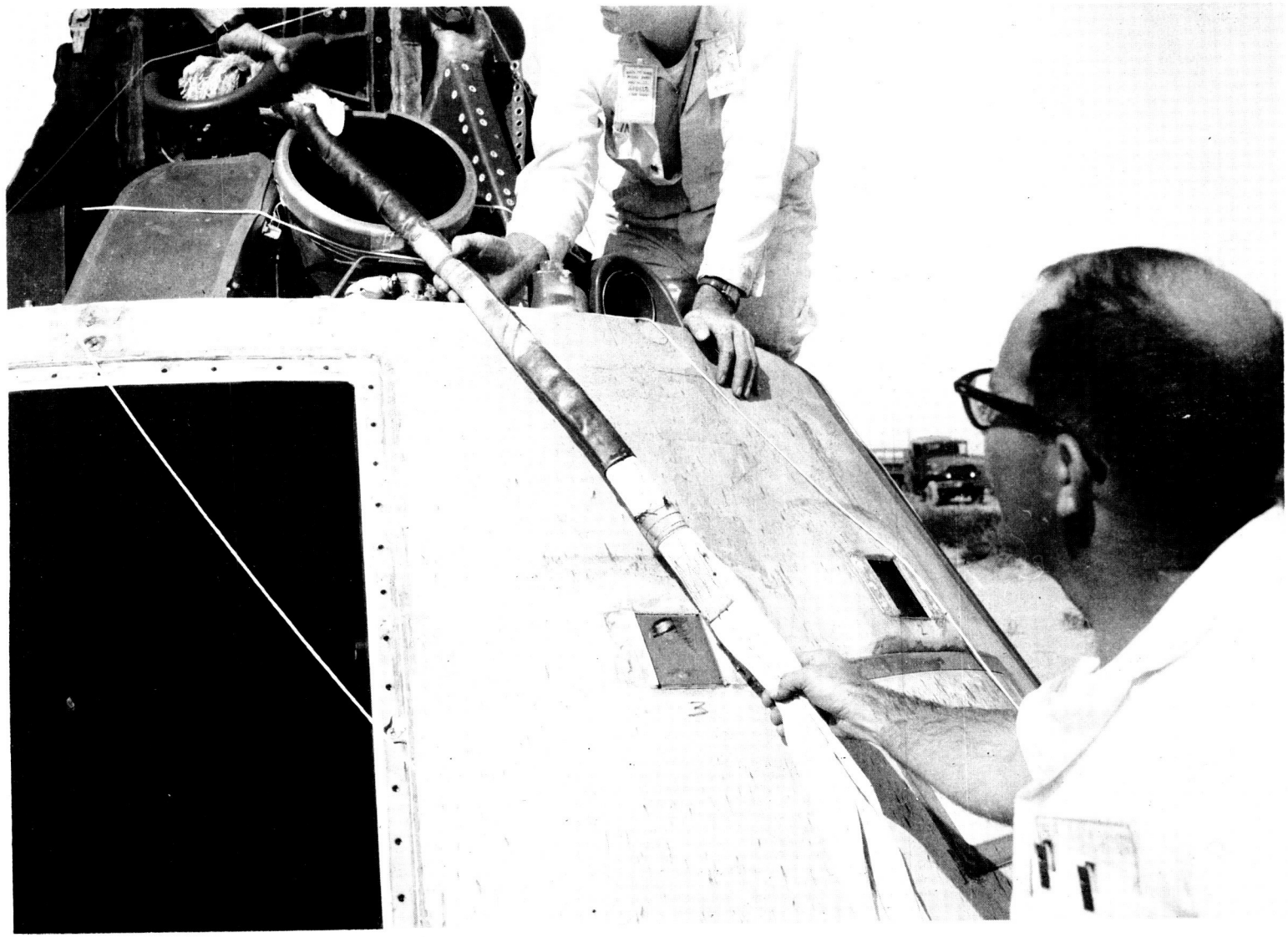

Figure 4.3.5-6.- Upper portion of failed riser showing abrasion of command module Thermo Fit Sleeving and riser.

Figure 4.3.5-7.- Failed riser showing abrasion of command module skin by parachute connector links.

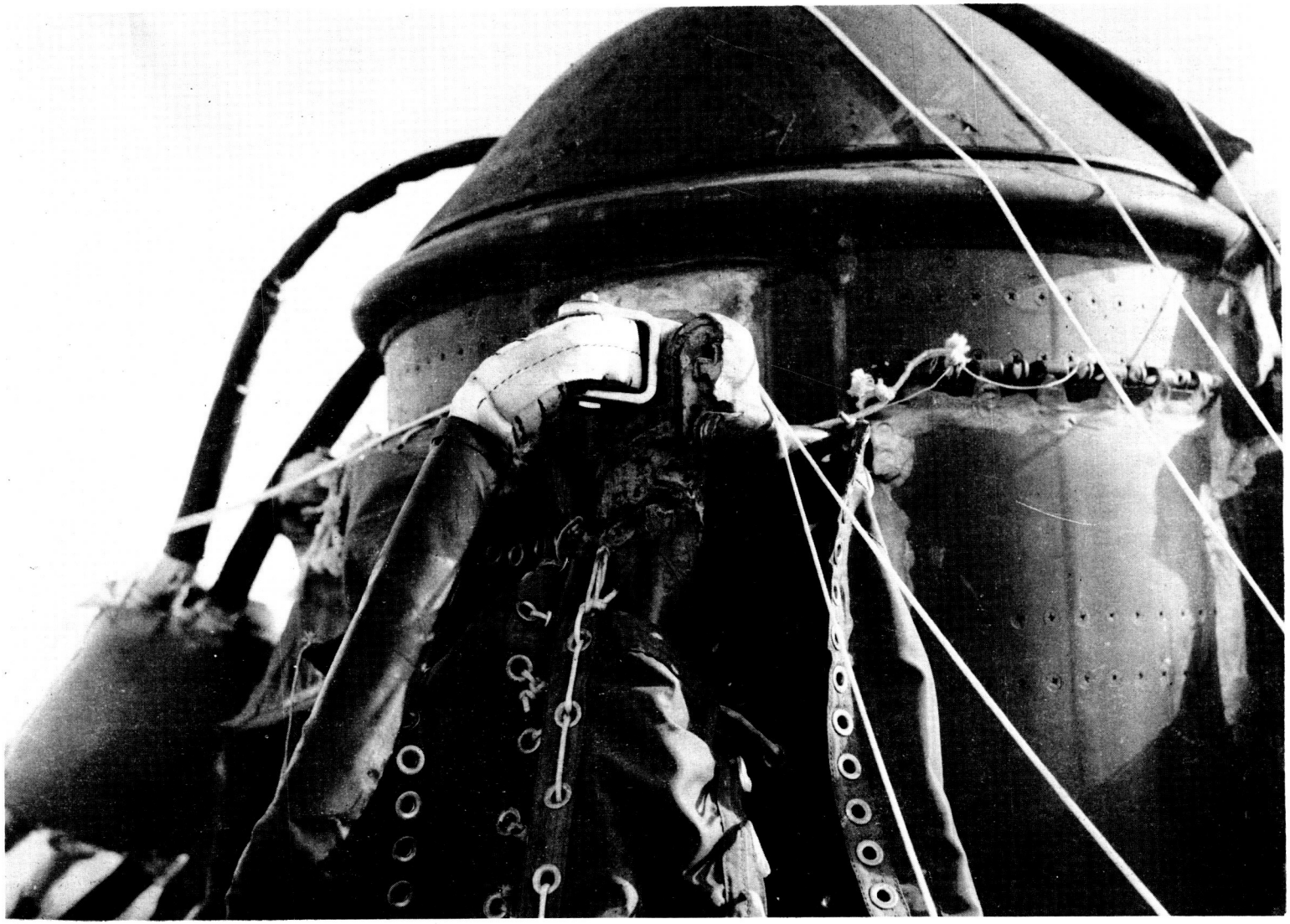

Figure 4.3.5-8.- No. 1 main parachute riser damage to no. 2 longeron.

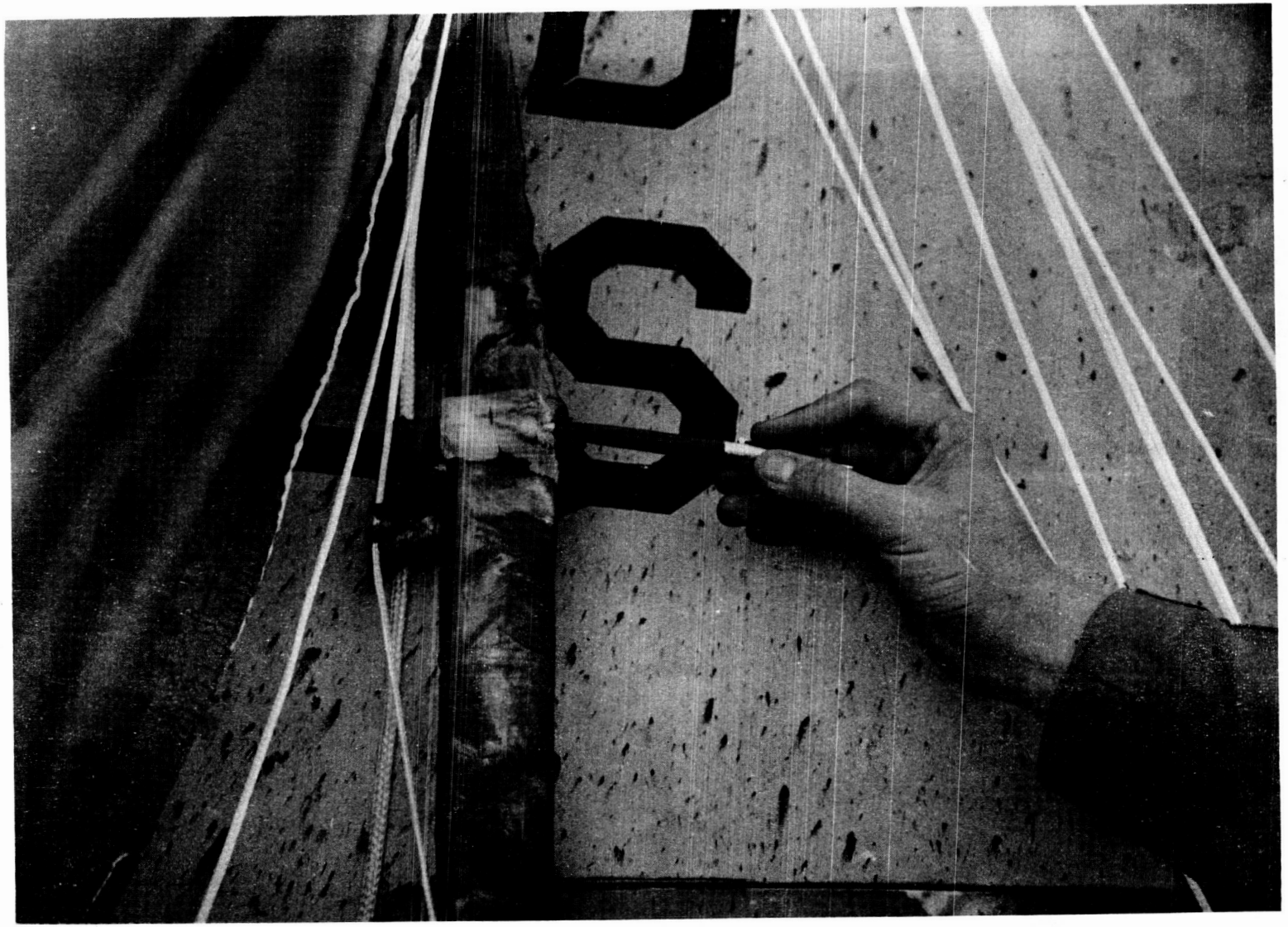

Figure 4.3.5-9.- Area of no. 1 parachute riser damaged by abrasion over no. 2 longeron.

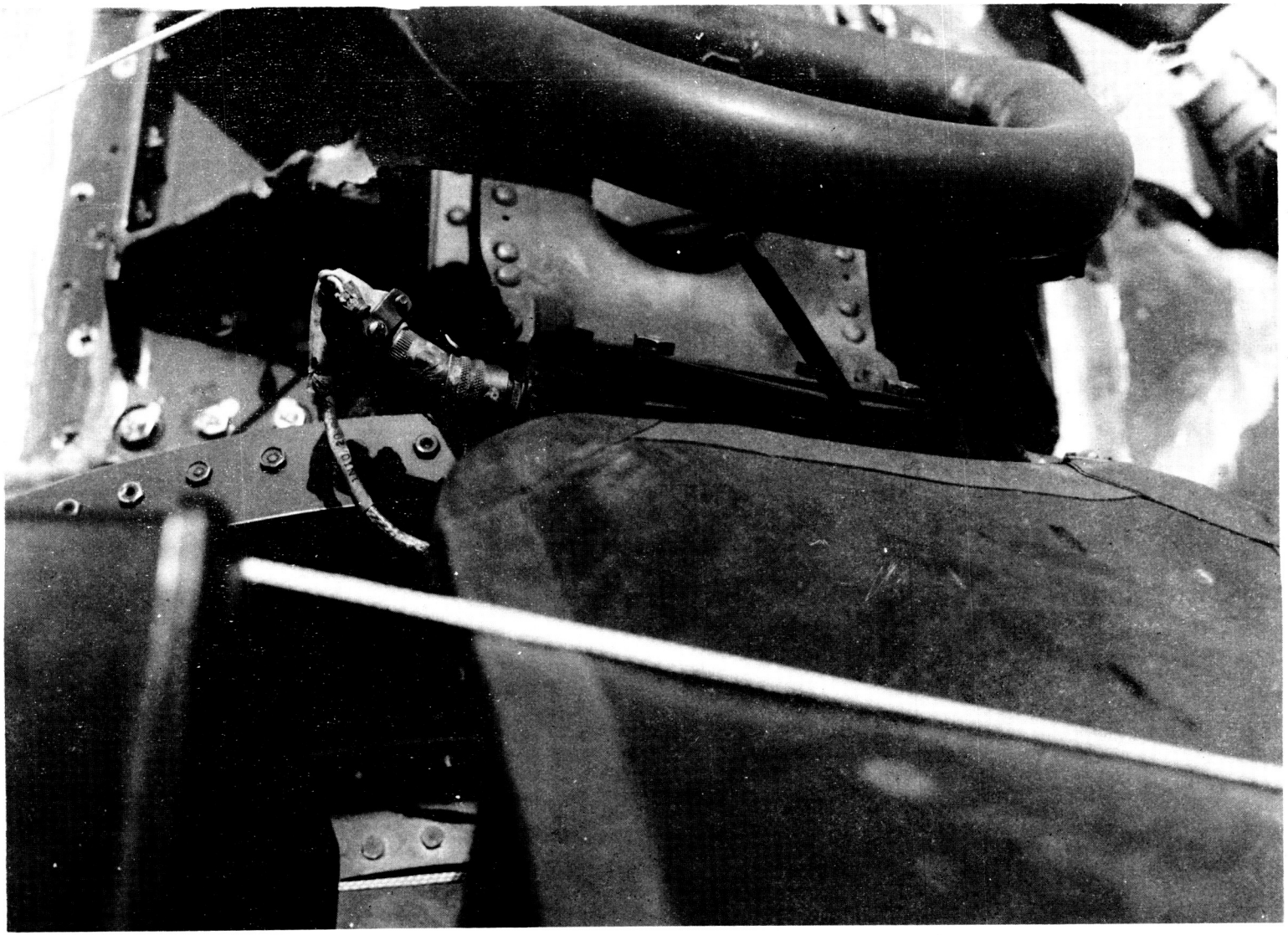

Figure 4.3.5-10. - Drogue disconnect assembly showing damaged electrical connector and charge holder. Note nylon tuft at upper right.

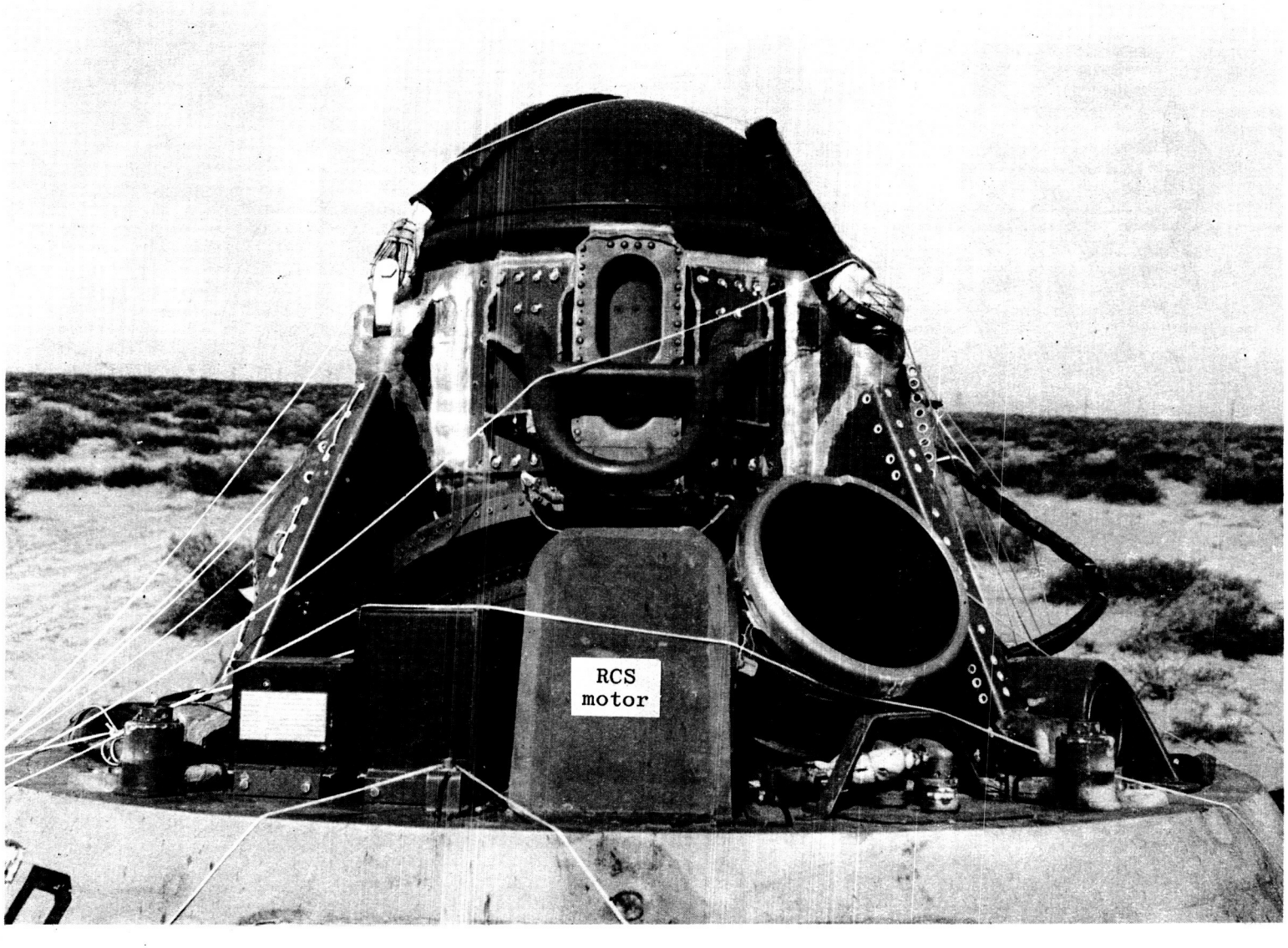

Figure 4.3.5-11.- Command module showing bent simulated reaction-control-subsystem motor.

[redacted]

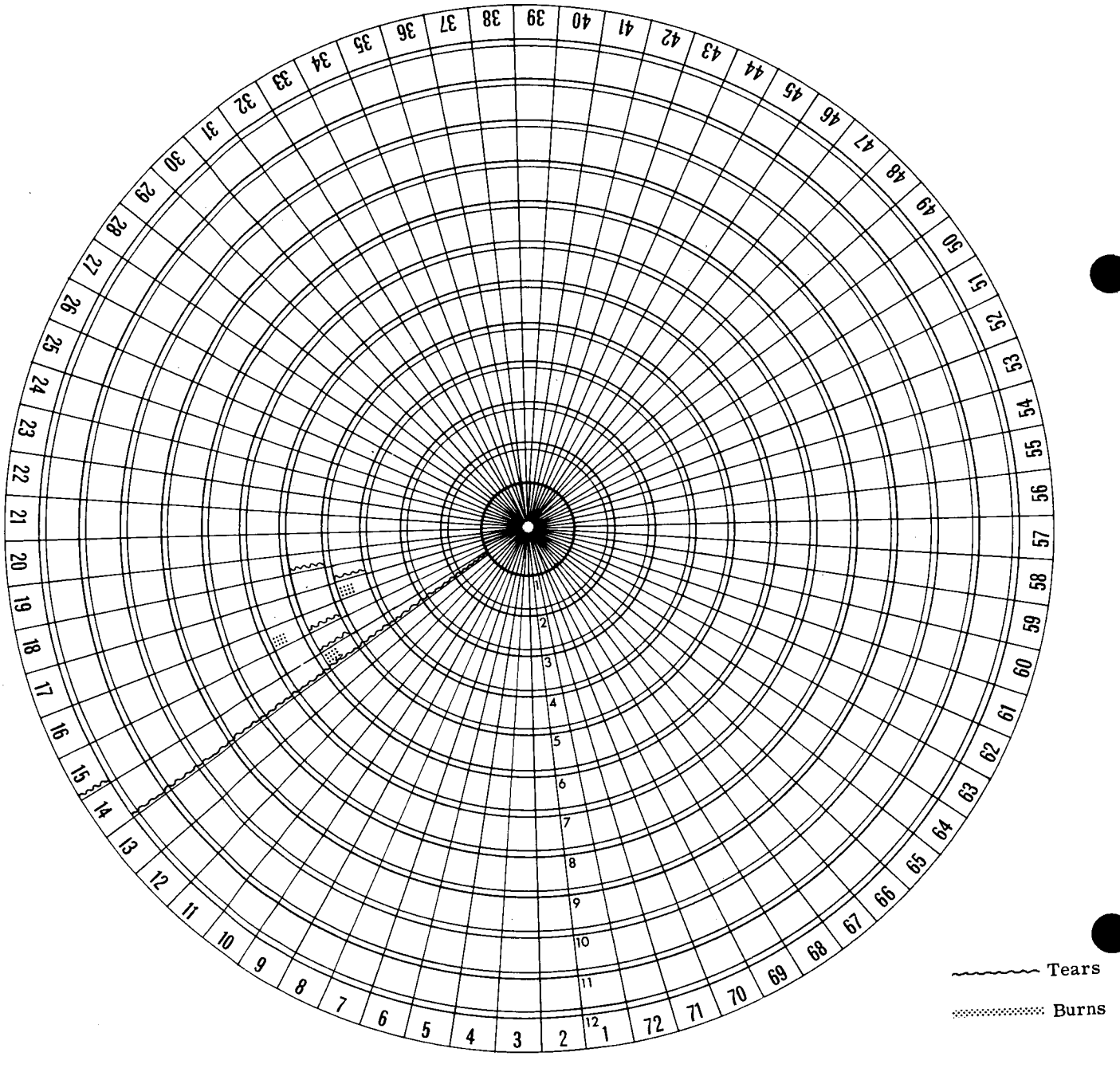

Figure 4.3.5-12.- Chart showing damage to no. 3 parachute.

[redacted]

4.3.6 Structures.- The structure for the boilerplate 12 flight-test vehicle consisted of a launch-escape subsystem in combination with boilerplate command and service modules. A 10-inch adapter was attached to the aft end of the service module for mating to the Little Joe II launch vehicle.

Measurements of such characteristics as vehicle accelerations, angle of attack, Mach number, and dynamic pressure permit inflight structural loads to be determined. Thrust-termination loads evidently caused some damage to the command module aft heat shield as a result of the structural failure of the fiber-glass pressure bulkhead located at the service module-adapter interface. A first-order test objective was to "demonstrate the structural integrity of the escape tower."

The boilerplate 12 tower structure performed well under the conditions which were encountered, and there was no evidence of structural problems. Table 4.3.6-1 shows a comparison of estimated flight loads with a comparable design condition. The estimated loads fall well within design values.

TABLE 4.3.6-1.- COMPARISON OF BOILERPLATE 12 TOWER LOADS WITH DESIGN LOADS DURING ABORT

Parameter	Design values for non-tumbling abort	Estimated flight values
Flight time, sec	----	32.0
Mach number	1.10	1.08
Dynamic pressure, lb/sq ft .	585	750
Angle of attack, deg	10	10
Angle of sideslip, deg . . .	----	0
Normal load factor[a]	-2.39	-1.7
Lateral load factor	----	0.0
Axial load factor	6.19	-1.9
Pitch acceleration, deg/sec^2	-70	-20
Yaw acceleration, deg/sec^2 .	----	0
Shear, lb	3,400	2,160
Axial load, lb	120,000	84,400
Bending moment, in.-lb . . .	438,150	250,000

[a]Measured at command module center of gravity

[redacted]

Four linear accelerometers were located in the command module as shown in figure 4.3.1-6. The specified frequency response was 0 to 30 cycles per second. Acceleration time histories along the three major axes are presented in figures 4.3.6-1 and 4.3.6-2 for two significant events. Figure 4.3.6-1 shows the accelerations experienced at thrust termination; figure 4.3.6-2 is a time history of command module acceleration at main parachute deployment. These figures obtained from oscillograph records of the telemetered continuous acceleration data are presented to provide information on two events which caused significant accelerations. In reviewing these figures, it should be noted that some of the oscillations exceed the specified frequency response of the accelerometers.

The thrust of the Algol sustaining rocket motor was successfully terminated as scheduled. The explosion which occurred as a result of thrust termination destroyed the launch-vehicle forebody and most of the afterbody and also caused a failure of the pressure bulkhead and some resulting damage to the aft heat shield of the command module. Figures 4.3.6-3 to 4.3.6-5 show the magnitude of the explosion. Figure 4.3.6-3 shows the vehicle just as a few holes appeared in the launch-vehicle skin. A few milliseconds later, the launch-vehicle forebody began to disintegrate as shown in figures 4.3.6-4 and 4.3.6-5. In an effort to determine the severity of the explosion, an investigation of possible blast overpressure ranges and fragmentation effects has been made.

If it is assumed that none of the Algol propellant detonated, then the overpressures may be assumed to consist of the expanding Algol chamber pressure, the primacord detonation, and the shaped-charge detonation. The following table shows the estimated overpressure resulting from each source. The igniter and shaped-charge overpressures were based on an average of a 5-foot separation from the pressure bulkhead.

Overpressure source	Overpressure at pressure bulkhead, psia
Expanding chamber pressure gases	16
Primacord and igniters	19.4
Shaped charge	25.2
Total	60.6

[redacted]

The blast overpressure probably ranged between 16 and 60 psia. The pressure bulkhead was designed to withstand a differential pressure of 22 psia, ultimate. A combination of any two of the overpressure sources would exceed the pressure bulkhead design ultimate differential pressure. Figure 4.3.6-3 shows the launch-vehicle skin bulging because of internal pressure. Recovered pieces of launch-vehicle skin were stretched flat because of the overpressures.

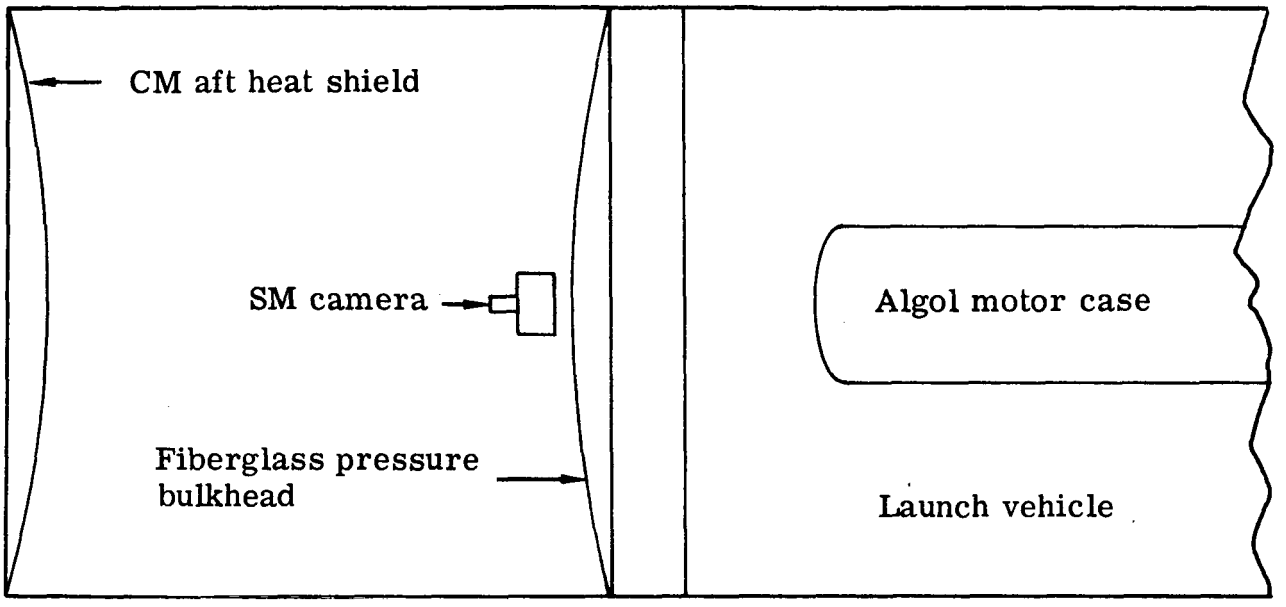

Another possible cause of the failure of the pressure bulkhead was fragmentation of the Algol motor case. There is extensive evidence that such fragmentation occurred. The sketch shows the relative location of the items of interest in considering fragmentation effects. Indications are that the forward end of the Algol motor was driven through the service module pressure bulkhead, striking the camera and driving the combined mass into the aft heat shield.

Orange paint from the service module camera was scuffed onto the aft heat shield in three separate places. In addition, a plate from the camera case was recovered with a definite fiber-glass design imprinted in the orange paint. The only orange-painted equipment in the launch vehicle and service module was the camera. Figure 4.3.6-1(a) shows a positive X-axis acceleration of about 17g at the time of thrust termination.

 [redacted]

Pieces of aft heat shield were seen to peel off after command module separation, suggesting blast damage. Figures 5.5.1-3, 5.5.1-6 and 5.5.1-7 show the damage to the heat shield. The photographs clearly show where a layer of fiber glass, approximately 3 feet by 10 feet, became delaminated, and was torn off. The heat shield also received two large dents and a crack several feet long. The command module floor was pushed inward approximately 10 inches in the +Z and -Z quadrants. Some of this damage may have occurred when the command module landed on an 18-inch high sand hummock.

Suggestions as to a solution to the thrust-termination problem include installation of a stronger pressure bulkhead, perhaps of a different material, to resist overpressure as well as fragments, and moving the igniter and shaped charges to the afterbody section of the Algol motor since overpressure resulting from the igniters and shaped charges decreases rapidly with distance.

The spacecraft was instrumented with 36 static pressure measurements on the conical portion of the command module and 12 static pressure measurements on the aft heat shield for determining the effects of escape-motor jet-plume impingement on the aerodynamic stability characteristics and on the structural loads. A preliminary investigation was made of the command module local pressures obtained during powered flight. The primary purpose of the pressure instrumentation was to provide detailed pressure distributions on the command module for eventual correlation with vehicle stability characteristics and for structural evaluation. The local pressure distribution and vehicle aerodynamic stability are interrelated and affect the loads accordingly. The stability characteristics determine the flight parameters which affect the overall loads, and the local pressure distributions affect the design of the local structure. The local pressures are affected considerably by the jet plumes from the four escape-motor nozzles.

Figure 4.3.1-8 shows the location of the static pressure transducers on the command module. The data indicate that good information was obtained from all except 2 of the 36 conical measurements. Conical surface pressure no. 16 remained at approximately 4.0 psia following thrust termination and conical surface pressure no. 22 read approximately 1.0 psia high at command module landing. Measured pressures were compared with wind-tunnel data. The condition chosen for comparison was based upon a rough estimate of angles of attack and sideslip; however, agreement appears to be fairly good.

[redacted]

The flight condition analyzed was:

$t = 32$ sec

$M = 1.08$

$q = 730$ lb/sq ft

$\alpha \approx 11^\circ$

$\beta \approx 0^\circ$

$P_{amb} = 6.23$ psi

Figure 4.3.6-6 shows a comparison of flight-measured pressure with wind-tunnel measurements along a ray opposite the jet plume in the +Z quadrant. Agreement is especially good. One point from the flight measurement is quite high but appears to be good data. The cause of this localized high coefficient is not definitely known. A comparison in the yaw plane is shown in figure 4.3.6-7. Agreement is fair; however, the flight-test data seem to be consistently higher than wind-tunnel data. Flight-test data from both rays in the yaw plane are shown suggesting that there are no known yaw effects in the results.

Data are also compared along rays between jet plumes. This comparison, shown in figure 4.3.6-8, also shows fair agreement. Again the flight-test measurements are higher.

The comparison around the periphery of the command module at a typical station also shows fair agreement in figure 4.3.6-9. All flight-test data were taken directly from tabulated data.

Plume impingement caused some slight scorching of the cork insulation on the command module in the quadrants opposite the escape-rocket nozzles. Local temperatures were measured by temperature sensitive paint and are discussed in section 4.5.2.

A second-order test objective was to"determine aerodynamic loads due to fluctuating pressures on the command module and service module during a Little Joe II launch." For this purpose, 11 fluctuating pressure transducers, three on the command module and eight on the service module, were included in the instrumentation, as shown on figures 4.3.1-7 and 4.3.1-8. As closely as practicable, the transducer orifice was flush-mounted to the spacrcraft skin and to assure that the spacecraft vibration would not be recorded, the service module mounts were

[redacted]

isolated from the structure. However, the pressure sensors were acceleration sensitive, and the data were biased during the boost phase at T+0 and T+29 seconds. No data are presented for these times.

All data were collected with an onboard tape recorder with the exception of measurement SA0184 which was included on the telemetry system. The frequency response for the transducer and associated equipment of each station was not the same; the limiting frequencies are shown in table 4.3.6-2.

As predicted for the Apollo launch configuration, the large fluctuating pressures occur at the command module—service module interface during transonic flight. A maximum root-mean-square (rms) pressure of 0.64 psi (167 decibels, that is 0.0002 dynes/cm^2 over-all sound pressure) did occur on measurement SA0182, 18 seconds after lift-off.

Data of particular interest for discussion are presented in figures 4.3.6-10 and 4.3.6-11.

Figure 4.3.6-10 indicates the variation of rms pressure with station location for Mach numbers of 0.80, 0.85, 0.90, and 0.95. These data indicate that the fluctuating pressures become significant at a Mach number of 0.80 at station 974, and as the Mach number increases, the maximum rms pressure moves to the forward end of the command module.

For comparison, wind-tunnel data are also presented in figure 4.3.6-10 for similar angles of attack, dynamic pressure, station location, and Mach number. A deviation of only 2 or 3 decibels indicates that the two sets of data compare favorably.

Figure 4.3.6-11(a) depicts two points of interest. The data indicate that the fluctuating pressure at X_c 100 does not exceed the ambient noise levels until after command module separation. The measurement stabilized at T+33 sec. and the rms pressure on this transducer remained nearly uniform until launch-escape-tower jettison where the measurement was terminated. Plots (b) to (g) in figure 4.3.6-11 show root-mean-square pressure time histories which were significant.

[redacted]

TABLE 4.3.6-2 LIMITING FREQUENCY RESPONSE FOR FLUCTUATING PRESSURE

[Data recording and reduction]

Measurement ID number	Fluctuating pressure	Station location	Frequency response, cycles/sec
CA0179 P	1	X_c 119, 7°	0 to 400
CA0180 P	2	X_c 70, 357°	0 to 400
CA0181 P	3	X_c 40, 357°	0 to 400
SA0182 P	4	X_a 1012, 357°	0 to 400
SA0183 P	5	X_a 1012, 177°	0 to 400
SA0184 P	6	X_a 974, 357°	0 to 300
SA0186 P	8	X_a 974, 177°	0 to 300
SA0187 P	9	X_a 974, 267°	0 to 600
SA0188 P	10	X_a 930, 357°	0 to 600
SA0189 P	11	X_a 881, 357°	0 to 600
SA0190 P	12	X_a 881, 177°	0 to 600

Time histories of the fluctuating pressures are presented in figure 4.3.6-11. These data characterize the changes in rms pressure as a function of flight duration as sensed by each transducer. Fourteen seconds after lift-off at M = 0.54 the fluctuating pressure became significant. These pressures continue to increase until command module separation. At this point, all fluctuating pressure transducer measurements were terminated except for those at stations X_c 119, SC 70 and X_c 40.

[redacted]

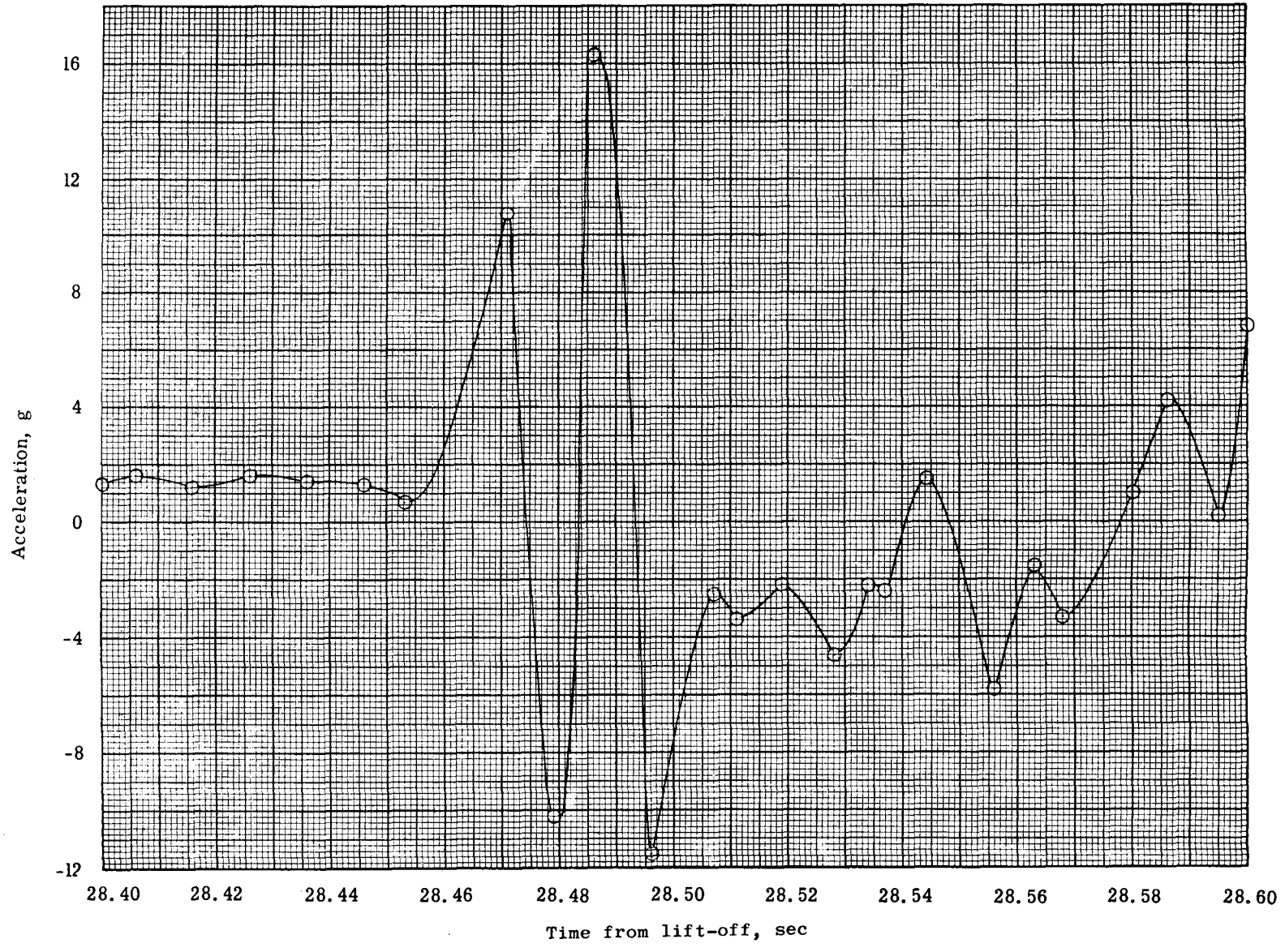

[redacted]

(a) X-axis acceleration (high range accelerometer).

Figure 4.3.6-1. - Time history of command module accelerometers during thrust termination.

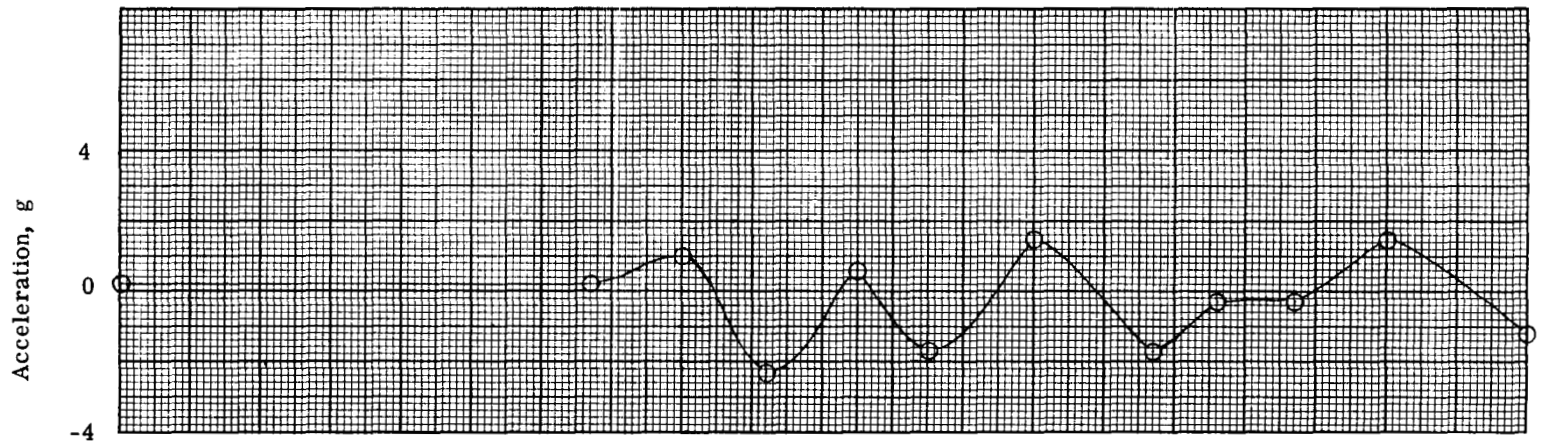

(b) Z -axis acceleration.

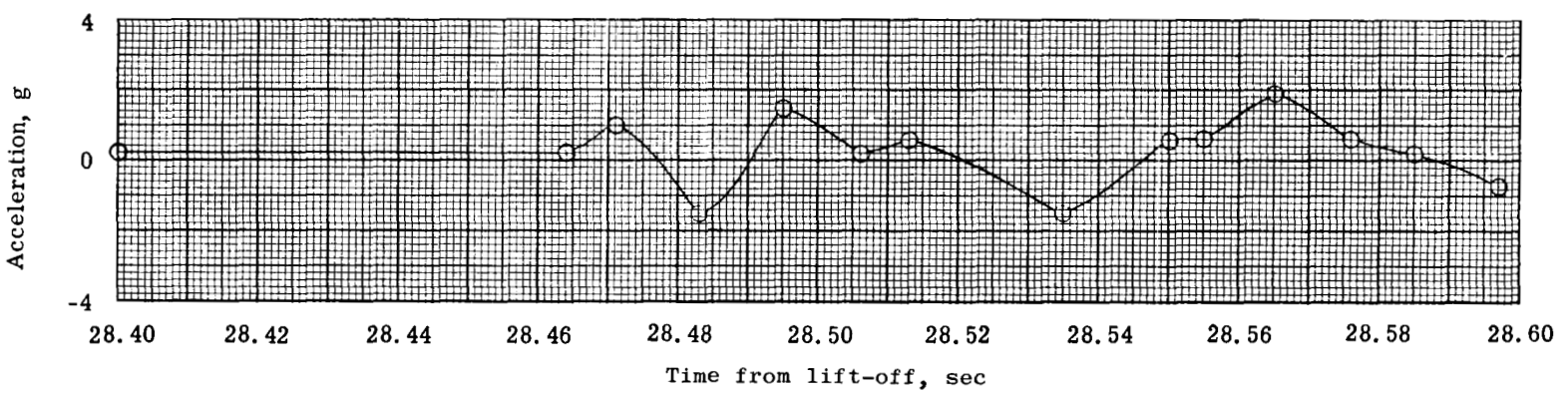

(c) Y-axis acceleration.

Figure 4.3.6-1.- Concluded.

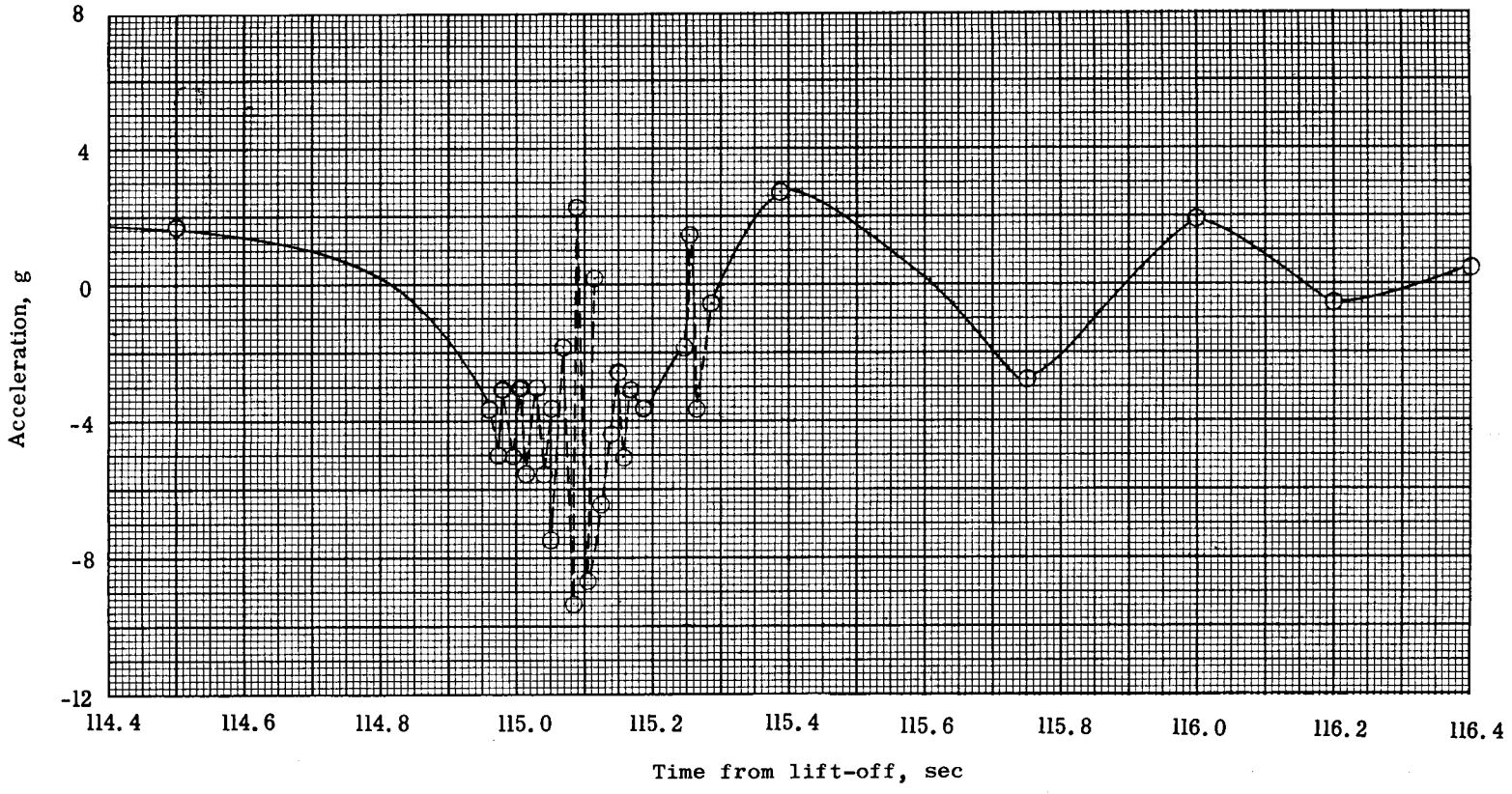

(a) X-axis acceleration (high range accelerometer).

Figure 4.3.6-2. - Time histories of command module accelerometers during main parachute deployment.

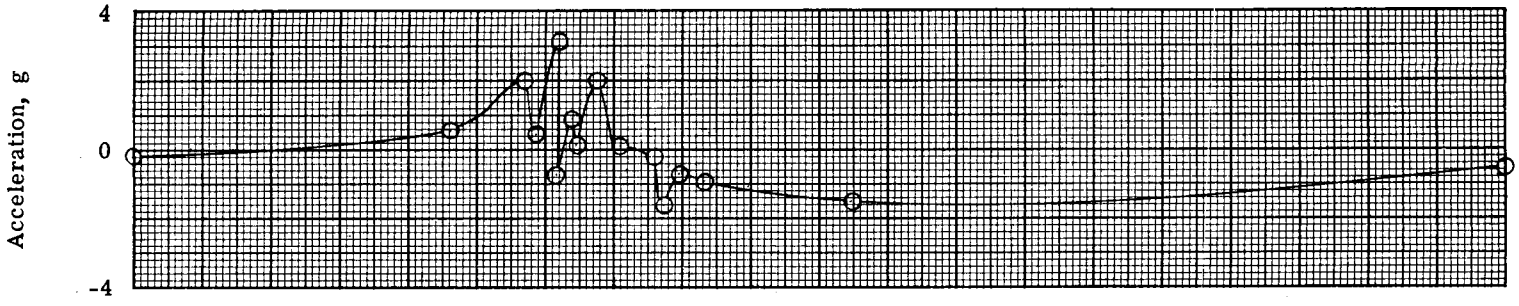

(b) Z -axis acceleration.

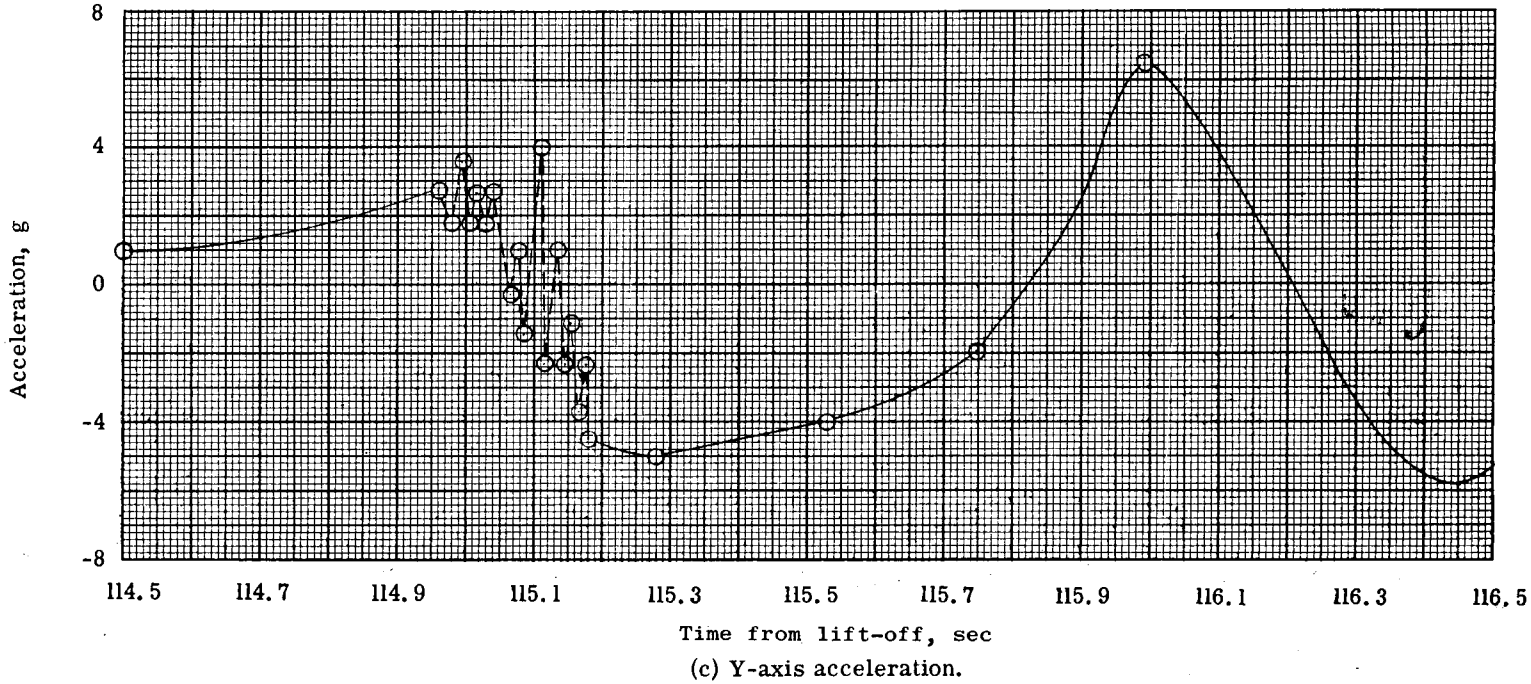

(c) Y-axis acceleration.

Figure 4.3.6-2. - Concluded.

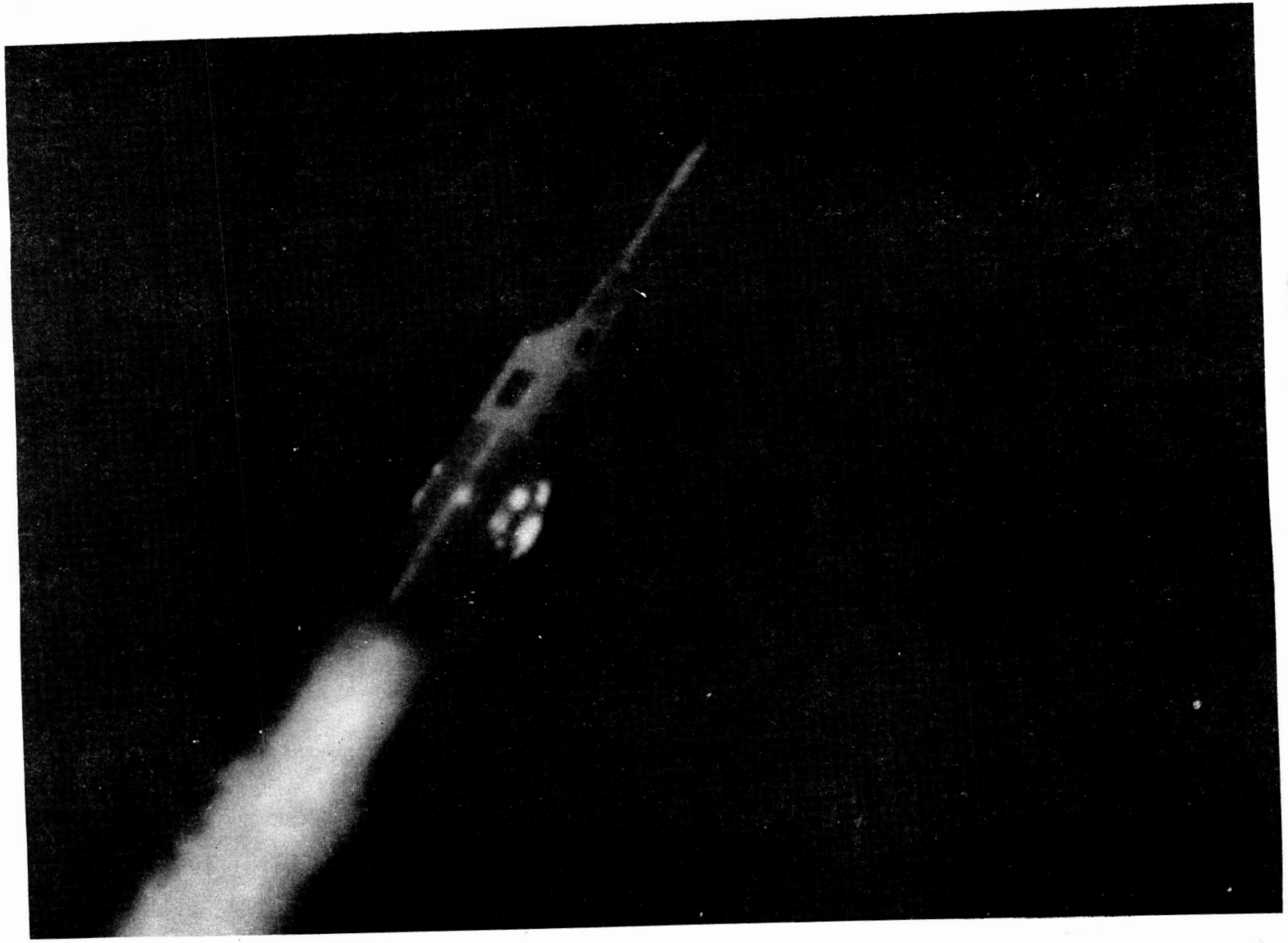

Figure 4.3.6-3.- Beginning of thrust termination.

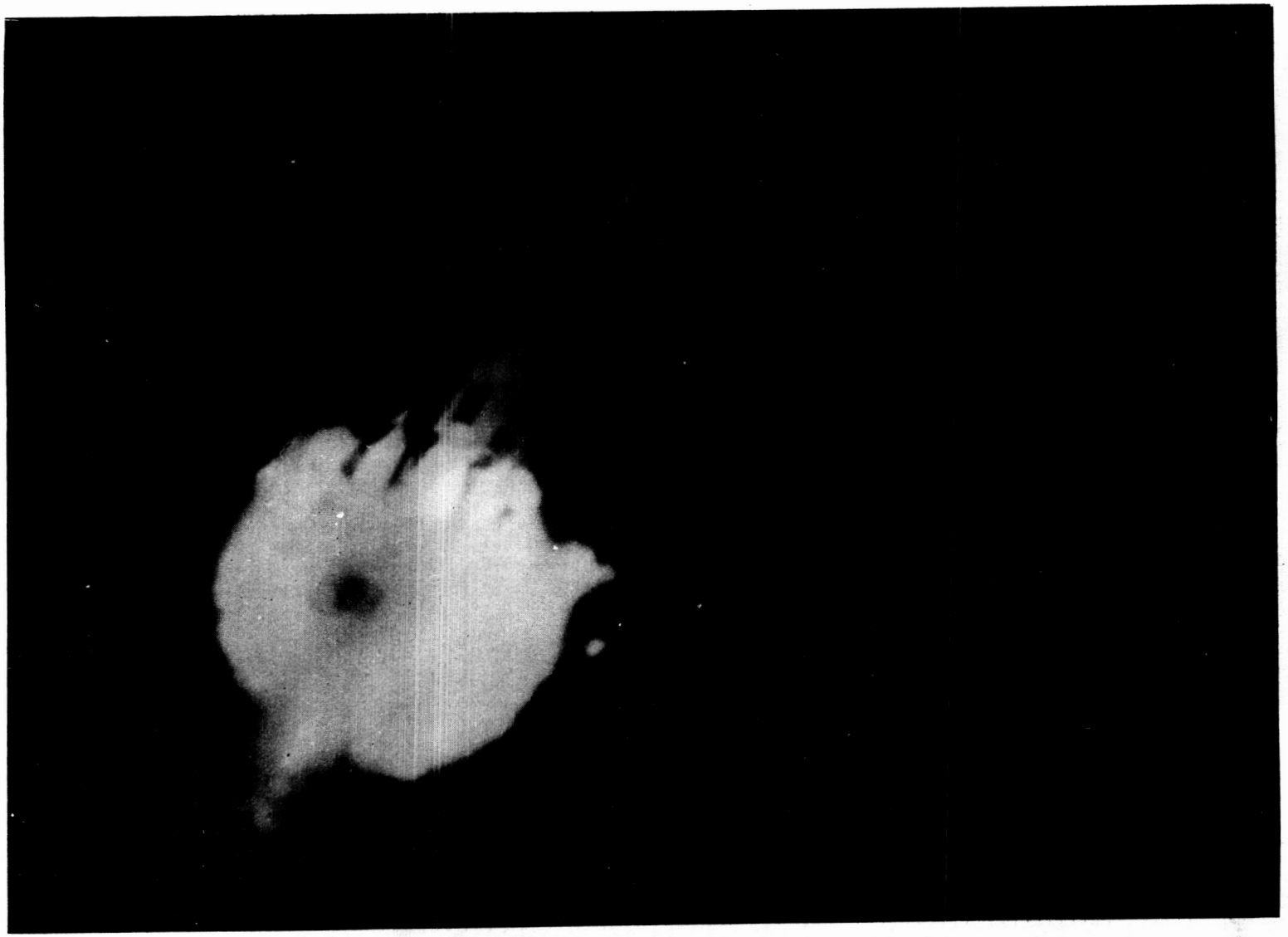

Figure 4.3.6-4. - Thrust termination as fireball engulfs launch vehicle.

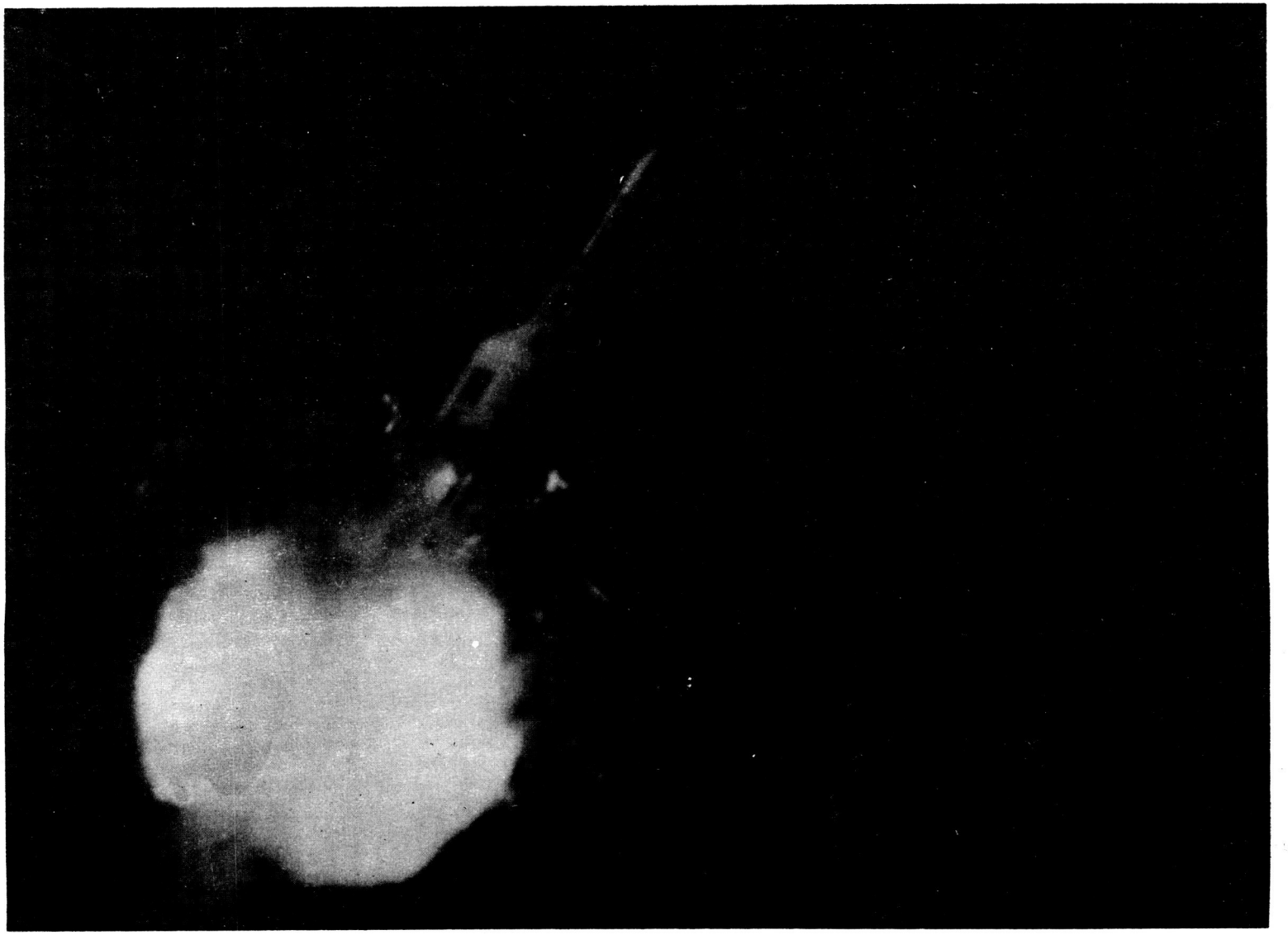

Figure 4.3.6-5.- Launch vehicle disintegrates during thrust termination.

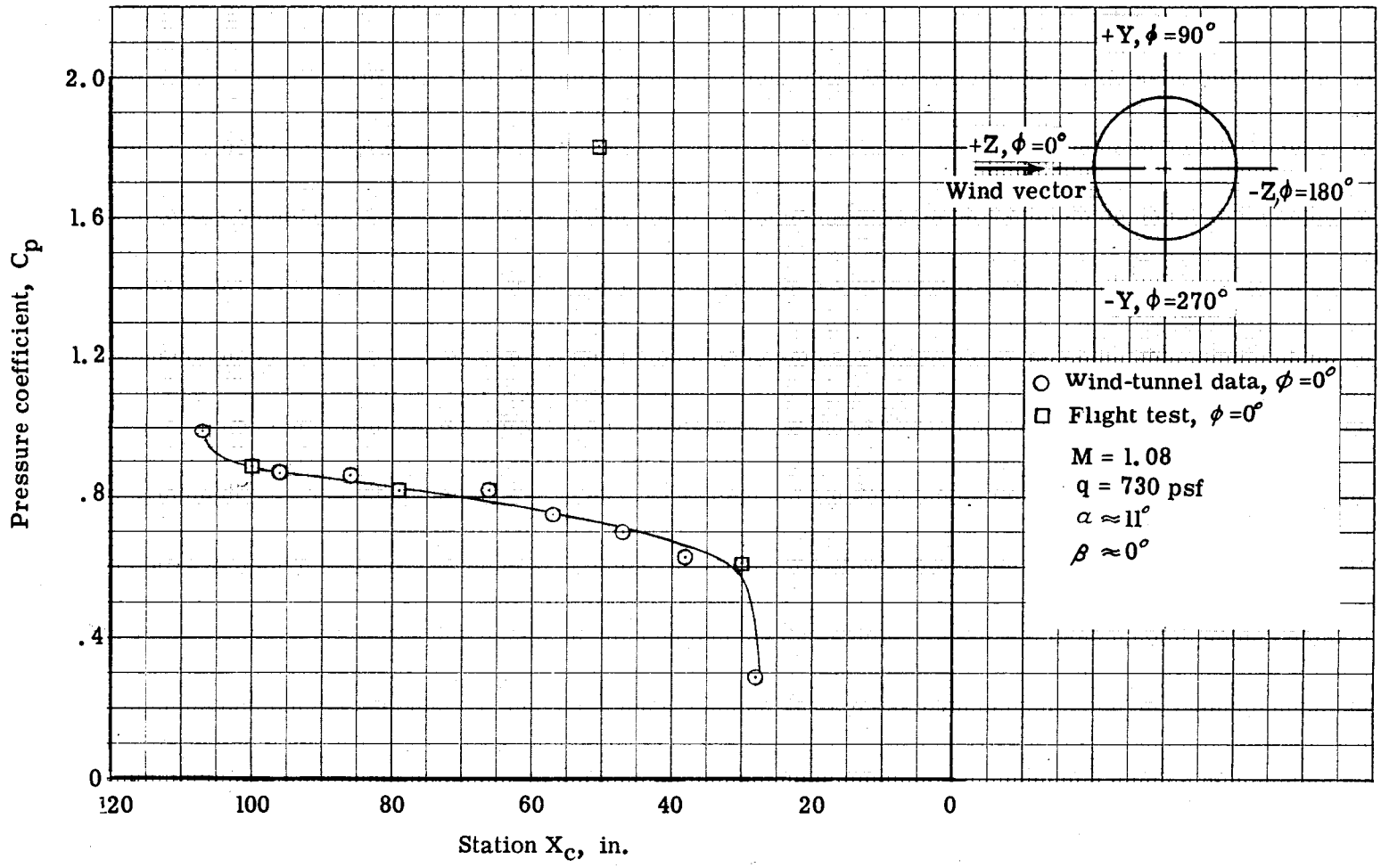

Figure 4.3.6-6. - Pressure coefficient comparison in the pitch plane +Z quadrant.

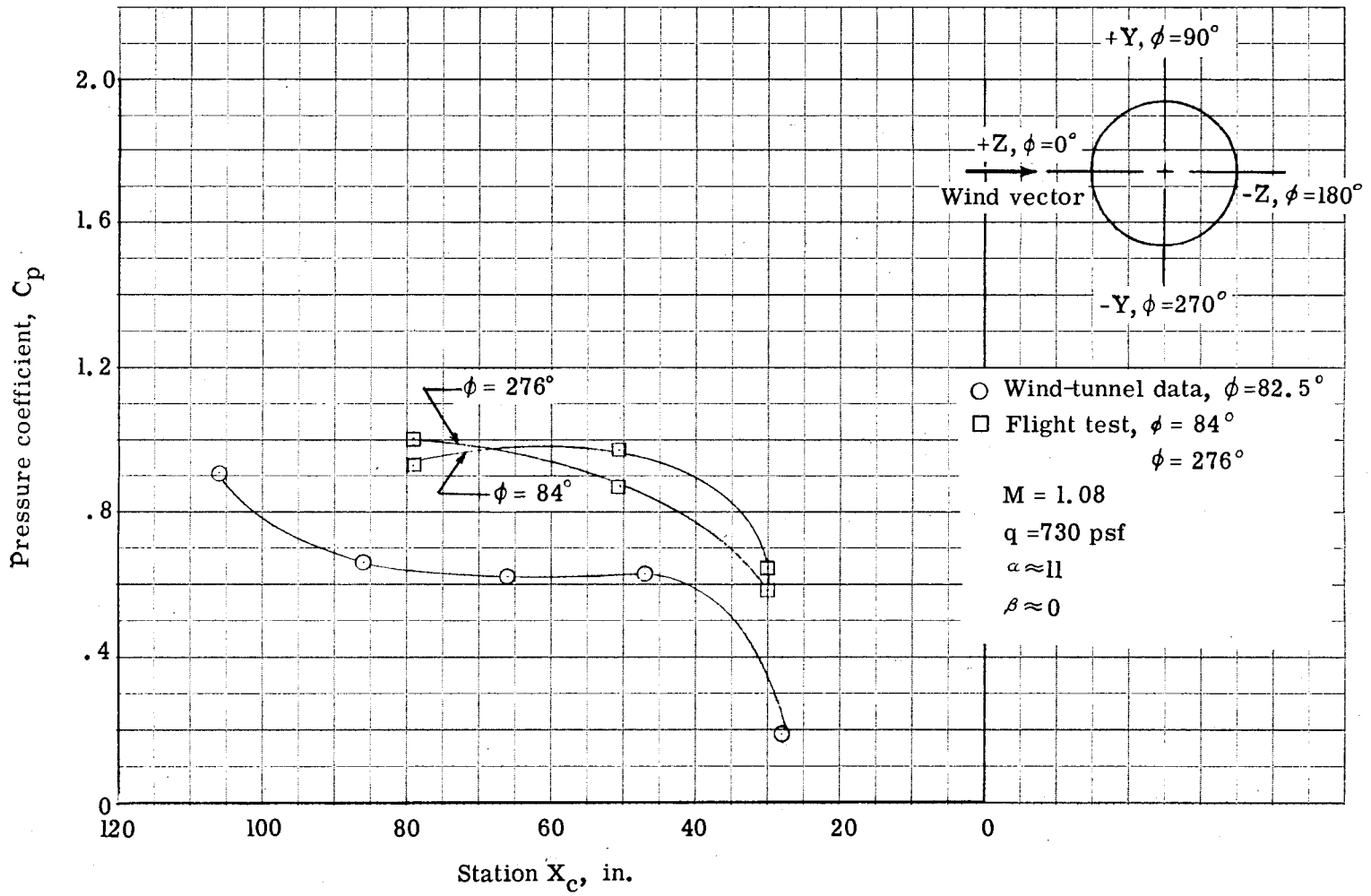

Figure 4.3.6-7.- Pressure coefficient comparison along two rays in the yaw plane.

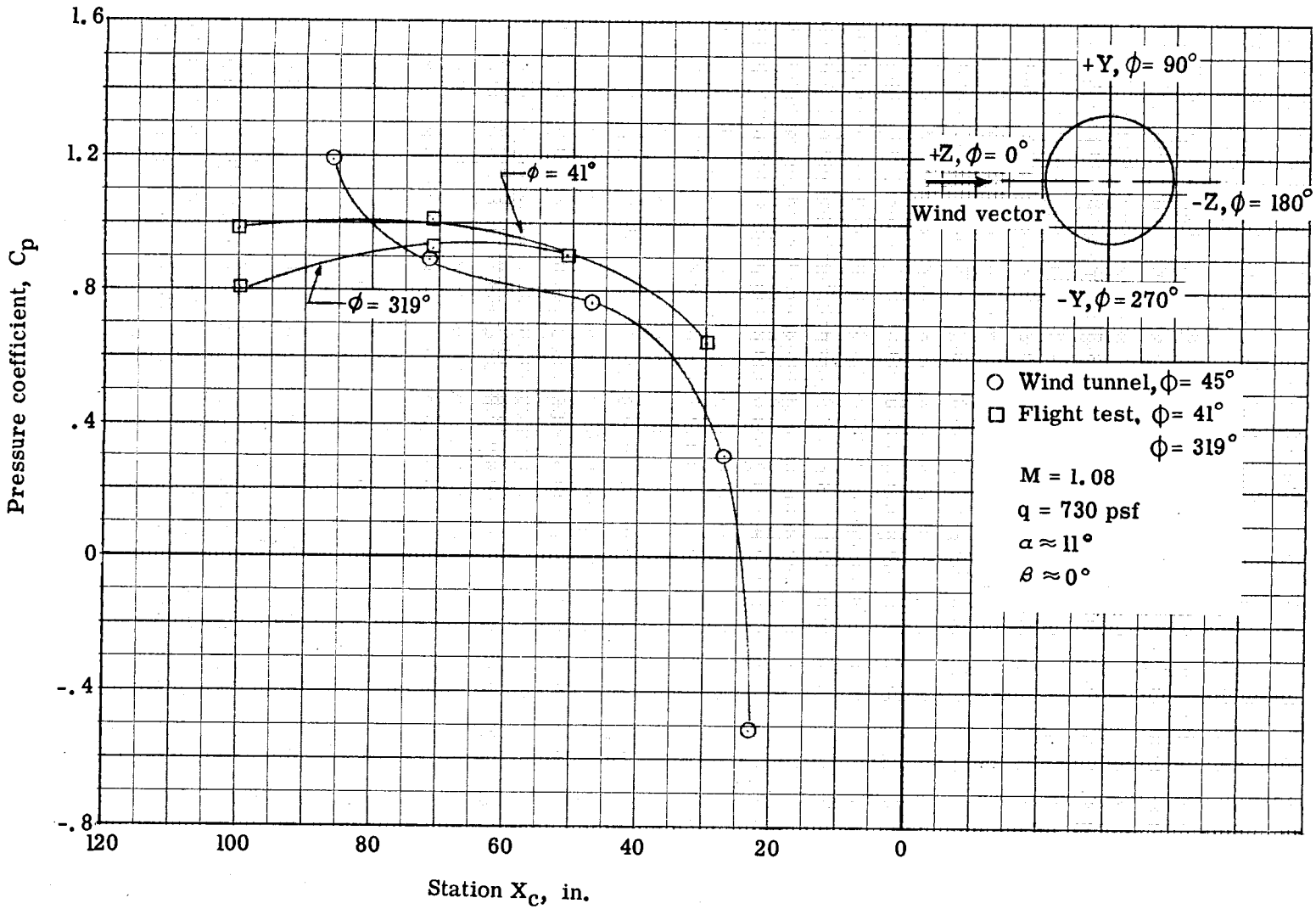

Figure 4.3.6-8. - Pressure coefficient comparison in planes between jet plumes.

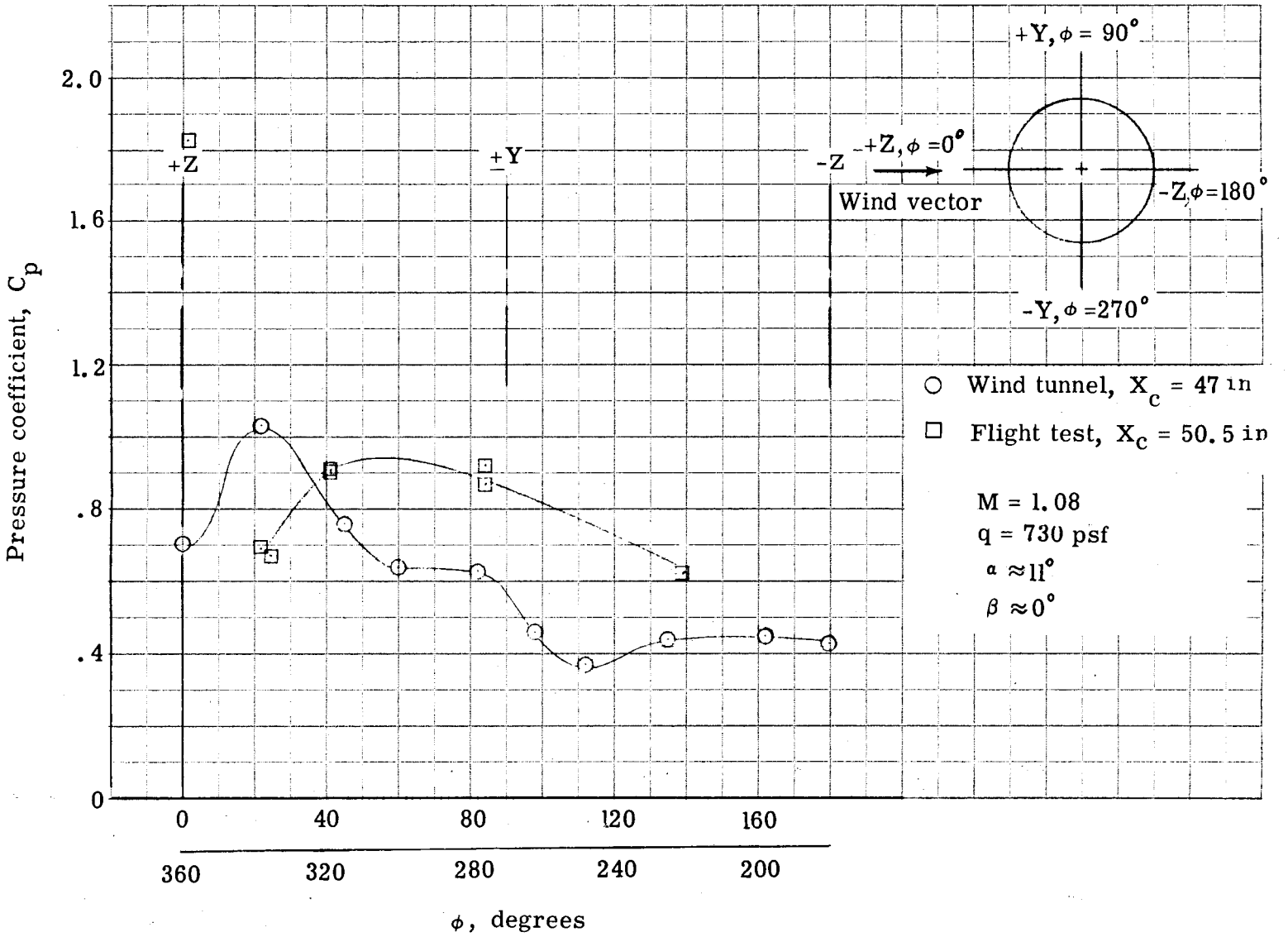

Figure 4.3.6-9. - Pressure coefficient comparison at a typical station.

[redacted]

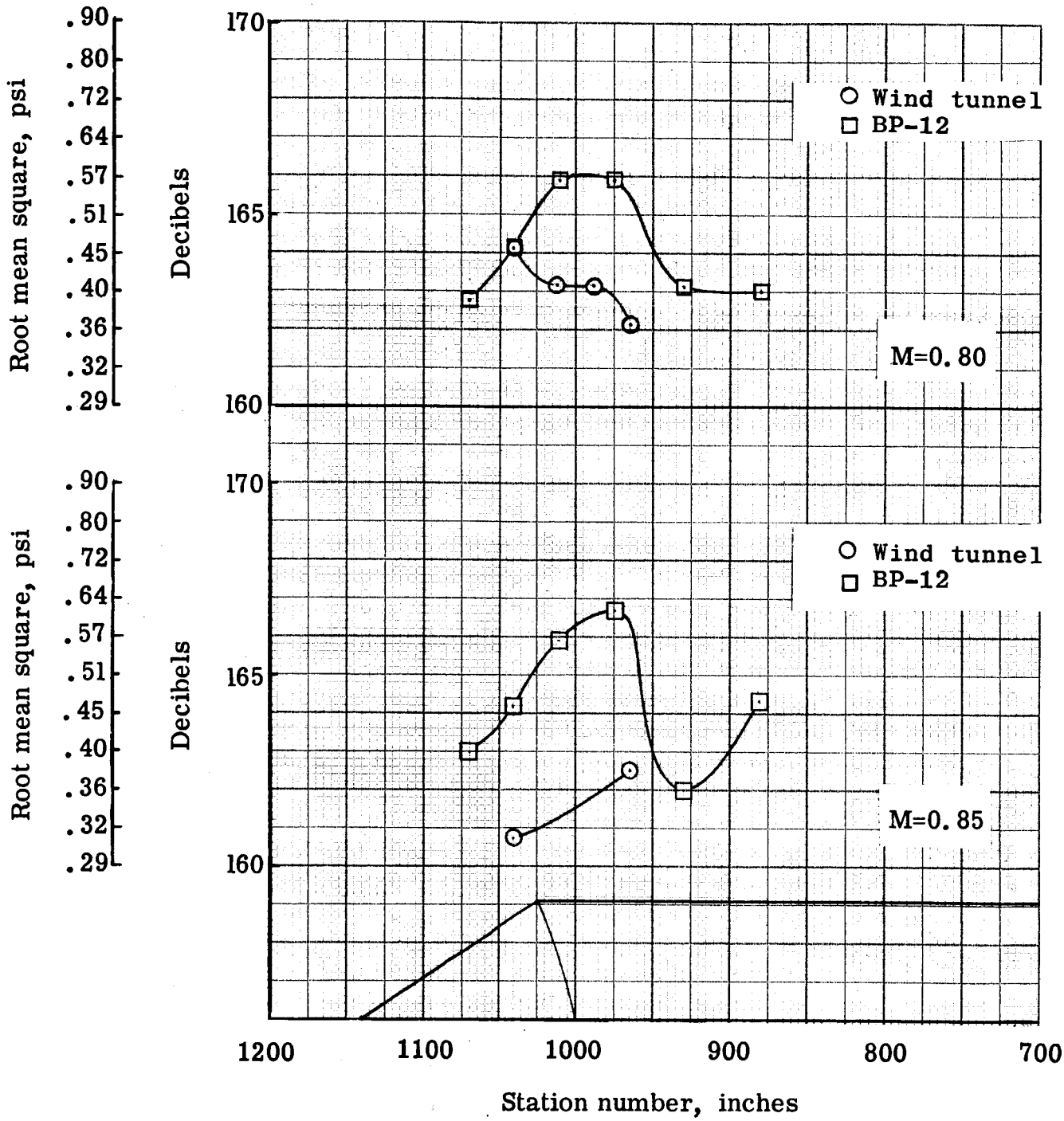

(a) M = 0.80 and 0.95.

Figure 4.3.6-10.- Comparison of BP-12 fluctuation pressures with wind-tunnel data.

[redacted]

[redacted]

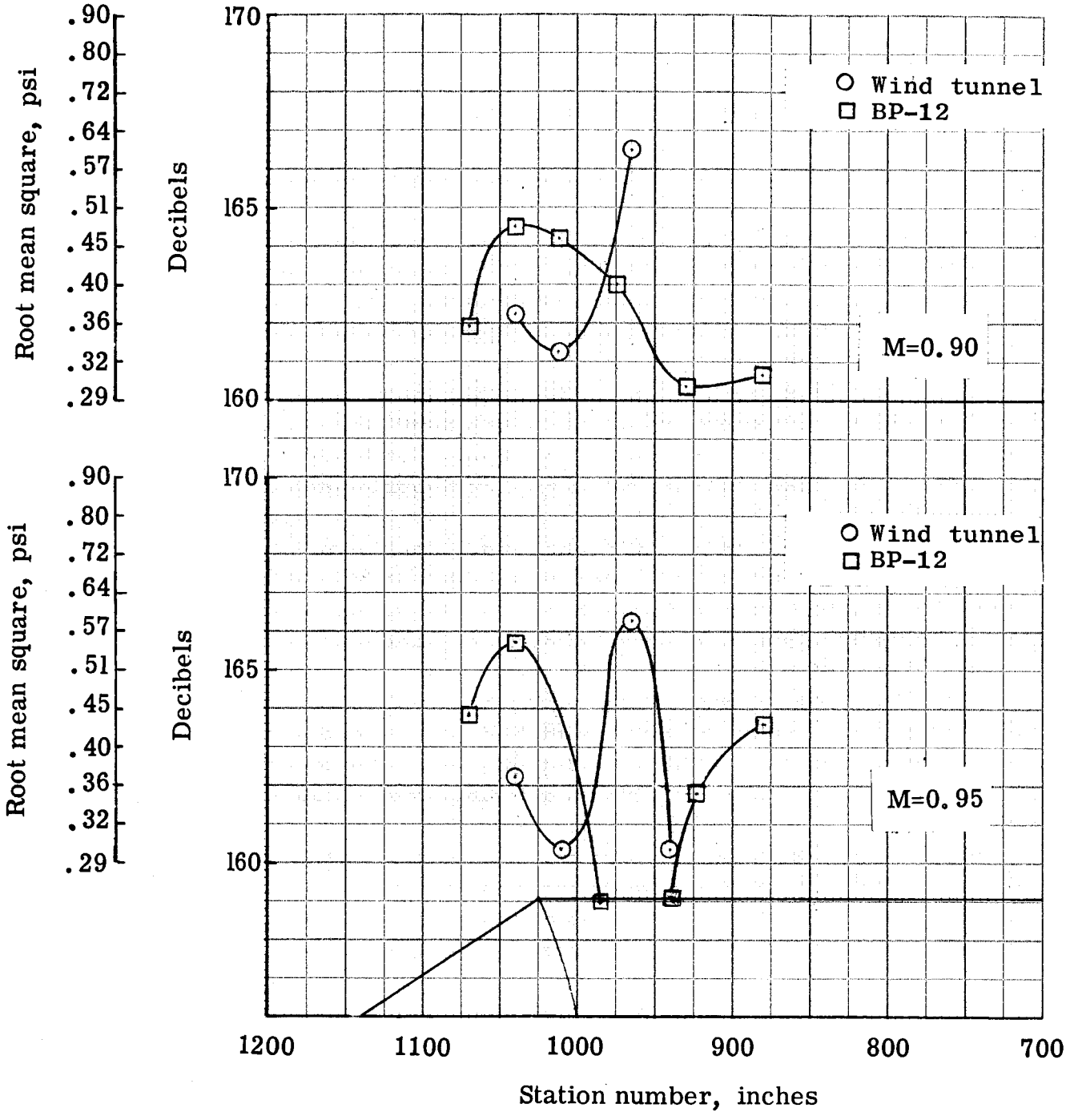

(b) M = 0.90 and 0.95.

Figure 4.3.6-10. - Concluded.

[redacted]

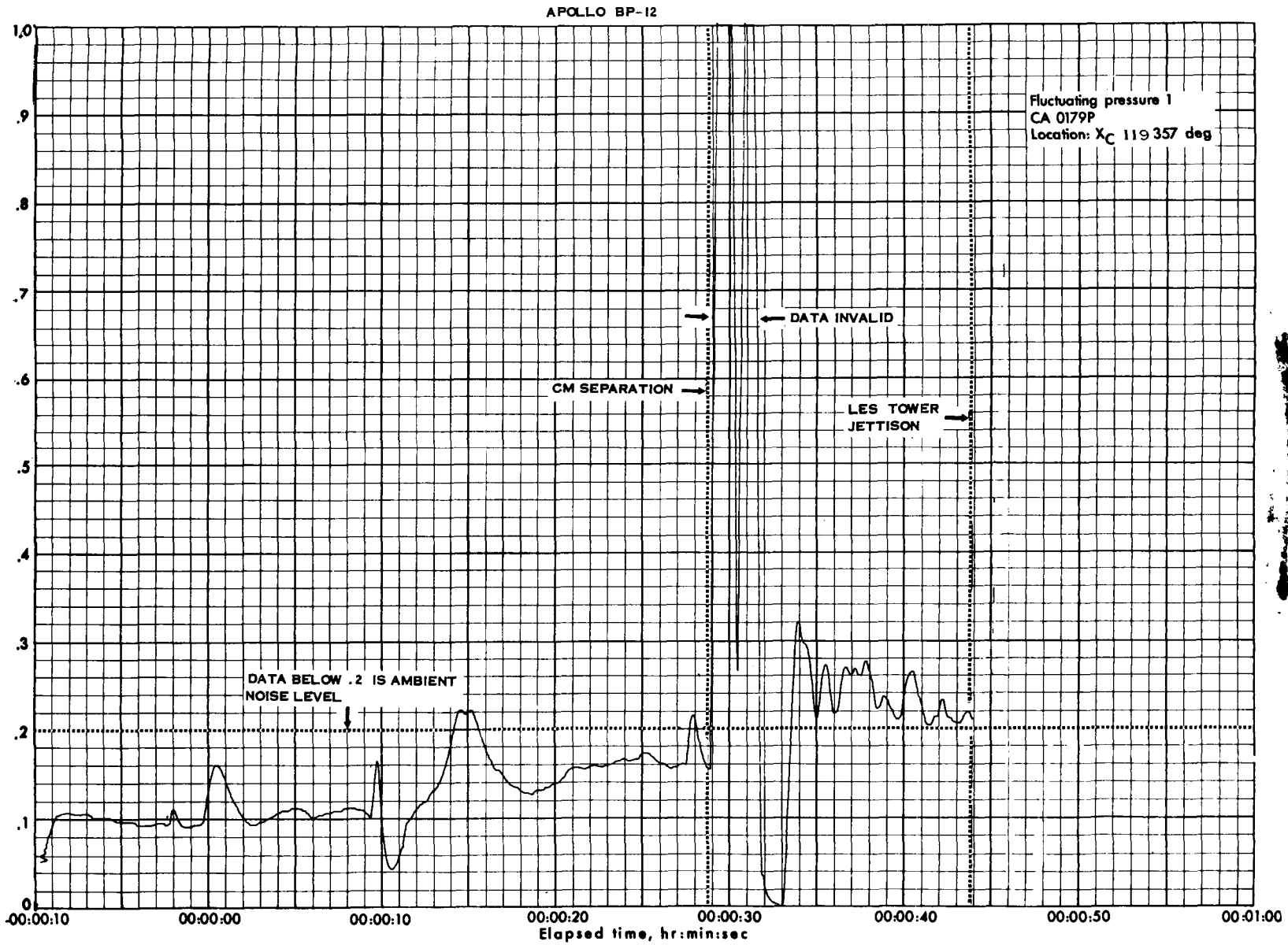

(a) Fluctuating pressure 1.

Figure 4.3.6-11. - Root mean square pressure time history.

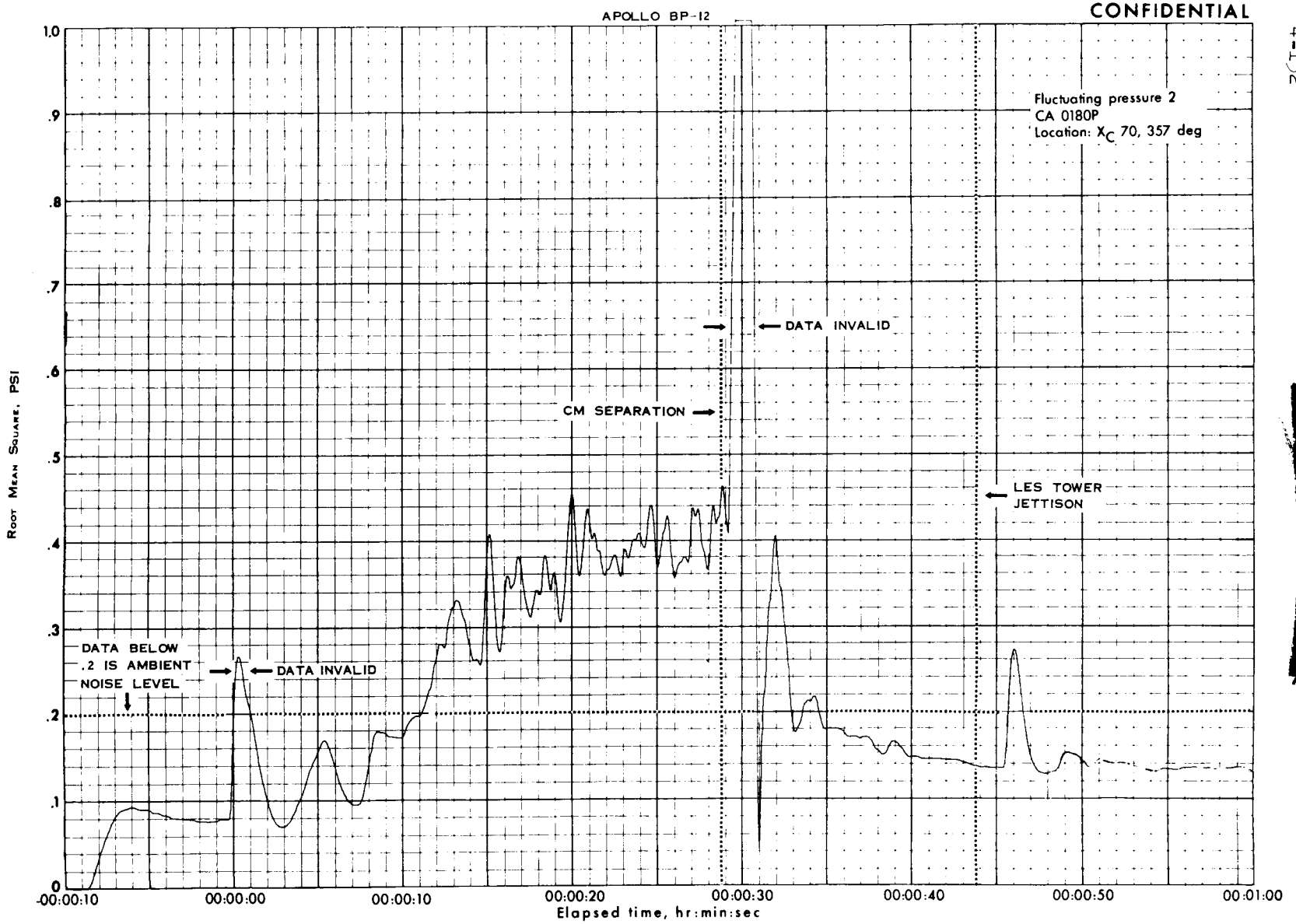

(b) Fluctuating pressure 2.

Figure 4.3.6-11. - Continued.

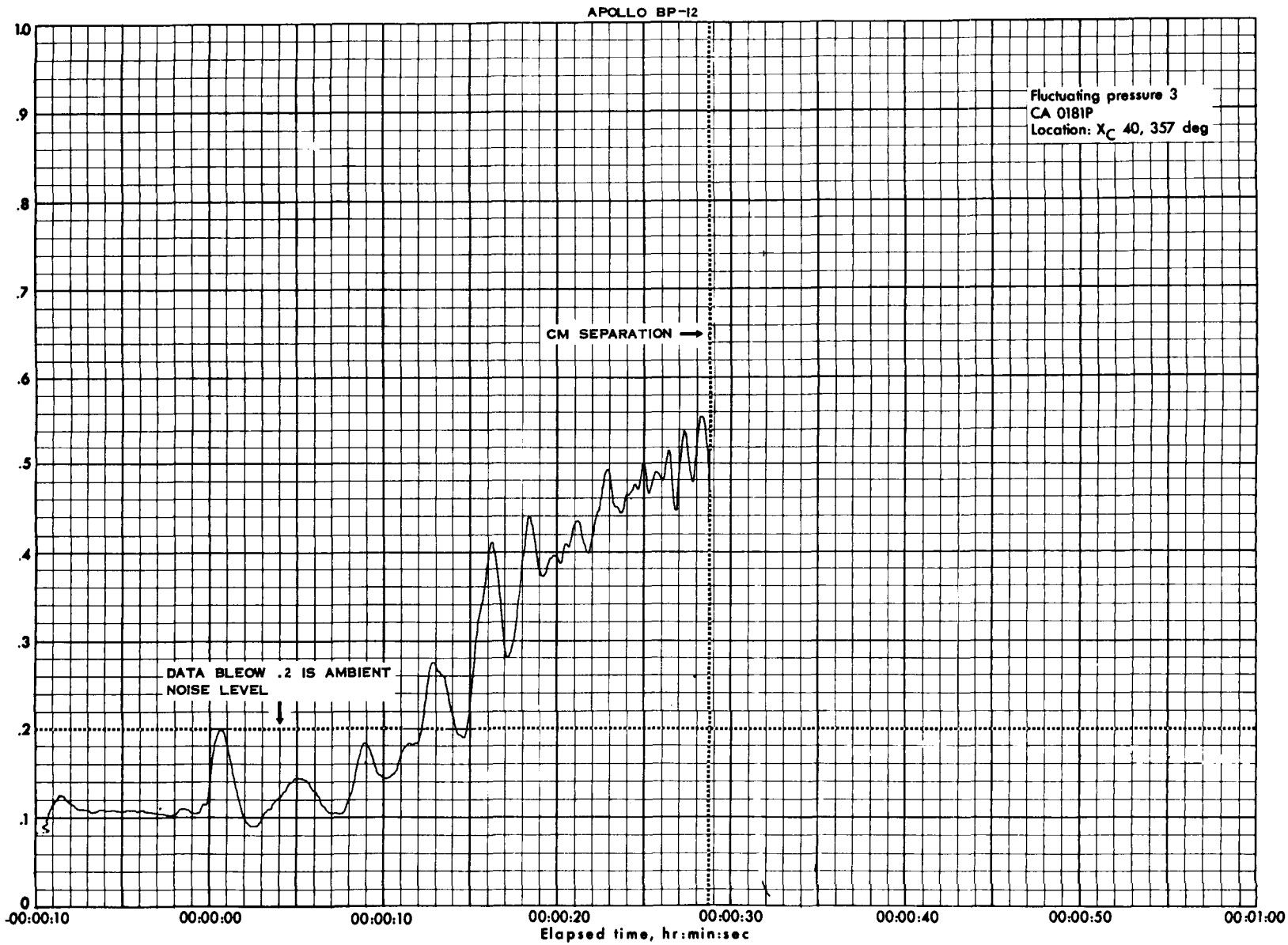

(c) Fluctuating pressure 3.

Figure 4.3.6-11. - Continued.

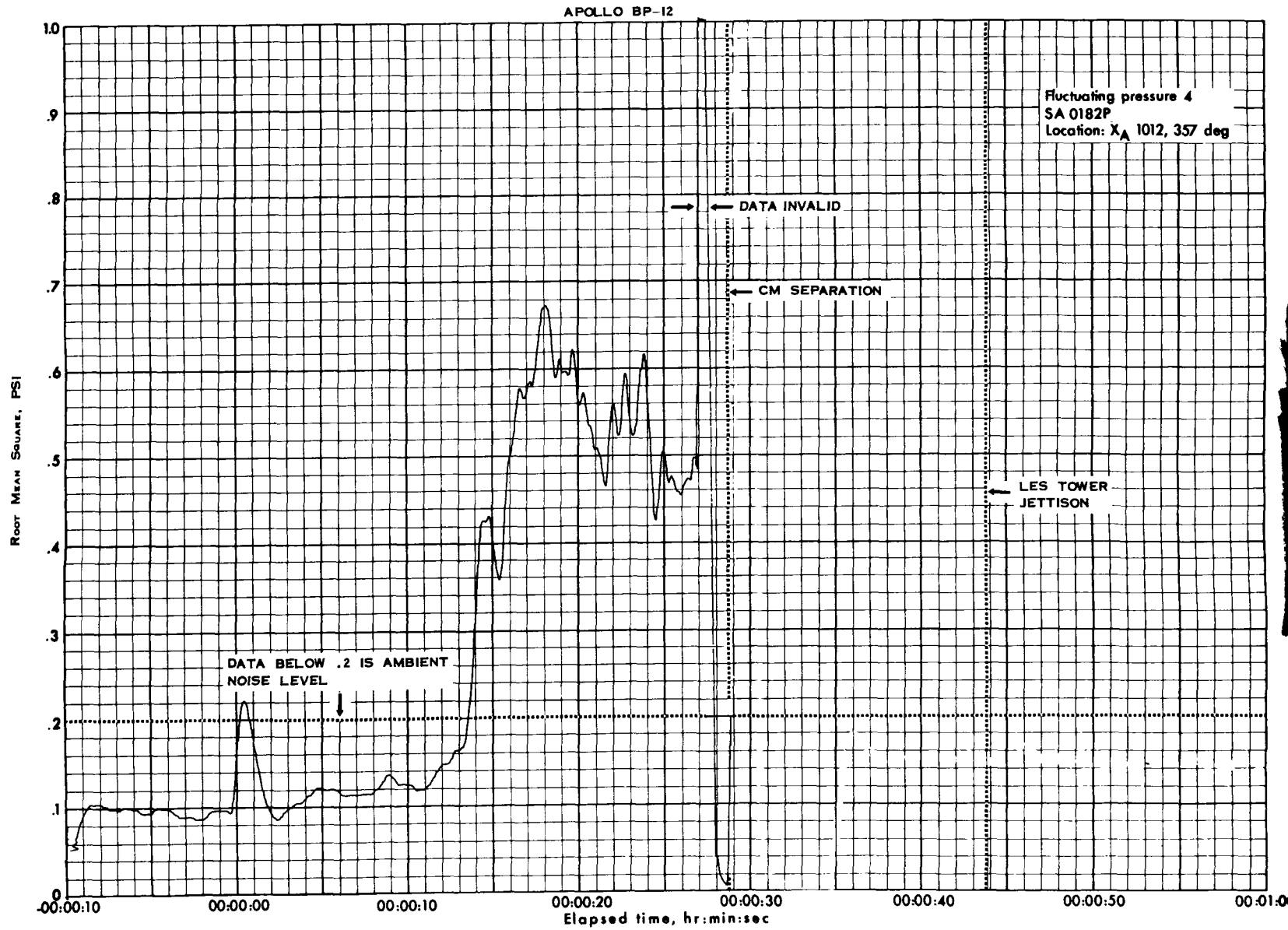

(d) Fluctuating pressure 4.

Figure 4.3.6-11. - Continued.

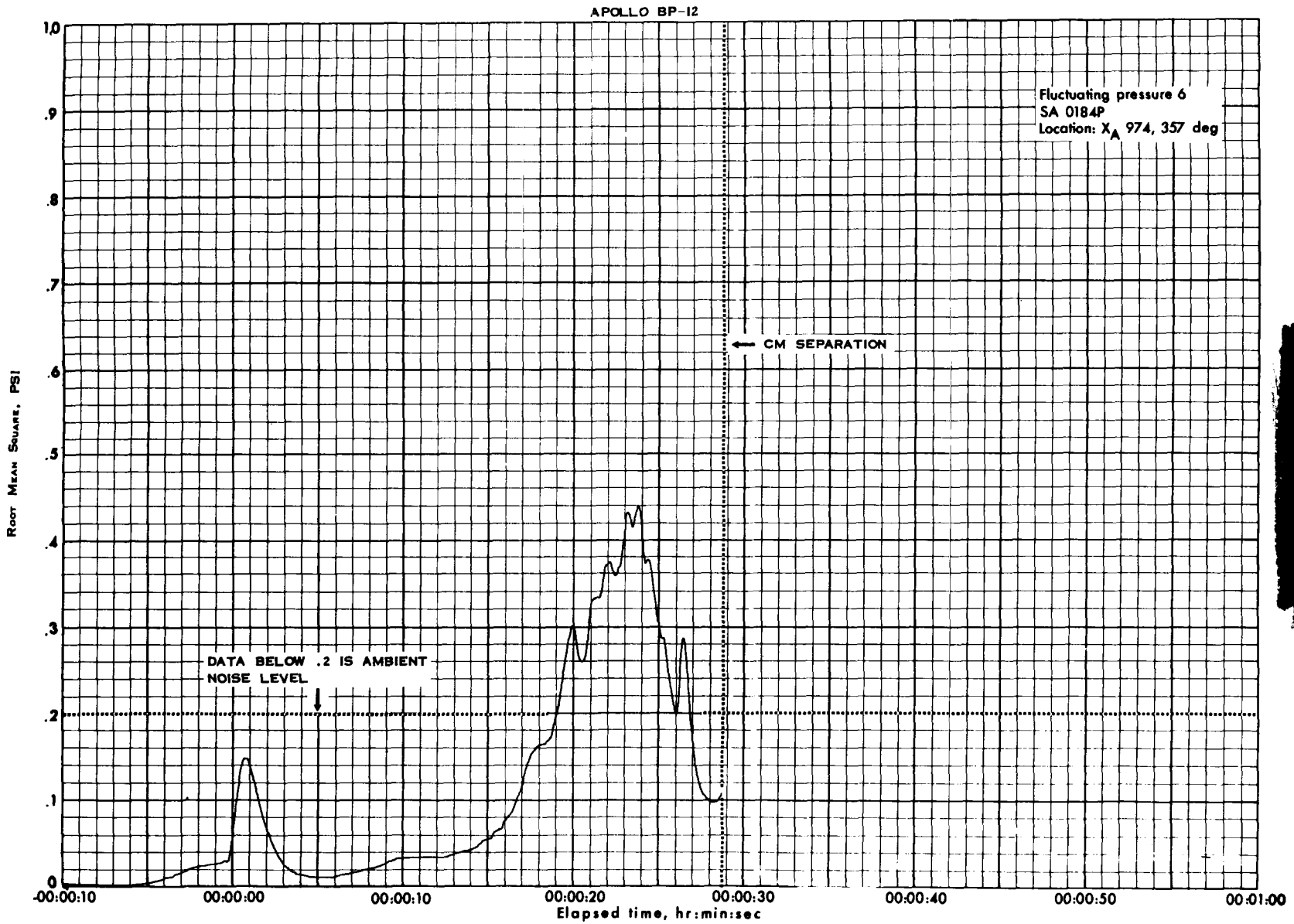

(e) Fluctuating pressure 6.

Figure 4.3.6-11. - Continued.

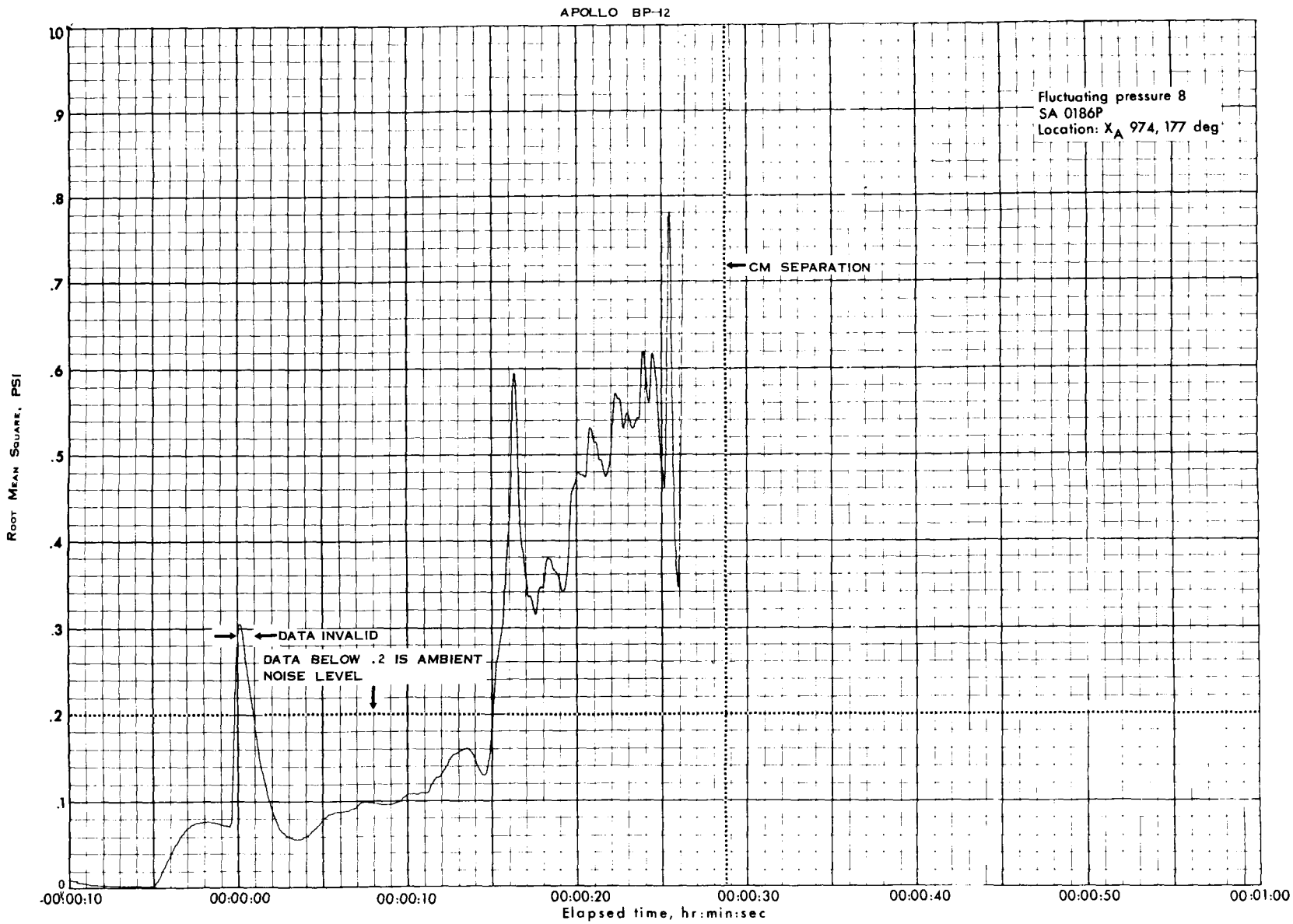

(f) Fluctuating pressure 8.

Figure 4.3.6-11. - Continued.

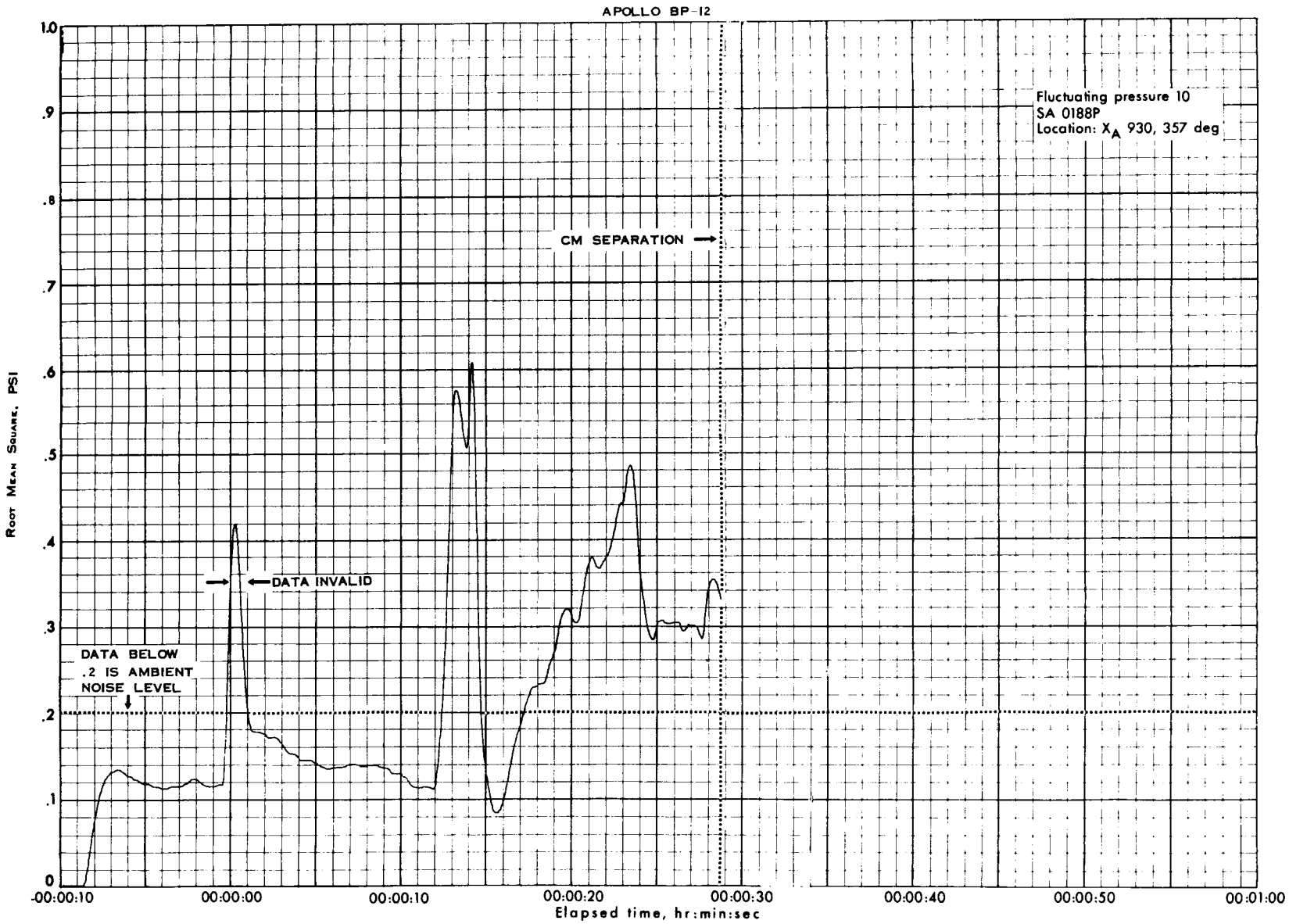

(g) Fluctuating pressure 10.

Figure 4.3.6-11. - Concluded.

00:00:28.5 CM-SEPARATION
00:00:28.4 LES AND P/C MTR IGNITION
00:00:43.7 LES TOWER JETTISON
00:00:47.1 DROGUE DEPLOYMENT

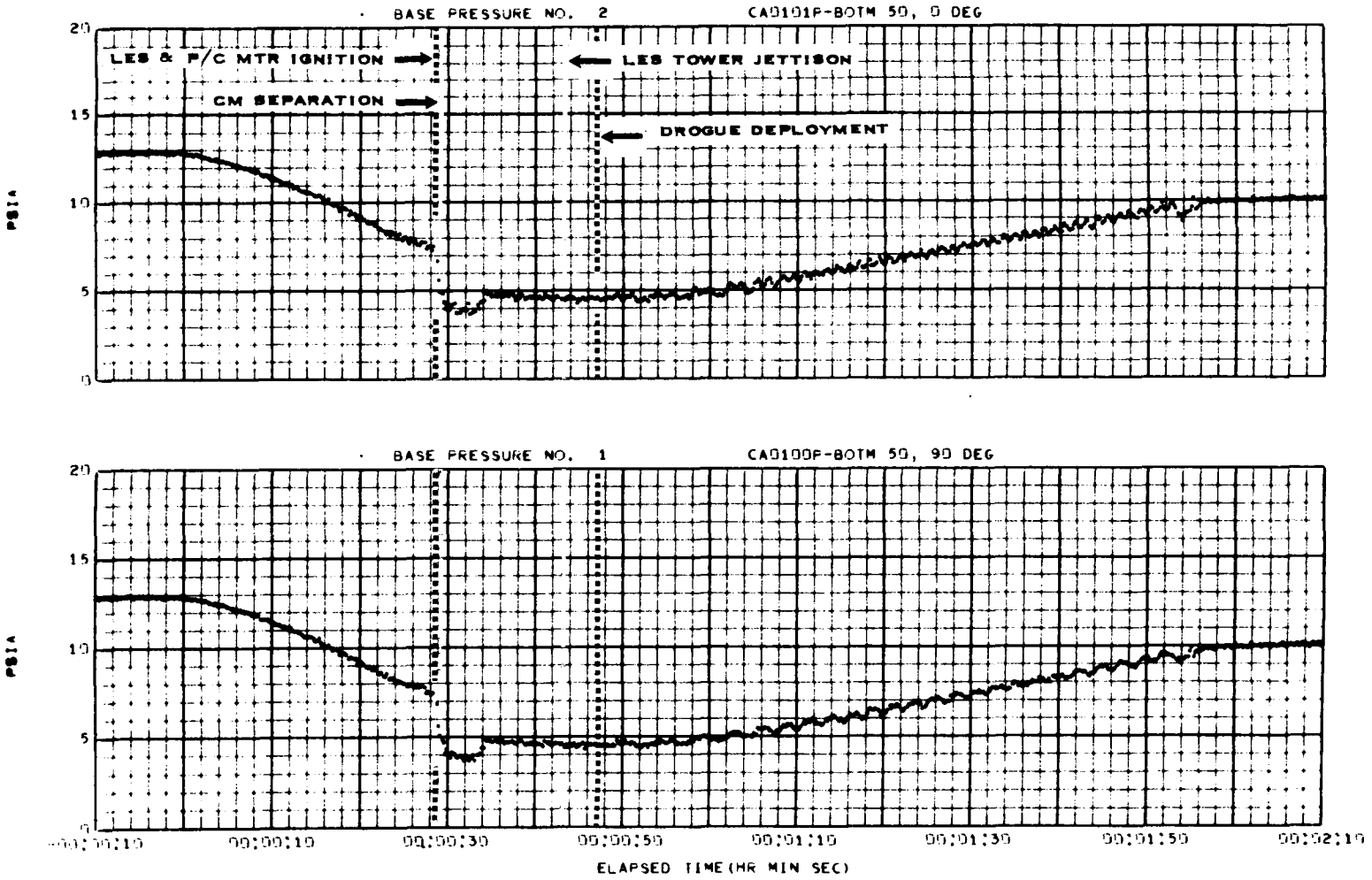

(a) Base pressures 1 and 2.

Figure 4.3.6-12. - Time histories of base pressures.

00:00:28.5 CM-SEPARATION
00:00:28.4 LES AND P/C MTR IGNITION
00:00:43.7 LES TOWER JETTISON
00:00:47.1 DROGUE DEPLOYMENT

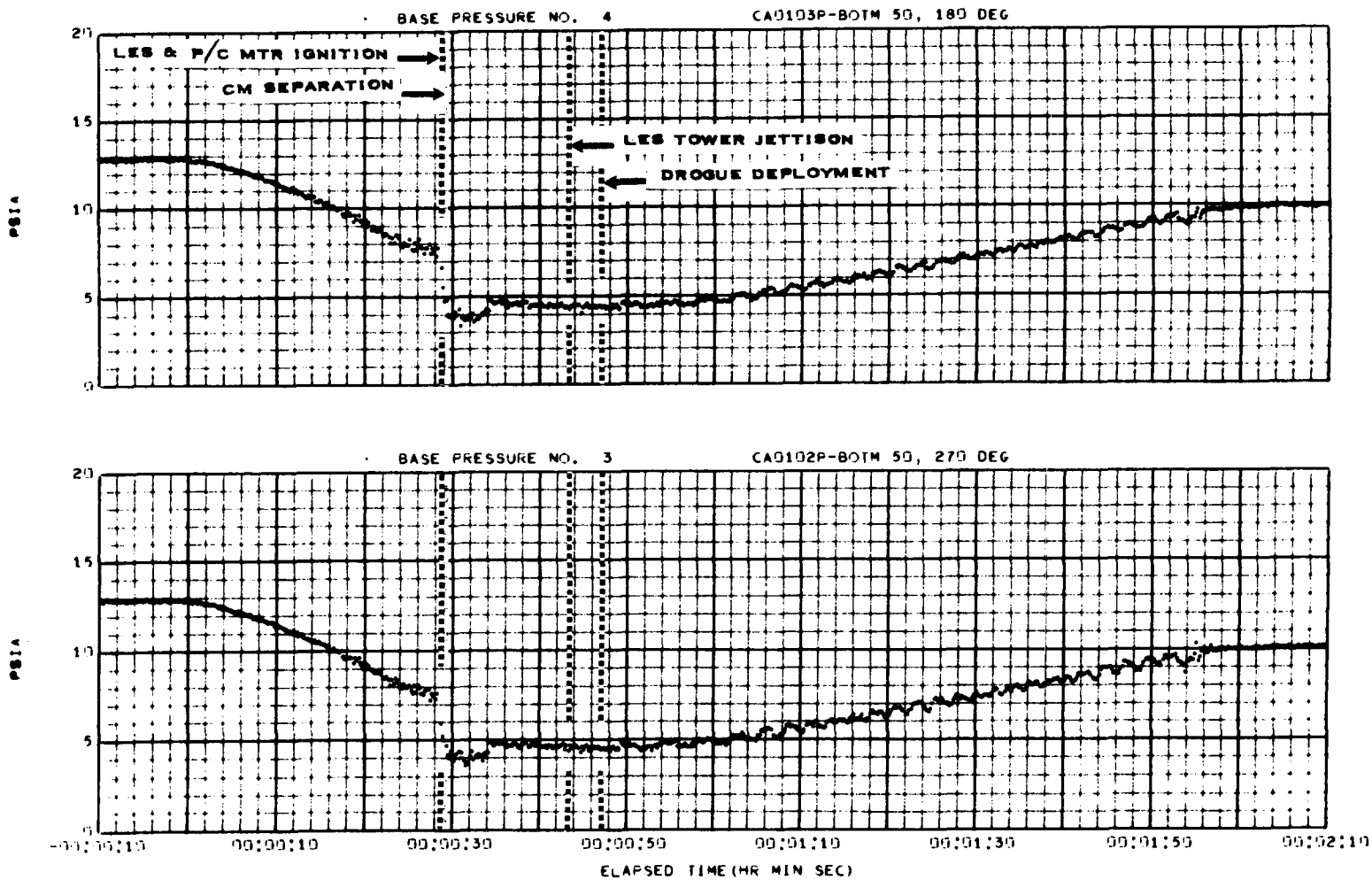

(b) Base pressures 3 and 4.

Figure 4.3.6-12. - Continued.

00:00:28.5 CM-SEPARATION
00:00:28.4 LES AND P/C MTR IGNITION
00:00:43.7 LES TOWER JETTISON
00:00:47.1 DROGUE DEPLOYMENT

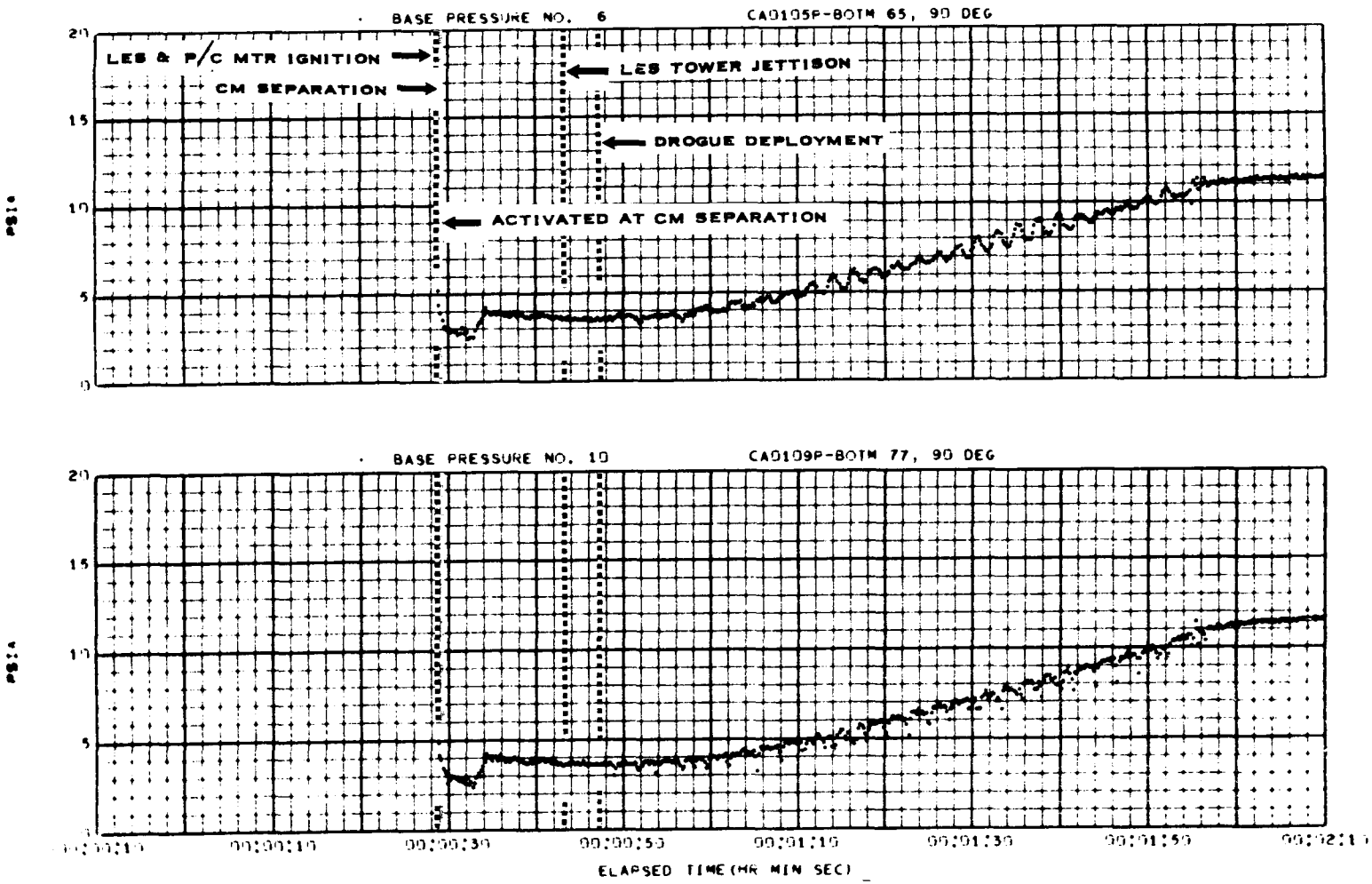

(c) Base pressures 6 and 10.

Figure 4.3.6-12. - Continued.

00:00:28.5 CM-SEPARATION
00:00:28.4 LES AND P/C MTR IGNITION
00:00:43.7 LES TOWER JETTISON
00:00:47.1 DROGUE DEPLOYMENT

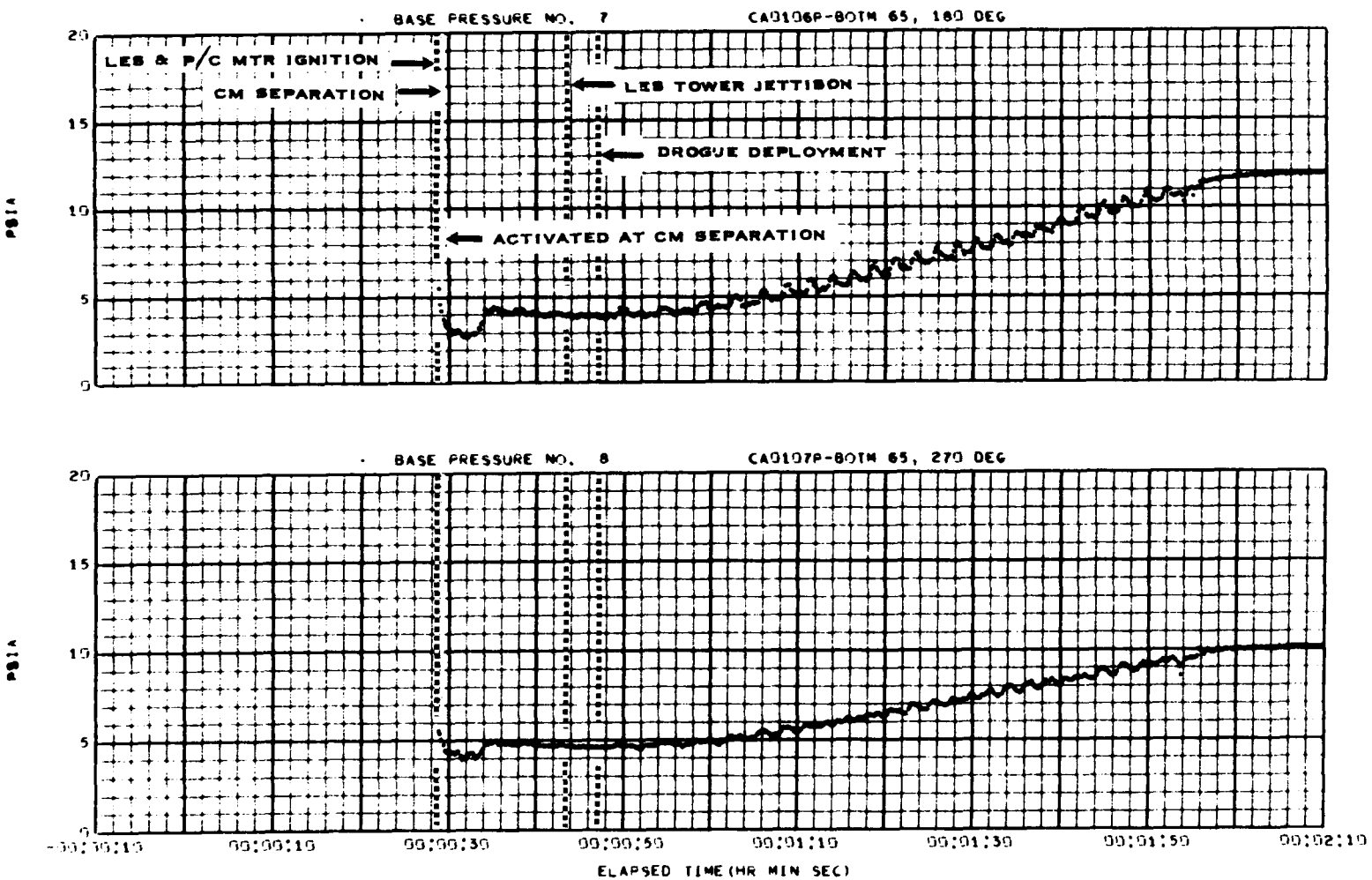

(d) Base pressures 7 and 8.

Figure 4.3.6-12. - Continued.

00:00:24.5 CM-SEPARATION
00:00:28.4 LES AND P/C MTR IGNITION
00:00:45.7 LES TOWER JETTISON
00:00:47.1 DROGUE DEPLOYMENT

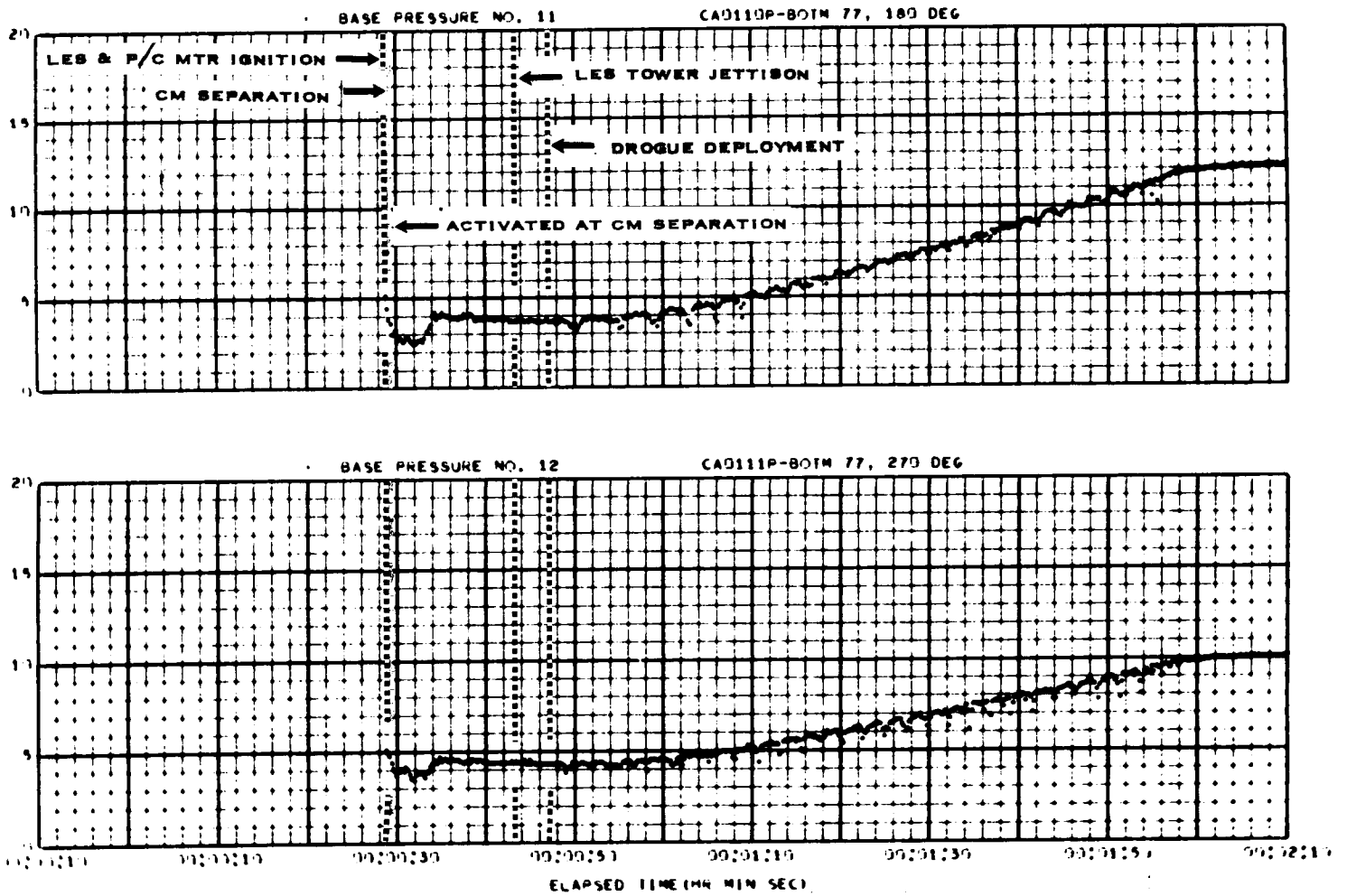

(e) Base pressures 11 and 12.

Figure 4.3.6-12. - Concluded.

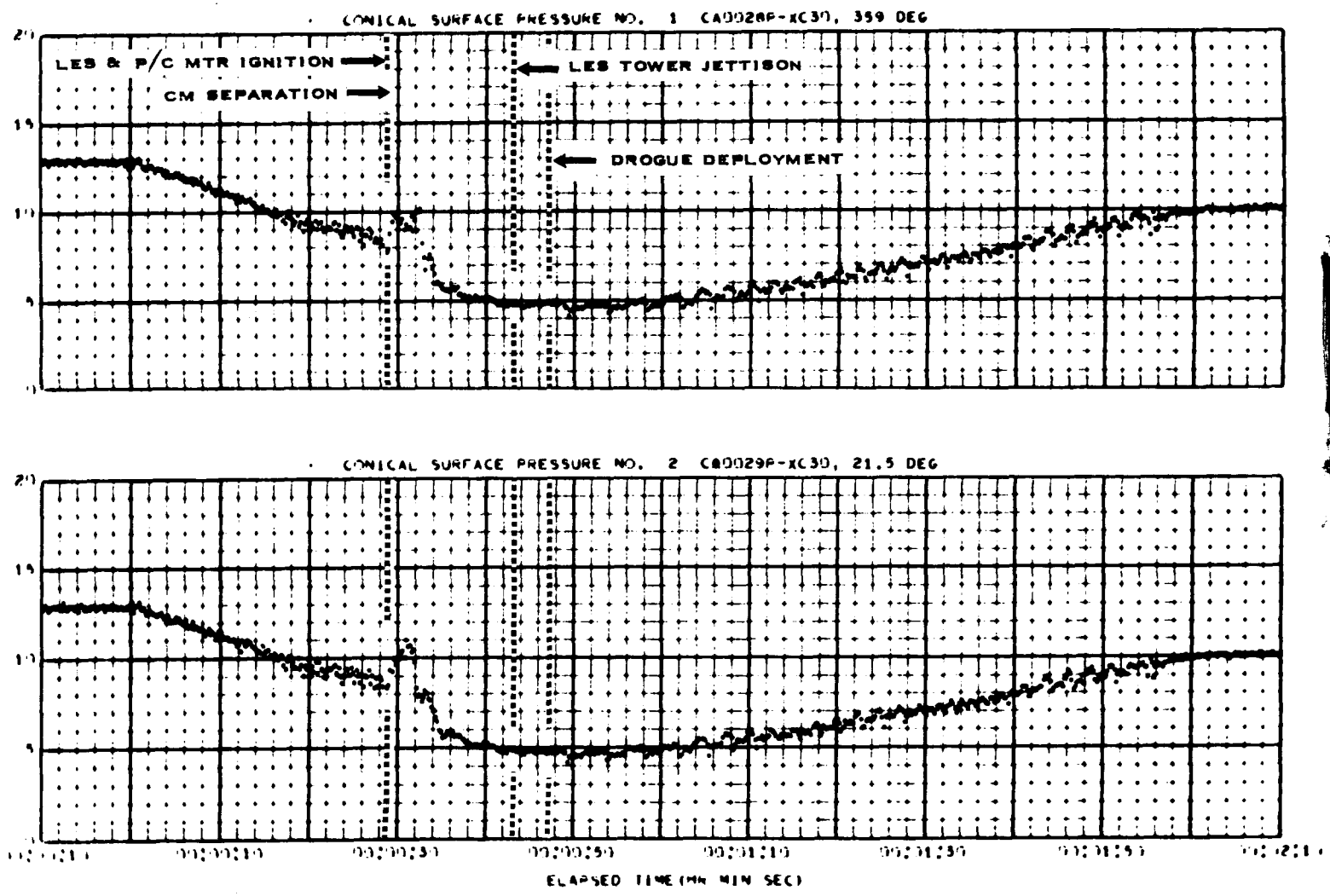

(a) Conical surface pressures 1 and 2.

Figure 4.3.6-13.- Time histories of conical surface pressures.

00:00:28.5 CM-SEPARATION
00:00:28.4 LES AND P/C MTR IGNITION
00:00:43.7 LES TOWER JETTISON
00:00:47.1 DROGUE DEPLOYMENT

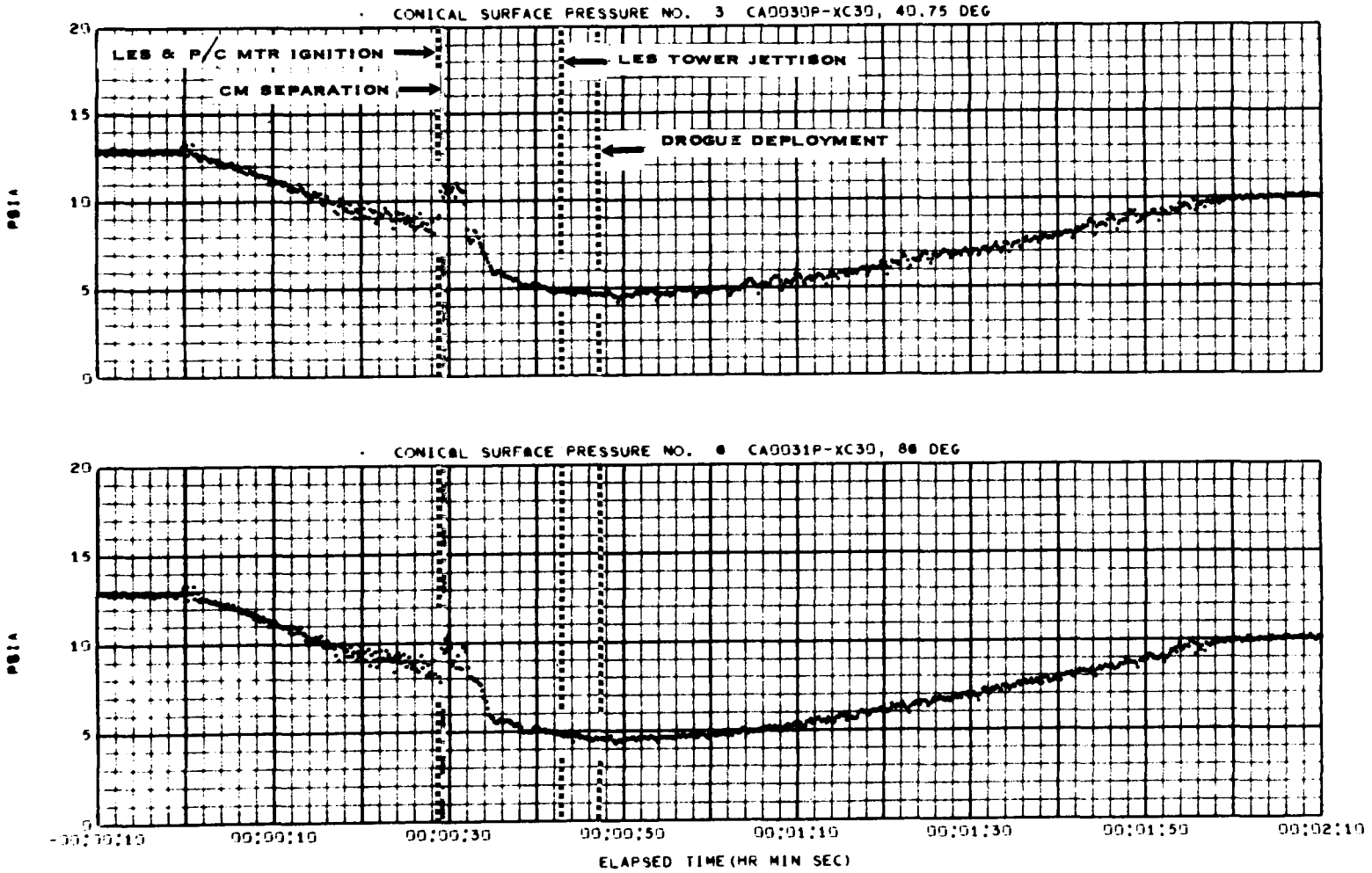

(b) Conical surface pressures 3 and 4.

Figure 4.3.6-13. - Continued.

00:00:24.5 CM-SEPARATION
00:00:28.4 LES AND P/C MTR IGNITION
00:00:43.7 LES TOWER JETTISON
00:00:47.1 DROGUE DEPLOYMENT

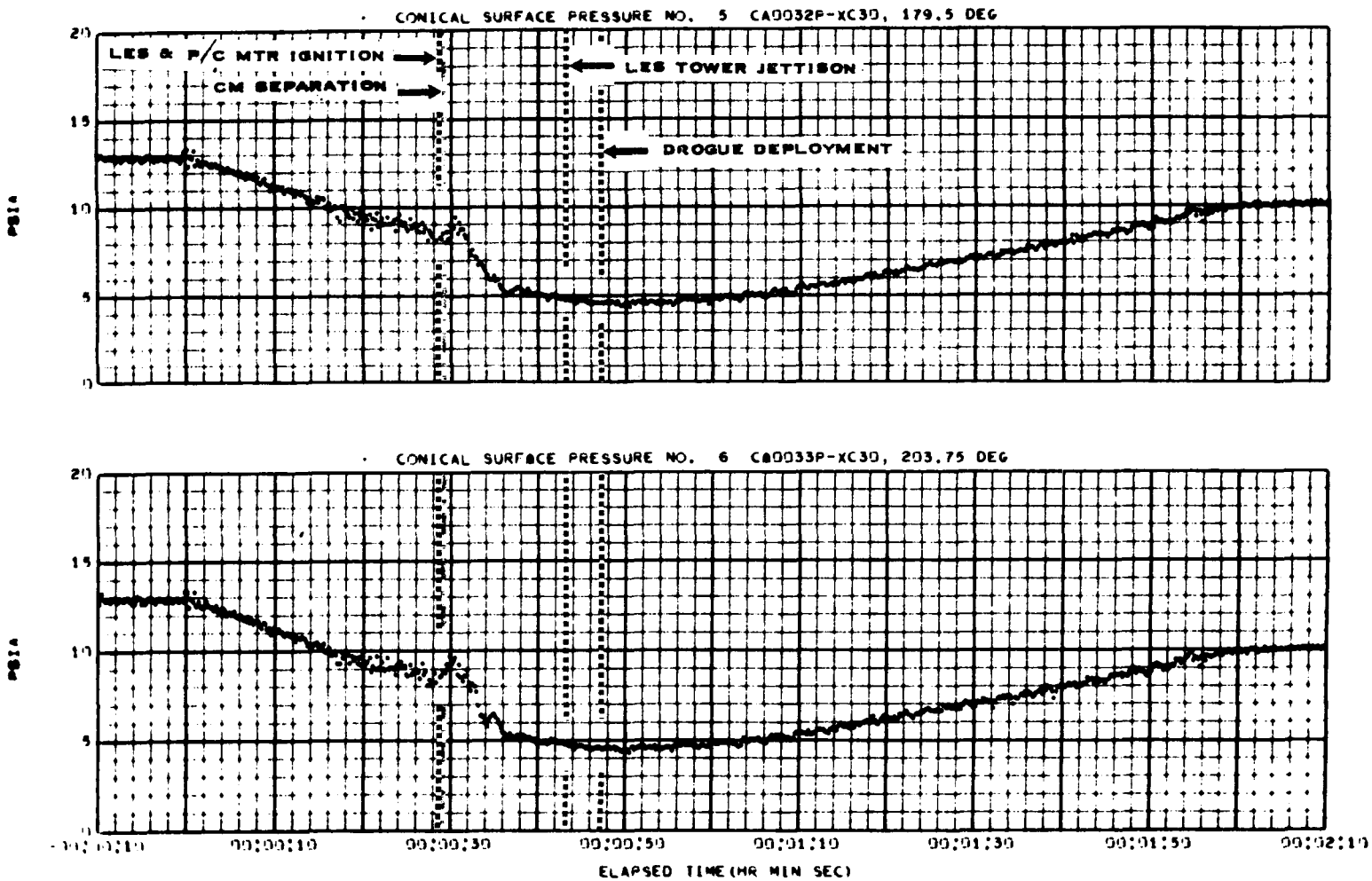

(c) Conical surface pressures 5 and 6.

Figure 4.3.6-13. - Continued.

00:00:24.5 CM-SEPARATION
00:00:24.4 LES AND P/C MTR IGNITION
00:00:45.7 LES TOWER JETTISON
00:00:47.1 DROGUE DEPLOYMENT

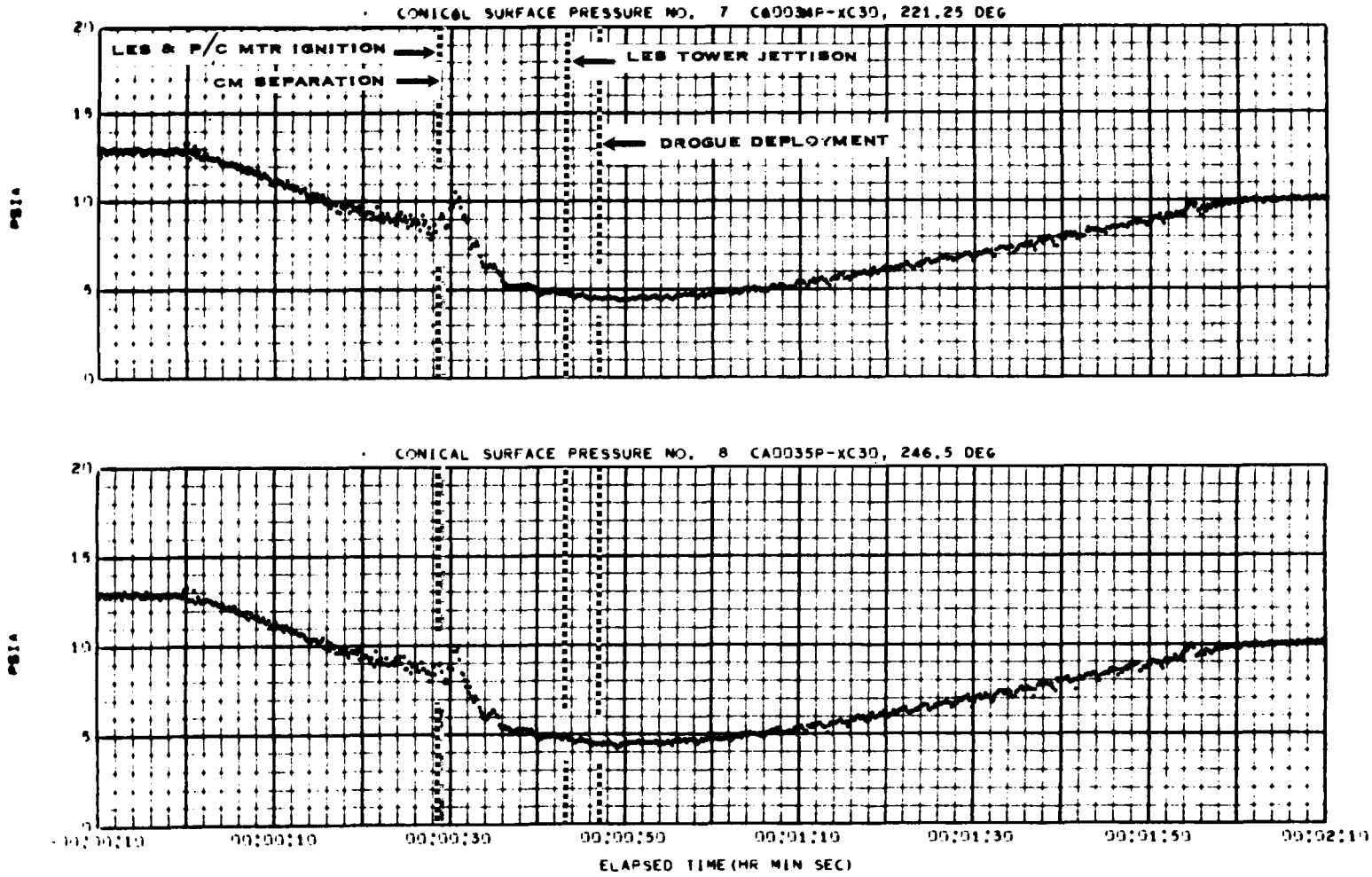

(d) Conical surface pressures 7 and 8.

Figure 4.3.6-13. - Continued.

00:00:28.4 LES AND P/C MTR IGNITION
00:00:43.7 LES TOWER JETTISON
00:00:47.1 DROGUE DEPLOYMENT
00:01:52.7 MAIN CHUTE DEPLOYMENT

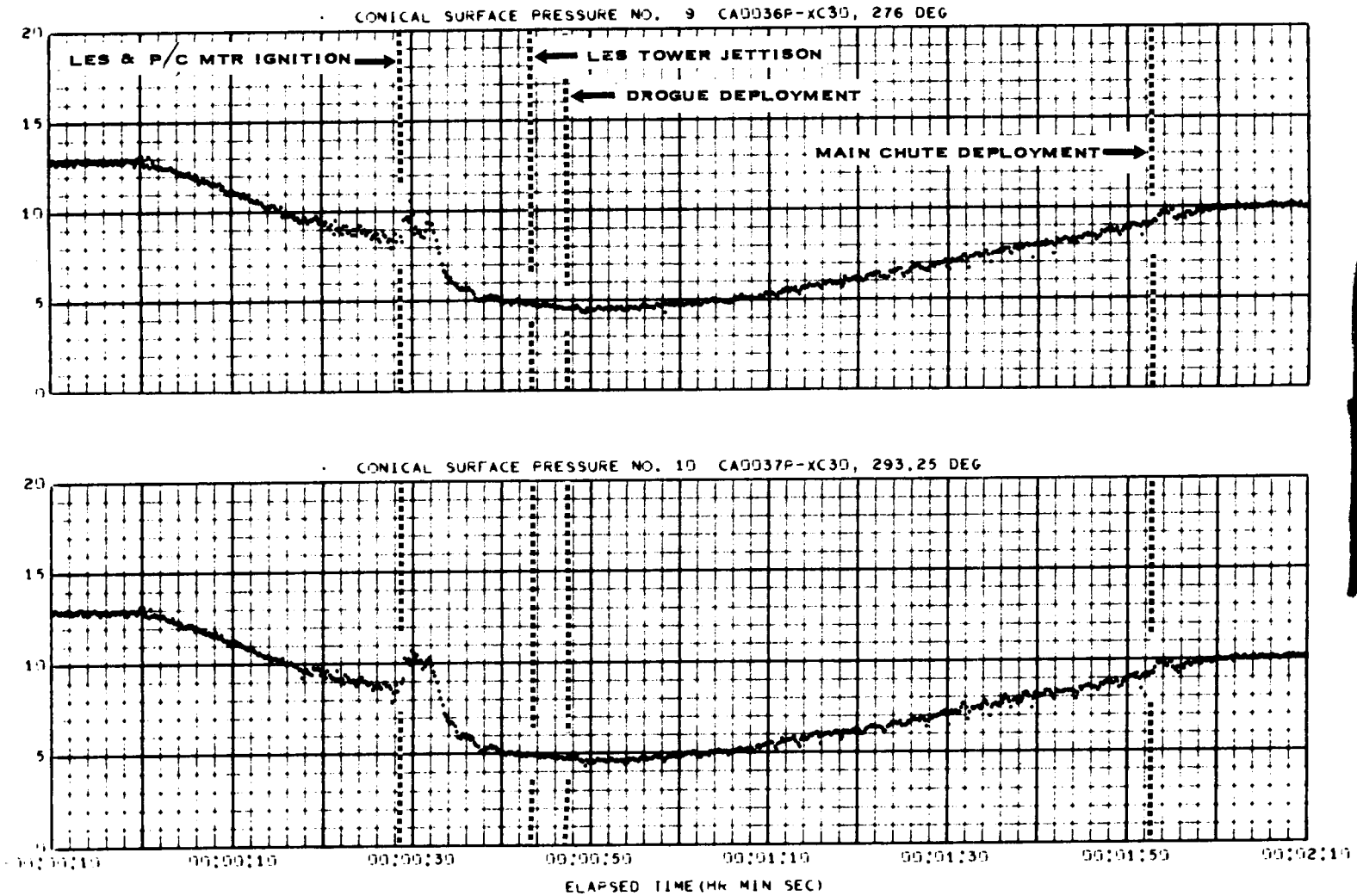

(e) Conical surface pressures 9 and 10.

Figure 4.3.6-13. - Continued.

00:00:28.4 LES AND P/C MTR IGNITION
00:00:43.7 LES TOWER JETTISON
00:00:47.1 DROGUE DEPLOYMENT
00:01:52.7 MAIN CHUTE DEPLOYMENT

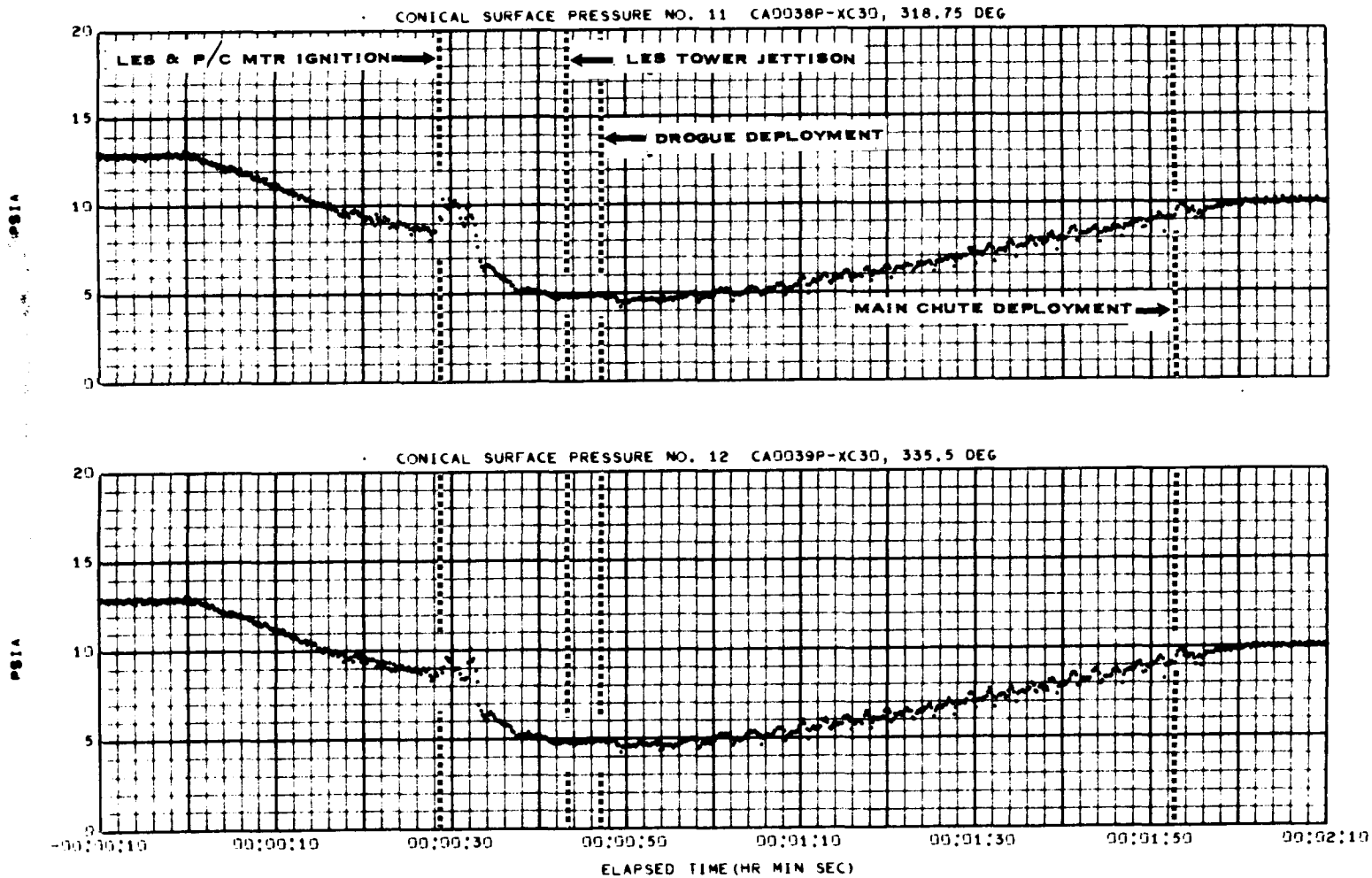

(f) Conical surface pressures 11 and 12.

Figure 4.3.6-13. - Continued.

00:00:28.4 LES AND P/C MTR IGNITION
00:00:43.7 LES TOWER JETTISON
00:00:47.1 DROGUE DEPLOYMENT
00:01:52.7 MAIN CHUTE DEPLOYMENT

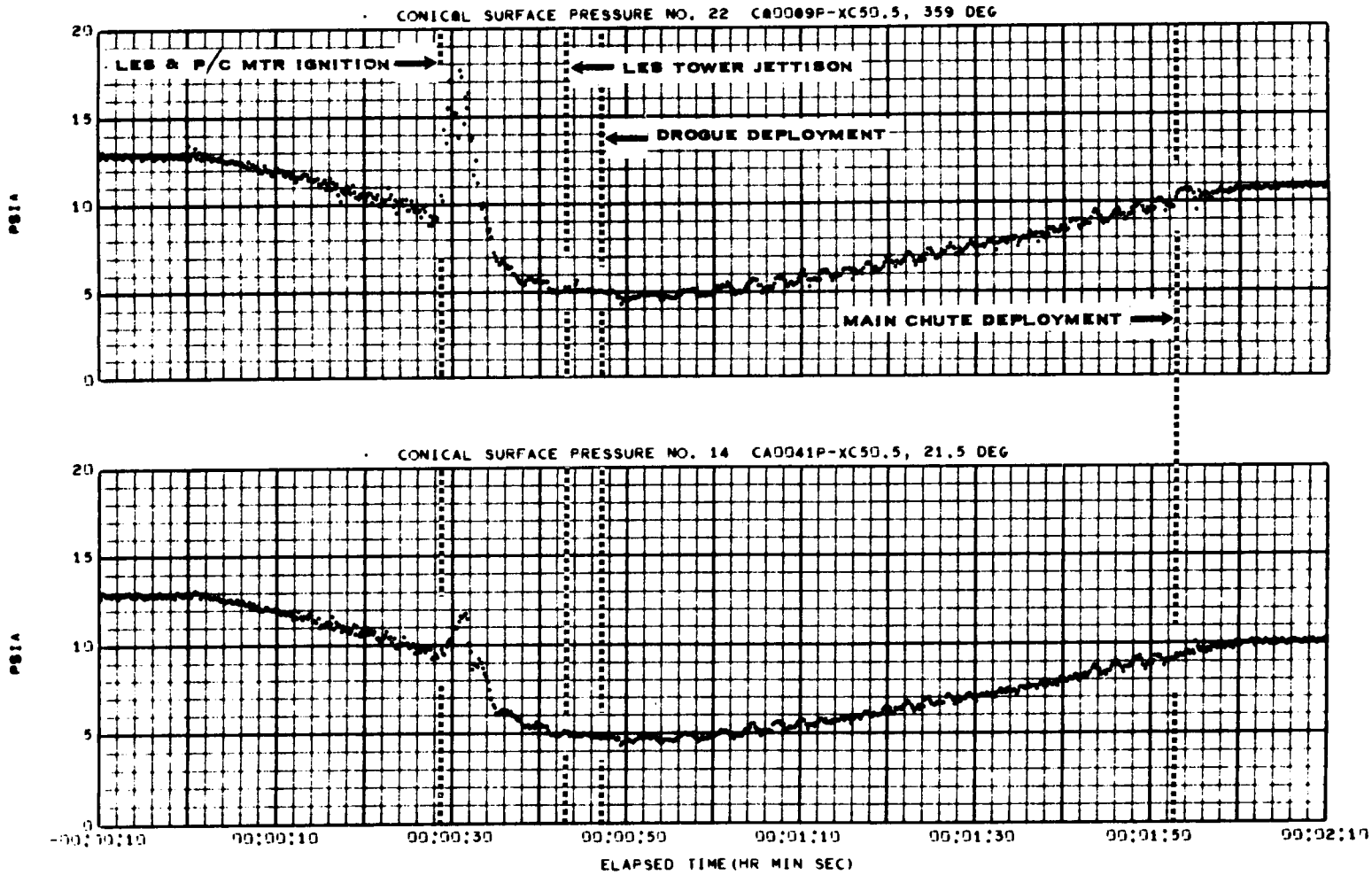

(g) Conical surface pressures 14 and 22.

Figure 4.3.6-13. - Continued.

00:00:28.4 LES AND P/C MTR IGNITION
00:00:43.7 LES TOWER JETTISON
00:00:47.1 DROGUE DEPLOYMENT
00:01:52.7 MAIN CHUTE DEPLOYMENT

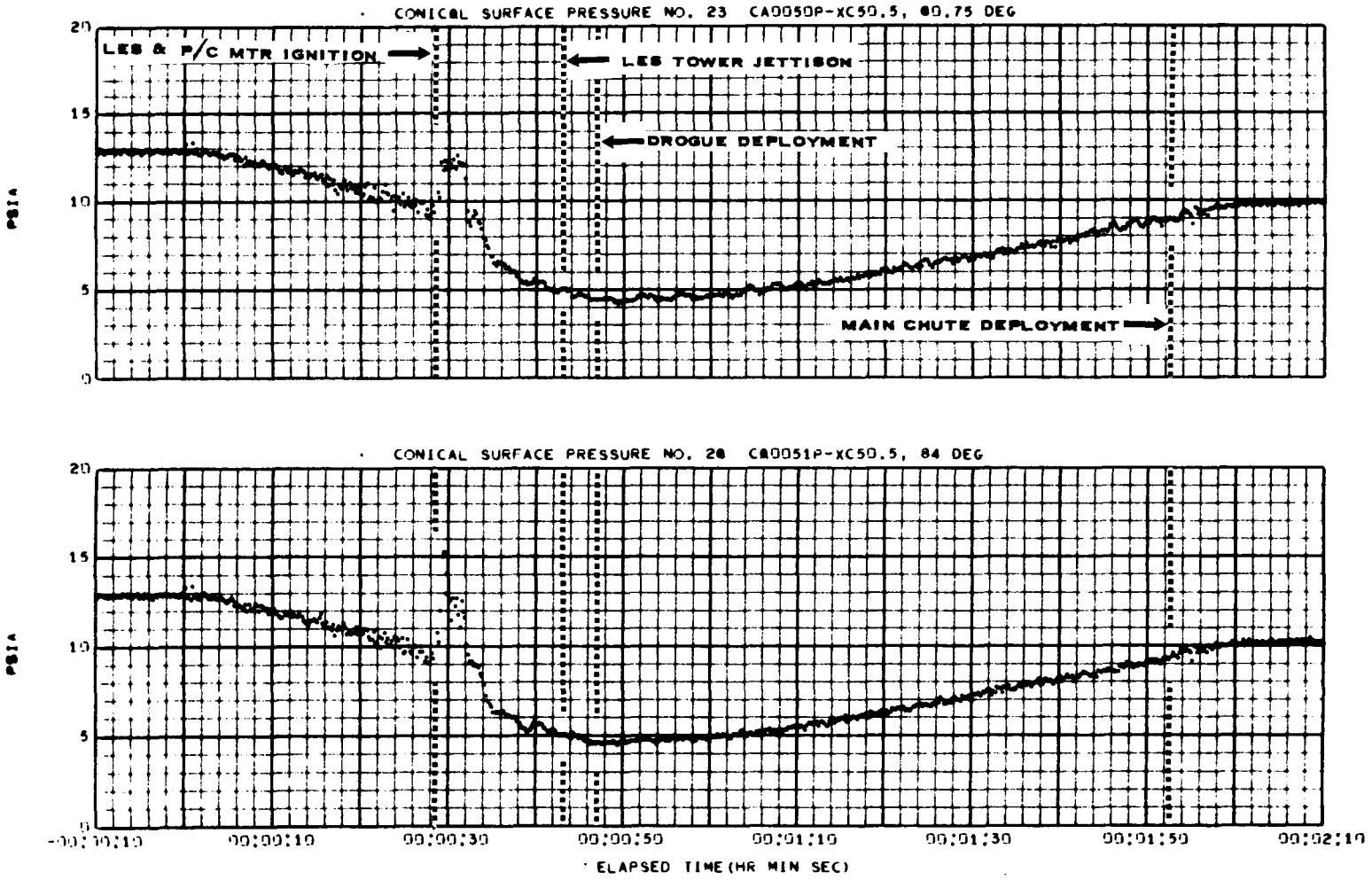

(h) Conical surface pressures 23 and 24.

Figure 4.3.6-13. - Continued.

00:00:28.4 LES AND P/C MTR IGNITION
00:00:43.7 LES TOWER JETTISON
00:00:47.1 DROGUE DEPLOYMENT
00:01:52.7 MAIN CHUTE DEPLOYMENT

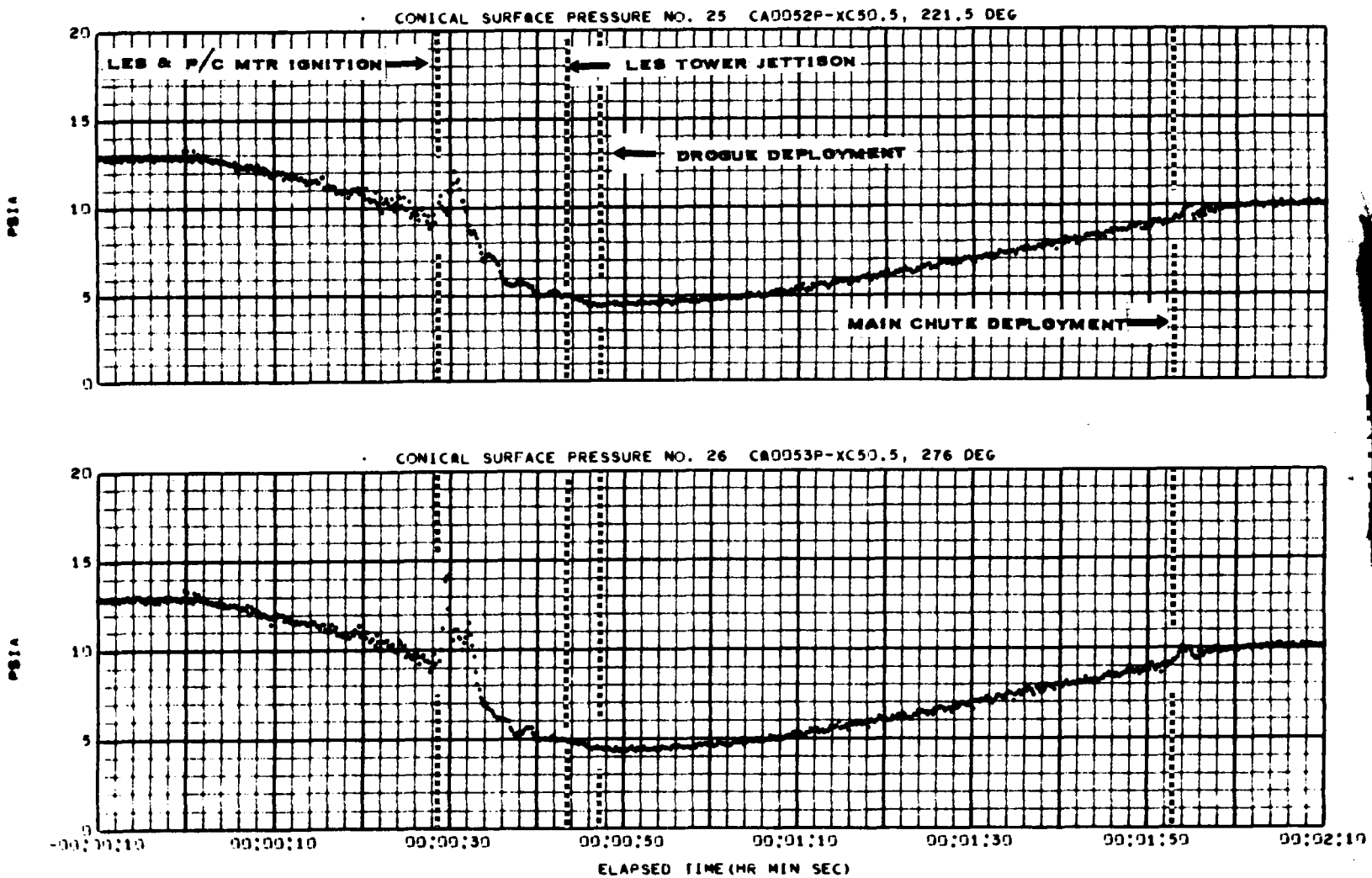

(i) Conical surface pressures 25 and 26.

Figure 4.3.6-13. - Continued.

00:00:28.4 LES AND P/C MTR IGNITION
00:00:43.7 LES TOWER JETTISON
00:00:47.1 DROGUE DEPLOYMENT
00:01:52.7 MAIN CHUTE DEPLOYMENT

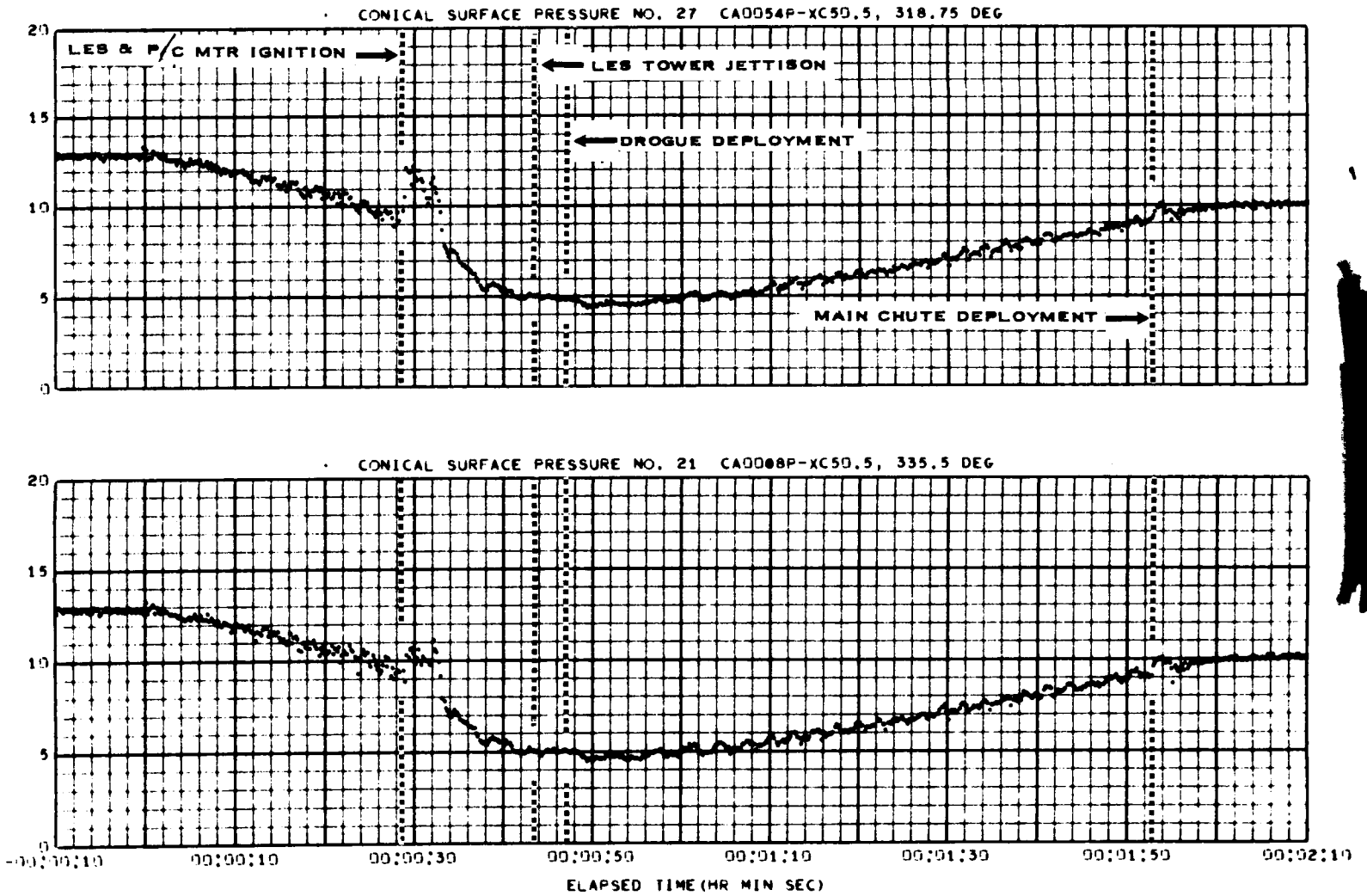

(j) Conical surface pressures 21 and 27.

Figure 4.3.6-13. - Continued.

00:00:28.4 LES AND P/C MTR IGNITION
00:00:43.7 LES TOWER JETTISON
00:00:47.1 DROGUE DEPLOYMENT
00:01:52.7 MAIN CHUTE DEPLOYMENT

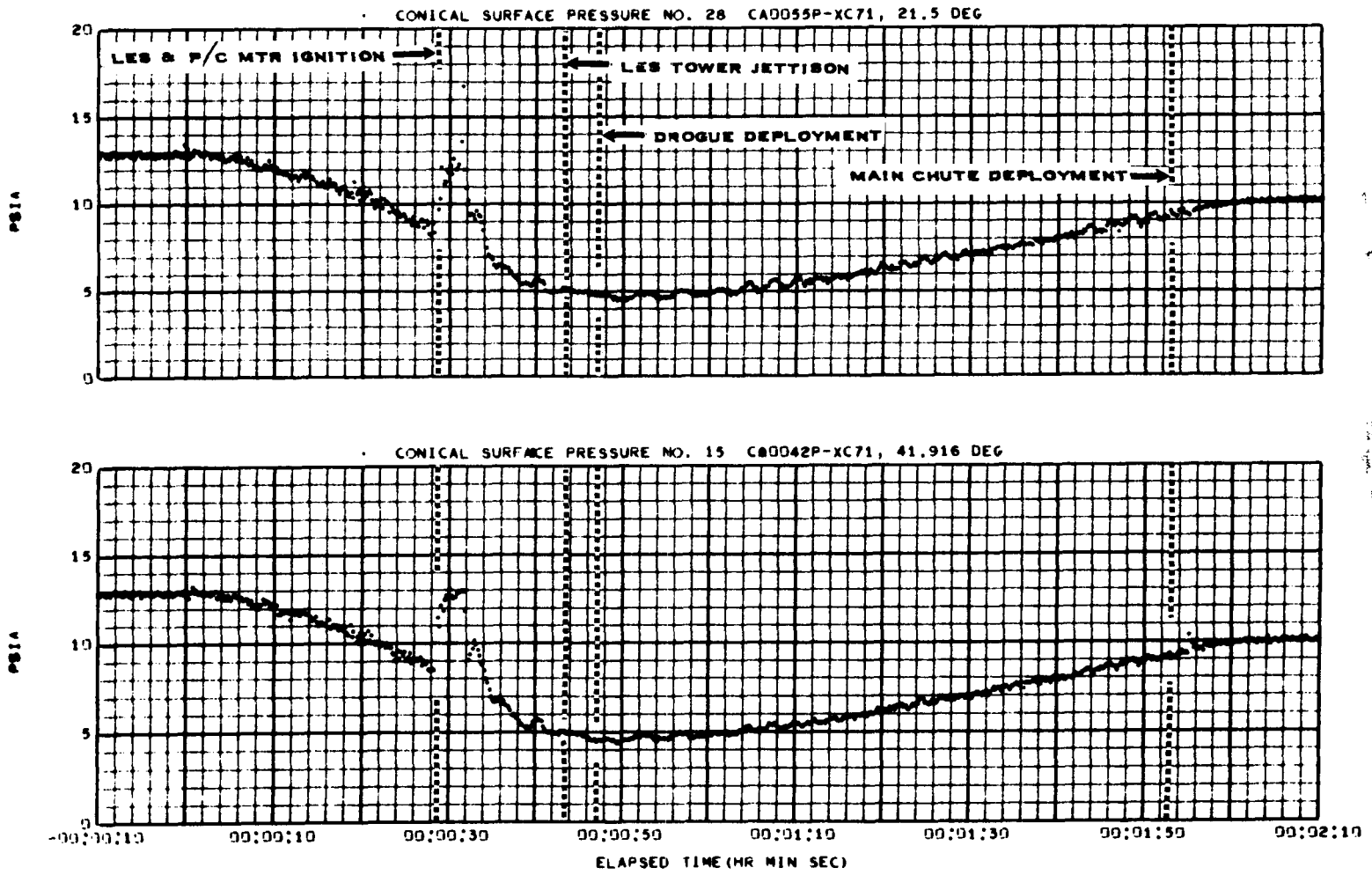

(k) Conical surface pressures 15 and 28.

Figure 4.3.6-13. - Continued.

00:00:28.4 LES AND P/C MTR IGNITION
00:00:43.7 LES TOWER JETTISON
00:00:47.1 DROGUE DEPLOYMENT
00:01:52.7 MAIN CHUTE DEPLOYMENT

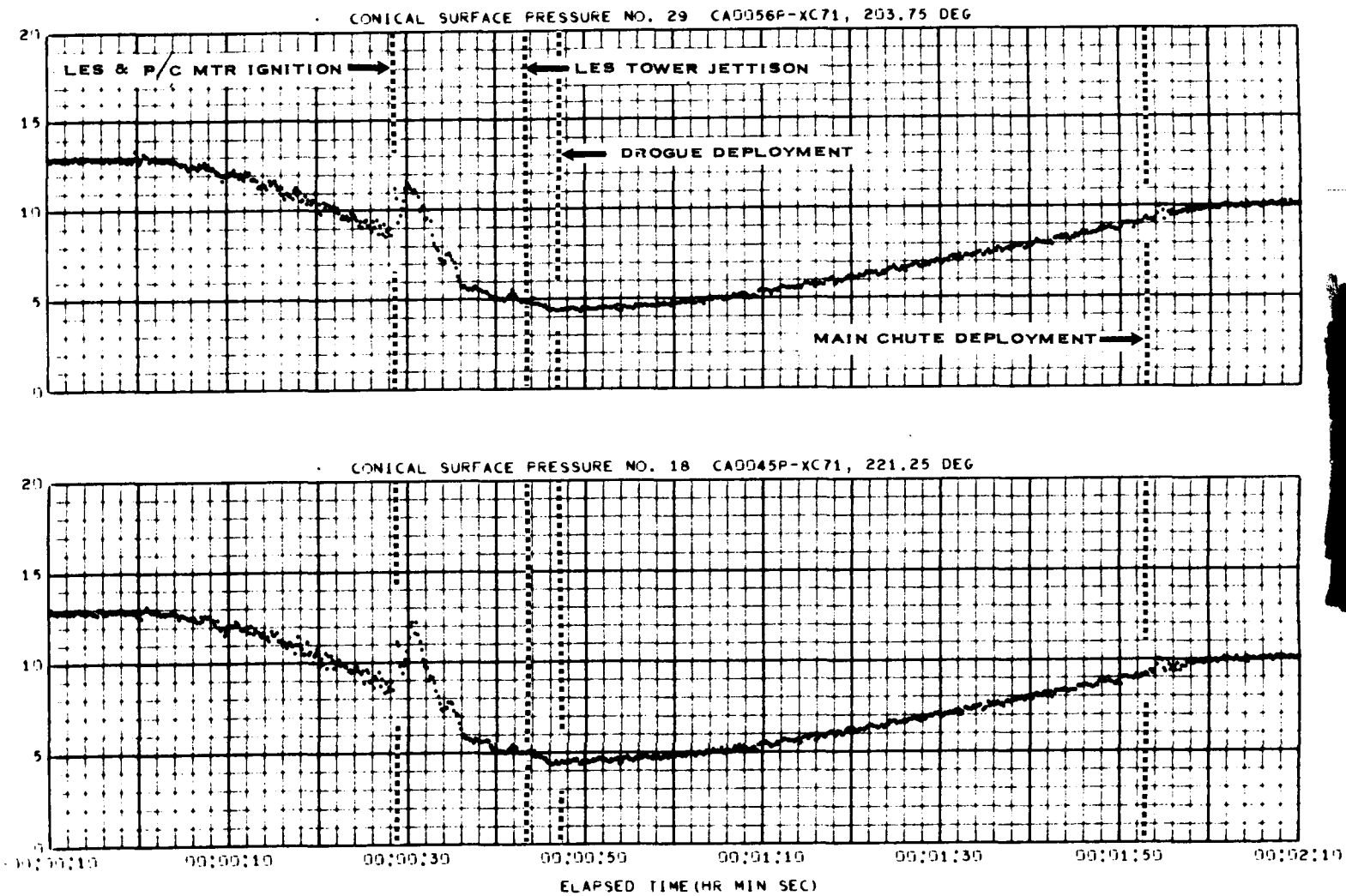

(l) Conical surface pressures 18 and 29.

Figure 4.3.6-13. - Continued.

00:00:28.4 LES AND P/C MTR IGNITION
00:00:43.7 LES TOWER JETTISON
00:00:47.1 DROGUE DEPLOYMENT
00:01:52.7 MAIN CHUTE DEPLOYMENT

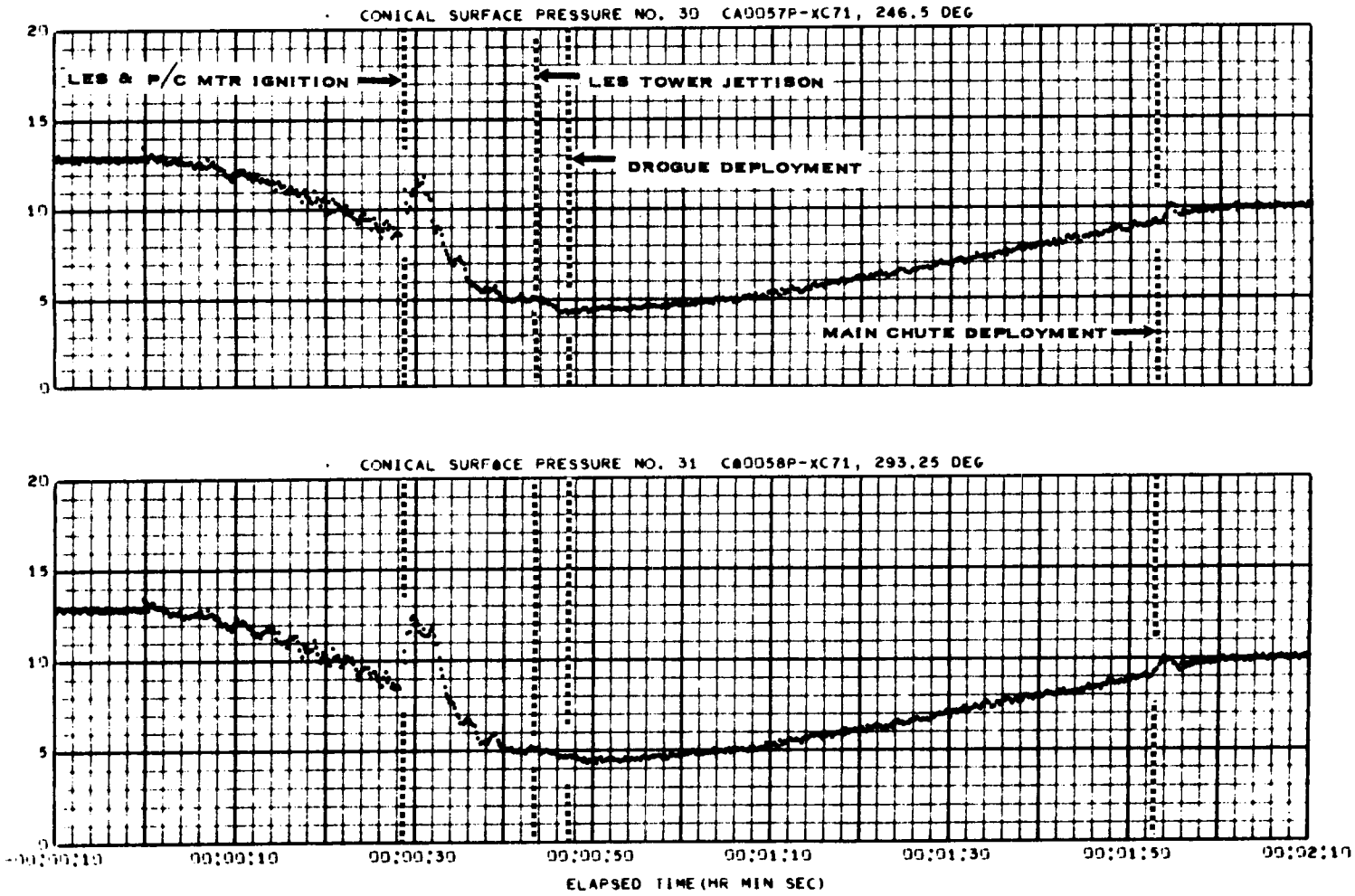

(m) Conical surface pressures 30 and 31.

Figure 4.3.6-13. - Continued.

00:00:28.4 LES AND P/C MTR IGNITION
00:00:43.7 LES TOWER JETTISON
00:00:47.1 DROGUE DEPLOYMENT
00:01:52.7 MAIN CHUTE DEPLOYMENT

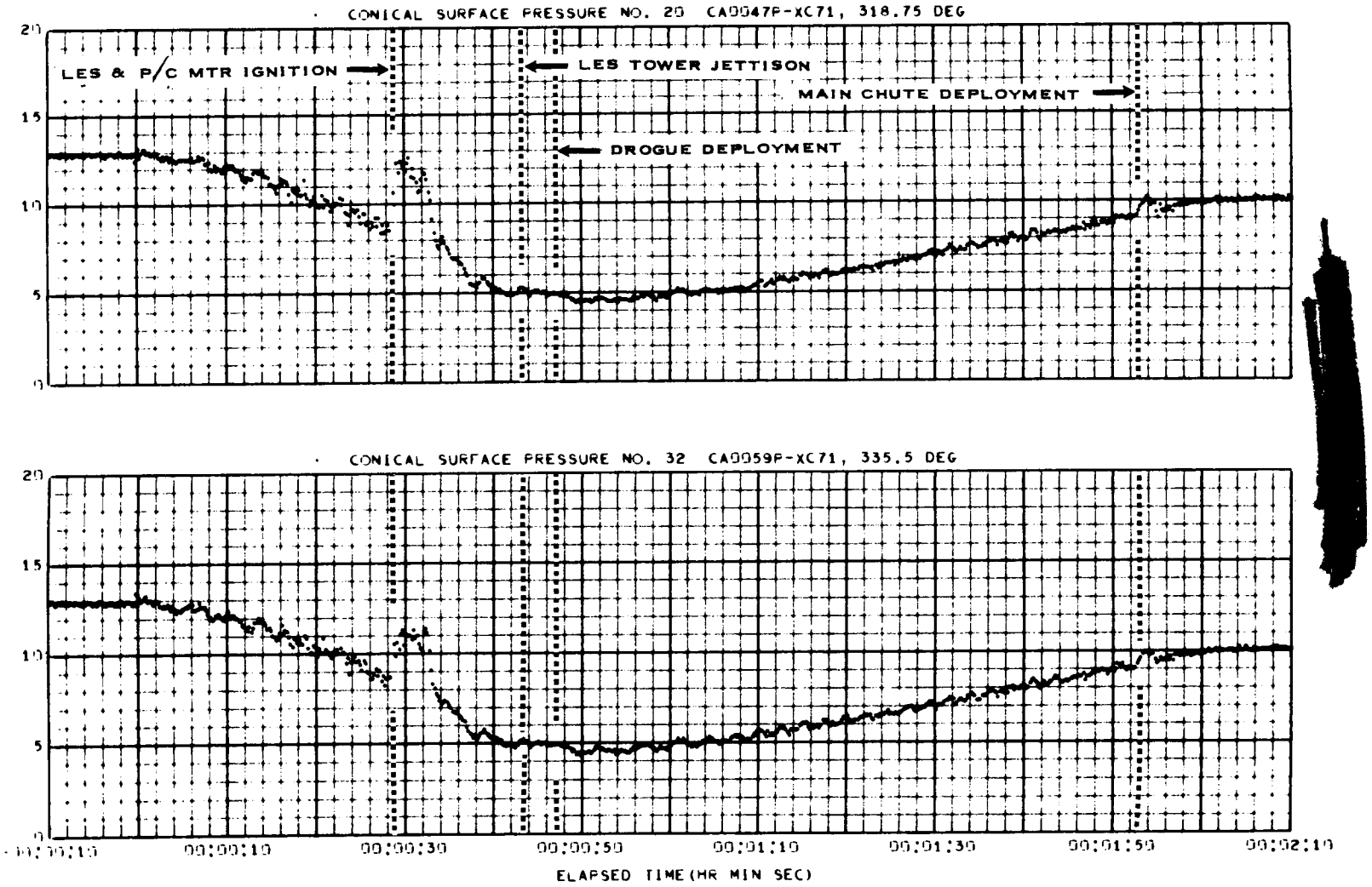

(n) Conical surface pressures 20 and 32.

Figure 4.3.6-13. - Continued.

00:00:28.4 LES AND P/C MTR IGNITION
00:00:43.7 LES TOWER JETTISON
00:00:47.1 DROGUE DEPLOYMENT
00:01:52.7 MAIN CHUTE DEPLOYMENT

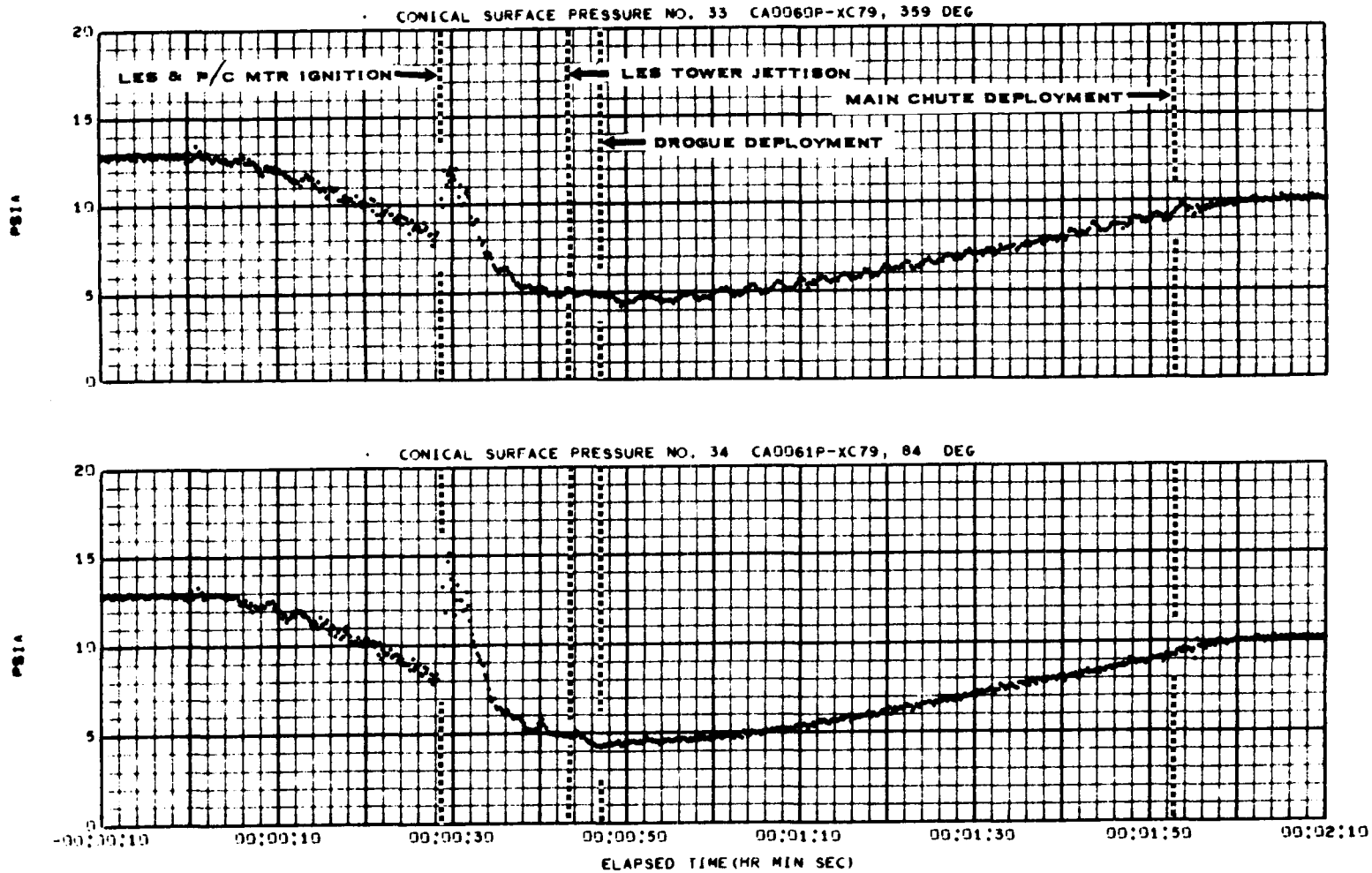

(o) Conical surface pressures 33 and 34.

Figure 4.3.6-13. - Continued.

00:00:28.4 LES AND P/C MTR IGNITION
00:00:43.7 LES TOWER JETTISON
00:00:47.1 DROGUE DEPLOYMENT
00:01:52.7 MAIN CHUTE DEPLOYMENT

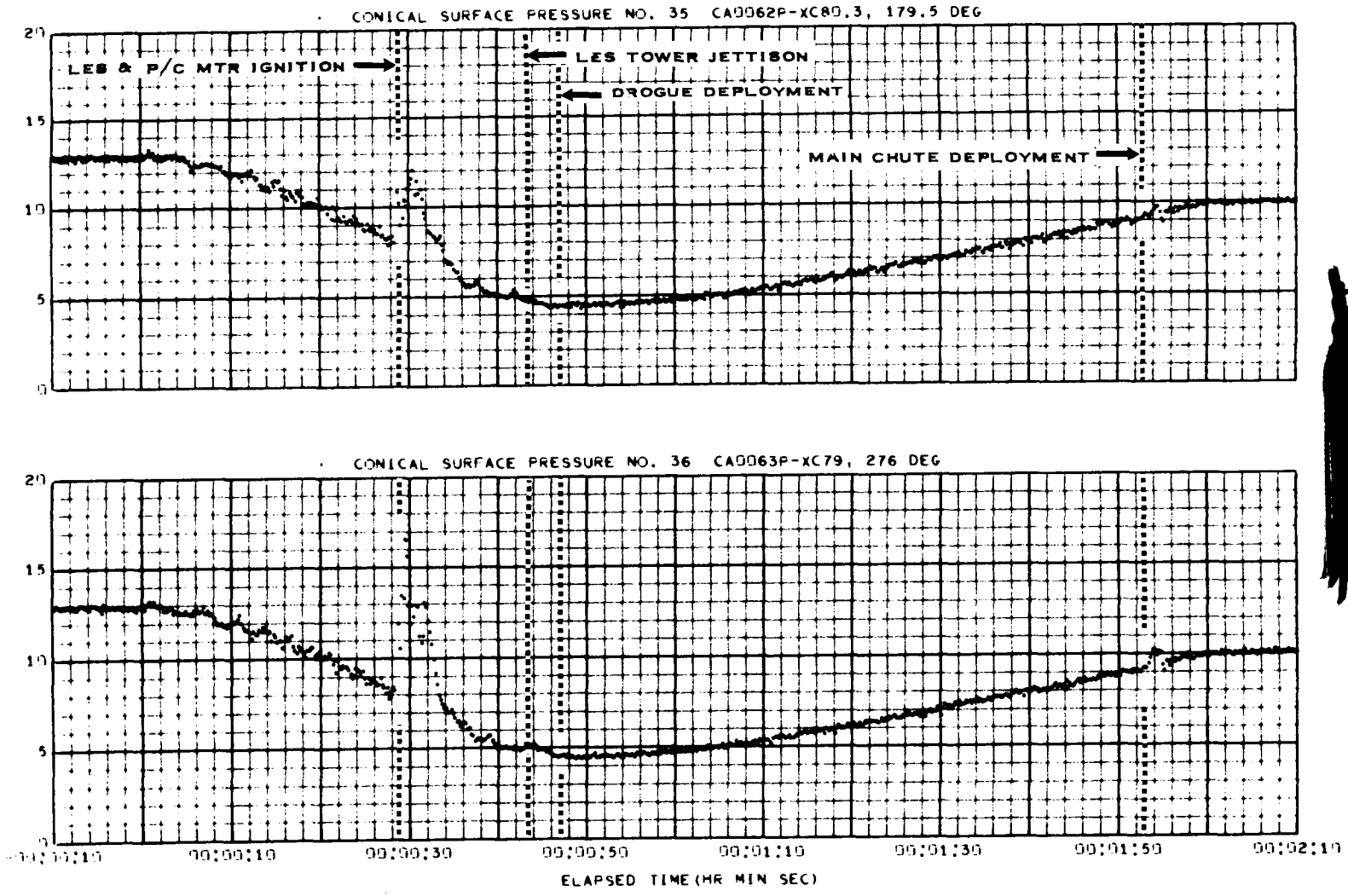

(p) Conical surface pressures 35 and 36.

Figure 4.3.6-13. - Continued.

00:00:28.4 LES AND P/C MTR IGNITION
00:00:43.7 LES TOWER JETTISON
00:00:47.1 DROGUE DEPLOYMENT
00:01:52.7 MAIN CHUTE DEPLOYMENT

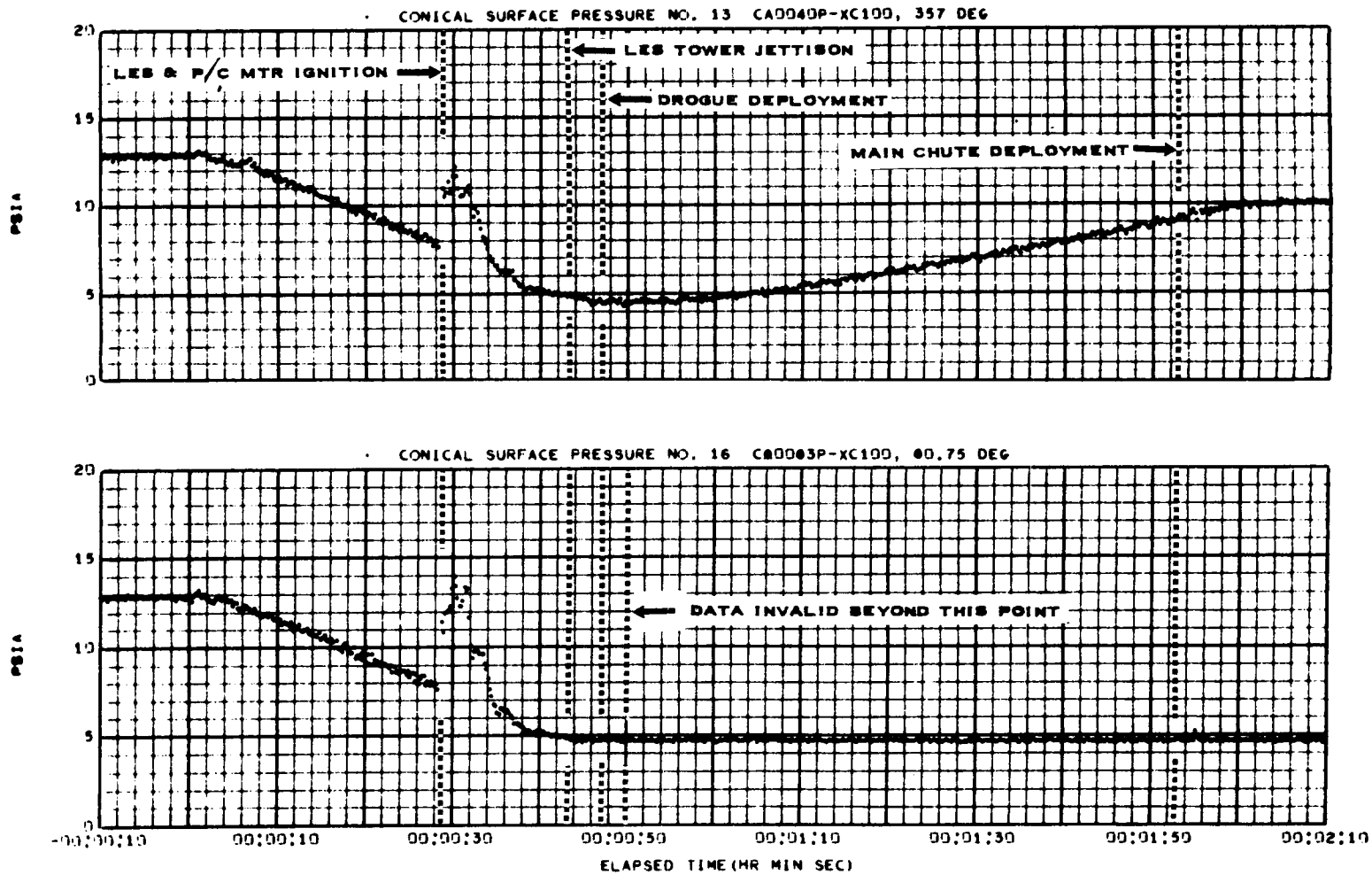

(q) Conical surface pressures 13 and 16.

Figure 4.3.6-13. - Continued.

00:00:24.4 LES AND P/C MTR IGNITION
00:00:43.7 LES TOWER JETTISON
00:00:47.1 DROGUE DEPLOYMENT
00:01:52.7 MAIN CHUTE DEPLOYMENT

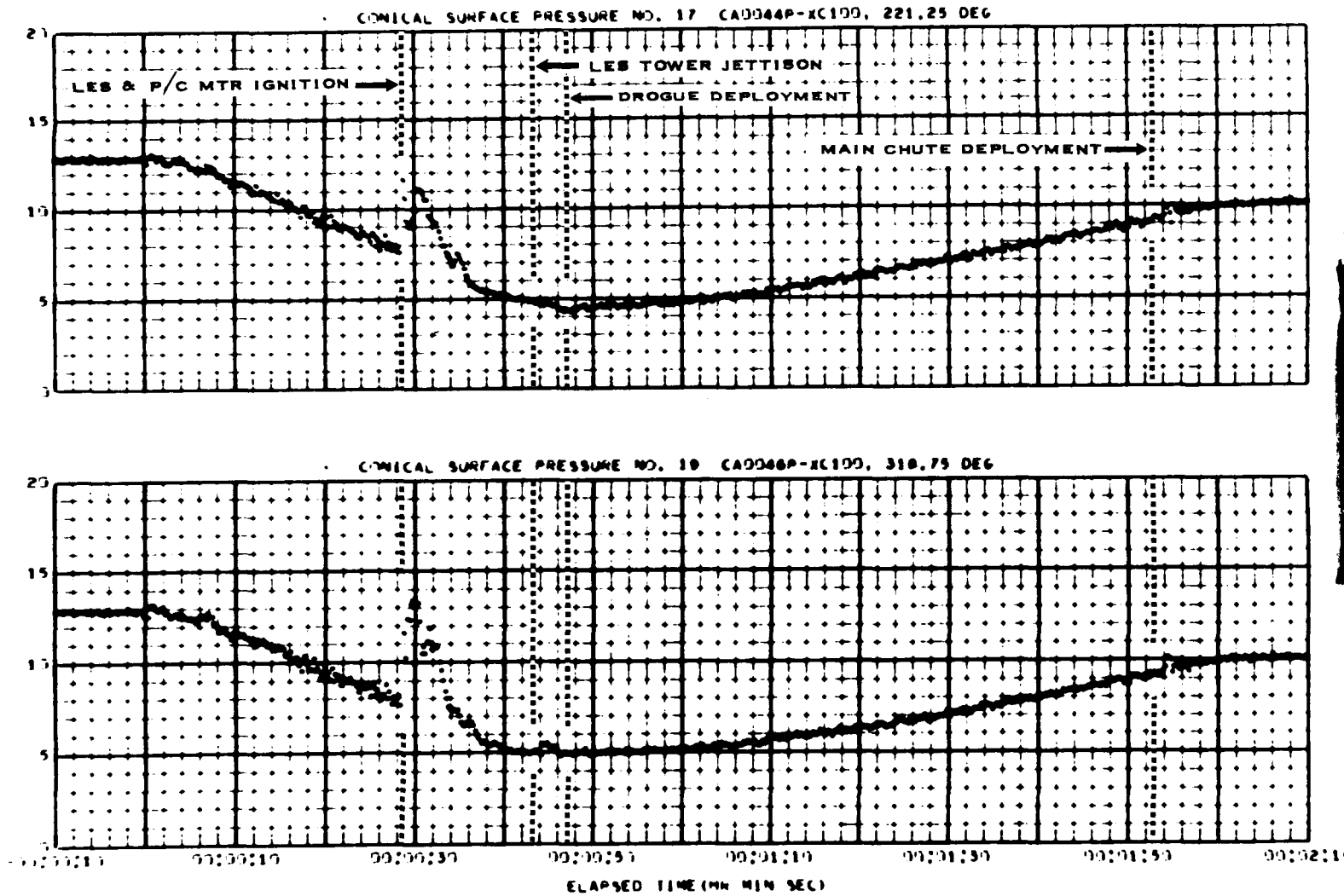

(r) Conical surface pressures 17 and 19.

Figure 4.3.6-13. - Concluded.

4.3.7 Equipment-cooling subsystem.- An equipment-cooling subsystem was provided to protect certain instrumentation from excessive operating temperatures. The subsystem consisted of a 5-gallon reservoir filled with water at approximately 70° F, a pump for circulation, and four cold-plates on which the two C-band transponders and the telemetry package were mounted.

During all tests and operations conducted on this vehicle at WSMR, the temperature at the RF amplifier and the transmitter were monitored with the equipment-cooling subsystem off and were well below maximum levels permitted (71.1° C). The equipment-cooling subsystem was intentionally disabled prior to the launch. The temperatures recorded by way of telemetry from T-25 minutes to T+80 minutes were well below the maximum level of 71.1° C. These recorded temperatures were:

Time, minutes	Temperature, °C
T-25	31
T-0	31
T+80	38

[redacted]

4.3.8 Stability and motion.- The flight motions experienced during launch-escape vehicle flight are dependent upon the flight conditions at abort as well as many other parameters. Off-nominal characteristics in any of the parameters will have an effect on the motions which will result in a difference from predicted values. The factors affecting flight in addition to abort conditions are aerodynamics, rocket-motor performance and thrust-vector alinement, weights, inertias, center-of-gravity location, and atmospheric characteristics.

At abort initiation, the launch-escape motor and the pitch-control motor are simultaneously ignited. The purpose of the launch-escape motor is to propel the launch-escape vehicle safely away from the launch vehicle following an abort. The thrust from the pitch-control motor, acting at the nose of the launch-escape vehicle, creates angular accelerations in the pitch plane. These accelerations are reduced by the moments created by the launch-escape motor thrust. At the time of abort, the high dynamic pressure produces large aerodynamic moments. These moments combine with the thrust moments to establish an oscillatory motion as the vehicle seeks its trimmed condition. Oscillatory motions in the yaw plane and roll motions are also established by thrust and aerodynamic moments.

The predicted data presented in this section were obtained from a six degree-of-freedom digital computer simulation. The preflight simulations utilized aerodynamic estimates obtained from results of wind-tunnel model testing. The effect of launch-escape motor burning on aerodynamic stability was obtained from a model which decomposed hydrogen peroxide to simulate the rocket exhaust. The rocket-motor performance used was the predicted boilerplate 12 motor characteristics presented in figure 4.3.3-4 with the launch-escape motor thrust-vector alinement presented in figure 4.2.4-1. Preflight estimates of weight, center of gravity, and inertias presented in figures 4.2.2-1, 4.2.2-2, and 4.2.2-4 to 4.2.2-6 were also utilized. The standard 1959 ARDC atmospheric properties were used. The initial conditions used were those predicted for a nominal Little Joe II launch.

The flight angular velocities and roll attitude presented in this section were determined from onboard gyroscopes. No pitch or yaw attitude data are presented since the gyroscopes measuring these attitudes became inoperative during the flight. The onboard instrumentation is discussed in section 4.3.1. The flight angle of attack and angle of sideslip were computed by using the Q-ball pressures together with Mach number and dynamic pressure from the real-time-data system. The real-time-data system is discussed in section 4.1.1. The Q-ball is a nose-mounted, conical-shaped, airflow direction sensor located forward of the pitch-control motor on the launch-escape subsystem. The Q-ball consists of three sets of pressure ports producing three differential pressure

[redacted]

readings. The three measurements taken together are sufficient to determine angle of attack, angle of sideslip, and dynamic pressure through a limited range of angles. Procedures are available to utilize ground tracking dynamic pressure and Mach number to extend the range of angles over which the Q-ball is valid.

The flight and preflight predicted vehicle pitch and yaw angular velocities are presented in figures 4.3.8-1 and 4.3.8-2, respectively. Analysis of the pitch and yaw rates shows that the vehicle was stable as predicted throughout the launch-escape-vehicle flight. The differences in oscillation amplitude and frequency can probably be attributed largely to the differences in abort conditions and to deviations in thrust characteristics from the predicted. Any deviations in launch-escape motor thrust could have been determined from the measured chamber pressure; however, the instrumentation which would have provided this pressure measurement was inoperative during launch-escape vehicle flight. The flight and predicted pitch-control motor characteristics are presented in figure 4.3.3-6. To analyze the deviation of flight from preflight predicted motions completely, evaluation of the effects of the maximum expected launch-escape motor thrust deviations is required. These thrust deviations are shown in figure 4.3.3-4. The associated mass characteristics are presented in section 4.2.

The flight and preflight predicted roll angular velocity and roll attitude time histories are presented in figures 4.3.8-3 and 4.3.8-4, respectively. At abort initiation there was a difference of 135° in roll attitude and 9 deg/sec in roll rate. The vehicle rolled negatively approximately 1.5 revolutions during launch-escape vehicle flight.

The flight and preflight predicted angle-of-attack time histories are presented in figure 4.3.8-5(a). The maximum positive and negative flight angles of attack were 13° and 5°, respectively. Time histories of the flight and preflight angle of sideslip are presented in figure 4.3.8-5(b). The flight angle of sideslip varied between 6° and -5°. Analysis of the angle of attack and angle of sideslip shows, as did the pitch and yaw angular velocity data, that the launch-escape vehicle was stable as predicted.

[redacted]

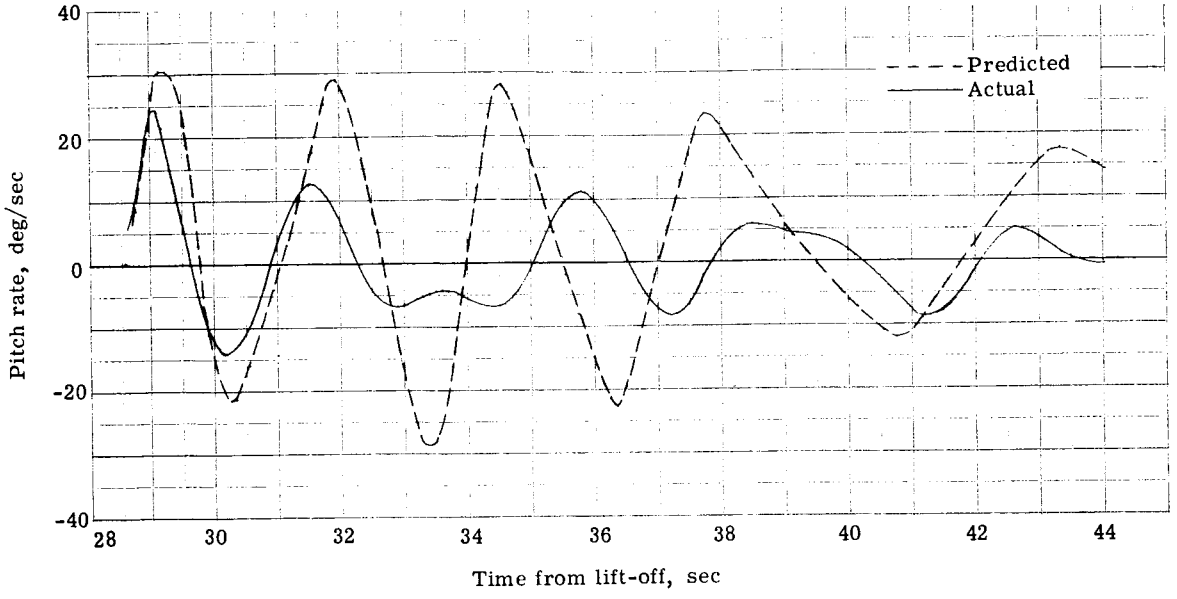

Figure 4.3.8-1.- Predicted and actual launch-escape-vehicle pitch rate time histories.

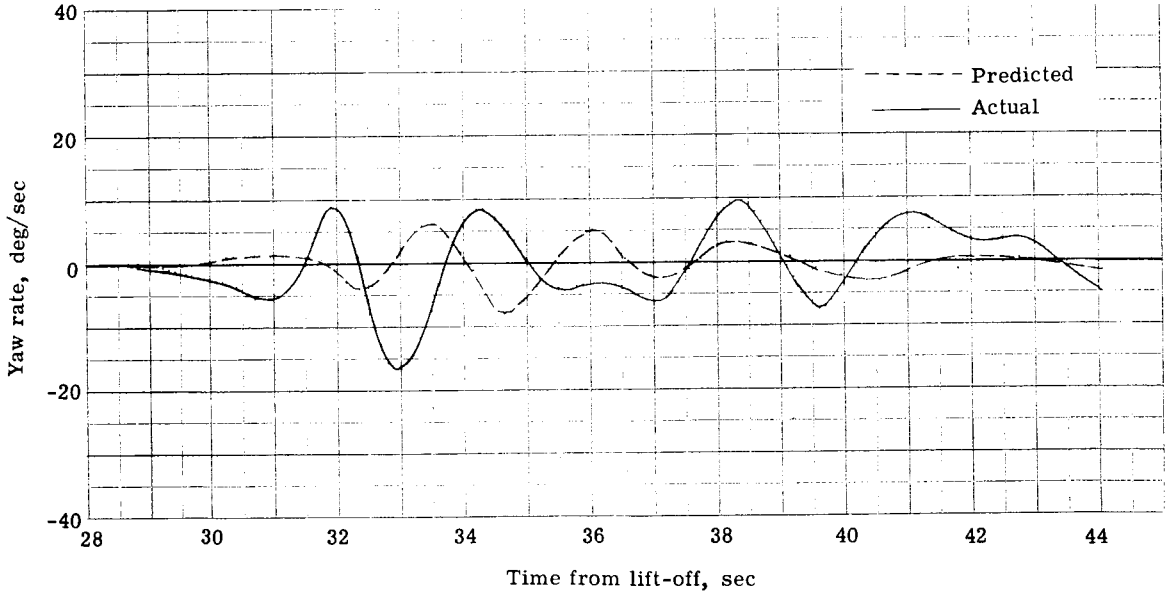

Figure 4.3.8-2.- Predicted and actual launch-escape-vehicle yaw rate time histories.

[redacted]

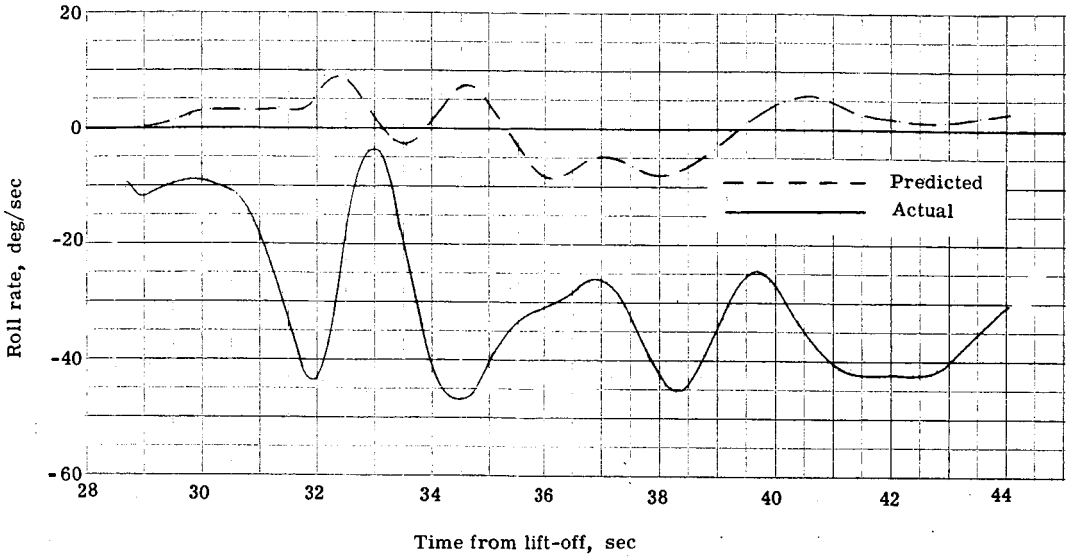

Figure 4.3.8-3. - Predicted and actual launch-escape-vehicle roll rate time histories.

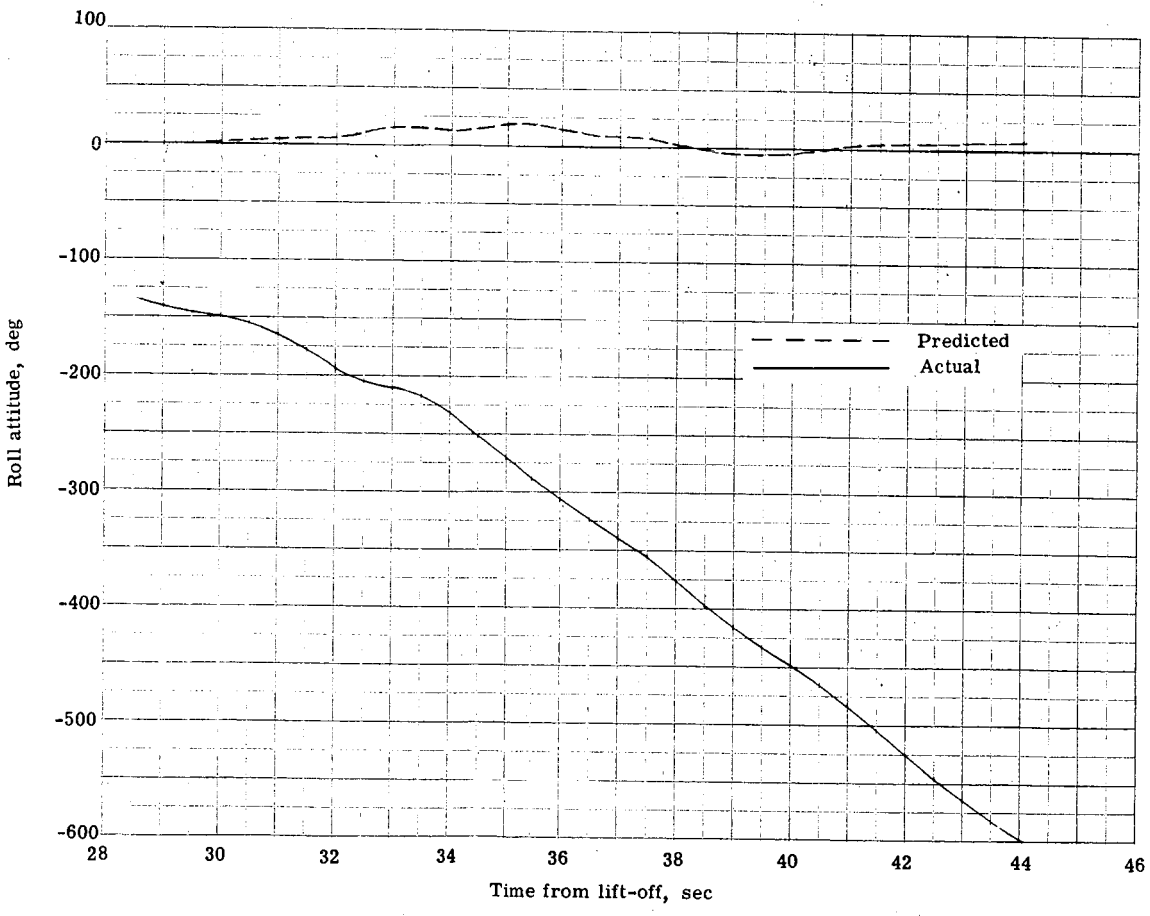

Figure 4.3.8-4. - Predicted and actual launch-escape-vehicle roll attitude time histories.

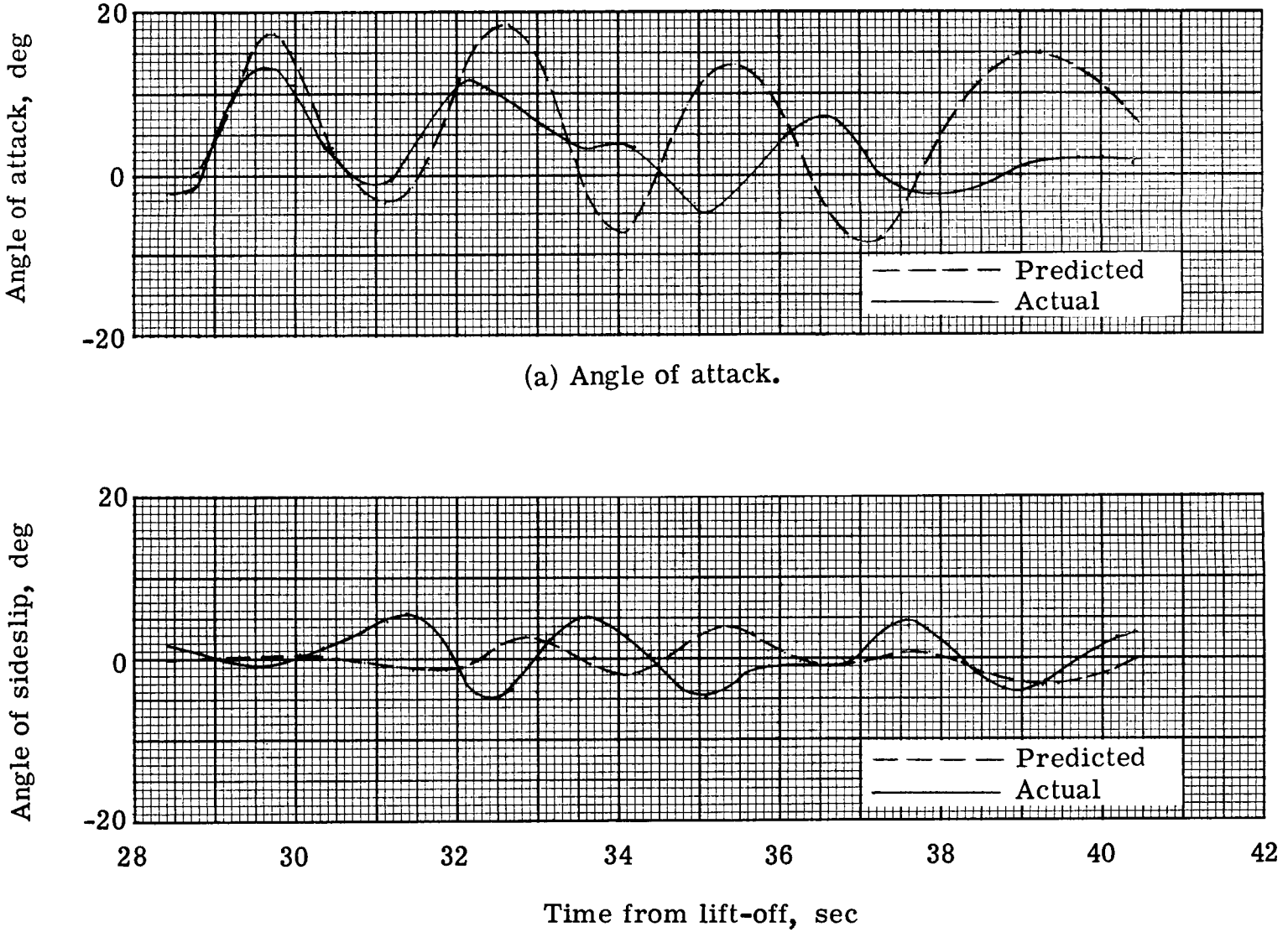

Figure 4.3.8-5.- Predicted and actual angles of attack and sideslip time histories.

00:00:28.4 THRUST TERMINATION
00:00:28.5 CM-SEPARATION
00:00:28.4 LES AND P/C MTR IGNITION
00:00:43.7 LES TOWER JETTISON

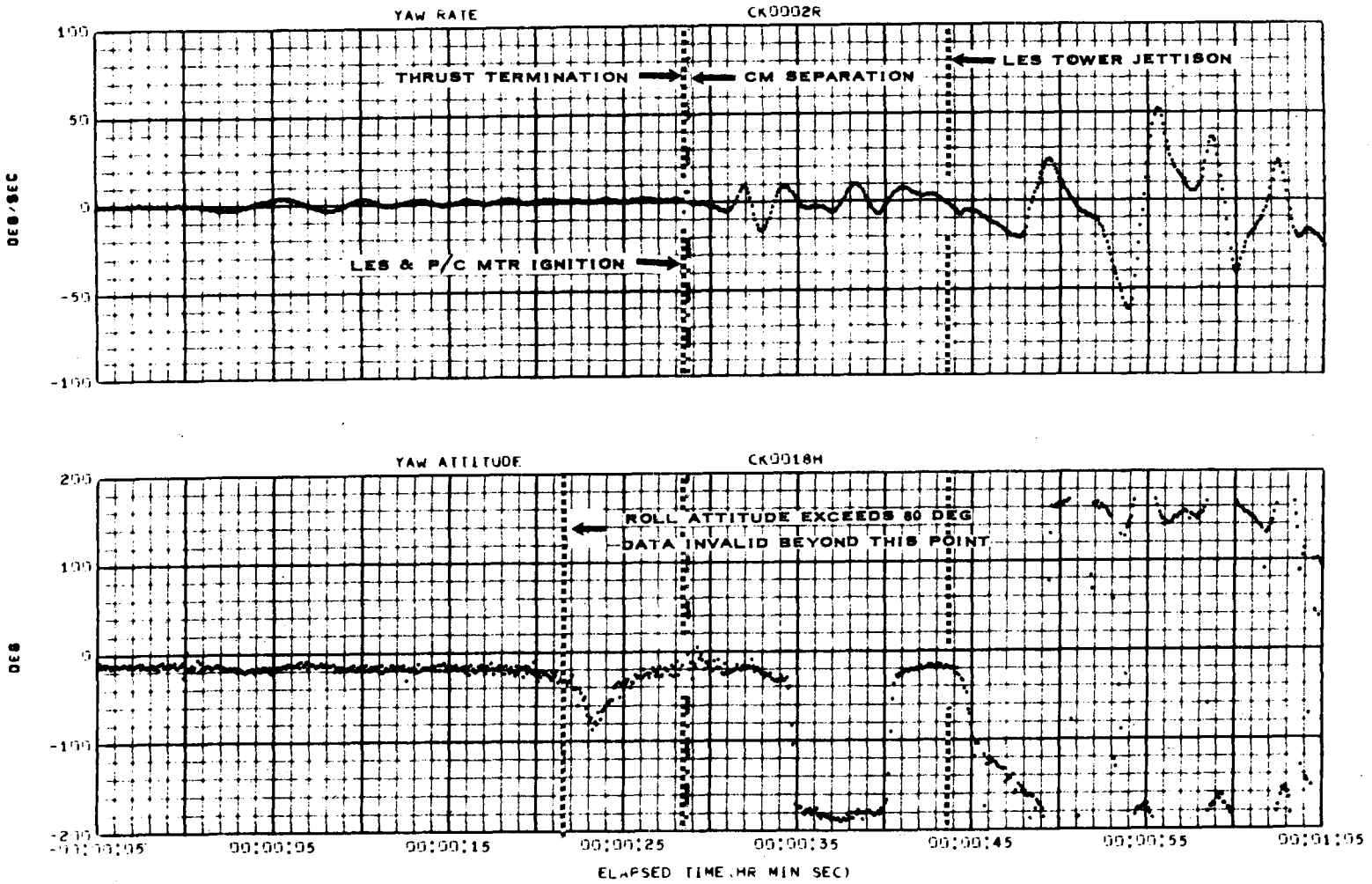

Figure 4.3.8-6.- Time histories of yaw rate and attitude.

00:00:28.4 THRUST TERMINATION
00:00:28.5 CM-SEPARATION
00:00:28.4 LES AND P/C MTR IGNITION
00:00:43.7 LES TOWER JETTISON

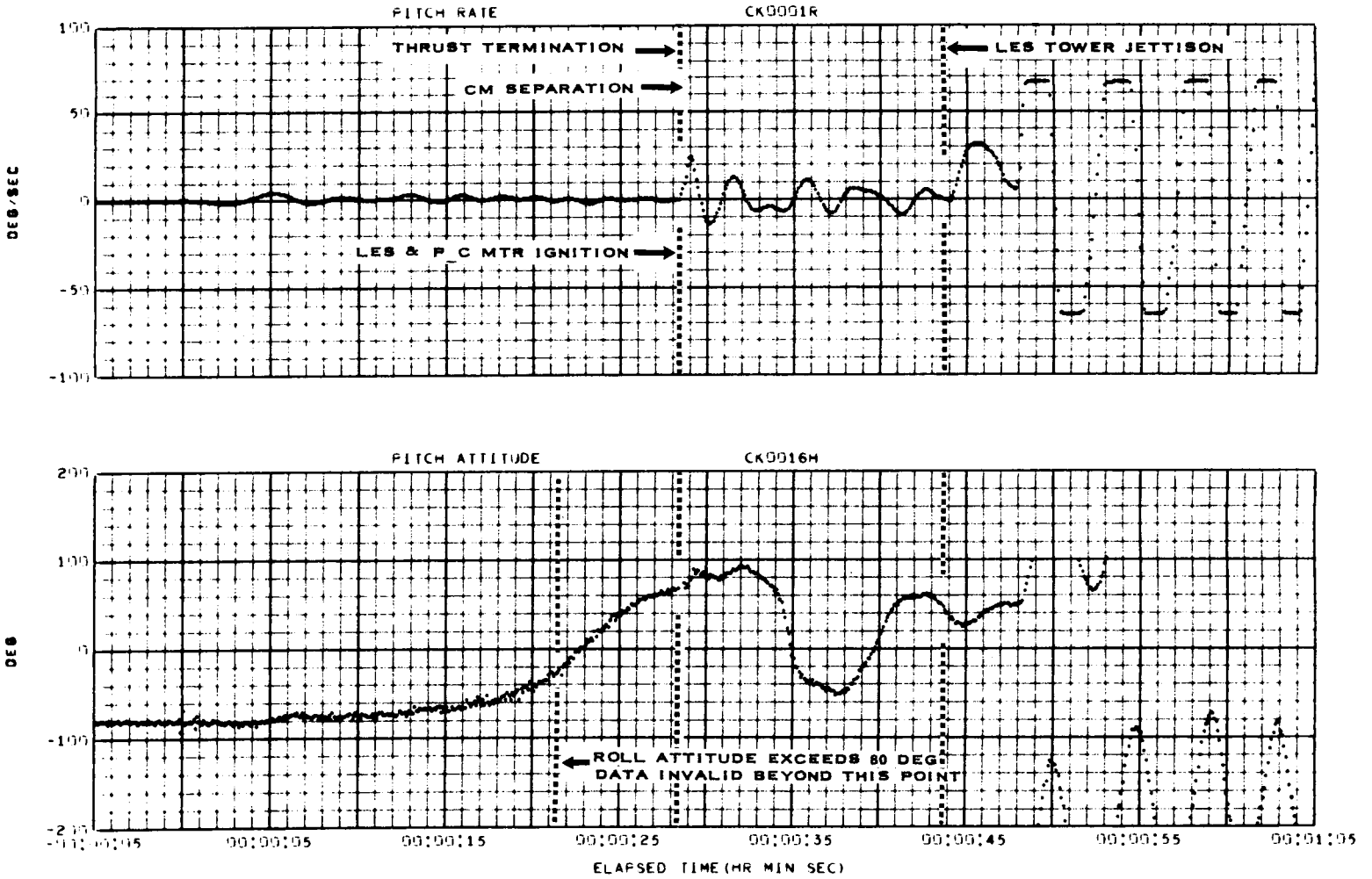

Figure 4.3.8-7.- Time histories of pitch rate and attitude.

00:00:28.4 THRUST TERMINATION
00:00:28.5 CM-SEPARATION
00:00:28.4 LES AND P/C MTR IGNITION
00:00:43.7 LES TOWER JETTISON

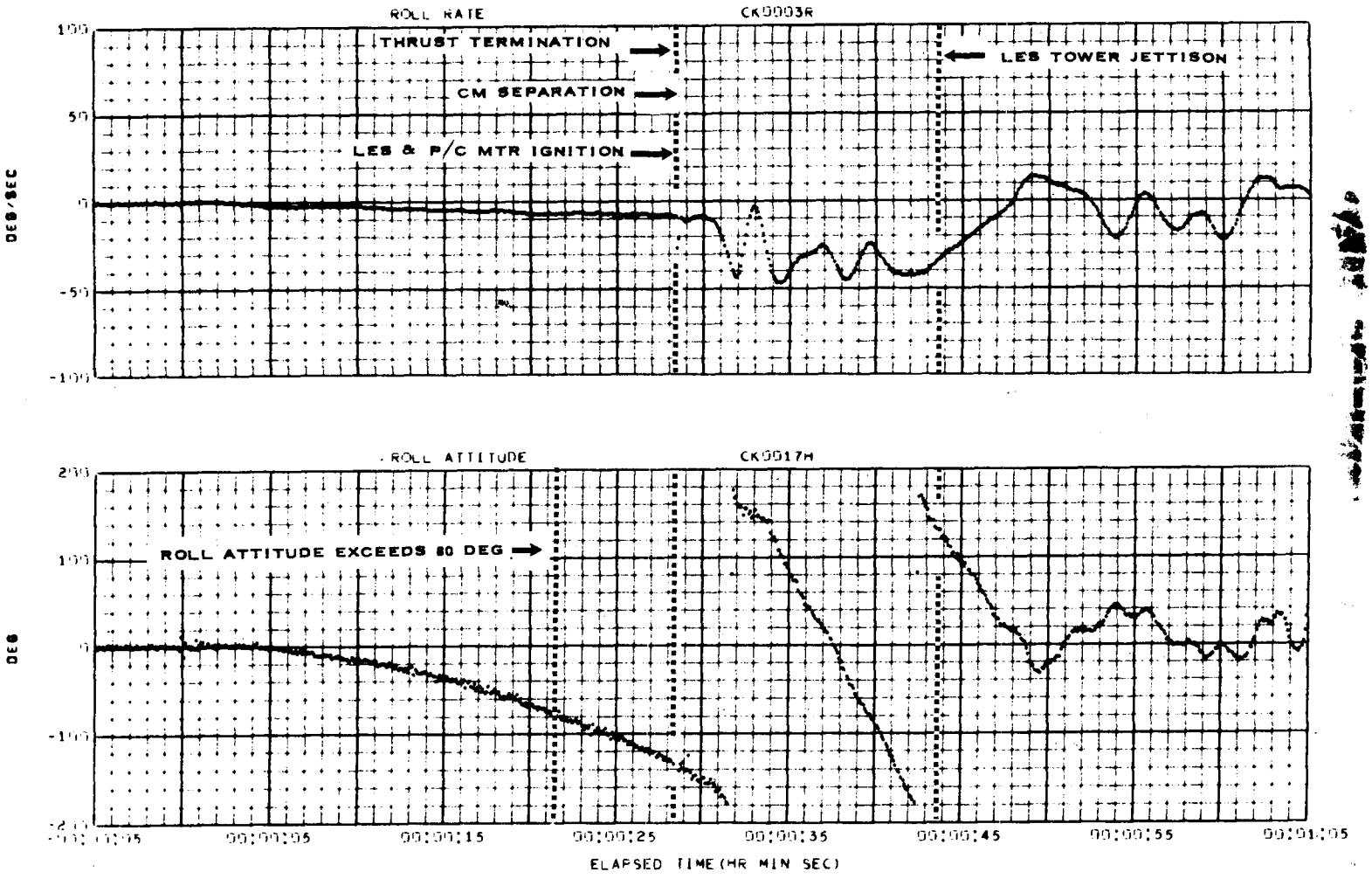

Figure 4.3.8-8. - Time histories of roll rate and attitude.

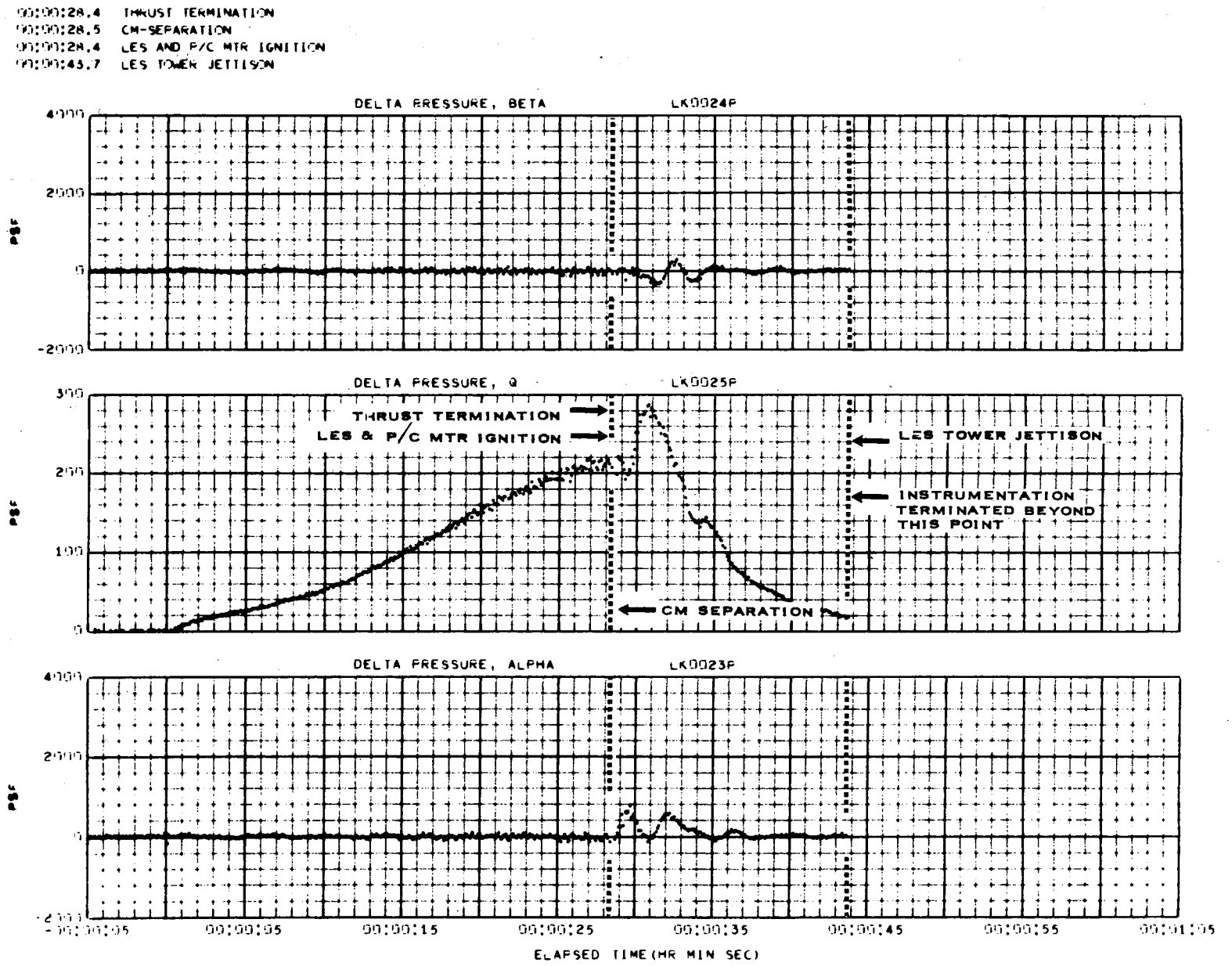

Figure 4.3.8-9.- Time histories of Q-ball delta pressures.

4.4 Launch Vehicle

4.4.1 Structures.- The Little Joe II launch vehicle encountered no adverse loading or structural problems during the launch phase of the flight. Bending loads during boost were estimated to be about 10 percent of maximum design αq loads. At thrust termination, the launch vehicle forebody and most of the afterbody were destroyed.

The effect of thrust termination on the spacecraft was more violent than had been anticipated. The X-axis accelerometer recorded a change in acceleration of approximately 27g. As described in section 4.3.6, there is evidence that the pressure bulkhead was fragmented. Portions of the launch vehicle and service module interior structure struck the command module aft heat shield resulting in structural damage to and delamination of this component. One side (side A) of the 41.1-second backup abort timer timed out early during thrust termination. During preflight and postflight tests, this timer functioned properly; however, during thrust termination it was subjected to accelerations above the qualification test level. It is apparent that the severity of thrust termination may have been the cause of this early time out. Many other components were subjected to accelerations higher than their qualification level but no other failures are known to have occurred at this time.

Loads of the launch vehicle during the time of maximum dynamic pressure were computed at the adapter-launch-vehicle interface. The bending moment was estimated to be about 30 percent of design bending moment for a comparable flight condition.

The loads were estimated by calculating resultant angles of attack and sideslip based on the measured winds up to abort altitude. This should provide an upper limit to the loads encountered by the fin-stabilized vehicle. The computed angle combined with the dynamic pressure gave a value of αq = 945 deg lb/sq ft as compared with an αq = 2,067 deg lb/sq ft for a comparable design condition. The structure of the Little Joe II launch vehicle is designed to withstand an αq of 10,000 deg lb/sq ft. The flight parameters and estimated loads are compared with design values in table 4.4.1-1.

[redacted]

TABLE 4.4.1-1.- COMPARISON OF BOILERPLATE 12 BOOST PHASE LOADS WITH COMPARABLE DESIGN LOADS

Parameter	Design loads	Approximate flight loads
Flight time, sec	37.5	28.5
Mach number	1.17	0.94
Dynamic pressure, lb/sq ft	689	630
αq, deg lb/sq ft	2,067	945
Resultant normal and lateral load factor, g.	0.86	0.2
Axial load factor, g	2.89	1.4
Combined pitch and yaw plane acceleration, radians/sec^2	1.97	0.0
Shear, lb	4,900	400
Axial load, lb	99,843	59,200
Bending moment, in.-lb	1,933,000	580,000

[redacted]

4.4.2 Propulsion and pyrotechnic subsystem.-

4.4.2.1 Propulsion subsystem: The propulsion subsystem for the Little Joe II launch vehicle consisted of one Algol ID, Mod II, solid-propellant rocket motor and six Recruit TE-29-II, Mod 1B, solid-propellant rocket motors. The Algol motor was bolted to the center retaining ring in the thrust bulkhead of the vehicle afterbody, and was laterally supported by the bulkhead at vehicle station 34.75. The Recruit motors were bolted by means of adapter plates to the six peripheral retaining rings and were unsupported at the forward end.

The Algol ID, Mod II, motor used a polyurethane aluminum-case bonded fuel and an ammonium perchlorate oxidizer. The grain configuration was an 8-tooth internal-burning gear. The chamber and the fixed-straight nozzle, were steel with a graphite throat insert and a zirconium oxide partial nozzle liner. Ignition was by means of a top mounted pyrotechnic igniter which used two Algol initiators. The motor was rated at 103,200 pounds average sea-level thrust for the 70° F nominal propellant grain temperature at which it was fired. This motor performed a sustainer function, burning until thrust was terminated by venting the motor case by means of explosive shaped charges.

Algol thrust was calculated by using measured chamber pressure and the equation found in section 4.3.3.

Figure 4.4.2-1 shows the variation of C_D with time. This quantity was determined from the predicted thrust and chamber pressure for the motor. The variation of P_a with time was obtained from launch-time meteorological data (fig. 4.1.2-2) and cinetheodolite trajectory data (fig. 4.1.1-1).

Figure 4.4.2-2 shows actual and predicted P_c plotted against time, and figure 4.4.2-3 shows actual thrust compared with predicted thrust. It is apparent that motor performance was high, but this variation was within normal motor-to-motor variation.

The six Recruit motors used as boosters were rated at an average thrust of 33,395 pounds each. These 5-point, internal-burning, star configuration motors used a case-bonded, liquid polymer LP-33 binder-fuel, and an ammonium perchlorate oxidizer. The cases and nozzles were steel with graphite throat inserts. The nozzles were canted outboard 6.5° to direct the thrust vector through the vehicle center of gravity. Ignition was accomplished by using one head-mounted pyrogen igniter per motor with two initiators per igniter. The initiators were standard Apollo initiators, P/N 453-0009-0004, modified by removal of the washer, to Thiokol P/N E-16452-01.

[redacted]

No measurements were made of Recruit motor performance. Predicted Recruit thrust is shown in figure 4.4.2-4. Launch-vehicle total thrust is shown in figure 4.4.2-5.

4.4.2.2 Pyrotechnic subsystem: Included in the launch-vehicle-pyrotechnic subsystem were safe and arm units, primacord, and shaped charges. Figures 4.4.2-6 and 4.4.2-7 are simplified diagrams of the Algol and Recruit firing circuits. More detailed descriptions of the thrust-termination system and the rocket-motor initiators are given in sections 4.4.4 and 4.4.6, respectively.

A detailed analysis indicated that all pyrotechnic devices performed their function at the proper time. Postflight inspection of the pyrotechnics indicated that all were expended and the desired results were achieved.

[redacted]

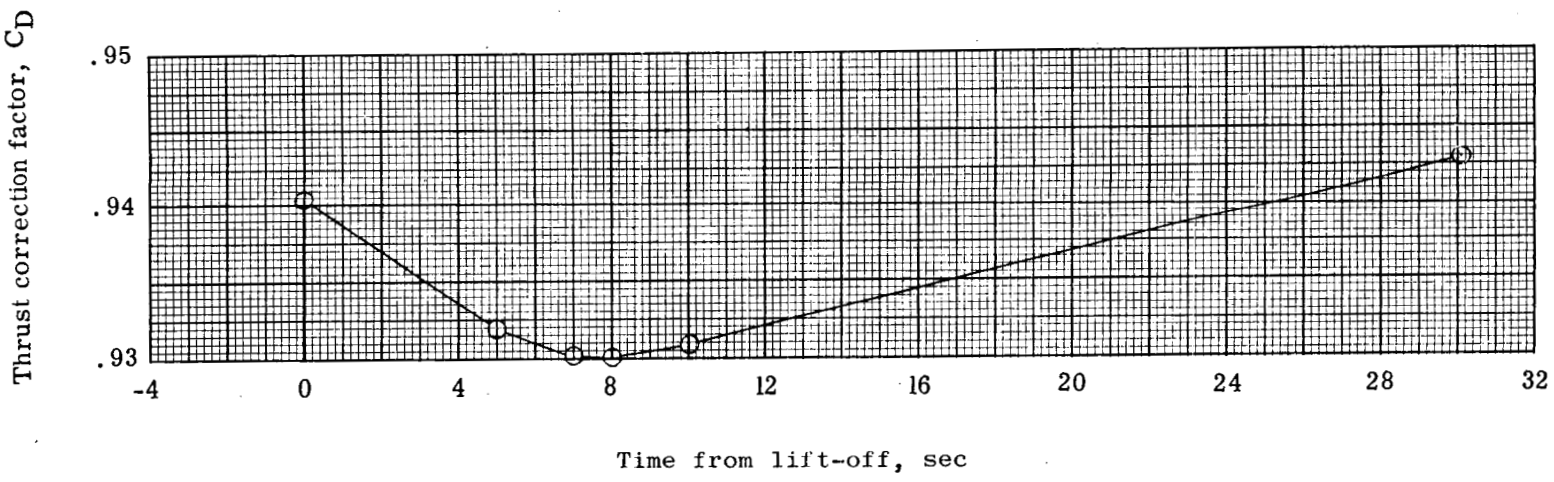

Figure 4.4.2-1. - Algol rocket motor thrust correction factor.

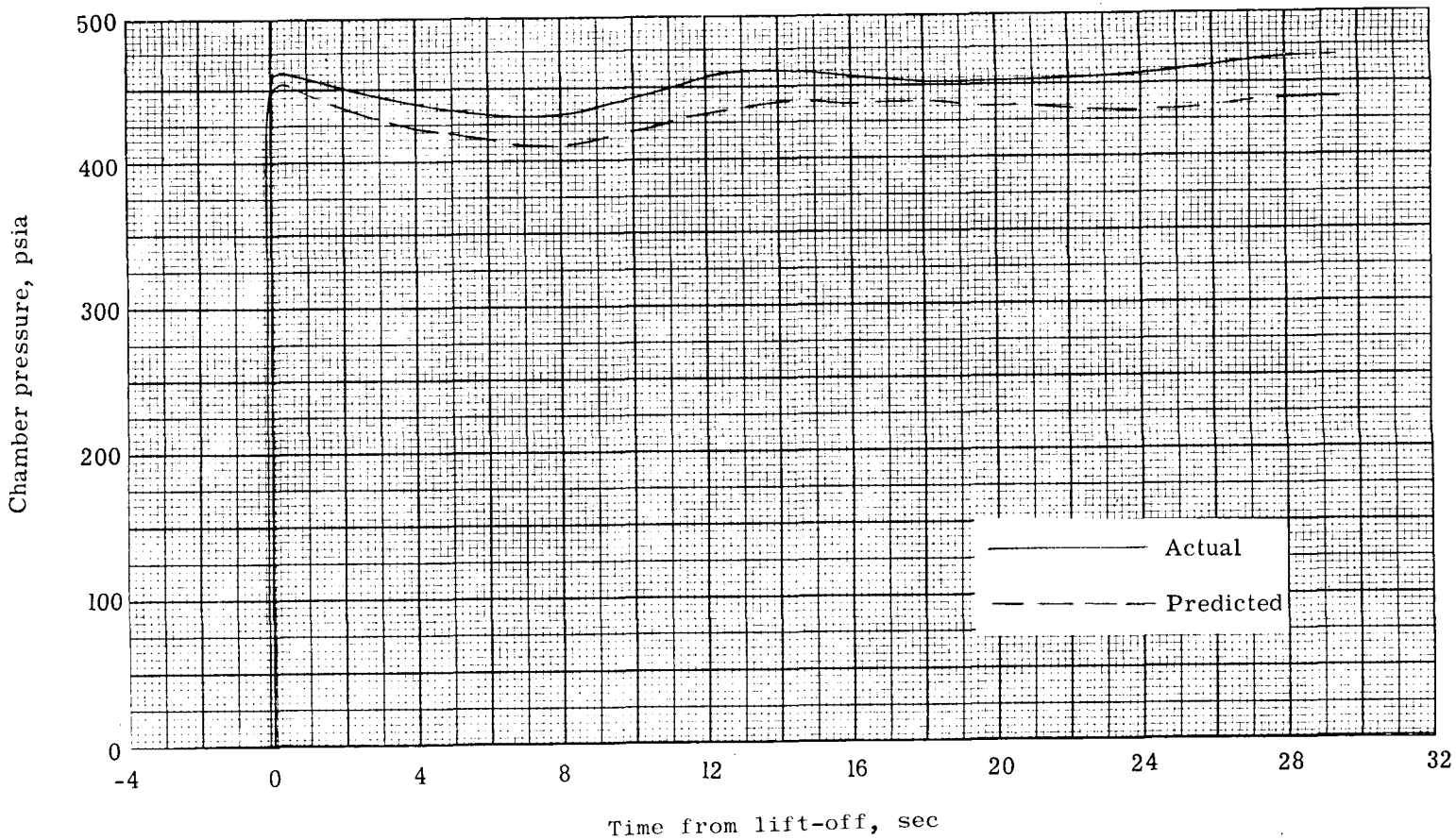

Figure 4.4.2-2. - Algol rocket motor chamber pressure plotted against time.

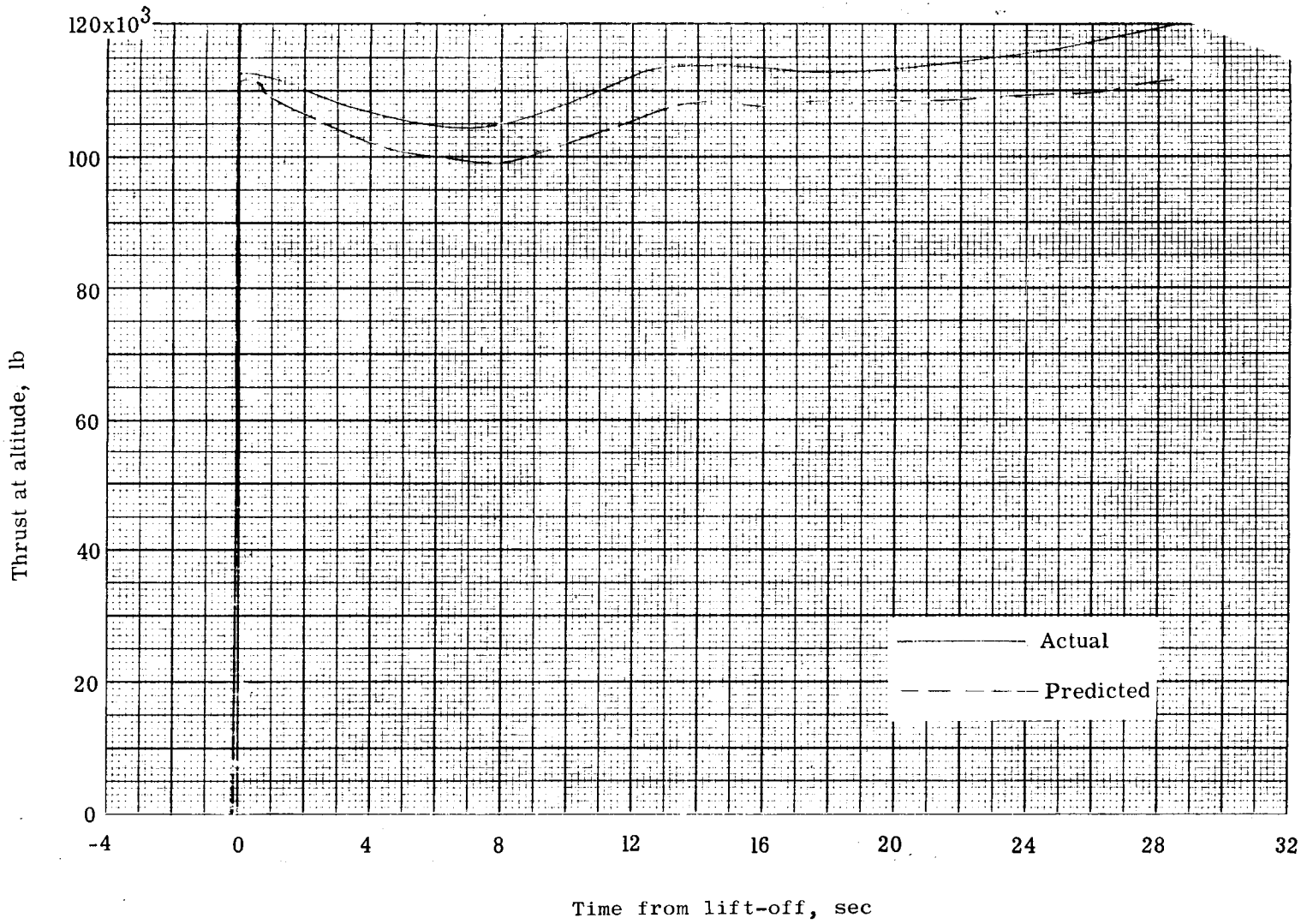

Figure 4.4.2-3. - Algol rocket motor thrust plotted against time.

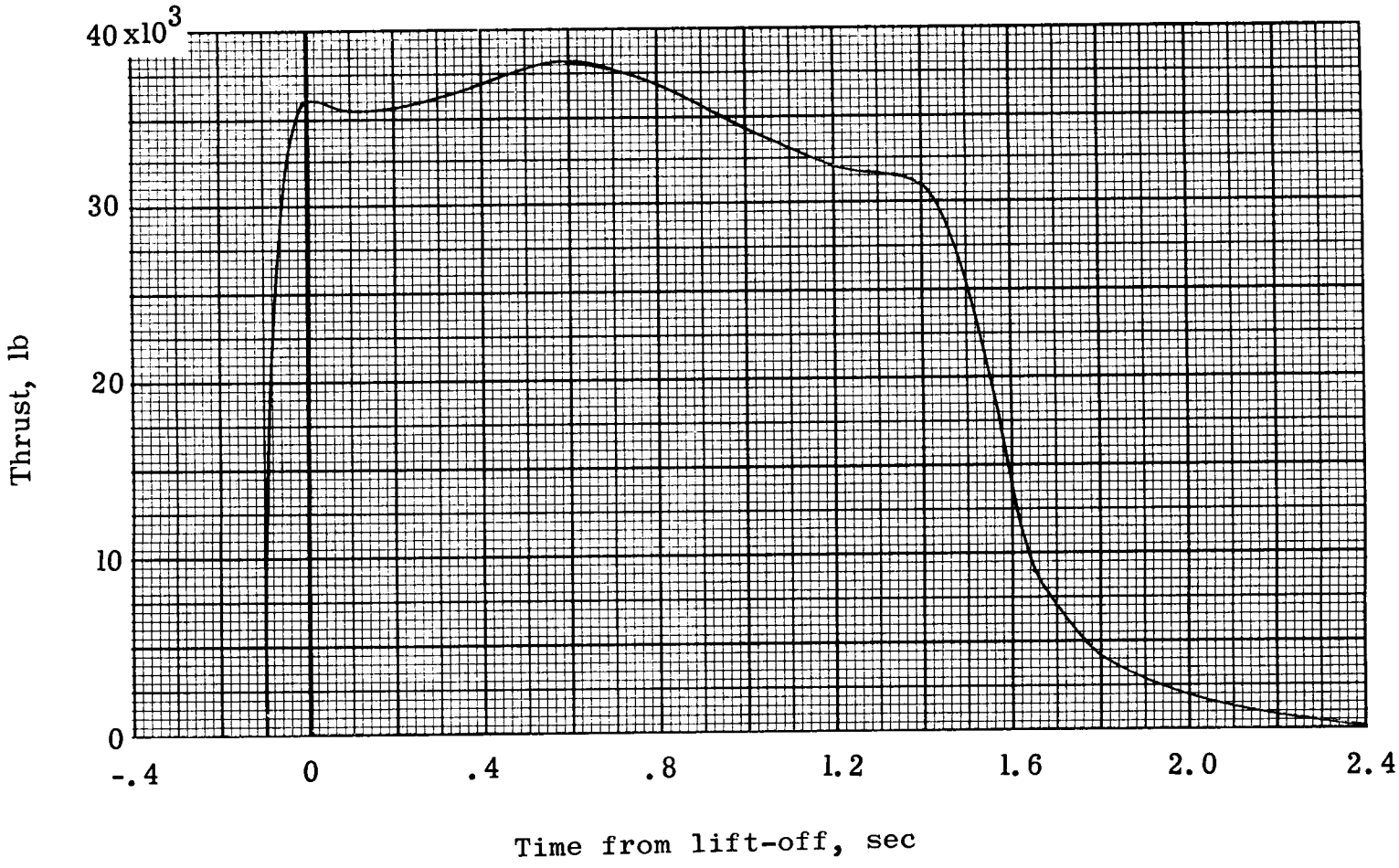

Figure 4.4.2-4. - Recruit rocket motor predicted thrust plotted against time.

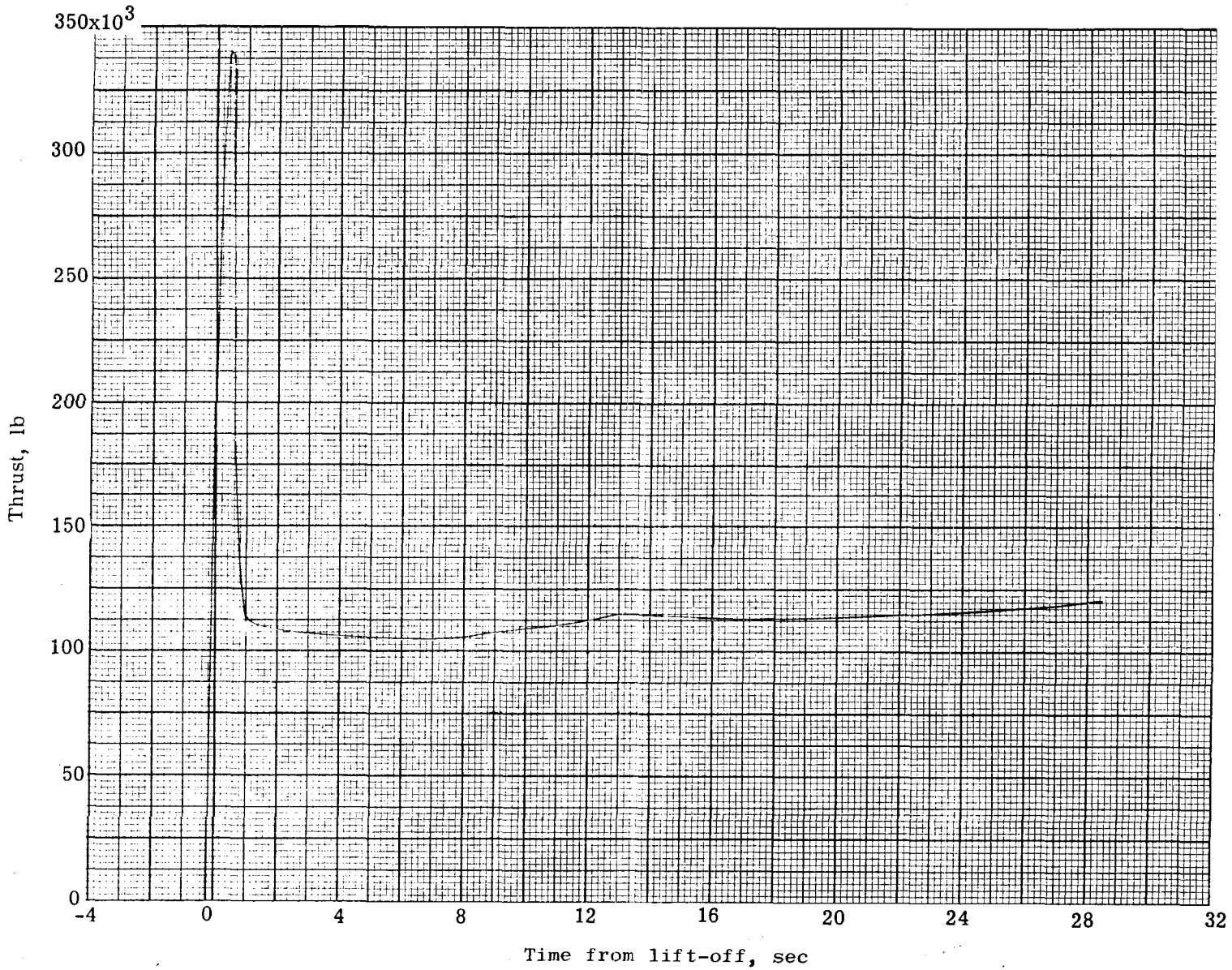

Figure 4.4.2-5. - Launch vehicle total thrust plotted against time.

[redacted]

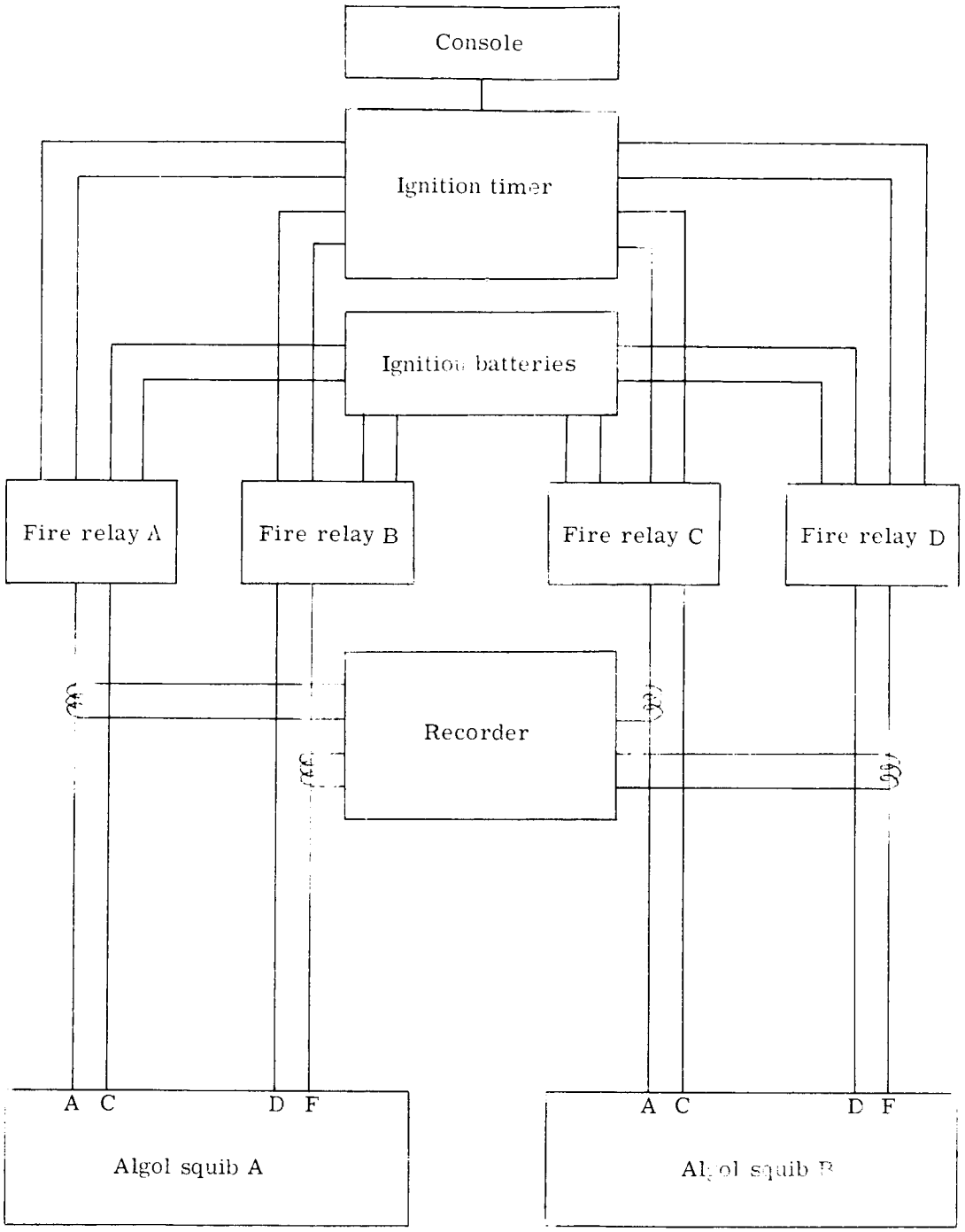

Figure 4.4.2-6.- Algol ignition subsystem diagram.

[redacted]

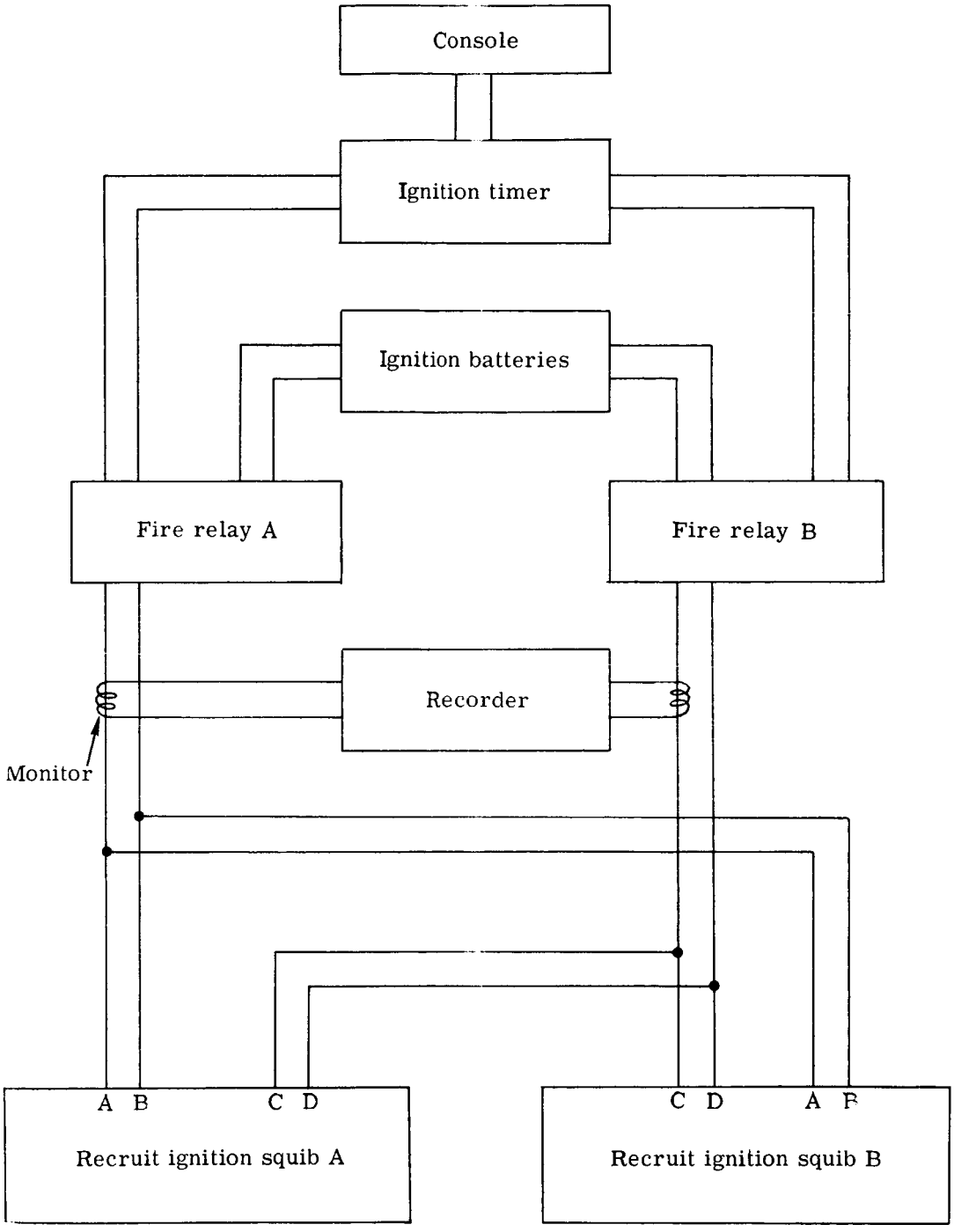

Figure 4.4.2-7.- Recruit ignition subsystem diagram. Typical for all Recruits.

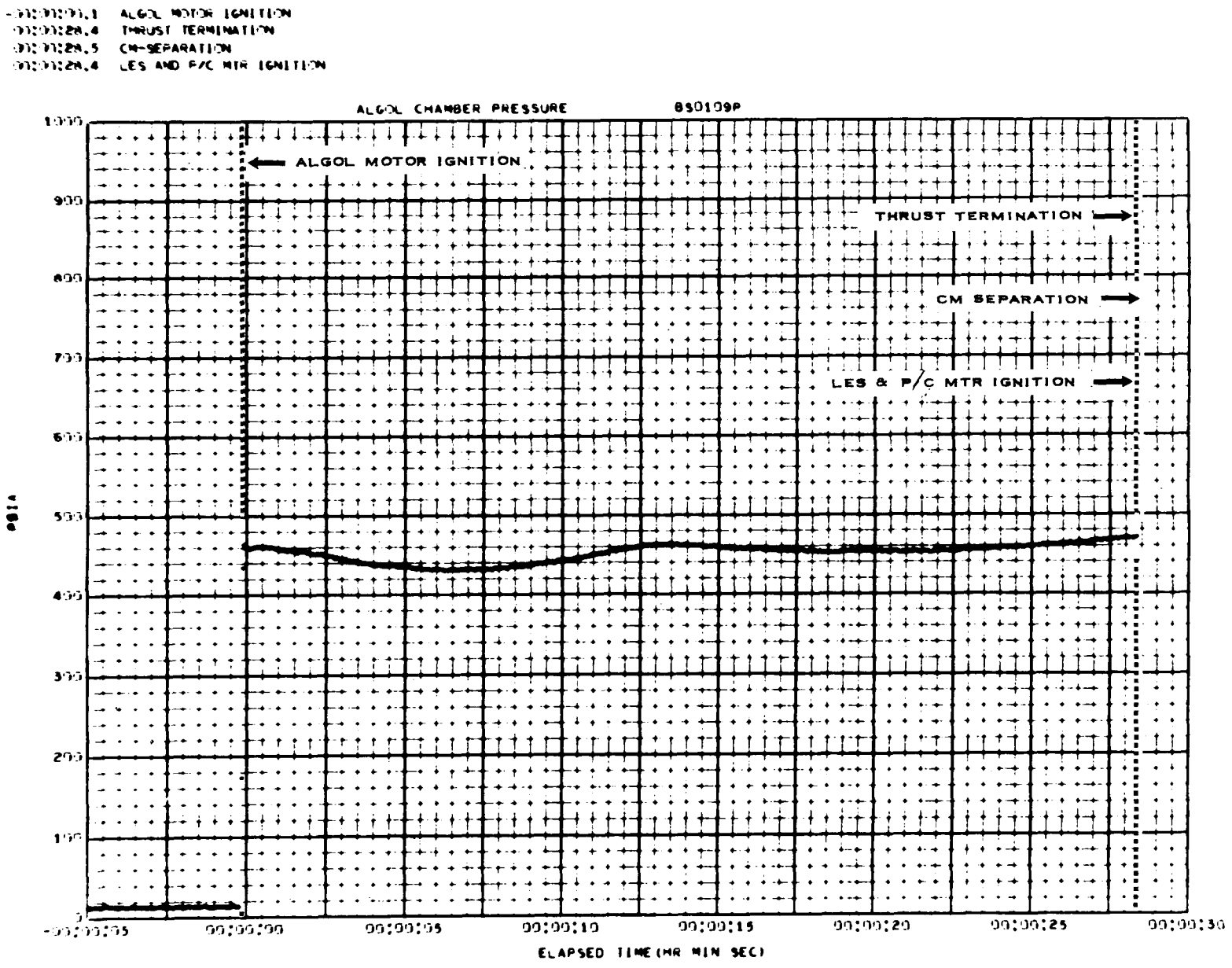

Figure 4.4.2-8. - Time history of Algol chamber pressure.

4.4.3 Aerodynamic analysis.- The test vehicle was stabilized aerodynamically by four symmetrically fixed fins. Analysis of the test vehicle pitch and yaw rates, determined from rate gyroscopes, indicated the vehicle was stable and responded to winds during the launch phase as was predicted. These rates are presented in figure 4.4.3-1 and figure 4.4.3-2, respectively.

Roll attitude and roll rate during launch vehicle flight presented in figure 4.4.3-3 and figure 4.4.3-4, respectively, were determined from the roll attitude and roll rate gyroscopes. The launch vehicle rolled 135° (counterclockwise looking forward from the vehicle base) from lift-off to abort initiation, and had a roll rate of -9 deg/sec at abort initiation. The roll motion was probably caused by small thrust-vector and/or fin misalinements.

The estimated launch drag used in test vehicle preflight performance predictions was obtained by adding the forebody drag determined from wind-tunnel test of scaled models to the base drag determined from base pressure measurements made on the Little Joe II Qualification Test Vehicle flight test. The Little Joe II QTV and Little Joe II launch vehicle 12-50-2 had the same rocket motor combination and base configuration. Comparison of the estimated drag with the flight drag computed from the longitudinal high range accelerometer data (fig. 4.3.6-1), the postflight estimated weight (fig. 4.2.2-1), and thrust (fig. 4.4.2-5) is presented in figure 4.4.3-5. The comparison shows that there is very good agreement between the estimated drag and the flight drag of the vehicle.

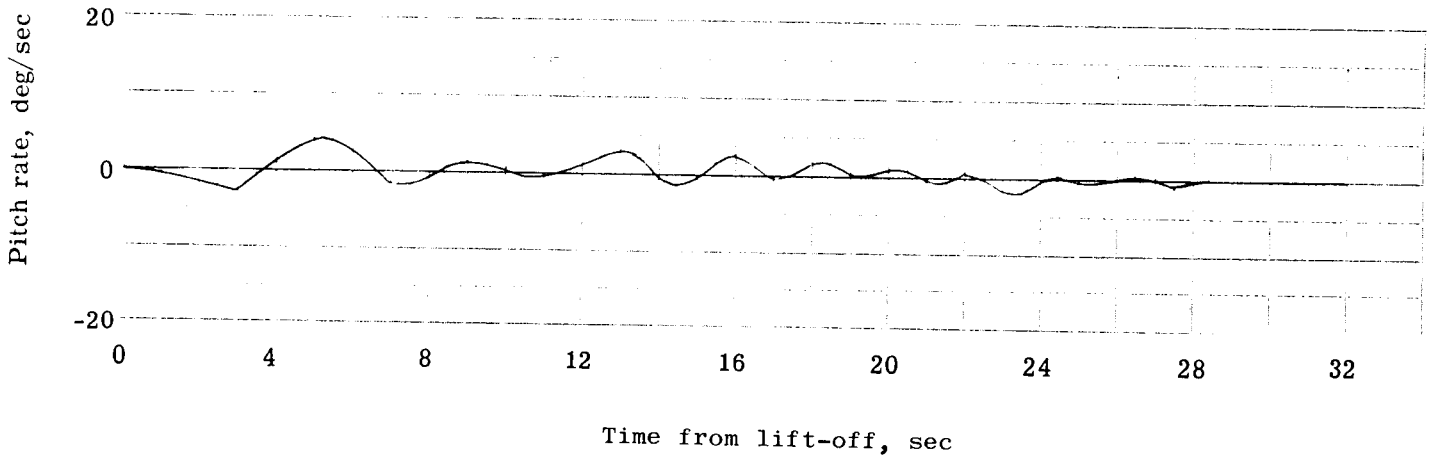

Figure 4.4.3-1.- Launch-vehicle pitch rate time history from lift-off to thrust termination.

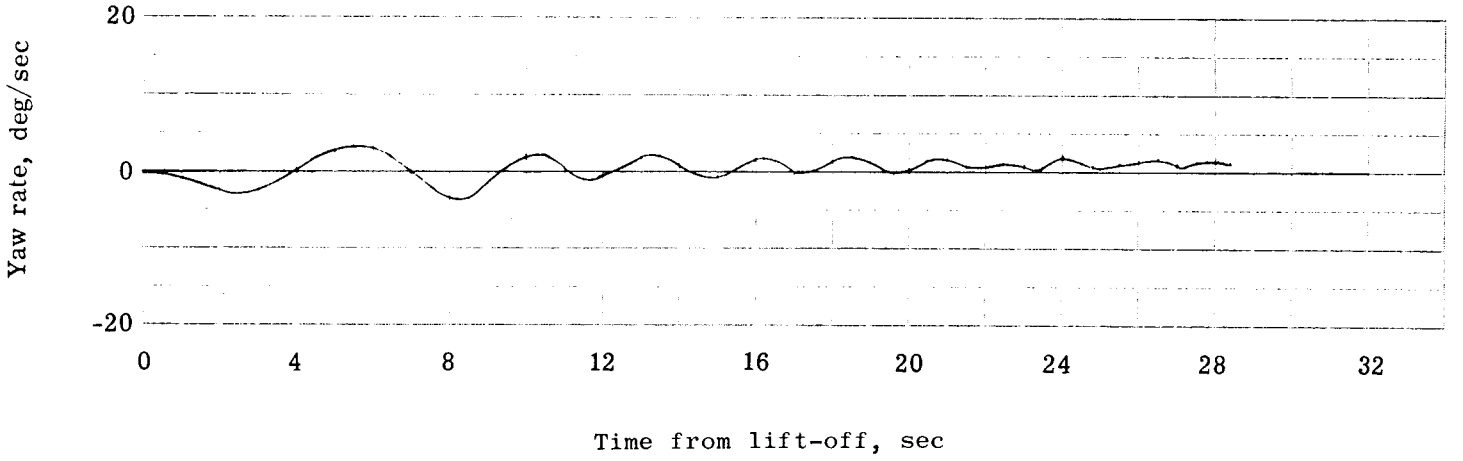

Figure 4.4.3-2.- Launch-vehicle yaw rate time history from lift-off to thrust termination.

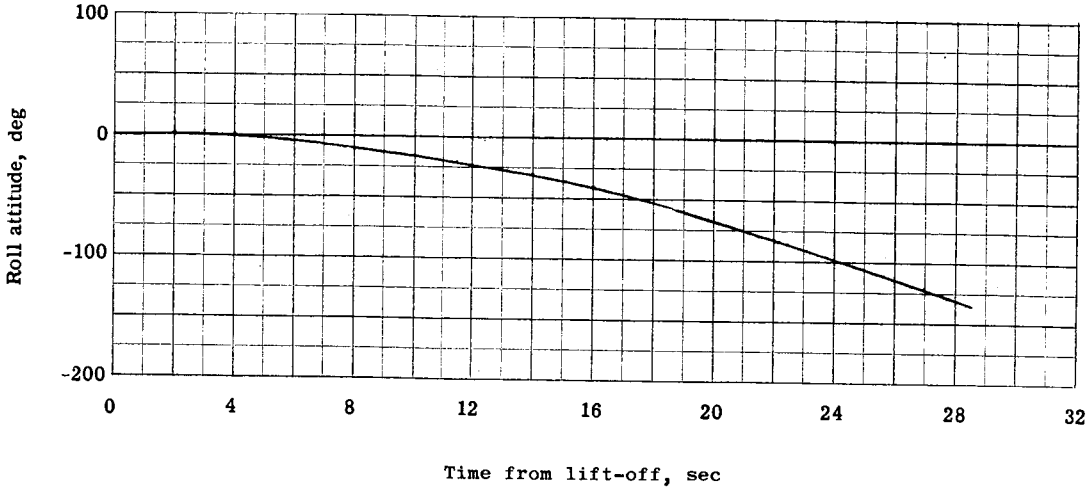

Figure 4.4.3-3.- Launch-vehicle roll attitude time history from lift-off to thrust termination.

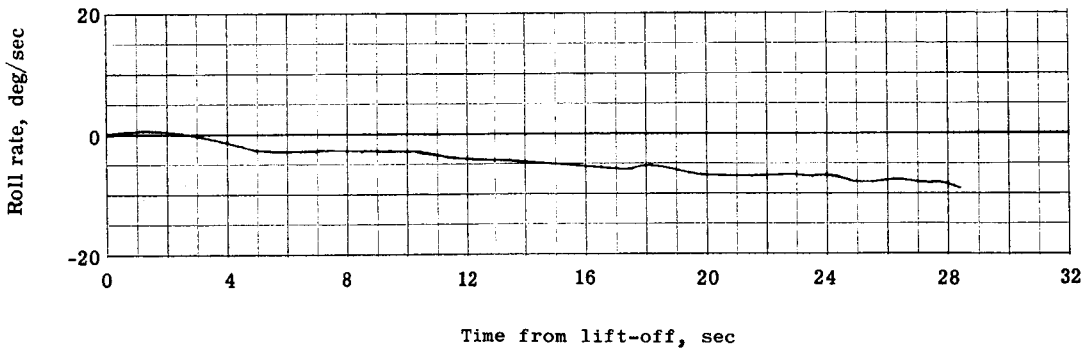

Figure 4.4.3-4.- Launch-vehicle roll rate time history from lift-off to thrust termination.

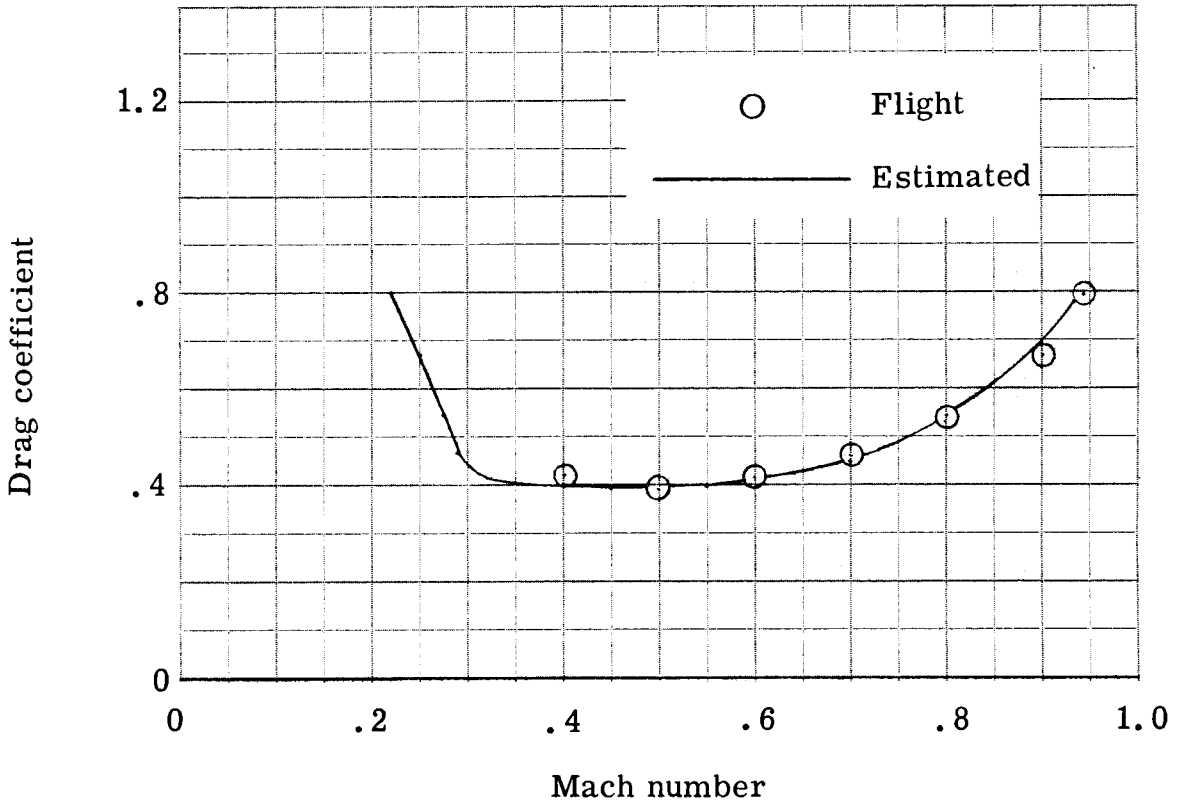

Figure 4.4.3-5. - Comparison of estimated drag with flight drag for various Mach numbers.

4.4.4 Thrust-termination subsystem.- The launch-vehicle thrust-termination subsystem was utilized for rupturing the Algol motor case, thus venting motor pressure and terminating thrust. The thrust-termination subsystem contained two fully redundant systems each consisting of a safe and arm (S and A) unit, two primacord lengths of 100 grains/ft RDX, and a shaped charge of 200 grains/ft RDX. The electrical portion of this system is discussed in section 4.4.6. The thrust-termination subsystem illustrated by the block diagram in figure 4.4.4-1 had the following capability: Electrical and pyrotechnic cross coupling and dual redundancy of primacord enabled thrust termination to be accomplished by firing any one of four primacords. Each S and A unit was equipped with primacords and two squibs. The Algol motor was equipped with two shaped charges, either of which was capable of rupturing the motor case.

The thrust-termination subsystem performed as designed. At T+28.435 seconds the abort command was transmitted from FRW-2 ground transmitter closing the firing relays which fired the S and A detonators, which, in turn, initiated the primacord lengths to the shaped charges. The resulting explosion cut the Algol motor case, thus terminating Algol thrust.

Visual observation at time of thrust termination, a review of the film after the flight, and inspection of the recovered launch-vehicle components revealed that thrust termination of the Algol rocket motor resulted in major destruction of the Little Joe II launch vehicle.

[redacted]

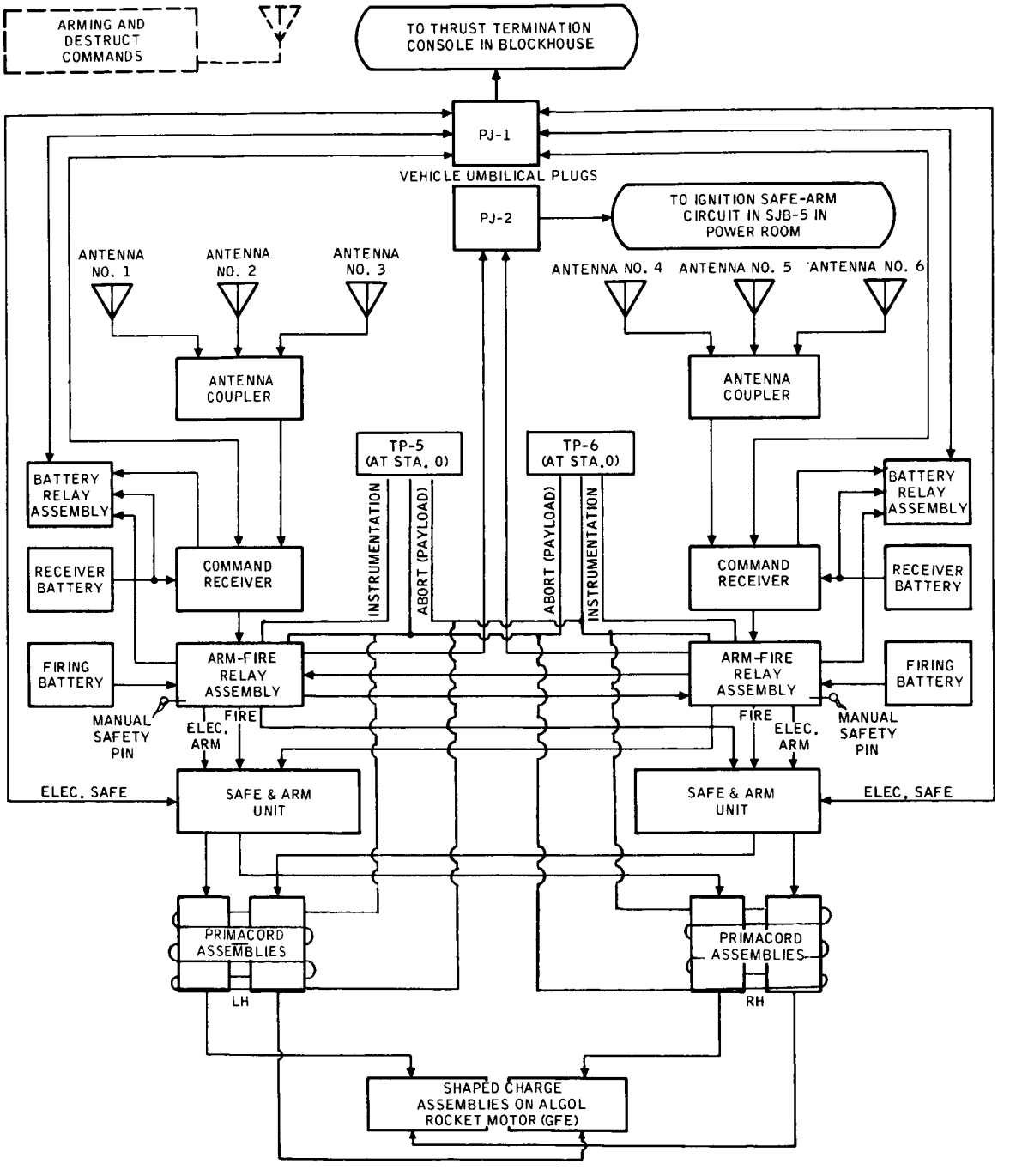

Figure 4.4.4-1.- Block diagram of dual thrust termination subsystem.

[redacted]

4.4.5 Instrumentation subsystem.- The measurement subsystem of the launch vehicle provided signals to landline instruments and to the Apollo command module instrumentation subsystem. Landline measurements consisted of prelaunch temperature environment monitoring for the test vehicle and the Algol motor, existence of firing currents, and a lift-off signal. The temperature data were recorded on a Brown recorder and the existence of firing currents on a visicorder. Landline measurements are shown in table 4.4.5-1.

The measurements to the command module instrumentation were Algol chamber pressure and thrust-termination subsystem A and B fire relay closures. Measurements are shown in table 4.4.5-2.

The Algol chamber pressure measurement gave satisfactory data. These data are presented in figure 4.4.2-8.

The thrust-termination fire relays operated satisfactorily at thrust termination. These measurements were made utilizing a 90×10 commutator at 10 samples per second. Thrust termination apparently occurred during a period when the commutator was not sampling these measurements. The only signal visible indicated the signal to the commutator became open probably because of destructing of the wiring in the launch vehicle.

The prelaunch rocket temperature system provided satisfactory data throughout the time the Algol rocket motor was installed. The final Algol grain temperatures were 70° F $\pm\frac{1}{2}^\circ$ F.

Satisfactory data were obtained from the firing current recorder. The data showed that two channels received no current. A postflight test using the facility portion of the ignition system was performed and is discussed in section 4.6.

TABLE 4.4.5-1.- LAUNCH VEHICLE LANDLINE MEASUREMENTS

Measurements				Recording		Sample rate	Frequency response, cps
Number	Type	Name	Location	Operating range, amp	Recording range, amp		
1	Current	No. 7 Algol, firing current, squib 7	Firing line	0 to 6	9 to 20	Continuous	600
2	Current	No. 7 Algol, firing current, squib 7	Firing line	0		Continuous	600
3	Current	No. 7 Algol, firing current, squib 8	Firing line	0		Continuous	600
4	Current	No. 7 Algol, firing current, squib 8	Firing line	0		Continuous	600
5	Current	No. 1 Recruit, firing current, squib 1	Firing line	0 to 10	0 to 20	Continuous	600
6	Current	No. 1 Recruit, firing current, squib 2	Firing line	0	0	Continuous	600
7	Current	No. 2 Recruit, firing current, squib 3	Firing line	0	0	Continuous	600
8	Current	No. 2 Recruit, firing current, squib 4	Firing line	0	0	Continuous	600
9	Current	No. 3 Recruit, firing current, squib 5	Firing line	0	0	Continuous	600
10	Current	No. 3 Recruit, firing current, squib 6	Firing line	0	0	Continuous	600
11	Current	No. 4 Recruit, firing current, squib 9	Firing line	0	0	Continuous	600
12	Current	No. 4 Recruit, firing current, squib 10	Firing line	0	0	Continuous	600

TABLE 4.4.5-1.- LAUNCH VEHICLE LANDLINE MEASUREMENTS - Concluded

Measurements				Recording		Sample rate	Frequency response, cps
Number	Type	Name	Location	Operating range, amp	Recording range, amp		
13	Current	No. 5 Recruit, firing current, squib 11	Firing line	0	0	Continuous	600
14	Current	No. 5 Recruit, firing current, squib 12	Firing line	0	0	Continuous	600
15	Current	No. 6 Recruit, firing current, squib 13	Firing line	0	0	Continuous	600
16	Current	No. 6 Recruit, firing current, squib 14	Firing line	0 to 20	0 to 10	Continuous	600
Number	Type	Name	Location	°F	°F	Sample rate	Frequency response, cps
17	Temperature	No. 7 Algol, temperature inner grain	Lower section	60 to 80	10 to 120	4/hr	1
18	Temperature	No. 7 Algol, temperature outer grain	Algol lower case	60 to 80	10 to 120	4/hr	1
19	Event	Missile lift-off		(a)		Continuous	
21	Temperature	No. 7 upper case temperatures	Sta 3475 on Algol motor case	60 to 80	10 to 120	4/hr	

NOTE: Landline systems do not allow measurements of each squib current as noted. Only the existence of current is indicated.

(a) Available at 5- to 0-volt step at NAA interface and 0- to -28-volt step at power building equipment rack. Maximum movement before indication = 4 inches.

TABLE 4.4.5-2.- LAUNCH VEHICLE AIRBORNE MEASUREMENTS

Measurement ID	Measurement description	Channel	Data range			Response		Location
			Low	High	Unit	Rate	Unit	
		L SC COM K NO SEG						
B S0109P	Algol chamber pressure	A - 16	0	+500	psia	0-300	cps	Little Joe II launch vehicle
B S0110X	Little Joe II thrust-termination fire system A	A-E-70			Event	10	s/s	Little Joe II launch vehicle
B S0111X	Little Joe II thrust-termination fire system B	A-E-79			Event	10	s/s	Little Joe II Launch vehicle

4.4.6 Electrical subsystem.- The launch-vehicle electrical subsystem consisted of batteries and the associated circuitry for the thrust-termination subsystem and the motor-ignition subsystem.

The thrust-termination electrical subsystem is composed of two subsystems each consisting of three antennas coupled into a command receiver, an arming and firing relay box, a battery monitor relay box, a receiver battery, a firing battery, and the electrical circuitry in the Safe and Arm unit used to arm and fire the igniters. The block diagram of the thrust-termination subsystem is shown in figure 4.4.4-1.

The receivers, AN/DRW-11, and the circuitry used to safe or arm the S and A units were controlled and monitored from the blockhouse. Four Yardney batteries (YEC 5500) were used for onboard power. Two batteries were used by the thrust-termination receivers and two were used to provide the firing current to the safe and arm units.

The electrical portion of the motor ignition subsystem consisted of standard lead-acid batteries, an ignition timer, and firing circuits terminating in the launch vehicle. Seventeen cells of the motor ignition batteries were used to provide the proper firing line current to all seven motors. Motor ignition was controlled by the ignition timer which was located in the power building. However, the ignition timer was started remotely in the blockhouse.

The launch-vehicle ignition battery charger was turned off at T-110 minutes. From the graph of figure 4.4.6-1, it was determined that the firing voltage was 36.3 volts d-c at lift-off. The ignition timer functioned properly. A check of oscillograph records, which gives an event readout of all motor firing line currents, showed no event indication on channels 7 and 12. These channels corresponded to one bridgewire in each of the following initiators: KSQ9, KSQ10, KSQ13, and KSQ14. A postflight test run to determine the lack of indication on channels 7 and 12 is described in section 4.6.

The Algol firing lines all operated satisfactorily.

The thrust-termination receivers were turned on and the safe and arm units were armed by an RF signal from the FRW-2 transmitter at T-4 minutes. The armed indicator at the blockhouse indicated the proper operation of the safe and arm units and associated circuitry. At T+28.435 seconds, the thrust-termination command was transmitted from the FRW-2 transmitter and as a result, thrust of the launch vehicle was terminated. Simultaneously with thrust termination, an abort signal was sent to the spacecraft by firing line relay contacts in parallel with an abort harness which was severed by primacord propagation. Operation of the launch-vehicle electrical subsystem was totally successful during the A-001 mission.

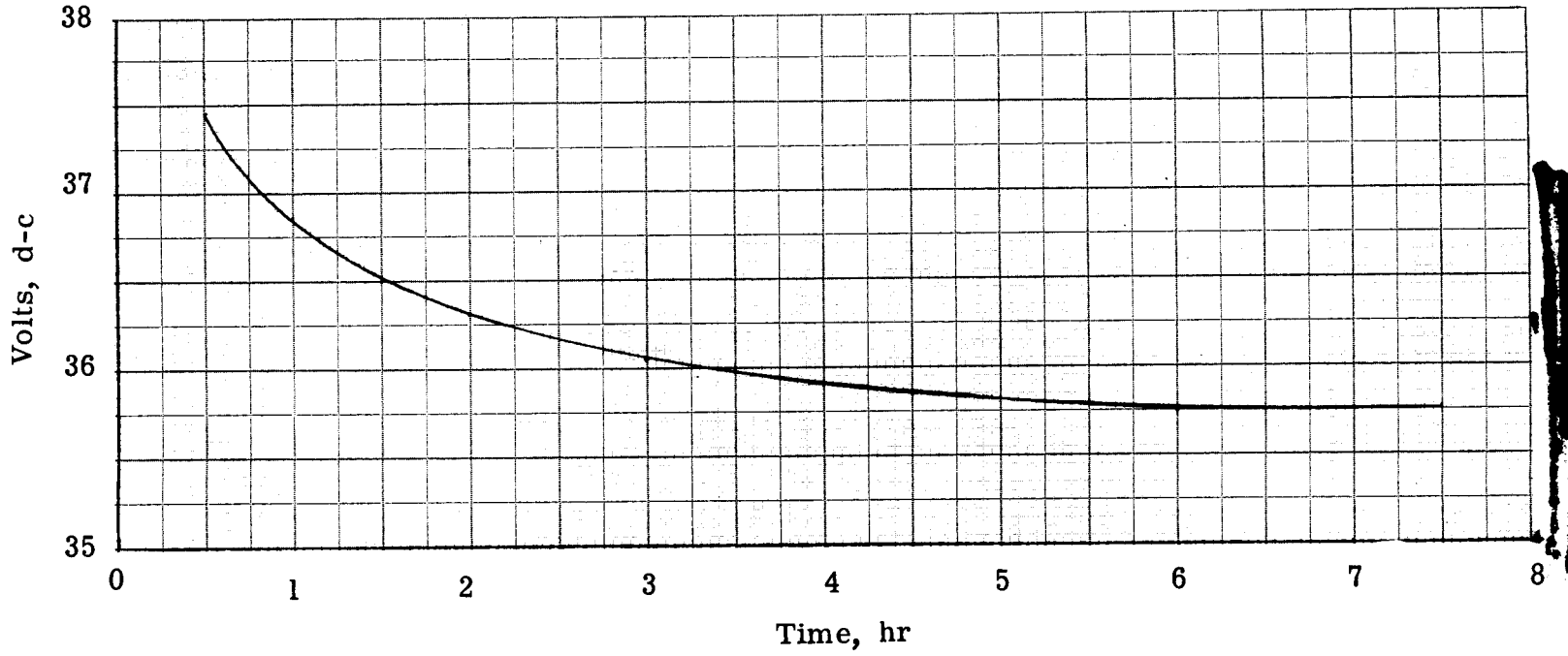

Figure 4.4.6-1. - Variation of ignition battery voltage with time after removal of battery charger.

4.5 Inflight Experiments

Two inflight experiments were conducted during Apollo mission A-001. Glass samples were placed on the conical surface of the command module for a study of rocket motor exhaust effects, and temperature-sensitive paint samples were placed around the conical-surface pressure orifices and on particular members of the LES tower structure to determine gross surface temperature at those locations.

4.5.1 Glass samples.- Glass samples of two types were located on the boilerplate 12 command module conical surface and around the periphery of the aft heat shield as indicated in figures 4.5.1-1 and 4.5.1-2 The two samples were 4 in. by 5 in. and 0.5 in.-thick code 7940 (coated) glass and 2 in. by 2 in. and 0.250 in. - thick code 1723 (uncoated) glass.

The samples were intended to determine effects of the launch-escape-subsystem and tower-jettison-motor exhaust gases and solids on command module windows. Samples were successfully recovered. Deposits caused by smearing of a main parachute riser were found on only one sample. Analysis is proceeding according to the following plans and results will be made available at a later date.

Boilerplate 12 Window Specimen

Examination Procedure

1. Open sealed boxes containing code 7940 glass specimens. Visually examine 4 in. by 5 in. by 0.5 in.- thin film-coated specimen which has been stored.

2. Qualitative photographic examination. Take pictures of a fluorescent grid ($\frac{1}{16}$-inch wide lines and 2 in. by 2 in. grid) through both boilerplate 12 thin film-coated specimens and a virgin thin film-coated specimen. Camera settings, lighting, grid lighting, and all other conditions will be identical for boilerplate 12 and virgin specimens. Qualitatively compare photographic prints.

3. Quantitative examination. Conduct transmissibility tests to determine the percent transmission of light wavelengths ranging from approximately 380 millimicrons to 1200 millimicrons. These determinations are to be made on both boilerplate 12 thin film-coated specimens and a clean virgin specimen. Quantitative data will constitute the difference, at any or all wavelengths, between virgin and boilerplate 12 specimens. State values of Δ in percent transmission loss.

4. Quantitative soot composition. If windows are "sooted" or otherwise contaminated, the deposited material will be physically and/or

[redacted]

chemically removed from the outboard face of specimens and subjected to quantitative spectrographic analysis. Care will be exercised to avoid removal of the thin film, vacuum-deposited window coatings. The greater the quantity of contaminant available the more accurate will be the analysis.

5. Microscopic examinations. After removal of deposited material, a microscopic study of the thin film-coated specimen surface will be conducted in an attempt to determine the extent of damage to coatings and/or to the polished glass surface.

6. The 2 in. by 2 in. by 0.250-in. samples which were polished on one side (mount facing out) of code 1723 (uncoated) will be examined visually for evidence of thermal damage. If sooted or otherwise contaminated, deposits will be removed and added to the material taken from the code 7940 windows for quantitative analysis.

7. Two of the small (code 1723) specimens will be intentionally fractured (after removal of surface deposit). The fracture pattern will be observed. If fragments are typical of heat-treated glass (not of diced shape), center birefringence readings may be necessary. Low birefringence values, given in mm/inch, would indicate that specimens were subjected to heat which was in excess of their annealing temperature (708° C or 1238° F).

[redacted]

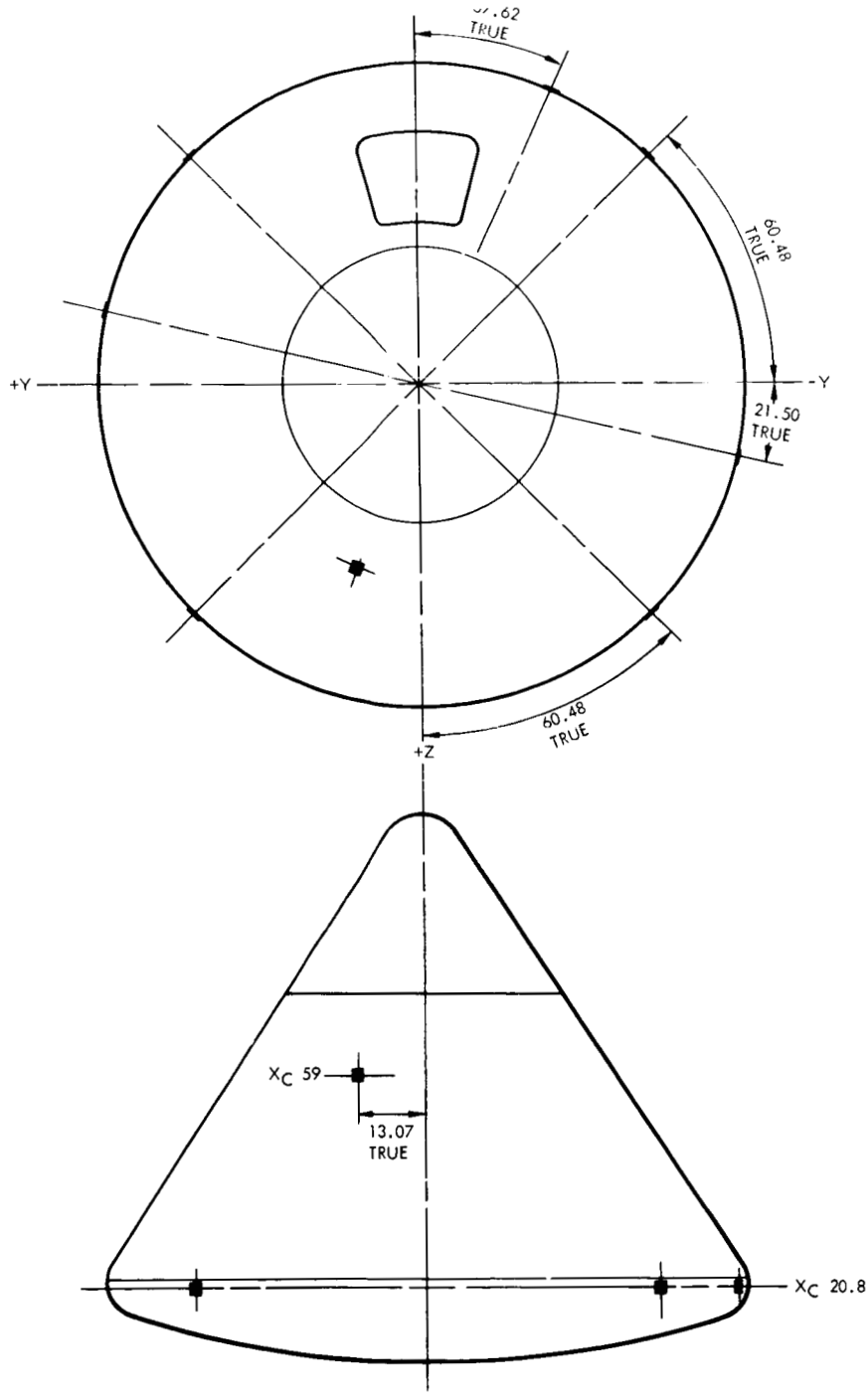

Figure 4.5.1-1. - Location of eight 2- by 2-inch glass samples on command module.

[redacted]

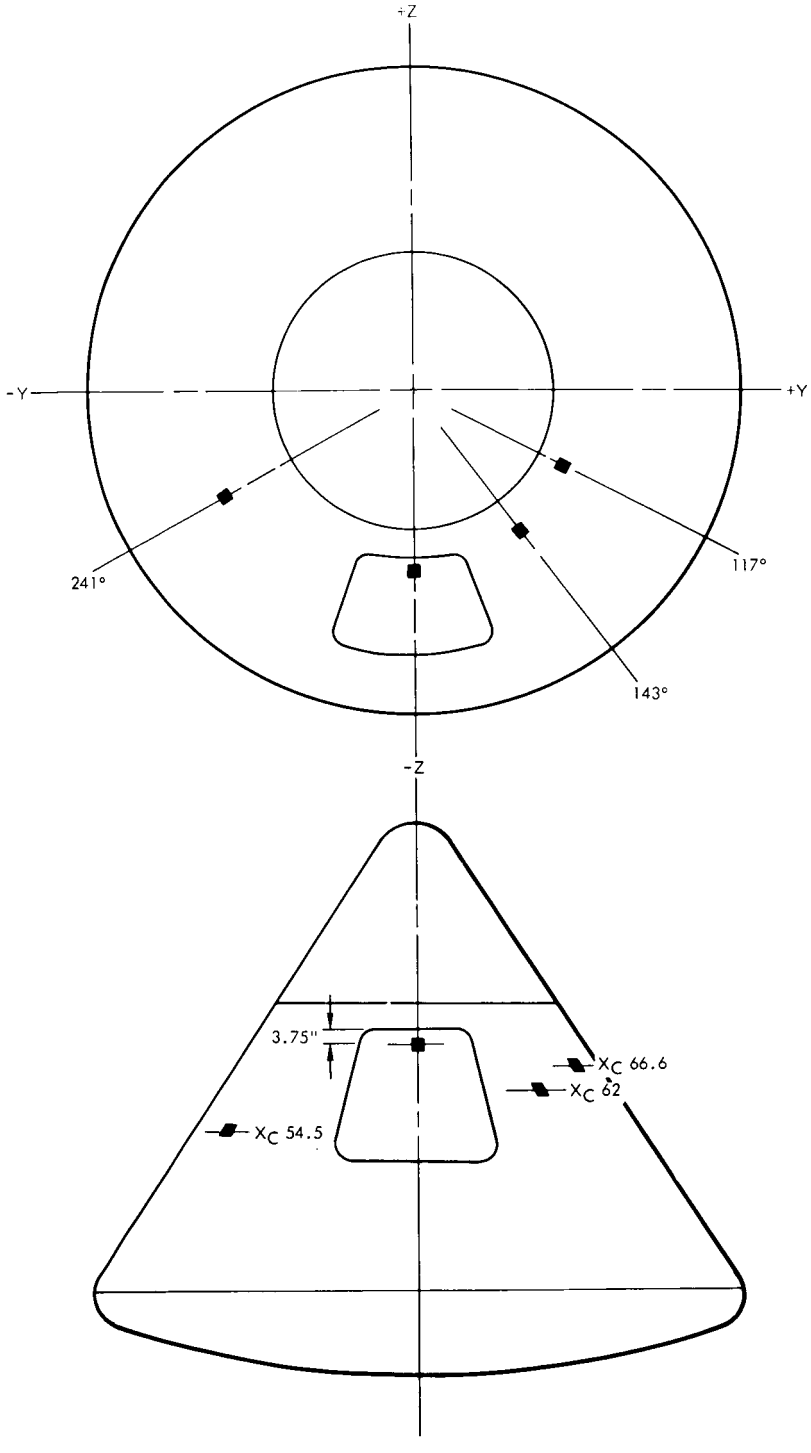

Figure 4.5.1-2. - Location of four 4- by 5-inch glass samples on command module.

[redacted]

4.5.2 Templaq sensitive paint.- Templaq paint was arranged around the command module as indicated in figure 4.5.2-1. The templaq pattern was placed on pressure orifice flanges at six axis locations. Station locations were from X_c = 30 inches to X_c = 78 inches with temperature ranges from 200° F to 850° F.

The highest temperatures were those around the base of the command module with the +Z axis recording the highest readings. Temperatures on the +Z axis were from 250° F (X_c = 78 in.) to above 850° F (X_c = 30 in.). The remaining axis ranges were from below 200° F to below 400° F.

The templaq patterns on the launch-escape tower (see fig. 4.5.2-2) were on the +Z, -Y axis. Temperature range of the patterns was 200° F to 600° F.

Generally, the patterns closest to the launch-escape motor were completely burned off. The readings on the lower patterns ranged from 200° F to 350° F.

[redacted]

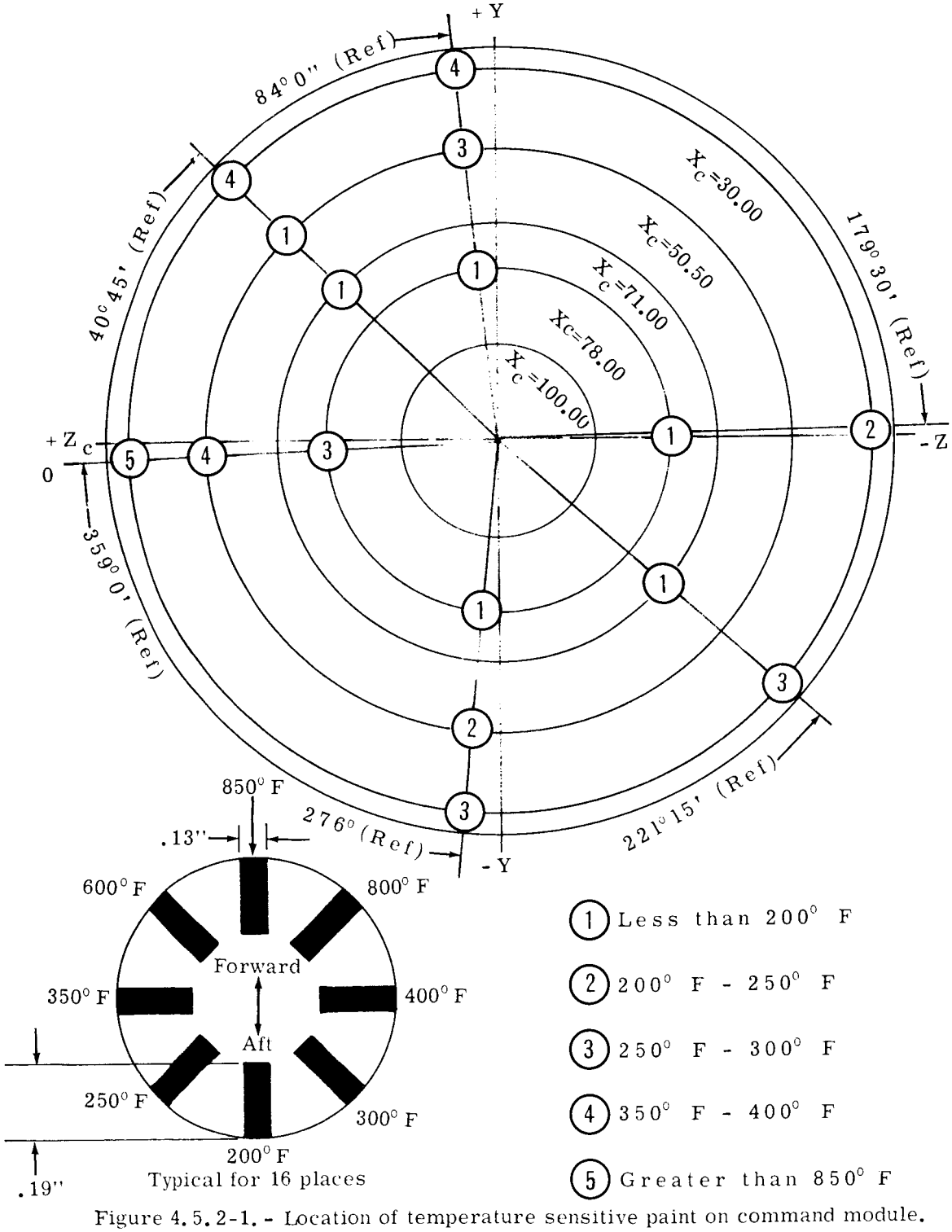

Figure 4.5.2-1. - Location of temperature sensitive paint on command module.

[redacted]

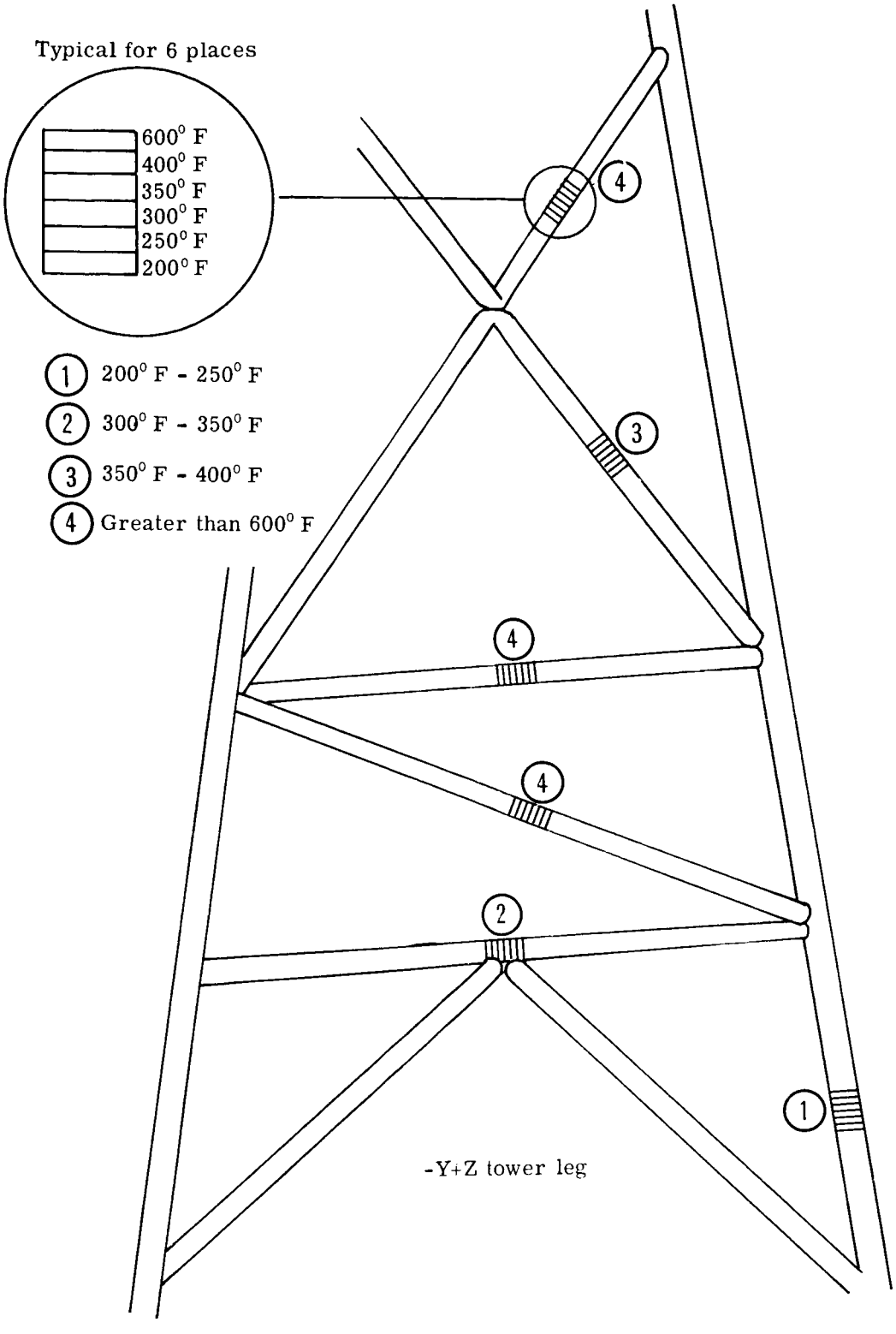

Figure 4.5.2-2.- Location of heat sensitive paint on launch-escape tower.

[redacted]

4.6 Postflight Testing

The postflight testing conducted at White Sands Missile Range (WSMR) consisted primarily of functional checks to verify overall hardware postflight status and specific tests to investigate anomalies noted in the flight data.

4.6.1 Launch vehicle postlaunch testing.- The only data anomaly noted on the launch vehicle was the absence of any current indication on channels 7 and 12 of the launch-vehicle-motor ignition current land-line recorder. Channel 7 monitored the current supplied to Recruit motor no. 4, squibs KSQ9 and KSQ10, bridgewires A to B. Channel 12 monitored the current supplies to Recruit motor no. 6, squibs KSQ13 and KSQ14, bridgewires C to D.

A postflight check of the instrumentation subsystem and GSE ignition system was performed. The test functionally checked the complete ignition system exclusive of the vehicle wiring. One-half ampere fuses were substituted for actual squibs.

Results of this test clearly indicated that there was a 1.5-millisecond delay between application of the current to the squibs which did not indicate current on the launch data and the redundant squibs in the same initiators which did indicate current application. It can be concluded from these data that the redundant bridgewires were destroyed prior to application of current when the adjacent bridgewires activated the initiator charges (fig. 4.4.2-7).

A physical check of all launch-vehicle-motor initiators showed no anomalies were evident.

4.6.2 Spacecraft postlaunch testing.- In addition to a functional verification of the over-all spacecraft electrical subsystem operation, most of the spacecraft postflight testing was devoted to investigation of the following three anomalies noted on the flight data:

1. Early time-out of the A system, 41.1-second back-up abort timer.

2. Failure of the launch-escape motor pressure instrumentation to yield any data.

3. Failure of command module base pressures nos. 5 and 9 to yield any data.

The following summaries include the scope, configuration, significant results, and applicable documentation of the postflight tests conducted on the BP-12 spacecraft hardware.

[redacted]

4.6.3 Over-all command module electrical subsystem test.- GSE power was applied to the command module using the postflight checkout box. Power supplies were used to supply 28 v d-c to the logic and main buses. No attempt was made to power or operate the pyrotechnic buses. During the power-on run, the following functions were performed: the onboard tape recorder was operated; gyros were caged and uncaged; the 5-point and R- and Z- calibrators were cycled; the instrumentation bus was activated; the telemetry package was turned on low power and recorded by RF link in the NASA telemetry trailer; and two 41.1-second back-up timer abort sequence runs were conducted.

Test results indicated that all sequencer time-delay relays operated within tolerance and all sequencer telemetry signals were normal. Opening and closing altitudes of the 25,000-foot and 12,500-foot baroswitches were checked using the C14-002 barometric console. Opening altitudes were recorded as 7.0 and 14.6 inches of mercury, and closing altitudes were 11.6 and 18.3 inches of mercury, which is within tolerance.

Command module electrical subsystem operation appeared normal in all respects and all data closely duplicated prelaunch test data.

4.6.4 Bench check-out of the ELS sequencer.- The bench check-out consisted of testing time-delay relays, telemetry readout circuitry, and functional operation of the baroswitches. Checkout of the flight ELS sequencer showed following conditions: all time-delay relays were within tolerance and consistent with times monitored during initial bench checkout and tests prior to flight; all transistors had normal resistance readings.

On the initial run of the bench checkout, one 25,000-foot baroswitch and one 12,500-foot baroswitch were slightly out of tolerance. The baroswitches were subsequently checked three more times and found to be operating normally.

All telemetry circuitry functioned normally during bench checks.

Telemetry tapes indicated the 25,000-foot baroswitches did not operate during the flight. However, the Northrop-Ventura data package states that the 25,000-foot baroswitches open at approximately 7.2 inches of mercury. The apogee of boilerplate 12 did not reach the altitude required to open the baroswitches.

4.6.5 Bench check-out of the LES sequencer.- The launch-escape-subsystem (LES) sequencer was bench-checked subsequent to the flight and was normal. No abnormality was noticed with system A of the 41.1-second timer, and all aspects of the check-out indicated normal operation.

[redacted]

During the flight, telemetry records indicated system A of the 41.1-second timer timed out prematurely, approximately 0.07 second after thrust termination and normal abort. It is possible that the exceedingly high g received by the spacecraft during thrust termination caused system A to malfunction, thus causing premature time out.

It is recommended that additional testing be conducted by the contractor to verify operation of the 41.1-second timer under high g loads similar to those imposed upon the command module at the time of launch-vehicle thrust termination.

4.6.6 Investigation of the launch-escape-motor pressure instrumentation.- Because of the damage incurred by the LES at impact, the only portion of the launch-escape motor pressure instrumentation that could be checked was the power and signal circuits between the tower disconnect and the telemetry package in the command module. Continuity checks of this circuitry indicated no apparent discrepancy. Checks of this circuitry during precount were satisfactory and did not reveal any problems in this area. The only conclusion is that a failure occurred in either the transducer itself or some portion of the LES tower wiring.

4.6.7 Investigation of the failure of command module base pressures nos. 5 and 9.- Both transducers were removed and functionally verified at the WSMR base calibration laboratory. Operation was normal and no significant change in calibration was noted. The power supply circuitry to these two transducers was then checked, and it was established that an open circuit common to both transducer power supplies existed in the signal conditioner box. This component will be forwarded to Downey for failure analysis.

[redacted]

5.0 MISSION OPERATIONS

5.1 Prelaunch Operations

5.1.1 Test vehicle history.- Relevant activities on the Little Joe II launch vehicle (12-50-2) commenced on April 22, 1963, when it entered final mate and assembly at the General Dynamics/Convair plant, San Diego, California. A chart depicting major milestone events is shown in figure 5.1.1-1.

The major assembly components of the launch vehicle consisting of forebody, afterbody, and 4 fins entered final mate and assembly on April 22, 1963. This activity was completed on September 3, 1963, and systems checkout was completed September 16, 1963. The vehicle was then placed in temporary storage at San Diego until November 14, 1963, when a design engineering inspection (DEI) was conducted. Subsequently, General Dynamics/Convair was directed to design and install a system which would terminate thrust of the launch vehicle in response to an RF signal. The thrust-termination subsystem design was approved on December 10, 1963. Three functional tests of the thrust-termination subsystem were accomplished using a wood and metal full-scale mock-up incorporating all wiring, primacord, and system components. A final design review approving the thrust-termination subsystem installation in the vehicle was held on February 1, 1964. Factory check-out of the vehicle was conducted from February 3 to February 8, 1964.

The fins and ground-support equipment for the launch vehicle arrived at WSMR on February 12, 1964. The launch vehicle forebody and afterbody combination arrived at WSMR on February 17, 1964. Offloading and receiving inspection proceeded as planned with completion on February 18, 1964. Receiving inspection on the Algol and Recruit motors was completed on January 15, 1964. The Algol was moved to the build-up area on February 20, 1964.

On February 19, 1964, the afterbody was moved from the Vehicle Assembly Building and placed on the launcher, initiating structural assembly.

Assembly of the launch vehicle was completed on February 26, 1964. Check-out of the vehicle systems was initiated on March 6 and, except for the thrust-termination subsystem, completed on March 20, 1964. The thrust-termination subsystem was not checked at this time.

During mid-March, it was deemed necessary to modify the abort signal circuitry and to install a redundant umbilical. Incorporation of these modifications, completion of the thrust-termination subsystem,

[redacted]

and performance of final vehicle check-outs were initiated on April 10, 1964. Complete launch vehicle validation was accomplished by April 24, 1964.

The Apollo boilerplate 12 spacecraft was released by the North American Aviation, Downey, manufacturing section to NAA Apollo Test and Operations on November 8, 1963. A chart depicting major spacecraft milestone events is shown in figure 5.1.1-2. The remainder of November and first 10 days of December 1963 were used for the incorporation of all outstanding modifications. Associated ground-support equipment (GSE) was checked and verified by December 13, 1963.

The period from December 10, 1963, to January 9, 1964, was utilized for the accomplishment of individual subsystems tests. Following this, electromagnetic interference tests (EMI) and integrated subsystems tests were performed and completed on February 17, 1964, freeing the vehicle and associated GSE for shipment to the White Sands Missile Range (WSMR).

Component items for spacecraft buildup started arriving at the Vehicle Assembly Building (VAB) in Launch Complex 36, White Sands Missile Range, on February 10, 1964, with final shipments received, unloaded, and inspected by March 9, 1964.

Actual spacecraft buildup began with the placement of the tower-jettison motor on the alinement stand on February 24, 1964. Instrumentation wiring, camera equipment installation, and weight and balance operations all proceeded concurrently. By March 24, 1964, the command module had been "closed out" with weight and balance measurements completed.

On March 24, 1964, the boilerplate service module was moved from the VAB to the launch pad and mated to the Little Joe II launch vehicle. Stacking of the command module on the service module and then the launch-escape subsystem (LES) on the command module completed mating procedures by March 30, 1964.

Individual subsystems tests were started April 2, 1964. At this time, testing was interrupted for spacecraft modification and troubleshooting of an apparent problem with the A-14-003 pyrotechnic simulator.

The modifications to the spacecraft included 41.1-second backup abort initiation timers, redundant disarming capabilities, and sequencer timer transient suppression circuitry. Compatible GSE modifications were made concurrently.

[redacted]

During the trouble-shooting procedure mentioned previously, a fusistor was inadvertently overheated in the earth-landing-subsystem sequencer, requiring replacement of the sequencer. The replacement sequencer with modified baroswitches was installed on May 22, 1964. The replacement sequencer was equipped with baroswitches set to activate at 12,500 feet; whereas, the originally installed sequencer baroswitches were set to activate at 15,000 feet m.s.l.

Throughout the month of April, there were concurrent efforts to perform a series of camera subsystem functional check-outs. In spite of numerous problems, all camera subsystem functional verifications were successfully completed by April 26, 1964.

After an open item review on April 27, 1964, the first combined spacecraft-launch vehicle operation, interface tests, was conducted April 28, 1964.

Subsequent integrated subsystems tests performed on April 30, 1964, proved compatibility of the individual subsystems while functioning as in flight.

The simulated countdown was performed on May 4 and 5, 1964, to establish the validity of the times estimated for performance of various tasks during the countdown.

On May 6, 1964, another integrated subsystems test was performed to reestablish confidence in the subsystems after connectors had been removed and replaced during the course of the simulated countdown.

A flight readiness review, conducted on May 8, 1964, established the readiness of the test vehicle for flight.

The countdown and launch were completed on May 13, 1964, culminating in a successful mission.

5.1.2 Spacecraft preparation operations.- North American Aviation (NAA) Operational Test Procedures (OTP's) approved by NASA and successfully performed at Downey and at White Sands Missile Range constituted the milestones by which flight preparation of the spacecraft were measured.

An OTP is a test and check-out procedure document originated by the cognizant launch operations systems engineer. If a deviation to an OTP was required, it was approved and signed by the NAA test project engineer, the NASA systems engineer, and the NASA test conductor. Before an OTP could be entered as valid documentation of a task performed, it was approved by both NASA and NAA quality control inspectors.

[redacted]

Figure 5.1.1-3 depicts the chronological sequence by week of significant events from the first factory subsystem test through the final preintegrated systems tests.

Permanent documentation of each OTP encompassing the final "as-run" procedure, test results obtained, and approval signatures is on file at NAA, Downey, and MSC, Houston.

At the BP-12 Flight Readiness Review meeting held on May 8, 1964, it became evident that all problems encountered during preflight testing had been satisfactorily resolved. The review board accepted the spacecraft, as well as the launch vehicle and GSE, as being ready for flight.

5.1.3 Launch vehicle preparation operations.- The check-out concept for Little Joe II launch vehicle 12-50-2 was identical to that used on the qualification test vehicle (QTV). Detailed building-block check-out operations were used to confirm that the facility and vehicle systems functioned as designed and were ready for the flight mission. This activity was accomplished according to GD/Convair Operational Check-out Instructions (OCI's).

An OCI for a system was originally prepared by the design engineer of the system. It was modified by using comments provided by GD/Convair launch operations engineers and MSC-RASPO/WSMR systems engineers. The OCI was conducted on the vehicle or support equipment at San Diego before delivery. Before use at WSMR, all OCI's were approved by MSC RASPO/WSMR systems engineers assigned to the operation.

Following vehicle assembly at WSMR, the systems were checked by using approved OCI's. Minor deviations to OCI's were made during the actual check-out operations if required. Complete testing of components and systems was accomplished at WSMR by GD/Convair personnel and observed by MSC RASPO/WSMR engineers, MSC/WSMR inspectors, and GD/Convair inspectors. The "as-run" copies of the OCI became permanent documentation for the vehicle and are available for review.

For this operation, an attempt was made to modify the OCI's to a format and test discipline consistent with future Apollo check-out procedures. The final OCI's used were satisfactory technically, but did not completely meet the Apollo format and discipline requirements as understood to apply by the NASA operations personnel assigned to the BP-12 operation.

All tasks of installation, modification, check-out, or operation were authorized by Test Preparation Sheets (TPS's) signed by cognizant RASPO/WSMR and GD/Convair engineers. These tasks were scheduled by weekly and daily schedule plans. Completion of tasks were confirmed

[redacted]

on the TPS by the signatures of the GD/Convair technician, GD/Convair inspector, and MSC/WSMR inspector.

For check-out operations prior to integrated operations with the spacecraft, OCI's were used. These tests were directed by a GD/Convair engineer and executed by GD/Convair engineers and technicians. The various steps were confirmed by both GD/Convair and MSC/WSMR inspectors.

For check-outs integrated with the spacecraft, Operational Test Procedures (OTP's) prepared by NAA with GD/Convair assistance and approved by RASPO/WSMR were used. These operations were directed by the RASPO/WSMR test director assigned to the operation. Procedures for execution and confirmation of the OTP's were identical to launch vehicle check-out procedures.

The OCI's that were accomplished and the week of performance are shown in figure 5.1.1-4.

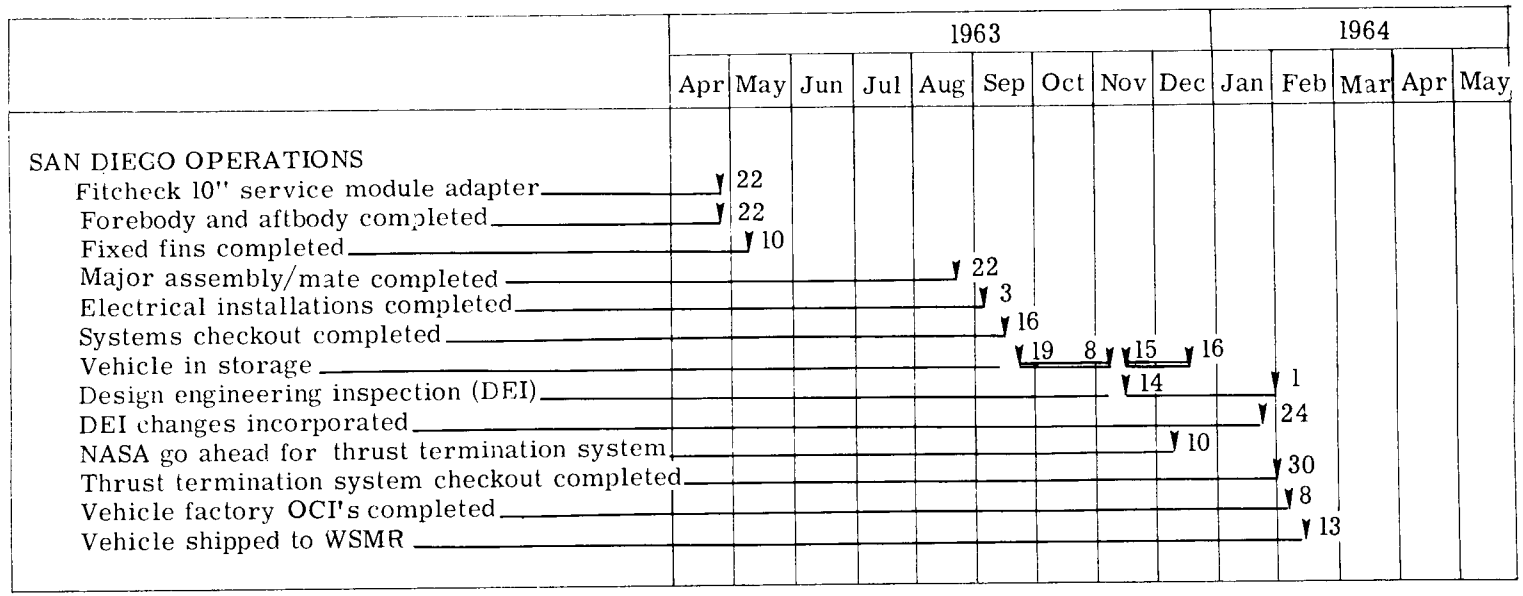

(a) San Diego operations.

Figure 5.1.1-1. - Launch vehicle 12-50-2 prelaunch milestones.

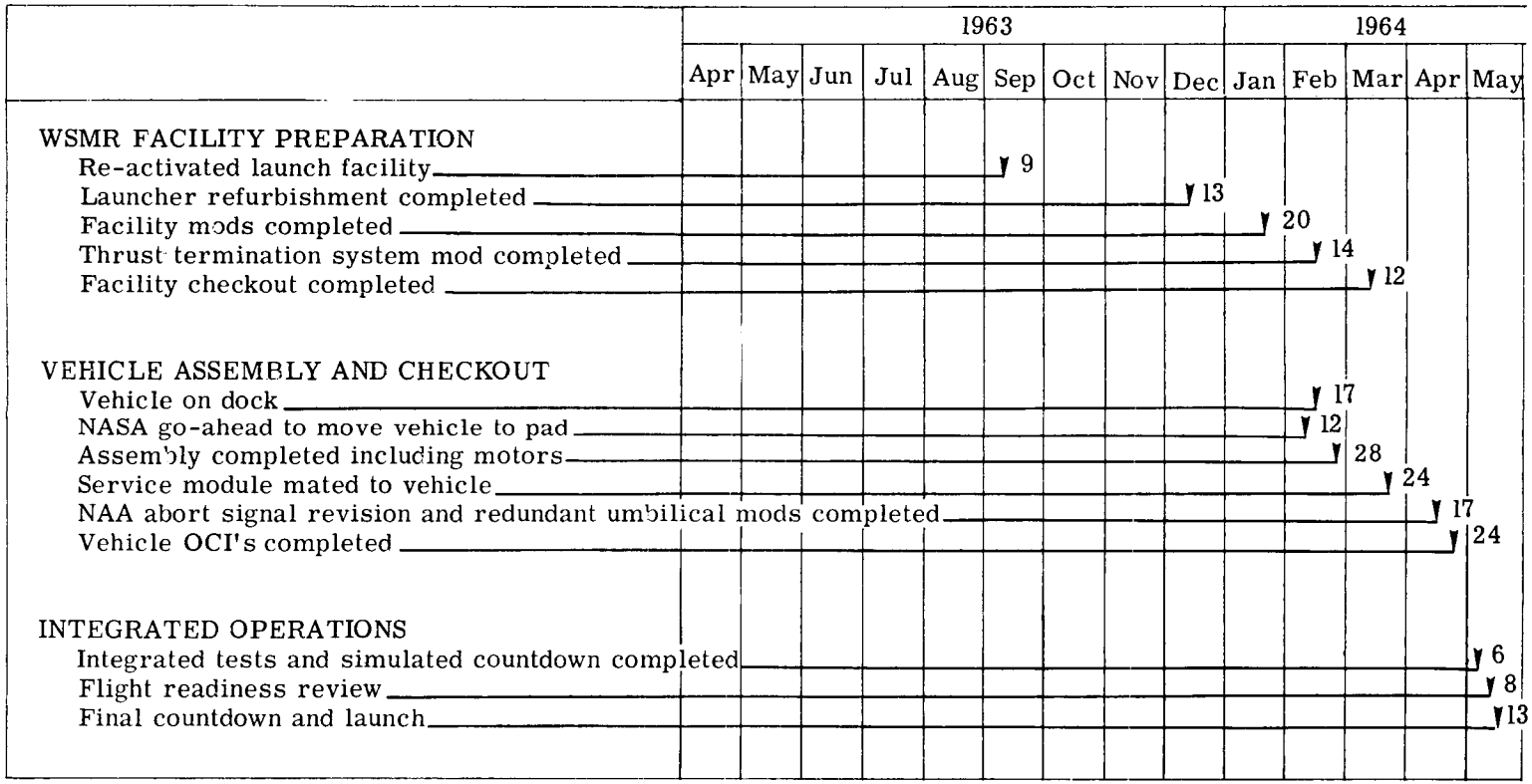

(b) WSMR facility preparation - Vehicle assembly and checkout - Integrated operations.

Figure 5.1.1-1. - Concluded.

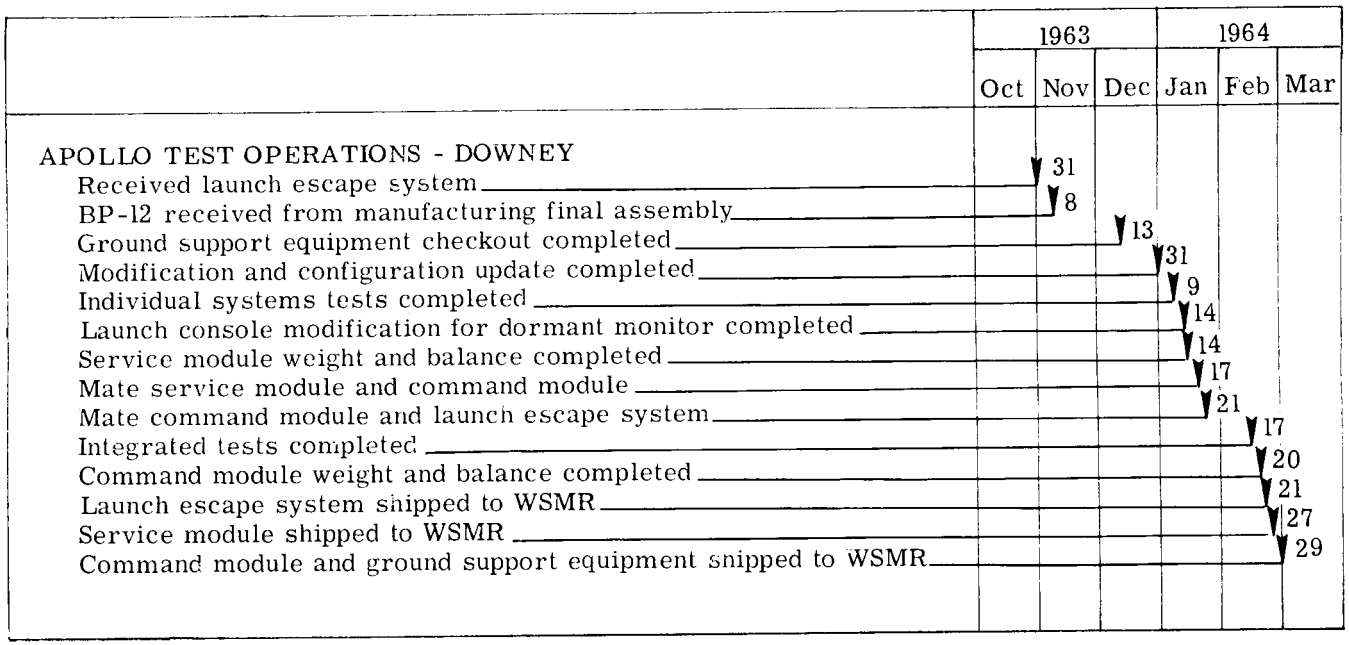

(a) Apollo test operations - Downey.

Figure 5.1.1-2. - Boilerplate 12 prelaunch milestones.

		Elapsed time in hours	1964 JAN 24	31	FEB 7	14	21	28	MAR 6	13	20	27	APR 3	10	17	24	MAY 1	8	15
FACILITY OCI'S																			
85108 - Blockhouse console		3:45	●	●															
85115 - Equipment rack	(2 times)	10:15	●					●											
85121 - Electrical distribution	(2 times)	17:05	●	●				●			●				●				
85110 - Pneumatic tubing installation		4:00		●															
86103 - Launcher positioning system	Run concurrent	1:10		●															
86104 - Launcher position indicator system	Run concurrent																		
86105 - Umbilical mast and support arms		:55		●															
85122 - Thrust termination console	(3 times)	1:52				●		●											
86112 - Integrated launcher		3:09							●										
VEHICLE OCI'S																			
82011 - Recruit motor assembly		8:00	●																
82014 - Recruit motor installation		6:30					●												
82017 - Algol motor assembly		4:00					●												
82018 - Algol motor installation		1:35						●											
85106 - Tie-down kit, vehicle		1:00						●											
85119 - Air conditioning system installation & checkout		3:00						●											
86604 - Support arm rigging		1:30						●											
86605 - Vehicle alinement		8:30						●	●										
86606 - Platform, destruct charge installation		5:00						●											
82016 - Algol igniter/squib check		5:20							●									●	
83208 - Primacord installation		3:00							●									●	
86008 - Vehicle electrical checkout		4:55							●					●		●			
81032 - Algol chamber pressure checkout		1:00								●									
85128 - Landlines instrumentation		4:00						●		●									
86204 - Ignition system resistance measurements	(2 times)	6:45								●	●			●					
86203 - Ignition system firing currents	(2 times)	4:49									●	●			●				
82013 - Recruit igniter/squib check		9:40											●					●	
83209 - Thrust termination system checkout		5:51														●			
83212 - Safe and arm pre-installation checkout		4:00																●	
83211 - Safe and arm pre-installation assembly		2:30																●	
82012 - Recruit igniter/squib installation		:30																	●
82015 - Algol igniter/squib installation		:05																	●

Figure 5.1.1-4.- Launch vehicle and associated facility pre-integrated tests.

[redacted]

5.2 Launch Operations

5.2.1 Launch procedures.- The planned launch countdown for Apollo Abort Mission A-001 consisted of a 2-day operation involving a 9-hour 10-minute precount on T-1 day and an 8-hour 15-minute final countdown. Bar charts indicating the scope and planned and actual times for the precount and countdown activities are shown in figures 5.2.1-1 and 5.2.1-2, respectively.

Actual T-1 day precount operations were initiated at 10:30 p.m. on Sunday, May 10, 1964, and were completed on schedule the following morning. The precount activities were conducted almost exactly as planned, and the times required for each major function were within a few minutes of the scheduled times. Only two significant problems were encountered during the precount. An intermittent return signal was experienced on the B system C-band beacon because the FPS-16 tracking radars were operated at 75-percent power instead of the normal 10 to 25 percent required for ground testing. In addition, the simulated mission was held up momentarily at T-2 minutes when the telemetry ground station reported loss of C-band beacon interrogation. This condition resulted because the FPS-16 radar operator secured the radars at T-2 minutes instead of T+2 minutes. Both of the aforementioned problems were recognized and resolved in time to preclude any slippage in the operation.

Countdown was started on May 11, 1964, at 9:45 p.m. and continued until T-55 minutes at 5:05 a.m. the following morning when a hold was called because of unfavorable wind conditions. The countdown operation was terminated at 6:50 a.m. m.s.t., when it became obvious that wind and visibility conditions were not improving. The initial portion of the countdown proceeded at a faster rate than anticipated and, by 11:45 p.m., the operation was approximately 45 minutes ahead of the count. The additional time was expended in replacing a safe and arm unit of the launch-vehicle thrust-termination subsystem which had malfunctioned during the system checks. No further problems were encountered prior to termination of the countdown operation.

Following termination of the countdown on May 12, the primacord of the launch-vehicle thrust-termination subsystem was disconnected and the launch-escape subsystem motors of the spacecraft were dearmed and safed. Covers were reinstalled on the exposed instrumentation components and the hatch of the command module was removed to provide access for securing the batteries. The resulting configuration made it possible to shorten the final countdown for the succeeding operation to 6 hours 40 minutes.

[redacted]

At 11:20 p.m. on May 12, 1964, the final countdown was again started. All operations proceeded according to schedule except for replacing the launch vehicle safe and arm unit which had been installed the previous night. This component indicated an excessive current demand during arming checks and was replaced and checked out without imposing a delay on the operation. The remaining portion of the countdown was completed without incident and the test vehicle consisting of the Little Joe II launch vehicle and the Apollo boilerplate 12 was successfully launched at 5:59:59.717 a.m. m.s.t. on May 13, 1964.

5.2.2 Launch pad damage assessment.- The damage to the launcher consisted of charring of the elevation screw jack boots, missing transite from one area of the X-frame, and normal damage to the expendable wiring. Spalling of pad firebrick covered a larger area than was experienced during Little Joe II Qualification Test Vehicle (QTV) test firing, but was not as severe.

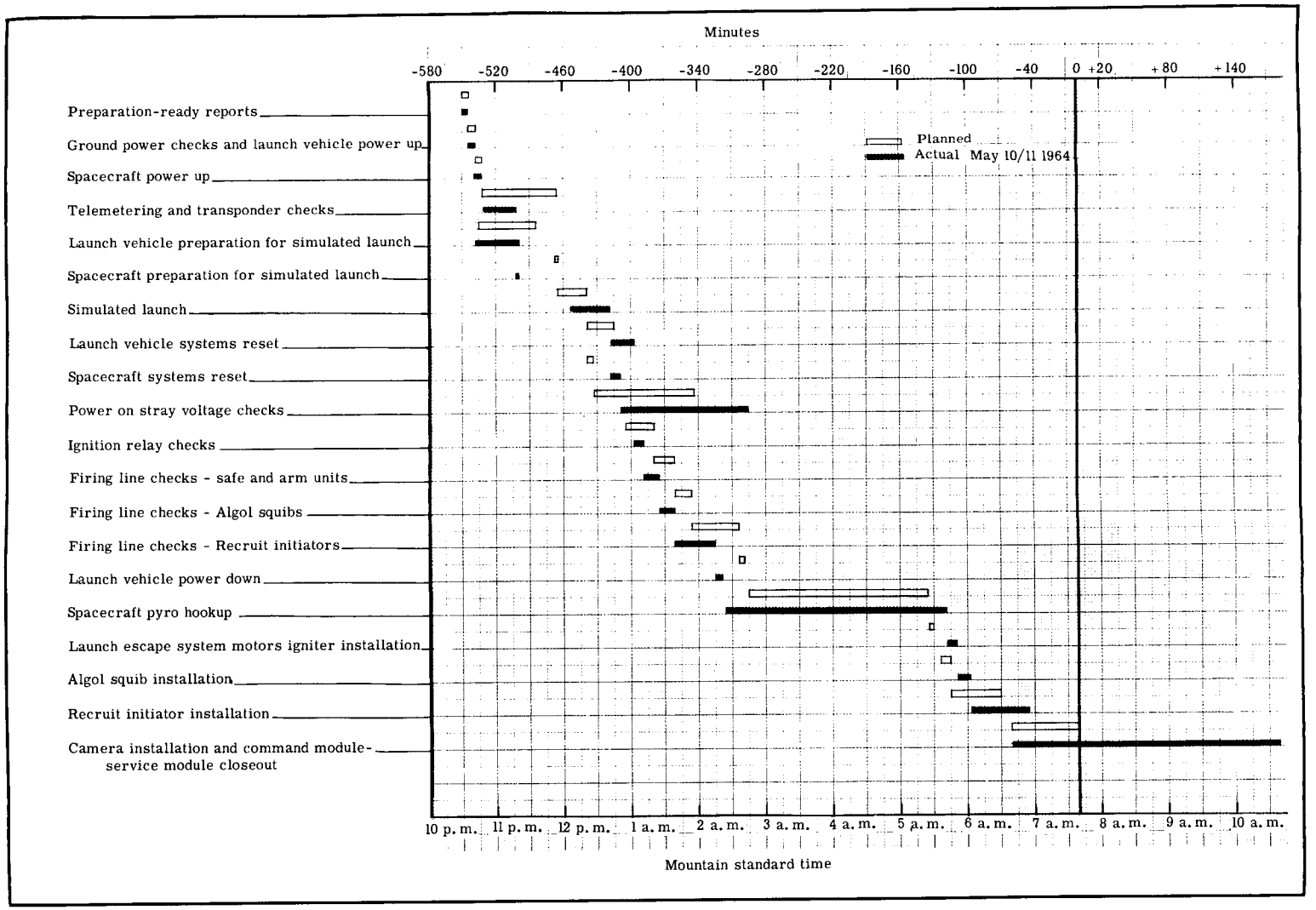

Figure 5.2.1-1.- Pre-count for boilerplate 12.

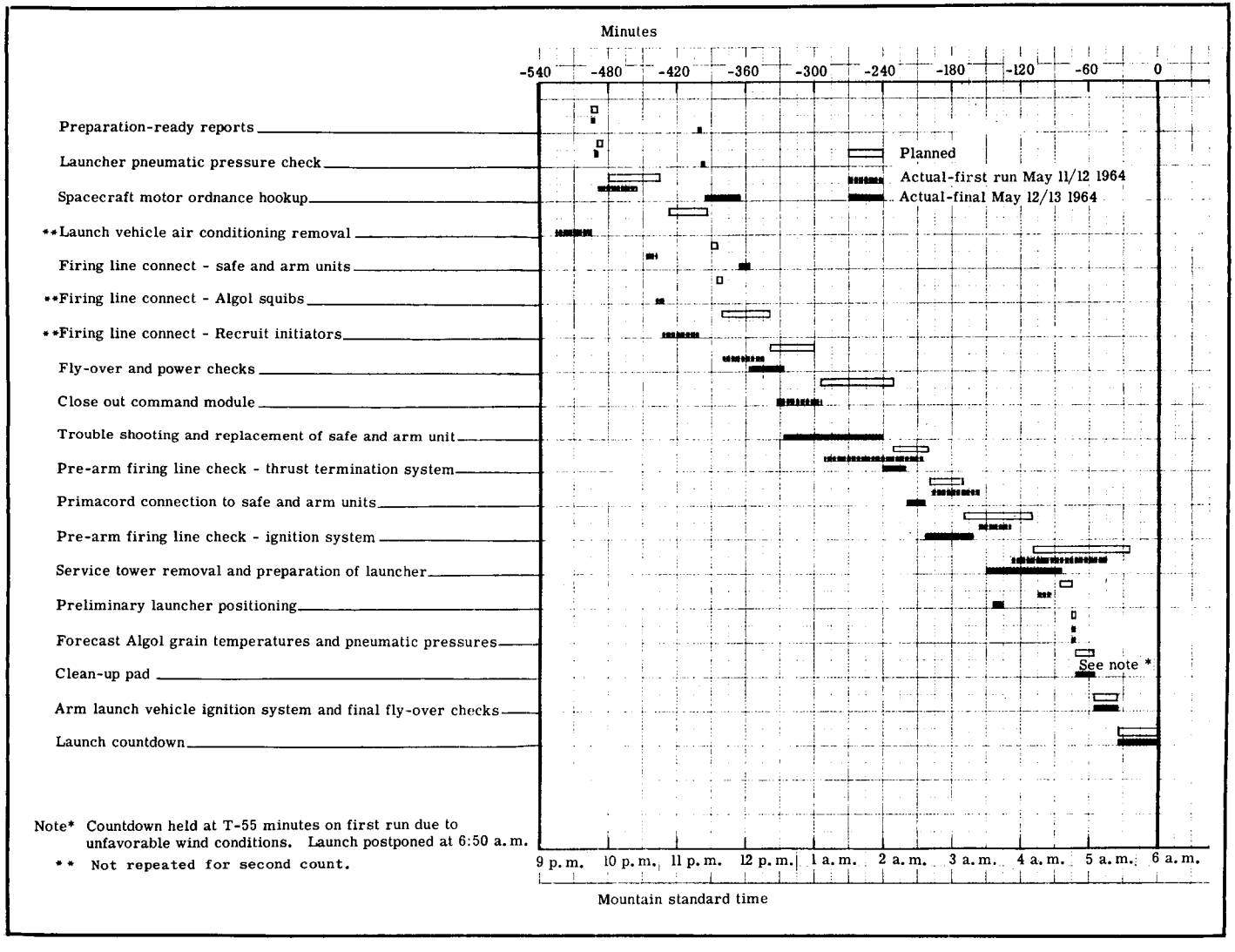

Note* Countdown held at T-55 minutes on first run due to unfavorable wind conditions. Launch postponed at 6:50 a.m.

** Not repeated for second count.

Figure 5.2.1-2.- Final countdown for boilerplate 12.

[redacted]

5.3 Data and Optical Instrumentation Coverage

The White Sands Missile Range provided range instrumentation and data reduction support for the Apollo boilerplate 12 mission. Radar, telemetry, meteorological, attitude, position, and geodetic data were satisfactory on this mission.

5.3.1 Optical instrumentation data.- Table 5.3.1-1 is a compilation of all optical instrumentation systems used to obtain optical data on the Apollo boilerplate 12 mission. Optical instrumentation station locations are shown in figure 5.3.1-1.

Four cameras located circumferentially from the launch pad (clock cameras) provided engineering sequential data in the event that a vehicle abnormality occurred during the initial 200 feet of flight. Four fixed cameras provided accurate position, attitude, and derivative data in the event that a vehicle abnormality occurred during the initial 700 feet of flight. Data reduction from these cameras was not requested because no vehicle abnormalities occurred during the flight. Table 5.3.1-1 lists pertinent data provided by these cameras.

Fourteen IGOR and telescope cameras provided attitude and events data throughout the flight. The following table itemized the attitude data received from the range.

Time coverage, sec	Objects tracked	Stations used	Remarks
0.333 to 28.333	Total vehicle	T-2, T-9, T-151, T-152, T-153, T-154, T-173, T-191, and T-198	An average of seven stations were used for attitude reduction during this period.

Nineteen cinetheodolite and Contraves camera provided position and derivative data throughout the flight. Certain cameras were assigned to track each stage throughout the flight. The table on the following page itemizes the coverage obtained for position and derivative data.

[redacted]

Time coverage, sec	Objects tracked	Stations used	Remarks	Frames/sec
0.033 to 349.283	Command module	G-80, G-81, G-82, G-106, G-107, G-108, G-109 G-110, G-154	An average of five stations were used for reduction during this period.	20
35.283 to 111.683	LES	G-101 and G-102	Two-station reduction	20
0.333 to destruct	Launch vehicle	G-81 and G-110	Two-station reduction	20

Table 5.3.1-1 lists optical coverage provided by the IGOR, telescope, cinetheodolite, and Contraves cameras.

Three cameras with their associated equipment were flown on board Apollo boilerplate 12. Manned Spacecraft Center, Houston, processed the only roll of film that was recovered from the flight. Coverage details on these cameras are listed in table 5.3.1-2.

The event data as recorded on film by the IGOR and telescope cameras are shown in table 5.3.1-3.

The telemetry station locations and the data handling time histories are shown in figures 5.3.1-2 and 5.3.1-3, respectively.

TABLE 5.3.1-1.- OPTICAL COVERAGE

Station	Film	Frame rate, per sec	Focal length	Object tracked	Time coverage, sec	Quality		Remarks
						Image	Film	
0199[a]	Color	500	6 in.	Fixed on launcher	0 to 1.131	Good	Good	Covered 10 to 200 ft of flight
0499[a]	Color	500	6 in.	Fixed on launcher	0 to 1.283	Good	Good	Covered 10 to 200 ft of flight
0799[a]	Color	500	6 in.	Fixed on launcher	0 to 1.242	Good	Good	Covered 10 to 200 ft of flight
1[illegible]9[illegible][a]	Color	1,000	6 in.	Fixed on launcher	0 to 1.421	Good	Good	Covered 10 to 200 ft of flight
F-[illegible]195	B and W	60	80 mm	Fixed on launcher	0 to 3.183	Good	Good	Covered 0 to 700 ft of flight. (70 mm film)
F-[illegible]196	B and W	60	80 mm	Fixed on launcher	0 to 3.183	Good	Good	Covered 0 to 700 ft of flight. (70 mm film)
F-1197	B and W	60	80 mm	Fixed on launcher	0 to 3.277	Good	Good	Covered 0 to 700 ft of flight. (70 mm film)
F-1198	B and W	60	80 mm	Fixed on launcher	0 to 3.476	Good	Good	Covered 0 to 700 ft of flight. (70 mm film)
T-7	B and W	30	80 in.	Command module	0 to 160.283	Blurred	Dark	
T-9	B and W	30	80 in.	Command module	2.759 to 350.647	Good	Hazy	
T-151, T-255	Color	30	48 in.	Command module	0 to 349.876	Good	Good to fair	
T-151, T-255	B and W	60	60 in.	Command module	0 to 286.083	Good	Light	

TABLE 5.3.1-1. - OPTICAL COVERAGE - Continued

Station	Film	Frame rate, per sec	Focal length	Object tracked	Time coverage, sec	Quality		Remarks
						Image	Film	
T-153, T-226	Color	250	24 in.	Command module	38.283 to 47.283	Not too clear	Good	
T-153, T-226	B and W	30	24 in.	Command module		Very good	Very good	No timing on film
T-153, T-226	B and W	30	70 in.	Command module	0 to 349.683	Out of focus	Good	Poor timing on film
T-154	B and W	30	96 in.	Command module	0 to 322.783	Out of focus	Fair	
T-173, T-156	Color	250	48 in.	Command module	42.283 to 47.283	Good	Good	
T-173, T-156	Color	30	96 in.	Command module	0 to 349.895	Very good	Very good	
T-191, F-212	B and W	30	109 in.	Command module	0 to 349.880	Good	Good	
T-197	B and W	30	180 in.	Command module	0 to 202.083	In and out of focus	Fair	70 mm film
T-193	Color	30	96 in.	Command module	0 to 147.783	Very good	Very good	
T-198	Color	30	24 in.	Command module		Good	Good	No events
T-2, T-220	B and W	30	80 in.	LES	0 to 103.346	Fair	Light	
T-126	Color	90	24 in.	LES	0 to 56.283	Fair	Poor	
T-126	Color	250	60 in.	LES		Good	Good	Timing erratic
T-128	B and W	90	24 in.	LES	0 to 347.283	Good	Very good	

TABLE 5.3.1-1.- OPTICAL COVERAGE - Continued

Station	Film	Frame rate, per sec	Focal length	Object tracked	Time coverage, sec	Quality		Remarks
						Image	Film	
T-128	B and W	250	60 in.	LES	0 to 47.283	Good	Good to poor	
T-127, T-254	Color	90	48 in.	Launch vehicle		Good	Good	Timing erratic
T-127, T-254	Color	250	48 in.	Launch vehicle	0 to 31.573	Good	Good	Poor tracking
T-155	B and W	250	24 in.	Launch vehicle	0 to 81.283	Good	Dark	
T-155	B and W	90	48 in.	Launch vehicle	0 to 328.883	Good	Very good	
T-152, T-6	Color	30	48 in.	Parachutes	0 to 349.543	Good	Good	Small image
T-152, T-6	B and W	250	80 in.	Parachutes	41.683 to 319.283	Good	Fair to good	
G-19	B and W	5	47 in.	Command module	0 to 41.30	Blurred	Fair	
G-26	B and W	5	100 cm	Command module	0 to 313.30	Good	Fair	
G-30	B and W	5	47 in.	Command module	Launch to 284.30	Blurred	Fair	
G-32	B and W	5	47 in.	Command module	Launch to 157.30	Blurred	Fair	
G-80	B and W	20	60 in.	Command module	Launch to 303.30	Fair	Light	
G-82	B and W	20	60 in.	Command module	Launch to 317.75	Faint-poor	Dark	

TABLE 5.3.1-1. - OPTICAL COVERAGE - Concluded

Station	Film	Frame rate, per sec	Focal length	Object tracked	Time coverage, sec	Quality		Remarks
						Image	Film	
G-106	B and W	20	60 in.	Command module	Launch to 228.10	Fair	Fair	
G-107	B and W	20	60 in.	Command module	Launch to 344.05	Fair	Light	
G-108	B and W	20	60 in.	Command module	Launch to 349.70	Fair	Fair	
G-109	B and W	20	60 in.	Command module	Launch to 350.00	Fair	Faint to Dark	
G-110	B and W	20	60 in.	Launch vehicle and command module	Launch to 350.05	Fair	Good	
G-81	B and W	20	60 in.	Launch vehicle	0 to 124.20	Faint	Fair	
G-111	B and W	20	60 in.	Launch vehicle	0 to 124.50	Fair	Fair	Dials slipped
G-83	B and W	20	60 in.	LES	0 to 29.15	Fair	Very dark	
G-101	Color	20	60 in.	LES	0 to 318.683	Good	Good	
G-102	B and W	30	60 in.	LES	0 to 111.685	Blurred	Fair	
G-154	B and W	20	60 in.	LES	0 to 130.00	Faint	Fair	
G-112	B and W	20	60 in.					No timing

a = Clock cameras
F = Fixed cameras
T = IGOR and telescope cameras
G = Contraves and cinetheodolite cameras

TABLE 5.3.1-2.- COVERAGE DETAILS FROM ONBOARD CAMERAS

Camera	Camera location	Speed, frames per sec	Film	Coverage period, sec	Coverage	Remarks
16-mm Milliken DBM-5A	LES tower	200	B and W	0 to 80	Entire top surface of command module including the tower leg attach points.	Camera did not expose any film because the film was not engaged on the take-up sprockets
16-mm Milliken DBM-5A	Command module egress hatch	100	Color	0 to 160	LES structure and engine exhaust nozzles.	300 feet of film exposed. Film quality deteriorated as the flight progressed.
16-mm Milliken DBM-5A	Service module	200	B and W	0 to 80	Lower heat shield	Camera was not recovered; therefore, no data are available

TABLE 5.3.1-3.- OPTICAL EVENT DATA

Event	Time, sec	Camera Station	Focal length	Film
Launch vehicle ignition	-0.127±0.001	T-199	6 in.	Color
Recruit motors burnout	1.896±0.005	T-126	24 in.	Color
Launch vehicle blowup	28.428±0.017	T-197	180 in.	B and W
Pitch-control motor ignition	28.510±0.016	T-7	96 in.	B and W
LES motor ignition	28.560±0.009	T-151, T-255	60 in.	B and W
Pitch-control motor burnout	29.463±0.005	T-126	24 in.	Color
LES motor begins gradual burnout	35.732±0.019	T-191, F-212	109 in.	B and W
Jettison-motor ignition	44.157±0.012	T-198	96 in.	Color
CM-LES separation	44.157±0.012	T-198	96 in.	Color
Apex heat shield jettison	46.365±0.002	T-173, T-156	48 in.	Color
Jettison-motor begins gradual burnout	45.397±0.002	T-153, T-226	24 in.	Color
Drogue parachute deployment	46.330±0.011	T-198	96 in.	Color
Drogue parachute fully inflated	48.052±0.002	T-153, T-226	24 in.	Color
Piece breaks off module	60.549±0.002	T-152, T-6	80 in.	B and W
Second piece breaks off module	89.662±0.002	T-152, T-6	80 in.	B and W
LES impact	111.696±0.007	T-128	24 in.	B and W

[redacted]

TABLE 5.3.1-3.- OPTICAL EVENT DATA - Concluded

Event	Time, sec	Camera station	Focal length	Film
Pilot parachute deployment	112.624±0.017	T-197	180 in.	B and W
Main parachute deployment	113.158±0.011	T-198	96 in.	Color
Shroud lines break on one parachute	115.469±0.012	T-198	96 in.	Color
First parachute fully inflated	121.182±0.010	T-198	96 in.	Color
Launch vehicle impacts	124.483±0.011	T-155	48 in.	B and W
Second parachute fully inflated	127.827±0.013	T-198	96 in.	Color

[redacted]

[redacted]

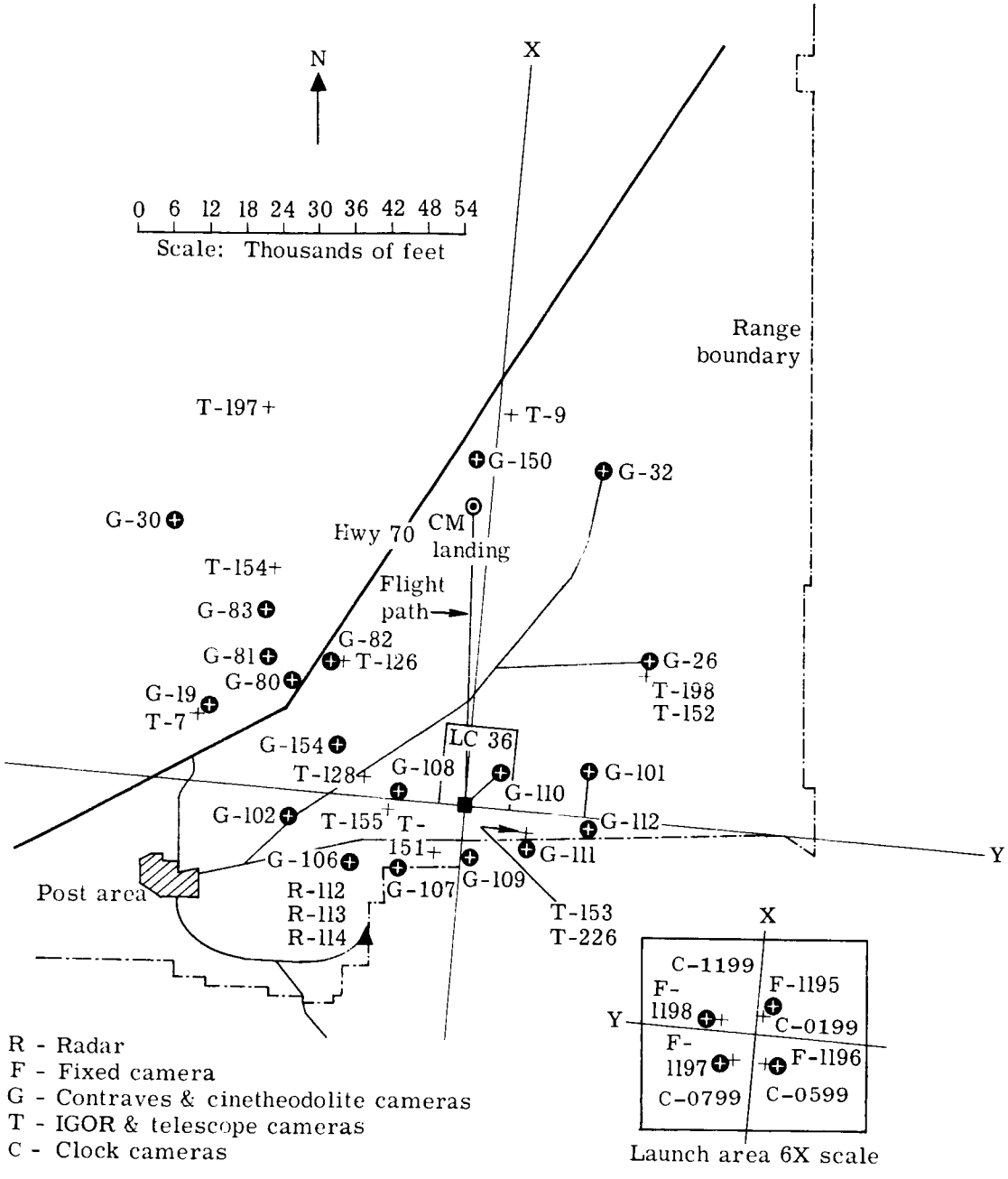

Figure 5.3.1-1.- Camera and radar locations for boilerplate 12.

[redacted]

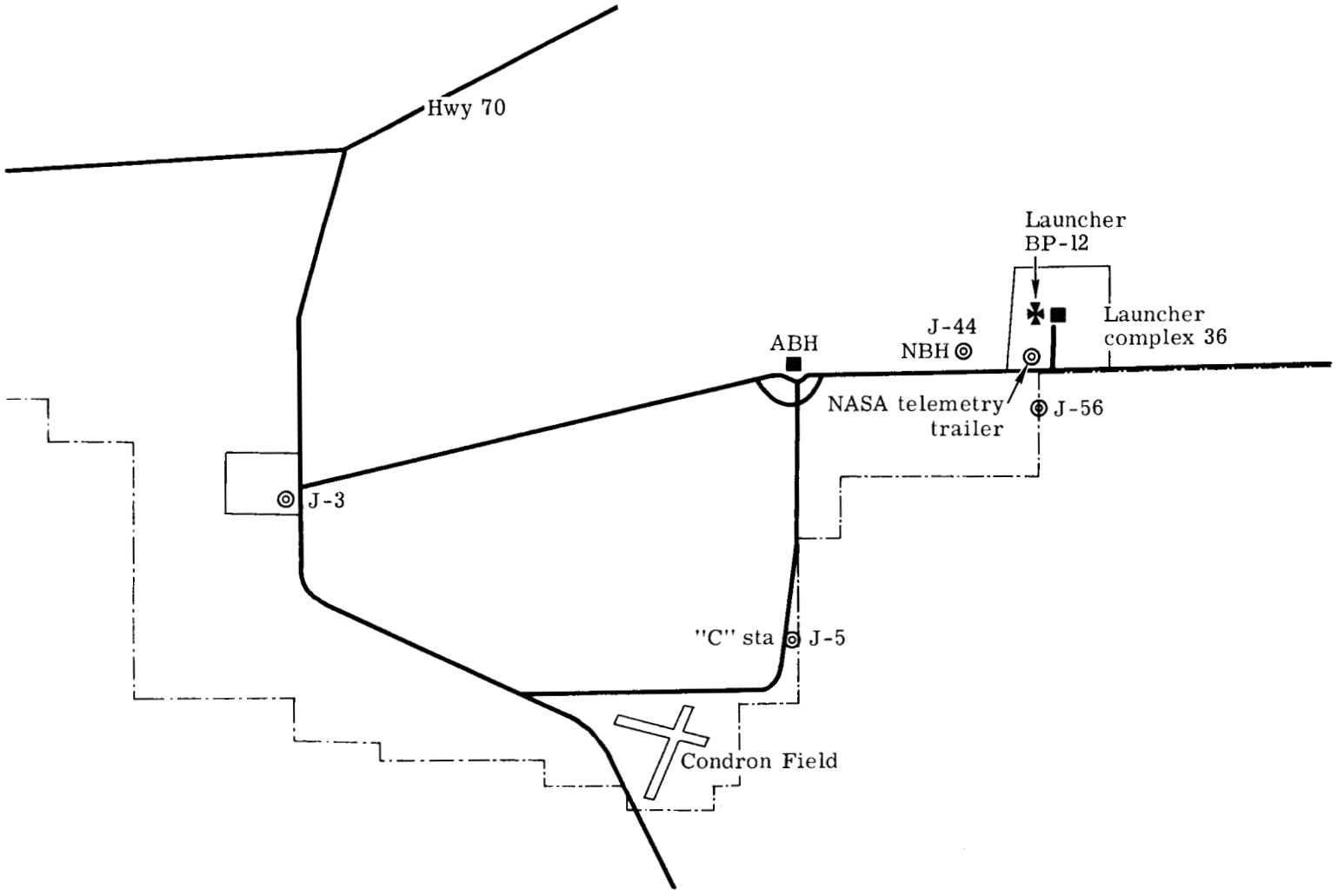

Figure 5.3.1-2.- Telemetry station locations for boilerplate 12.

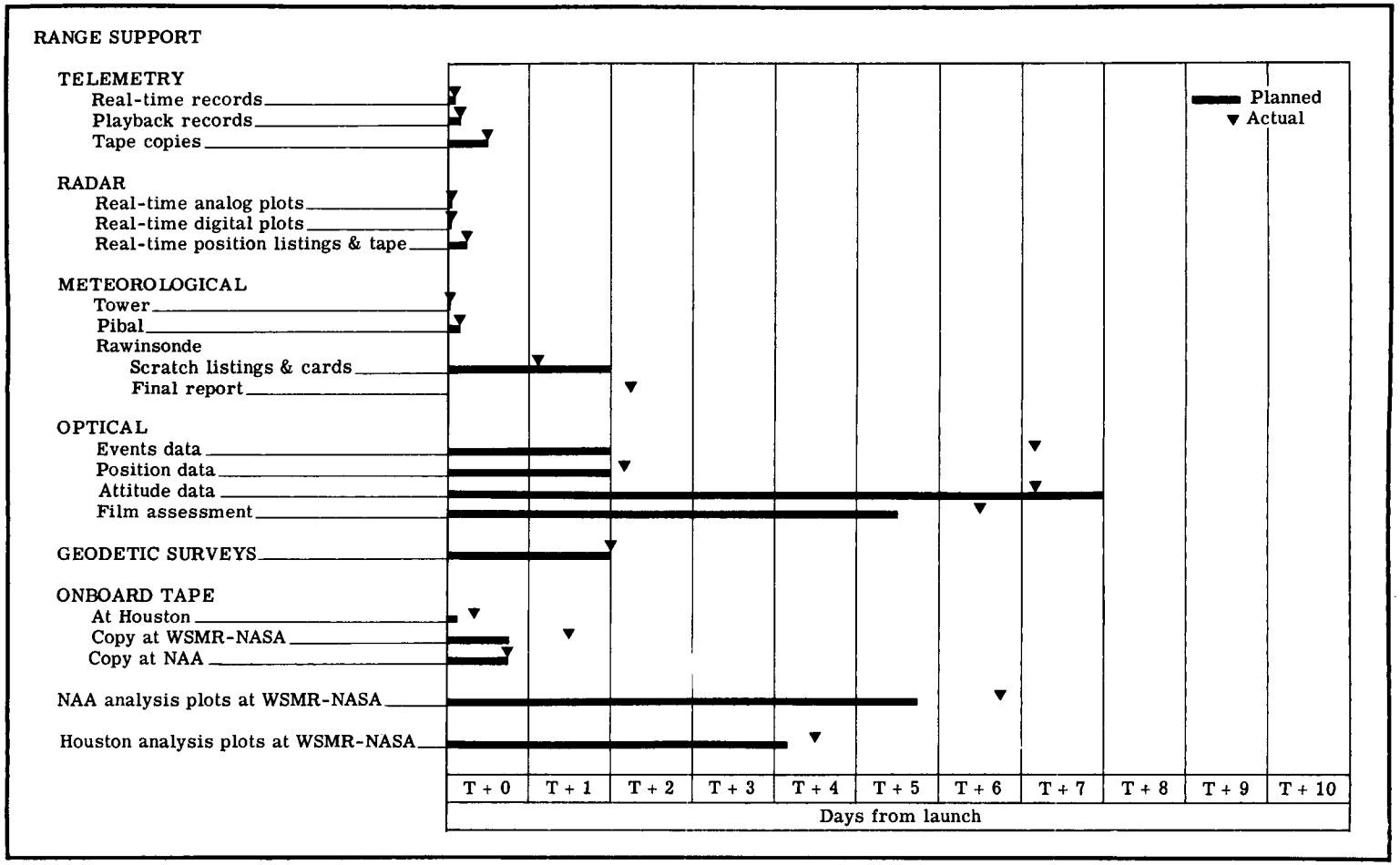

Figure 5.3.1-3.- Data handling time history.

[redacted]

5.3.2 Meteorological data.- Three systems were used to provide meteorological data for support of Apollo boilerplate 12 mission.

These data consisted of scratch listing, final reports, and IBM cards containing the following information:

1. Wind direction, degrees from true north
2. Wind velocity, knots
3. Temperature, degrees Centigrade
4. Pressure, millibars
5. Altitude, feet
6. Relative humidity, percent
7. Index of refraction
8. Density, grams/cubic meter
9. Density, slugs/foot squared-second

The following table lists pertinent information on the meteorological support provided by WSMR.

System	Location	Release times, a.m.	Measurements	Altitude above surface, ft
Rawinsonde	Desert Site Small Missile Range	2:25 4:00 6:00 7:30 5:40	Wind, temperature, pressure, and relative humidity	0 to 40,000
		Time read, a.m.		
PIBAL	Launch complex 36	4:30 5:15 6:07	Wind components against altitude	0 to 7,000
500-foot tower	Launch complex 36	4:00 4:45 5:35 6:00	Wind components against altitude	0,25,75,125, 175,225,300, 400,and 500

[redacted]

5.3.3 Geodetic data.- In the White Sands Transverse Mercator System (WSTM): X is measured in feet along a line passing through the point in question which crosses the central meridian, longitude 160°20'00.000" W., at a right angle and increases positively to the east.

Y is measured along the central meridian, longitude 106°20'00.00" W., increasing positively to the north.

H is measured in feet along a radius of the earth at the point in question, above mean sea level, 1929 datum, positive upwards.

The origin of this system is the intersection of latitude 32°10'00.00" N. and longitude 106°20'00.000" N. This origin has a value of X-500,000.00 feet and Y-100,000.00 feet.

In the White Sands Cartesian System (WSCS): E is measured in feet in the plane along a line passing through the point in question, crossing the north-south axis at a right angle, and increasing positively eastward.

N is measured in feet in the plane along a line passing through the point in question, crossing the east-west axis at a right angle, and increasing positively northward.

Z is measured positively upward from the normal to the plane.

The origin of this is the intersection of latitude 33°05'00.000" N. and longitude 106°20'00.000" W. This origin has a value of E-500,000.00 feet and N-500,000.00 feet. At this point, the plane is tangent to Clarke's spheroid of 1866 at sea level.

[redacted]

Geodetic surveys of various components of BP-12 are listed in the following table:

IMPACT FOR APOLLO MISSION A-001

Component	WSTM Coordinates, ft	WSCS Coordinates, ft
Launch-escape subsystem	X = 504,862 Y = 218,844 H = 3,984	E = 504,863 N = 285,303 Z = 2,878
Command module	X = 503,997 Y = 213,781 H = 3,985	E = 503,998 N = 280,239 Z = 2,827
Drogue parachute	X = 505,307 Y = 217,115 H = 3,988	E = 505,308 N = 283,574 Z = 2,864
Service module	X = 502,421 Y = 201,950 H = 4,009	E = 502,421 N = 268,406 Z = 2,722
Launch vehicle	X = 502,854 Y = 202,575 H = 4,011	E = 502,855 N = 269,031 Z = 2,731
Red box part BL 13158-122 REV-A	X = 502,656 Y = 203,024	
Skin section separation point	X = 503,996 Y = 201,458	
Range safety command battery; propellant	X = 503,799 Y = 200,997	

[redacted]

5.4 Range Operations

5.4.1 Communications.- The range provided the following communications services:

Range Command-Ready-Hold Network. This is the formal communications channel between range users and range operating personnel for transmitting range readiness and countdown information.

Range Telemetry Network. This is the intercommunications network linking all range telemetry stations with the telemetry systems controller at the range control station. Recording of prelaunch calibrations and telemetry checkouts were coordinated over this network.

Missile Flight Surveillance Network. This network included intercommunications network in the blockhouse, the real-time-data system display room, and the FRW-2 transmitter building from which the abort command was transmitted. Checkout and arming of the thrust-termination system, checks of the plus time clocks at each of the network terminations, and initiation of the back-up abort command were coordinated over this network.

Flight Dynamics Officer's (FIDO) Network. This network was installed solely for use by NASA. Intercommunication stations on this network were provided for the flight dynamics officer in the real-time-data system display room, the NASA prelaunch computation program manager at the computer for the NASA visual observer atop the Vehicle Assembly Building, for the flight dynamics meteorological coordinator (METRO), the NASA operations director, and the NASA range support coordinators in the blockhouse. Launcher pointing order, real-time-data system performance, METRO and FIDO go-no-go status, and meteorological conditions were discussed over this network. Inflight events, as observed by the visual observer, were announced on this network.

Thrust-Termination Command Circuit. This circuit provided the means for the flight dynamics officer in the real-time-data system display room to originate the thrust termination command transmitted by FRW-2 command transmitter.

Voice Recorder. A tape recording of channels 1 and 3 of the launch complex intercommunication system, the Range-Command-Ready-Hold Network, and the NASA flight dynamics officer's network was made on a multichannel recorder in the blockhouse.

[redacted]

An emergency maintenance and repair team was on duty in the blockhouse to repair system malfunctions and answer questions pertaining to range communications facilities.

All communications systems performed satisfactorily.

5.4.2 Radio frequency radiation control.- Control of electromagnetic energy radiated on the launch pad was maintained from approximately T-310 minutes during countdown until impact of the spacecraft. High-powered radars on the southern portion of the missile range were requested not to radiate in the direction of the NASA launch complex without the permission of NASA. No violations of the radio frequency radiation control were detected.

5.4.3 Closed-loop television.- Three closed-loop television systems were used to provide three views of the launch pad and flight vehicle. One camera was located southwest of the launcher for general surveillance of the launch pad, service structure, and flight vehicle. A remote control unit for this camera was provided on the test director's console for adjustment while viewing the monitor set. The second camera provided a similar view but from a different vantage point. The third camera was located just north of the Vehicle Assembly Building. This camera was operated manually to track the command module from launch to impact. The video signal from the third camera was transmitted by narrow beam microwave link to the blockhouse. A monitor set for each of the three cameras was located on the east wall of the operations room in the blockhouse in plain view of personnel at their duty stations.

One of the pad systems was inoperative at launch; otherwise the television system performed satisfactorily. The system, which displayed the vehicle in flight, was especially useful for observing lift-off and inflight events. Some difficulty was experienced by the tracker because smoke obscured the vehicle during some of the flight. A location to east or west, rather than behind the launcher, will be recommended for the next mission. This display and the verbal reports by the visual observer, as heard over the NASA flight dynamic officer's network, were used by the NASA range support coordinator to generate event reports on the Range-Command-Ready-Hold Network.

5.4.4 Timing.- A functional block diagram of the WSMR timing system is shown in figure 5.4-1. The lift-off signal generated after a 4-inch motion of the launch vehicle caused two events at the range timing generator — a lift-off tone is turned on, and the instantaneous value of the elapsed time codes is read out and displayed. The lift-off tone from the timing generator is sent to the various plus-time clocks, to other WSMR systems, and to each of the supporting Contrave cinetheodolites

[redacted]

to reset the frame counters automatically so that the Contrave data film may be readily correlated. Data from other WSMR systems are normally correlated by comparison of the time of occurrence of a particular event, as shown by the range timing signal recorded with the event, with the value of the range time codes recorded by the time code readout unit at lift-off.

The timing system performed satisfactorily. The value of the time recorded on the time code readout at lift-off was:

134 days 12 hours 59 minutes 59.717 seconds IRIG (G.m.t.) time
5 hours 59 minutes 59.717 seconds m.s.t.
46,799.717 seconds WSMR G-2 time
(an actual reading of 0.716905 second was rounded off to 0.717 second)

5.4.5 Meteorological.- Weather forecasting services and data from three meteorological data-gathering systems were utilized during countdown. Meteorological data on-surface, near-surface, and upper atmospheric conditions were obtained from Rawinsonde balloons released from Desert Site at 2:25 a.m., 4:00 a.m., 6:00 a.m., and 7:30 a.m., from the Small Missile Range at 5:40 a.m.; from four pilot balloons released in the launch area at 4:30 a.m., 5:40 a.m., and 6:07 a.m. m.s.t.; and from the 500-foot tower at the blockhouse at 4:00 a.m., 4:45 a.m., 5:35 a.m., and 6:00 a.m. The data tabulated in the field and telephoned to the computer for the Rawinsonde release at 4:00 a.m. were used in the real-time-data system program for inflight computation of dynamic pressure and Mach number. The same data supplemented with wind data from the pilot balloon released at 4:30 a.m. and from the tower reading at 4:45 a.m. were used in the final solution for launcher azimuth and elevation setting.

Final meteorological data from each of the Rawinsonde releases were received approximately 26 hours after launch.

Meteorological support was satisfactory.

5.4.6 Geodetics.- Location surveys of the launch-escape subsystem, command module, drogue parachute, service module, and launch vehicle were furnished 50 hours after launch. Data were supplied in the coordinate systems in azimuth and range from the launcher as described in section 5.3.

Performance was satisfactory.

5.4.7 Telescopes.- A detailed discussion of the telescope cinecamera coverage is included in section 5.3. Coverage generally was as requested.

[redacted]

5.4.8 Contrave cinetheodolites.- A detailed discussion of cinetheodolite coverage is included in section 5.3. Coverage was as requested. Because of the excellent parachute pictures on the boresight film from G101, copies of this film were requested by MSC-Houston.

5.4.9 Fixed cameras.- Data film was obtained from engineering sequential cameras and four position data cameras, as specified in section 5.3. Reduction of data from the position data cameras was not requested. Fixed camera coverage was satisfactory.

5.4.10 Telemetry.- Range telemetry support as set forth in section 5.3 was provided. Some delay in copying the range tapes was encountered because the ground station that was copying the tapes was required to support another range operation. Otherwise, telemetry support was satisfactory.

5.4.11 Radar.- The three C-station FPS-16 radars tracked the fly-by aircraft at T-30 minutes to verify the real-time-data system, and tracked the command module from launch to near impact.

Performance was satisfactory.

5.4.12 Missile flight surveillance office.- The WSMR missile flight surveillance office supported the mission by providing the FRW-2 command transmitter for checkout of the thrust-termination subsystem and for sending the inflight abort command. The flight dynamics officer transmitted the abort command at T+28.43 seconds (as recorded by way of range time at the transmitter) and immediately announced "abort" on the intercommunication network. On hearing the "abort" command, the operator at the transmitter manually transmitted the abort command as a back-up measure. The time recorded for this back-up abort transmission was T+29.17 seconds.

Performance was satisfactory.

5.4.13 Real-time-data system.- The Little Joe II real-time-data system consisted of the three FPS-16 radars at C-station; data links and timing to the radars and the 7094 computer in building 1512; the output digital displays and plots in the display room of building 1512; the meteorological data input systems.

The real-time-data system performed satisfactorily on the aircraft flyover at T-30 minutes and also on the mission. The abort command was initiated when Mach number, as indicated by the real-time-data system output, reached a value of 0.94. Preliminary analysis of optical position data showed excellent agreement between the real-time output and the postflight data as computed from optical tracking data after being compensated for the velocity error as described in section 4.1.1.

[redacted]

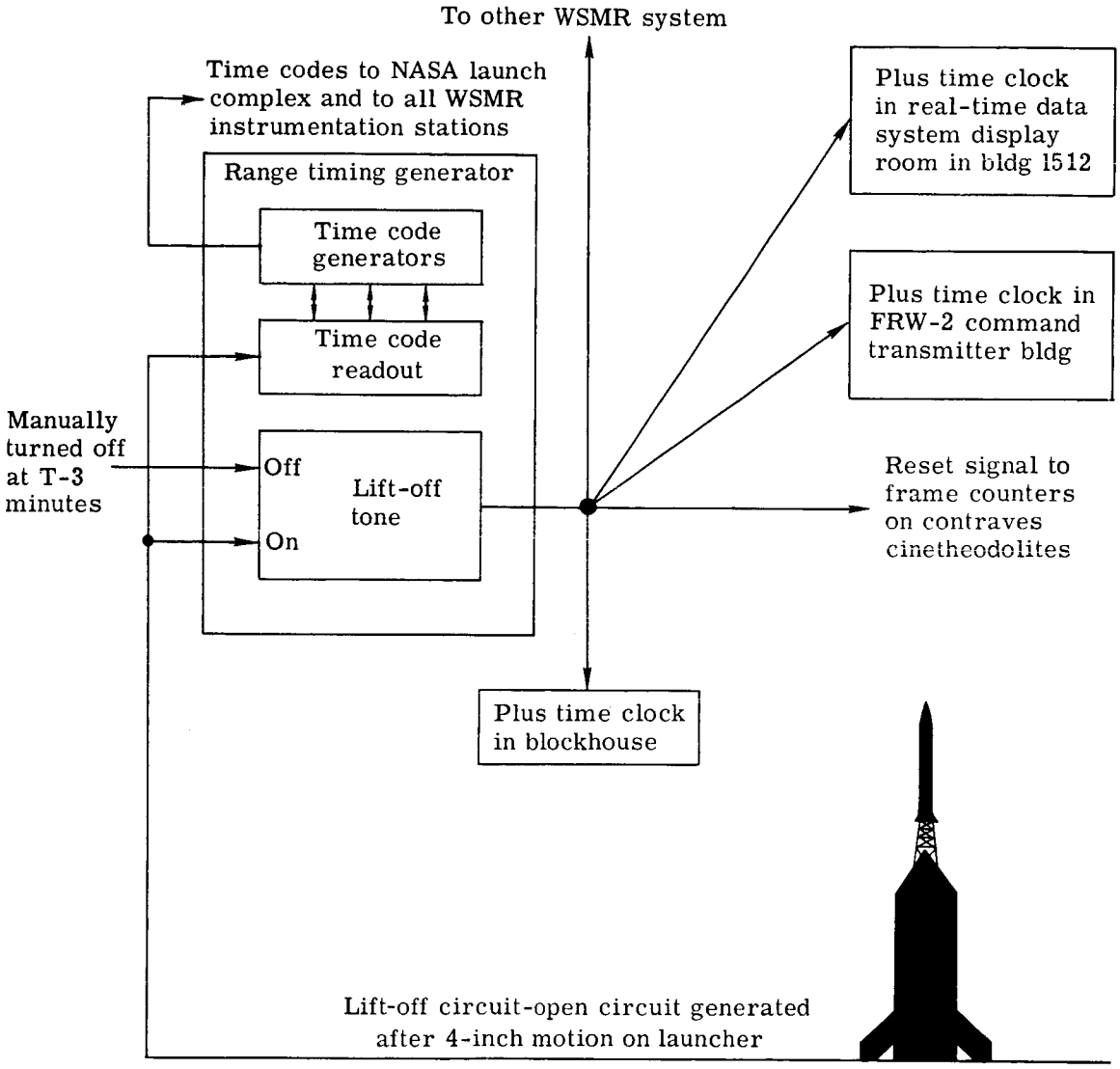

Figure 5.4.1-1. - Functional block diagram of WSMR timing system.

[redacted]

5.5 Recovery Operations

Recovery teams were established to provide for rapid location, inspection, and recovery of all flight hardware. The teams were prepositioned downrange to affort optimum utilization of time and equipment for the recovery operations.

5.5.1 Recovery teams and equipment.- The recovery force was composed of three recovery teams organized and equipped for downrange recovery operations. Prior to launch, the recovery teams were positioned in the vicinity of the expected landing and impact areas (fig. 5.5.1-1). These positions were selected based upon personnel safety, the latest wind and trajectory information available, and existing roads and trails on the range. Team no. 1 was assigned to the landing area of the command module, team no. 2 was assigned to the impact area of the launch-escape subsystem, and team no. 3 to the impact area of the launch vehicle.

A recovery helicopter was positioned downrange to direct the recovery vehicles to the landing areas. A photographic helicopter was on station to photograph the descent and landing of the command module, recovery team movements, and general landing and impact area scenes. The recovery teams consisted of personnel and equipment capable of making necessary on-scene inspections, evaluating and preserving scientific data, returning all recovered hardware, and conducting salvage operations in event of flight anomalies.

[redacted]

5.5.2 Command module recovery.- Upon inflation of the main parachutes, team no. 1 proceeded to the expected landing point of the command module and arrived on scene at T+10 minutes or about 4 minutes after command module landing. The command module landed in a relatively clear area and came to rest in an upright position at a slightly inclined angle on the edge of a small hummock approximately 18 inches high (figs. 5.5.1-2 to 5.5.1-4).

The two effective parachutes collapsed immediately after landing. The detached parachute landed approximately 100 yards southeast of the command module. Following general area photography and examination of pyrotechnic devices, recovery team personnel began a systematic inspection of the command module and parachutes. Close-up photographs of the glass samples were made prior to their removal and placement in protective containers. All heat-sensitive paint specimens were photographed and evaluated. The detached parachute was examined, photographed, and placed in a parachute bag. A sequence of detail photographs was then taken to indicate the probable position of the main parachute riser with respect to the command module at the time of riser failure. This position was reconstructed by matching the abrasions, scrape marks, and deformations on the command module with the associated paint deposits and breaks along the failed riser. This sequence of photographs is included in section 4.3.5.

The gyros were caged and the A and B bus powered down externally at T+45 minutes. The command module was entered through the side hatch at T+64 minutes. Following an inspection of apparent damage and complete photographic coverage of the command module interior, the onboard camera was powered down. The tape recorder and camera were removed at T+85 minutes and T+88 minutes, respectively. The camera was quite hot when removed, and the lens was coated with exhaust deposits. Both the tape recorder and the camera were immediately dispatched by helicopter to the Vehicle Assembly Building (VAB). At T+110 minutes, following the completion of postflight procedures and attaching lifting and tie-down hardware, the command module was raised and placed in the transportation dolly which was secured to the deck of the MM-1 balloon-tired Terracruiser (fig. 5.5.1-5). As the command module was raised, detail photographs of the heat shield were taken. Figure 5.5.1-6 shows a photograph of the command module landing imprint in the sand. Four hours 25 minutes after launch, the MM-1 vehicle with command module and escort vehicles proceeded to the VAB. The command module arrived at the VAB 5 hours 15 minutes after launch where it was off-loaded and placed in the pad adapter stand.

On-scene inspection of the command module revealed the following:

[redacted]

[redacted]

a. An approximate $\frac{3}{8}$-inch displacement of the aft heat shield in the -Z axis.

b. A layer of fiber glass in the -Z, -Y quandrant (fig. 5.5.1-7) torn from the aft heat shield of the command module. (Several pieces of this material were found by the recovery teams near Oboe site (fig. 5.5.1-1).

c. Evidence of riser rubbing on -Z, +Y quandrant of the conical surface of the command module.

d. Glass specimen no. 10 smeared by shroud line (matched with deposits on line).

e. Moisture beneath glass specimen numbers 10, 11, 12.

f. Evidence of highest temperature was observed on +Z axis (small sample, 1 in. by 2 in., of cork near the aft heat shield; conical surface parting line on +Z axis was removed for postflight analysis).

g. Very slight discoloration along -Z axis, moderate discoloration along +Y, -Z axis.

h. Exhaust deposits on egress cover.

i. Rub marks across egress cover matched marks on parachute riser.

j. Small sections of cord on C-band antennas and teflon on main antennas bulged outward.

k. Floor of command module deformed inward in some sections 8 to 10 inches with undulations on ±Z axis.

l. Main battery mount, rear rack rivets, failed, bottom of main battery damaged.

m. Top deck floor sections cracked circumferentially.

n. Damage to structure around several main parachute attach points.

o. Heat shield cracked and dented.

Team no. 2, using location assistance of the recovery helicopter, proceeded to the launch-escape subsystem immediately after impact, and arrived on scene at T+14 minutes or approximately 12 minutes after impact. After completion of the general area photography and an examination of the pyrotechnic devices, the onboard launch-escape subsystem camera was

[redacted]

located, placed in a special carrying bag, and dispatched to the VAB at T+34 minutes. The drogue parachute which landed approximately 400 yards from the launch-escape subsystem was located and retrieved at T+35 minutes. Team no. 2 completed its inspection, photography, and retrieval of all launch-escape subsystem hardware 3 hours 25 minutes after launch. All retrieved launch-escape subsystem hardware and the drogue parachute were returned to the VAB at T+4 hours.

The launch-escape subsystem broke apart at impact. The largest piece relatively intact was a 7-foot section of the motor case with nozzles and one tower leg attached. Figures 5.5.1-8 and 5.5.1-9 show the general condition of the launch-escape subsystem after impact.

5.5.3 Launch vehicle and service module recovery.- Upon impact of the service module and aft thrust bulkhead of the Little Joe II launch vehicle, team no. 3 proceeded toward the observed areas of impact and arrived on scene at T+18 and T+21 minutes, respectively. Very little damage was sustained by the service module which landed in an almost upright position; however, the service module camera was missing. A search of the area surrounding the service module did not yield the camera. A systematic search of the total impact area was then conducted in an effort to locate the remains of the camera. The camera was never located; however, two portions of the camera system were recovered. One section of the green camera cover support angle was found approximately $\frac{1}{2}$ mile east of the service module, and an orange camera mounting plate was found approximately 1 mile east of the service module. The search was terminated at T+36 hours. The service module was loaded and returned to the VAB at 10 hours 29 minutes after launch. Pieces of fiber glass from the service module pressure bulkhead were found over the entire launch vehicle and service module debris area. The heaviest accumulation, however, was near the service module.

The Little Joe II launch vehicle forebody and afterbody sections broke into many pieces at time of thrust termination. The rear thrust bulkhead of the launch vehicle landed intact with all Recruit motors and a short section of the Algol casing still attached. One fin was lost upon impact and lay on the ground a few feet away, and the remaining three fins were still attached. The fins showed a moderate coating of white combustion products toward the middle of the cord. All fin edge rivets had a cumbustion product coating on the inboard side. The nozzle of the Algol motor and the Recruit motors were in relatively good condition as was the thrust bulkhead. The heat protection material on the fin trailing edges showed some evidence of bubbling. Sections of Algol motor and propellant were found over the entire debris area. A section of the Algol motor cut by the thrust-termination charges and the top of the Algol motor were found approximately $\frac{1}{4}$ mile east of the rear bulkhead. A very heavy concentration of Little Joe II launch vehicle skin and support rings was found approximately 1 to 2 miles east of the rear bulkhead. Two large portions of the station 34.75 (web) bulkhead were found. This web exhibited heavy charring apparently from primacord propagation. No evidence was found of any unburned primacord. Smaller pieces of the launch vehicle were scattered over an area estimated to be about 7 square miles. Figures 5.5.1-10 and 5.5.1-11 show the postlanding condition of the service module and aft section of the launch vehicle, respectively. All flight hardware, which was declared to have postflight engineering value, was returned to the VAB. The following system components were recovered: one antenna, one antenna coupler, one S and A unit, two batteries, and two relay boxes.

5.5.4 Survey report.- WSMR Geodetic Branch personnel, who were part of the recovery teams, made surveys of the command module landing site and the launch-escape subsystem and launch-vehicle impact sites. The results of these surveys indicated that the command module landed on an azimuth of 3°37'11", 22,840 feet downrange from the launch pad. The launch-escape subsystem impacted 27,953 feet, bearing 4°44'05", from the launch pad and the service module impacted on an azimuth of 359°17'55", 10,964 feet from the launch pad. The aft section of the launch vehicle impacted 11, 592 feet, bearing 1°28'43", from the launch pad. Figure 5.5.1-12 shows a general layout of the survey.

[redacted]

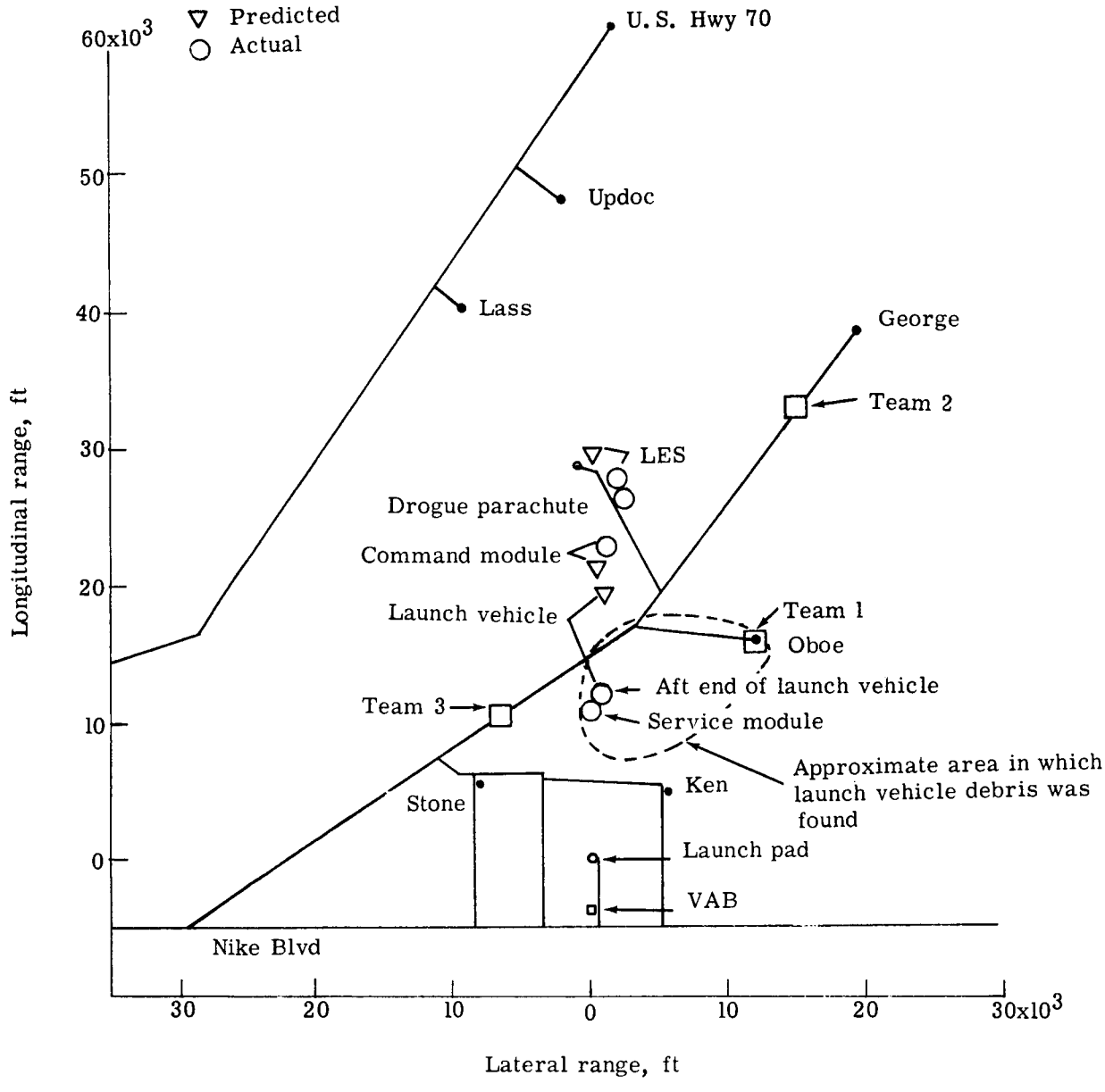

Figure 5.5.1-1.- Recovery team standby positions and location of predicted and actual landing/impact points.

[redacted]

Figure 5.5.1-2.- Photograph of command module after landing.

Figure 5.5.1-3.- Closeup photograph of command module after landing.

Figure 5.5.1-4.- Photograph of command module and parachute after landing.

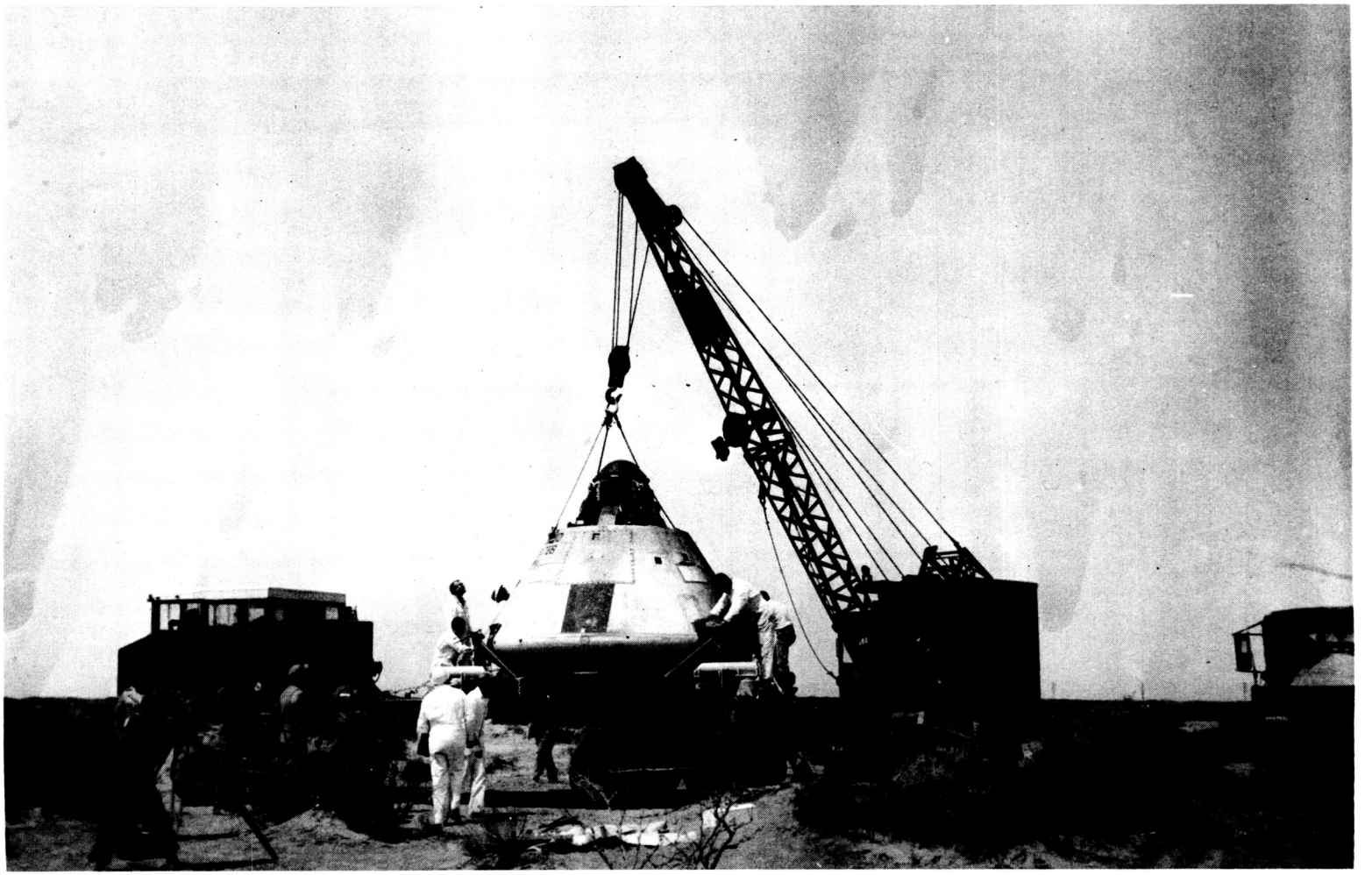

Figure 5.5.1-5.- Photograph showing command module being loaded on Terracruiser.

[redacted]

Figure 5.5.1-6.- Photograph of command module imprint on ground.

[redacted]

[redacted]

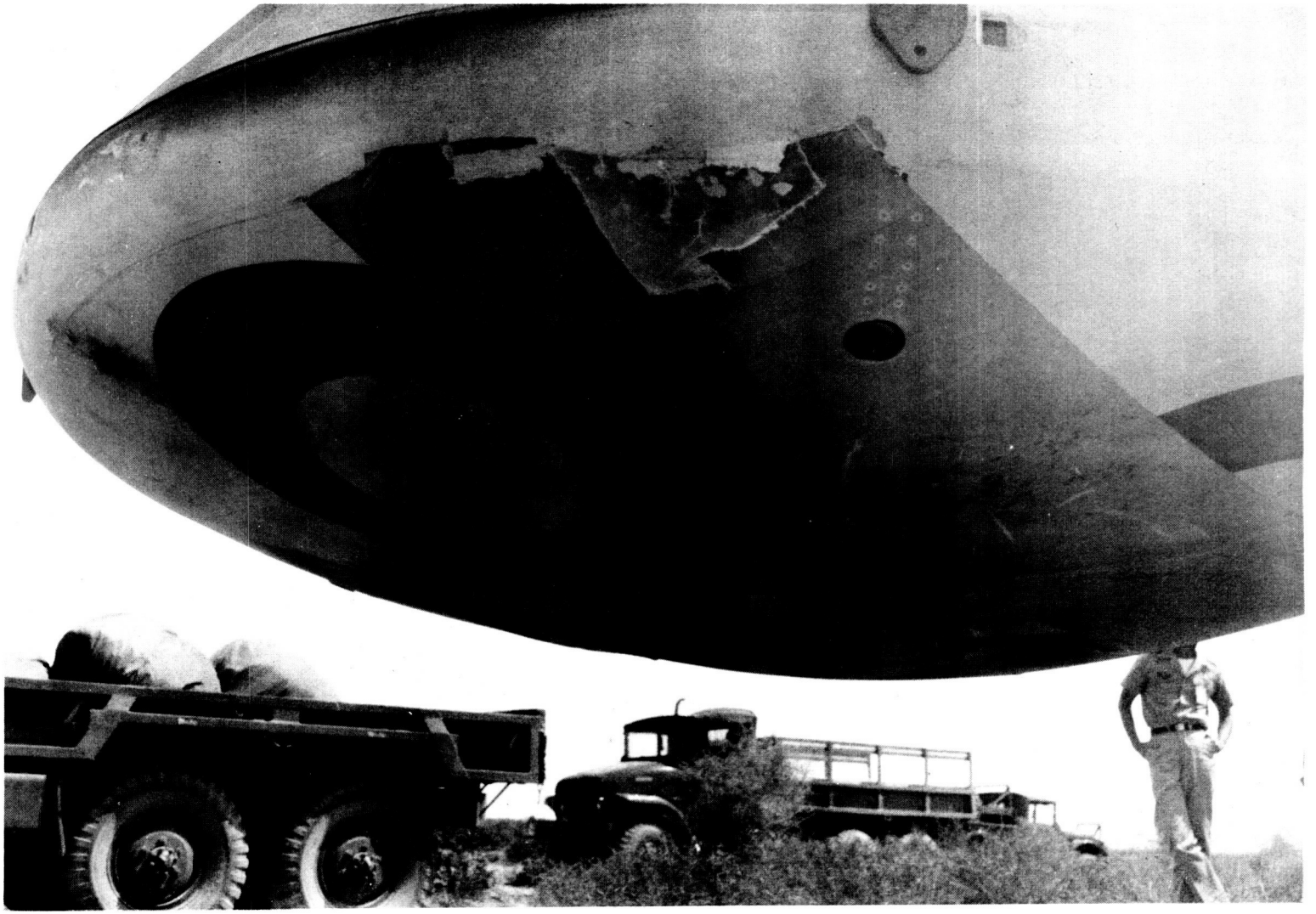

[redacted]

Figure 5.5.1-7.- Photograph showing fiberglass torn from aft heat shield.

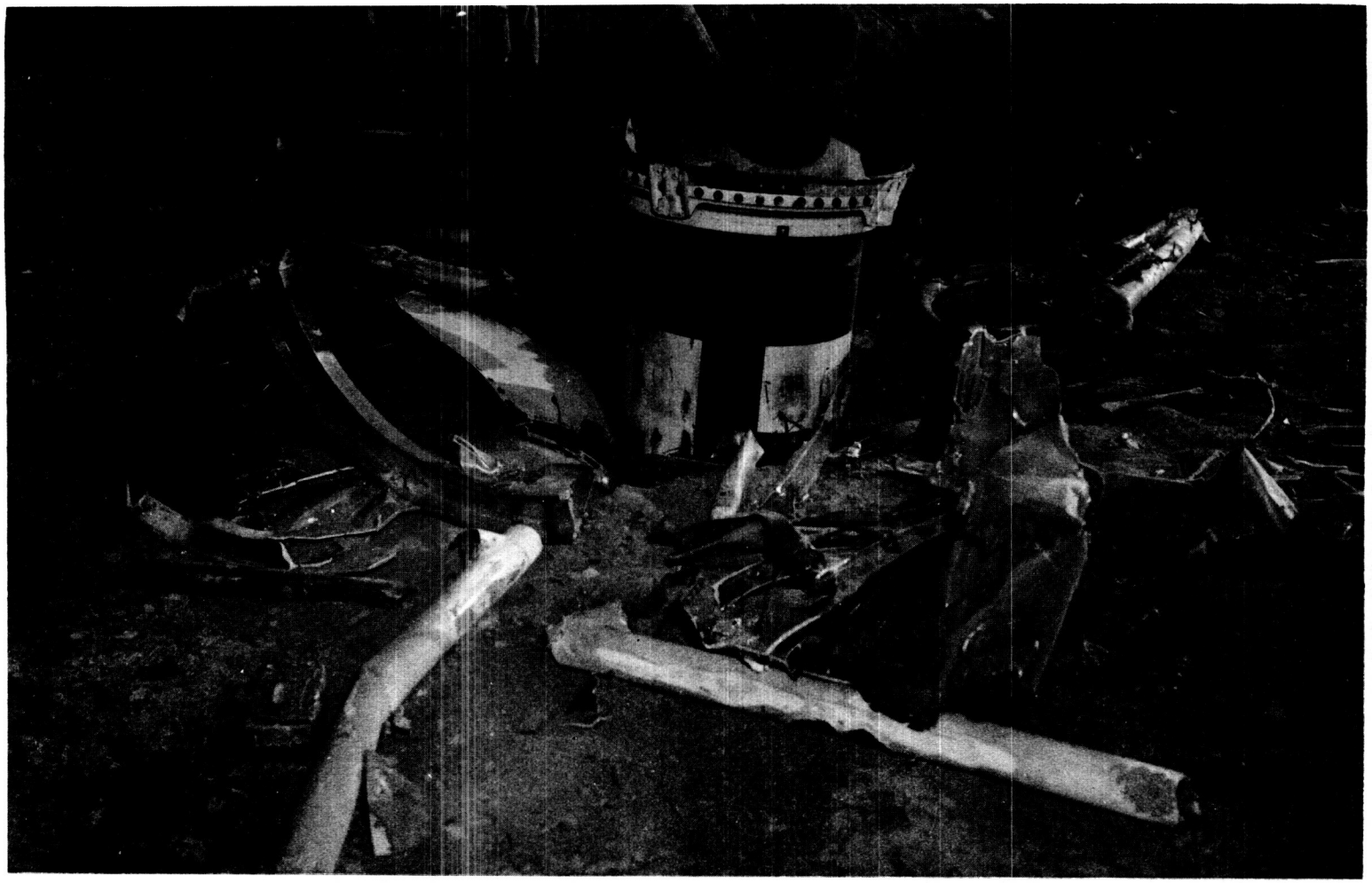

Figure 5.5.1-8.- Photograph of LES after impact.

[redacted]

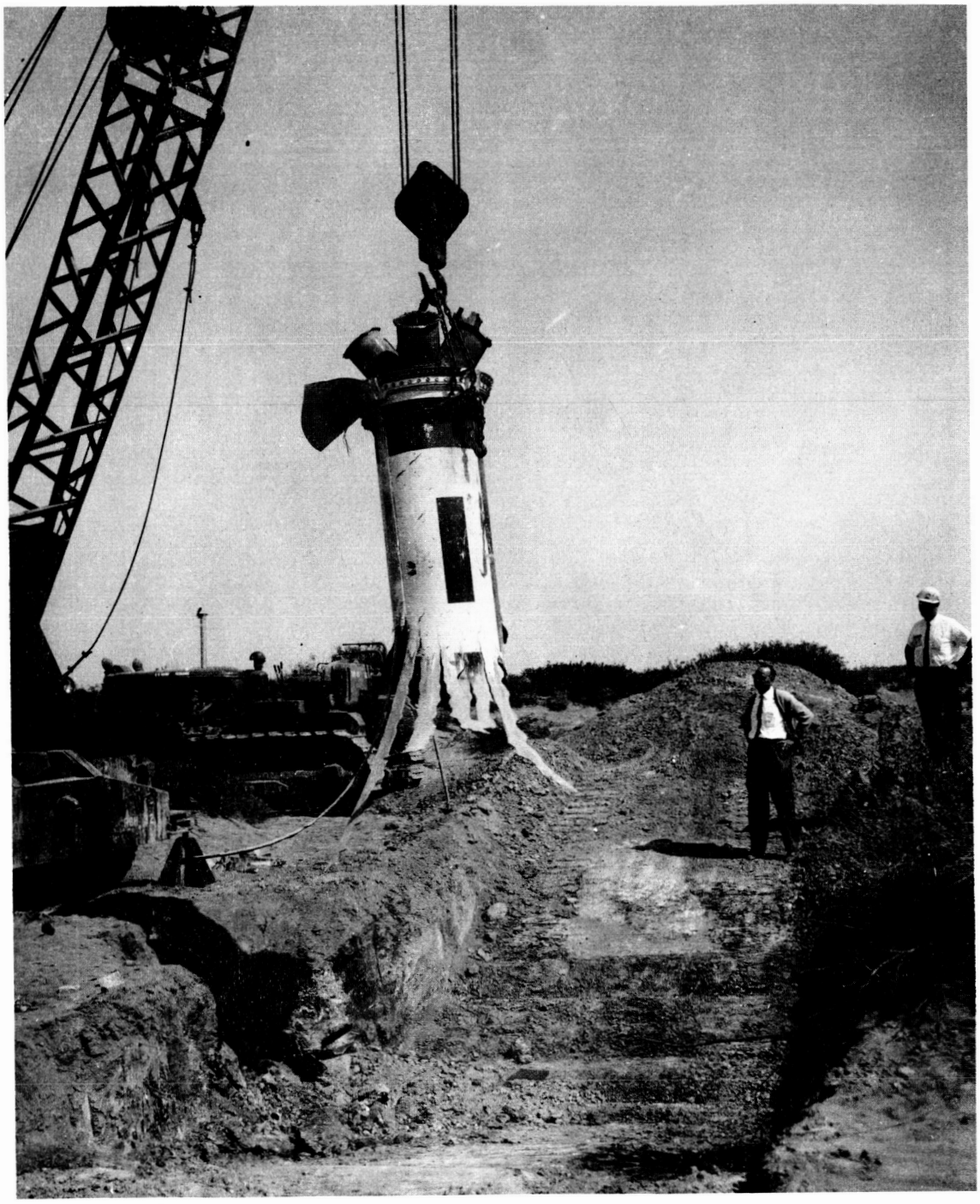

Figure 5.5.1-9.- Photograph of LES after removal from ground.

[redacted]

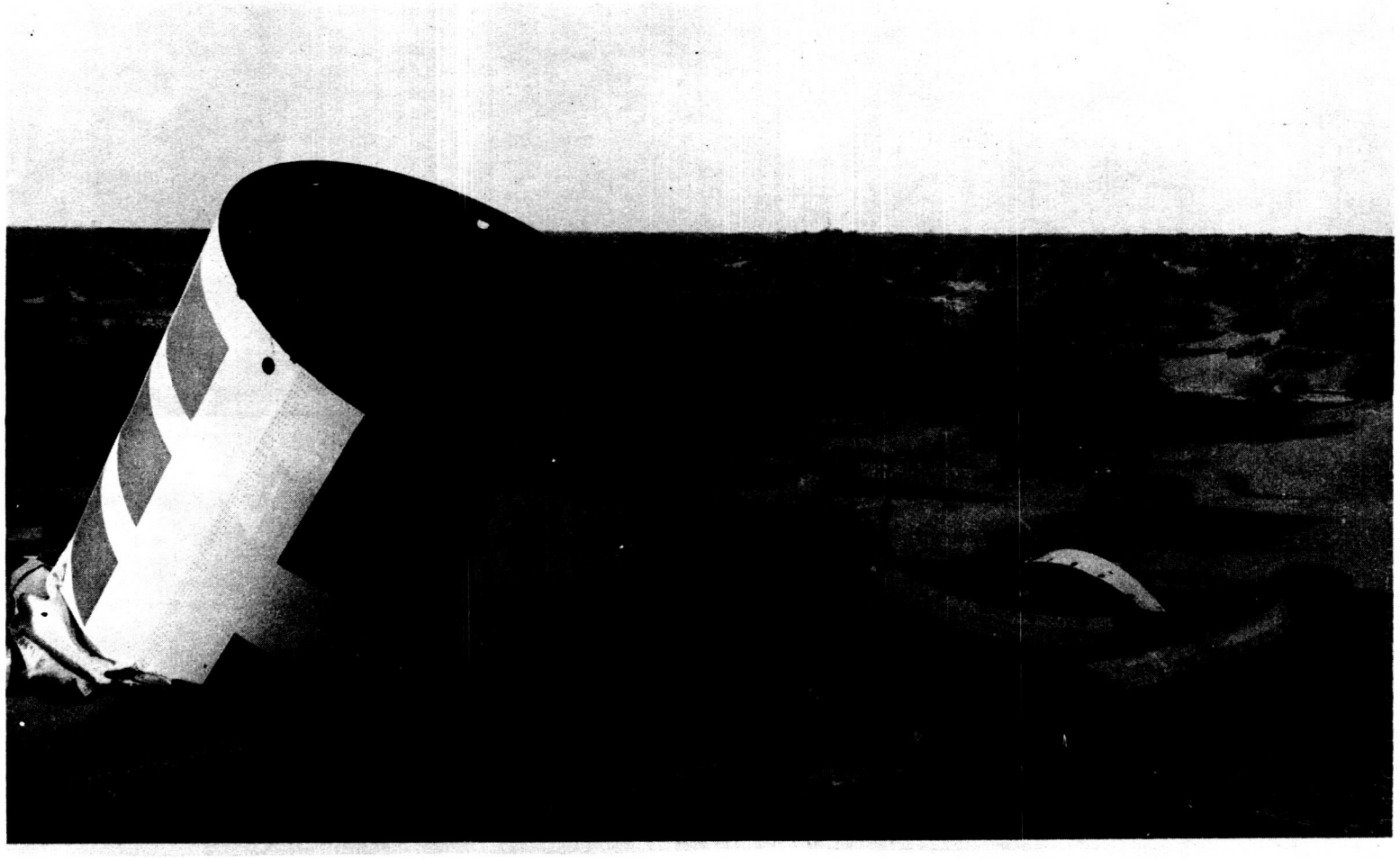

Figure 5.5.1-10.- Photograph of service module after impact.

Figure 5.5.1-11.- Photograph of aft section of launch vehicle after impact.

6.0 CONCLUSIONS

As a result of the Apollo boilerplate 12 Mission A-001, the following conclusions can be drawn:

1. There was no evidence of any damage to the launch-escape vehicle because of the environment experienced during Mission A-001 except during thrust termination and earth landing.

2. Thrust termination subjected the spacecraft to an environment more severe than expected and was above the qualification test level of many of the command module components. The command module aft heat shield was damaged by the force of the explosion. In addition, the failure of one side of the 41.1 second back-up abort timer occurring at thrust termination may have been caused by the severity of the explosion experienced during thrust termination.

3. The launch-escape vehicle was aerodynamically stable in the dynamic pressure and Mach number range of this mission.

4. The command module-service module separation system functioned as designed. The separation was effected with no indication of command module to service module recontact.

5. The time of occurrence of events was satisfactory in all respects. The loss of one main parachute was not attributable to either high dynamic pressure or any problem which could be a result of incorrect earth-landing subsystem timing events.

6. Little Joe II launch vehicle and spacecraft compatibility was proven satisfactorily during both the ground-testing phase and the flight phase of Mission A-001 operations.

7. The aerodynamic loads resulting from fluctuating pressures on the spacecraft were within those predicted from results of wind-tunnel testing.

8. The only test objective which was not fully satisfied was the second-order test objective on the earth-landing subsystem. This objective was:

> Demonstrate proper operation of the applicable components of the earth-landing subsystem.

[redacted]

The only applicable component of the earth-landing subsystem which did not demonstrate proper operation was main parachute no. 1 which did not have a chance to display proper reefing, disreefing, and inflation. This parachute broke loose from the spacecraft when the parachute riser parted shortly after line stretch because of abrading and cutting on the sharp edges of the drogue disconnect guide assembly structural gusset.

[redacted]

7.0 DISTRIBUTION

Number of Copies		Addressees
1	D	Director
6	AI4	Technical Library
2	AI6	Technical Information Division Records
3	E	Assistant Director for Engineering and Development
3	G	Gemini Program Office
6	P	Apollo Spacecraft Program Office
3	SR	Reliability and Quality Assurance Office
1	HM	Reliability and Flight Safety Office, Cape Kennedy, Fla.
2	SP	Public Affairs Office
1	SL2	Office of Patent Counsel
6	MD	NASA Headquarters
6	ATSS-6	NASA Headquarters Library
6		Ames Research Center Library
6		Flight Research Center Library
6		Goddard Space Flight Center Library
6		Langley Research Center Library
6		John F. Kennedy Space Center Library
6		Lewis Research Center Library
6		Marshall Space Flight Center Library

Number of Copies		Addressees
1		Ames Research Center Attn: Director
1		Flight Research Center Attn: Director
1		Goddard Space Flight Center Attn: Director
1		Langley Research Center Attn: Director
1		John F. Kennedy Space Center Attn: Director
1		Lewis Research Center Attn: Director
1		Marshall Space Flight Center Attn: Director
1	HR	MSC Florida Operations Office/Houston
2	OO	Office of Assistant Director for Flight Operations
4	OF	Flight Control Division
3	OL	Landing and Recovery Division
6	OM	Mission Planning and Analysis Division
6	EG	Guidance and Control Division
7	EC	Crew Systems Division
9	EA	Advanced Spacecraft Technology Division
7	ES	Structures and Mechanics Division
8	EE	Instrumentation and Electronic Systems Division
8	ED	Computation and Analysis Division

Number of Copies		Addressees
3	EP	Propulsion and Energy Systems Division
6	CO	Office of Assistant Director for Flight Crew Operations
2	CC	Aircraft Operations Office
2	CF	Flight Crew Support Division
5	CA	Astronaut Office
5	PD	Resident Apollo Spacecraft Program Office at NAA, Downey, California
3	PC	Command and Service Module - Project Officer
2	PB	Resident Apollo Spacecraft Program Office at Grumman, Bethpage, L.I., N.Y.
1	PG	Navigation and Guidance - Project Officer
1	PS	PACE Spacecraft - Manager
1	PL	Lunar Excursion Module - Project Officer
3	PA	Operations Planning Division
6	PP	Program Control Division
7	PE	Systems Engineering Division
3	PR	Reliability and Quality Assurance Division
35	PT	Test Division
12	PT1	WSMR Test Office - Attn: H. Van Goey P. O. Drawer "D" White Sands, New Mexico
2	HA1	AMR Test Office - Attn: A. E. Morse P. O. Box MS, Cocoa Beach, Fla.
12	HS	Operations Support, Plans and Programs Mail Code HS - Cape Kennedy, Fla.

Number of Copies		Addressees
1	A	Administration Directorate
3	AD	Photographic Division
5	AW	WSMR Operations - Attn: W. Messing P. O. Drawer "D" White Sands, New Mexico
6		NASA Wallops Station, Wallops Island, Virginia
5		Mr. J. B. Hurt, Program Manager, General Dynamics/Convair, Mail Zone 6-135, San Diego, California
2		Mr. Robert S. Mullaney, Program Manager Apollo LEM - Grumman Aircraft Engineering Corporation, Bethpage, L.I., N.Y.
35		Mr. E. E. Sack, Manager, Contracts and Proposals, North American Aviation, Inc. S and ID, 12214 Lakewood Blvd., Downey, California
1	AT	Office of Technical and Engineering Services, Office of Chief
1	AS	Security Division - Office of Chief
10	HO	MSC Manager - Fla. Operations - Office of Manager
2	AI	Technical Information Division - Office of Chief
1	DS	Special Assistant to Director
1	DA	Sr. Engineering Advisor to Director
1	DE	Executive Assistant to Director
1	SM	Center Medical Office
1	HA	RASPO - AMR - Cape Kennedy

Number of Copies		Addressees
1	O	Flight Operations Directorate
1	C	Flight Crew Operations Directorate
6		General Electric Co., Apollo Support Dept., MSC Support Operations, Houston, Texas
5		Dr. F. A. Speer Marshall Space Flight Center Code: R-AERO-F
1		Aerojet General Corporation Sacramento, California Attn: H. E. Halligan
10	AI6	Reports Distribution Branch
10	AA21	Publications and Forms Distribution Branch